Hot mill interstand model and practical applciations.

Cornelius, Paul Andrew

Hot Mill Interstand Model and Practical Applications

By

Paul Andrew Cornelius BEng(Hons)

Thesis submitted to the
University of Wales
for the Degree of
Engineering Doctorate

Department of Materials Engineering
University of Wales-Swansea

January 2001

Academic Supervisor : Professor R. W. Evans
Industrial Supervisor : Dr. N. Rudkins

ProQuest LLC.
789 East Eisenhower Parkway
P.O. Box 1346
Ann Arbor, MI 48106 – 1346

SYNOPSIS

Hot rolling is a highly complex physical problem. The difficult geometry and the hot deformation behaviour of Carbon strip steels during hot rolling render this process difficult to investigate during normal operations or within the laboratory. Numerical models can therefore be used to further understanding of hot rolling with their ability to predict variables that are difficult or even impossible to measure during normal hot rolling operations. A numerical model has been developed using the commercial ABAQUS Finite-Element software package to consider the effect of process variables such as temperature and microstructural evolution with their consequential effects upon the mechanical behaviour of the strip within a seven stand commercial finishing mill.

The roll-gap has been described as a thermal-mechanical coupled plane-strain problem with thermal and microstructural algorithms describing the interstand periods. The hot deformation characteristics of a high Carbon material have also been investigated using multi-deformation testing methods within the laboratory and numerically described using constitutive modelling techniques.

The numerical results include multi-pass thermal predictions and the calculation of microstructural evolution between successive deformations for high Carbon, Carbon Manganese and low Carbon strip steels. Rolling parameters such as rolling loads have been predicted as functions of strain, strain rate, temperature and retained strain from previous deformations. Rolling forces and thermal results have been shown to be in reasonable agreement with measured data from trials at the Corus strip mills at Port Talbot and Llanwern, Wales, UK.

The research programme has developed constitutive relationships for a high Carbon steel and demonstrated that coupled thermal-mechanical and microstructural algorithms can create sensitive and accurate numerical simulations of commercial hot rolling.

ACKNOWLEDGEMENTS

The author would like to thank Dr. B. J. Hewitt, Director R, D & T, Corus Strip Products for permission to publish this thesis. This research has been carried out at Corus Strip Products – Welsh Technology Centre and the University of Wales-Swansea as part of the research programme of the Engineering Doctorate Centre-Wales under sponsorship from the Engineering and Physical Sciences Research Council.

The author would also like to thank Professor R. W. Evans (Academic Supervisor, University of Wales-Swansea) for his original suggestion for this research and whose invaluable guidance and encouragement throughout the four-year period has provided the motivation to complete this thesis.

Thanks also go to Dr. N. T. Rudkins (Industrial Supervisor, Welsh Technology Centre) for his helpful advice concerning the direction of this work and his positive insights into the industrial applications of the research within Corus UK.

Finally, I would also personally like to thank my family for their unlimited support and care during my Engineering Doctorate Degree, for which I will be eternally grateful.

NOMENCLATURE

A	Area (m^2)
A_i	Instantaneous area (m^2)
C	Specific heat of steel ($Jkg^{-1}K^{-1}$)
C_p	Specific heat ($Jkg^{-1}K^{-1}$)
C_{pw}	Specific heat of water ($Jkg^{-1}K^{-1}$)
D	Thermal diffusivity (m^2s^{-1})
d_o	Initial austenite grain diameter (μm)
E	Emissivity factor
F	Force (N)
F^{el}	Elastic forces (N)
F^{pl}	Plastic forces (N)
Gr	Grashof number
h_i	Instantaneous height (m)
h_o	Original height (m)
$J_{1,2,3}$	1^{st}, 2^{nd} and 3^{rd} invariants of deviatoric stress
K	Empirical constant and material stiffness
K_g	Mean yield stress for torque ($tons/in^2$)
K_p	Mean yield stress for load ($tons/in^2$)
k	Thermal Conductivity ($Jm^{-1}s^{-1}K^{-1}$) and yield stress in pure shear
L	Characteristic length (m)
N	Roll speed (rev/min)
Nu	Nusselt number
n	Material constant
P	Rolling Load (N)
P_n	Contact pressures normal to the surface (Nm^{-2}).
Pr	Prandtl number
Q	Rate of heat generation due to plastic work
Q_{def}	Apparent activation energy
Q_g	Dimensionless parameter
Q_p	Heat generation in the roll gap
Q_{rex}	Apparent activation energy fo recrystallisation (kJ/mol)
R	Undeformed roll radius (m) and molar gas constant.
R'	Deformed roll radius (m)
R_e	Reynolds number
S	Stefan-Boltzmann constant ($Jm^{-2}\ s^{-1}\ K^{-4}$)
S_t	Austenite microstructure
s	Proportion of steam generated
T	Temperature (K)
T_a	Ambient temperature (K)
T_r	Roll Temperature (K)
t	Time (s)
$t_{0.5}$	Time to 50% recrystallisation (s)
V	Volume (m^3) or velocity (ms^{-1})
W_f	Water flow per unit width of plate ($m^2\ min^{-1}$)
w	Width of strip (m)
$(H \rightarrow h)$	Fraction reduction (%).
X	Fraction recrystallised

Z	Zenner-Hollomon parameter = $\dot{\varepsilon}$ exp Q_{def}/ RT (s^{-1})

Greek Symbols

α	Heat Conduction factor ($Jm^{-2}\ S^{-1}\ K^{-1}$) and material constant
α_{FC}	Forced convection heat transfer coefficient ($Jm^{-2}\ S^{-1}\ K^{-1}$)
β	Material constant = (αn)
δ	Draft (inch)
ε	Strain
$d\varepsilon$	Increment of strain
$d\varepsilon^{el}$	Elastic part if incremental strain
$d\varepsilon^{pl}$	Plastic part of incremental strain
$\dot{\varepsilon}$	Strain rate
Δ	Change in value of a quantity
μ	Friction coefficient
ρ	Density (kg m^{-3})
ρ_w	Density of water (kg m^{-3})
Δt_w	Temperature change in water (K)
λ	Latent heat of water (Jkg^{-1})
σ	Cauchy or True stress
σ_N	Effective normal stress
σ_P	Effective peak stress
σ_y	Effective yield stress
$\sigma_{0.5}$	Effective stress at large true strain
τ_F	Shear stress
τ_{max}	Maximum shear stress
θ_R	Temperature of the work roll (C)
θ_W	Temperature of the workpiece (C)
γi	Slip rate in direction *i*

TABLE OF CONTENTS

Appendix A

Mill Data

1 Introduction

Rolling is among the highest tonnage industrial processes where product dimensions are successively reduced by passing it between two counter-rotating rolls with the roll-gap progressively being reduced. However, harder and less ductile metals and alloys, such as steel, could not be given large reductions at room temperature. Hot rolling was therefore introduced to enable the processing of these materials where the stock is heated to reduce the energy required to deform these materials.

More recently steel manufacturers want to change from commodity businesses to manufacturers of a range of innovative, fit for purpose and ultimately high value products. This and the fact that steel makers are not only threatened by other steel makers but are also challenged by other materials provides the motivation to develop understanding of both the process and the products.

Hot rolling is extremely complex and difficult to investigate during normal commercial operations or within the laboratory. Numerous numerical models have been developed for further understanding of this process and to calculate loads and power requirements as functions of processing parameters such as reductions and rolling speeds. Researchers at the Welsh Technology Centre and Engineering Doctorate centre at University of Wales-Swansea have considered the complexities of hot rolling with an aim to model the deformation process with as few approximations as possible. Mathematical models using modern Finite Difference and Finite-Element techniques have been developed to describe the mechanical behaviour of plain Carbon steels during hot rolling. However there is a need to complement this work by modelling the thermal and microstructural behaviour of the strip between successive stands.

The ultimate aim of any thermomechanical model is to produce a complete and sensitive simulation of the hot rolling industrial process. Indeed, a fundamental goal of a process model is to reduce the necessity for physical mill trials. Furthermore, process modelling aims to optimise the use of equipment by allowing extreme mathematical, rather than experimental, scenarios to be executed. Optimisation of plant will lead to a decrease in

delays, improvements to both processes and products and hence the possibility of a faster payback on the heavy initial capital expenditure involved with the hot rolling process.

A brief description of the work completed during this research follows. The entire thesis consists of 11 chapters with the relevant figures after each chapter. The current chapter provides a general introduction to the field of hot rolling analysis. Chapter 2 forms the literature review of relevant theoretical and experimental research completed on numerical modelling of hot rolling.

As the work was carried out in partnership with Corus UK, chapter 3 gives some insight into the motivation behind the research and a brief description of the two South Wales hot strip mills. Chapter 4 introduces the methodology of the finishing mill multi-stand model with an overview of Finite-Element concepts and phases.

Chapter 5 explains the experimentation apparatus and procedures used to derive the hot deformation strength and the recrystallisation characteristics of a high Carbon steel to be used within the Multi-Stand Finite-Element model. This chapter begins with continuous straining experiments and concludes with multiple hit deformation experiments.

Chapter 6 describes the development of the roll-gap model including heat transfer considerations and desired output. Chapter 7 completes the finishing mill multi-stand description with the analysis of the interstand model development. This chapter focuses on the microstructural algorithm created within the interstand Finite-Element model.

Chapter 8 presents the results from the experiments conducted in chapter 5 with the calculated constants for the prediction of hot strength and recrystallisation kinetics of the high Carbon Steel. Also included in chapter 8 are the finishing mill simulations with comparison to rolling trials conducted at the two commercial South Wales finishing mills. Finally, the thesis is closed with the major conclusions from the research and suggestions for future work.

2 Literature Review

2.1 Introduction

In order to reveal the complexities of the mechanical, thermal and microstructural aspects of hot rolling it is necessary to investigate current understanding of the subject through the review of previous work. The Literature review begins with a brief introduction to the mechanics of strip rolling including some of the early theoretical understanding of the process. All these theoretical models of the flat rolling process can be conveniently divided into two groups. Firstly, the traditional techniques such as slab and slip-line methods are described. In each of these approaches an equation of equilibrium is combined with the constitutive relations of the rolled metal. Prescribed friction conditions are then applied at the roll/strip interface to derive variables such as rolling loads and power requirements. The main concern with these methods is that consideration of the workpiece temperature only appears through its effect on the mechanical properties.

Latter sections refer to the most recent developments and encompass both the Finite Difference and Finite-Element models. Some models calculate the microstructural as well as the combined thermal-mechanical events during hot processing. Aspects of this research will be discussed in some detail with an emphasis on the current understanding of process modelling technology. This chapter concludes with a detailed description of the essential aspects concerning numerical methods employed in the mathematical modelling of hot strip finishing mills.

2.2 Roll Gap Introduction

The rolling of steel strip can be readily understood in mechanical terms when we consider the roll gap geometry as elastic and plastic areas of deformation as shown in Figure 2.1. The relative surface velocities between the roll and the strip are such that it draws the material into the roll gap. The strip firstly deforms elastically and if the reduction and therefore the strains within the material are great enough, plastic flow will also occur. These two regions of elastic and plastic state are separated by a surface called

the elastic-plastic interface and the criterion of plastic flow will govern the manner in which this transformation occurs.

Due to the roll gap geometry plastic flow will increase as the material progresses through the roll gap. At exit the roll pressure is removed and a limited amount of elastic recovery occurs corresponding to the material's mechanical behaviour.

As the material enters the roll gap it is normally travelling slower than the surface speed of the roll. As a result of the interface conditions the strip accelerates forward into the roll gap until, at exit, the strip is travelling faster than the roll. The direction of friction between the strip and the roll must therefore change direction within the roll gap. This change in the relative surface velocities between roll and the strip renders rolling difficult to investigate and describe using numerical methods [1].

2.3 Traditional Techniques

Rolling steel has been the subject of numerical analysis since the first part of the 20th Century. The starting point for many of these off-line models has been the calculation of the most important of rolling variables, i.e. rolling load. Due to the complexity of rolling, the early work required several simplifying assumptions. These are shown below with some justification to their application: -

1. *Plane strain deformation.* As the width is far greater than the gauge any deformation in this direction can be neglected.
2. *Homogeneous Compression.* Material segments perpendicular to the rolling remain perpendicular and therefore, ignore any shear forces.
3. *Constant Yield Stress.* Material properties are assumed independent of temperature, strain and strain rate within the roll gap.
4. *Circular arc of contact.* Any roll flattening that may occur is ignored. During rolling of slabs and plates at relatively low roll forces no flattening is expected. However, during thin strip rolling the effect of roll flattening on the rolling load can be significant due to the increased contact area.
5. *Sticking Friction.* Friction is assumed constant along the strip/roll interface.

Von Karman [2] conducted a numerical analysis of flat rolling using the classical slab method. Within the slab method, a representative volume element in the body of the material or workpiece undergoing plastic deformation is isolated and the behaviour of this element is observed as it moves along the deformation zone of the pass. The slab technique can make use of all the assumptions mentioned above and is derived for the calculation of plastic deformation for an isolated sample of the work piece. It is then assumed that this sample will be representative of the entire body of material.

The first notable development in this area was published in 1943 when Orowan [3] dispensed with all the mathematical approximations and the assumption of a constant yield stress. For the first time the direct use of experimentally determined stress/strain curves could be included in what was termed the 'graphical-numerical method of computation.' In part II of the well renowned paper titled 'The Calculation of Roll Pressure in Hot and Cold Rolling,' the assumptions of sticking friction along the arc of contact and homogeneous deformation were also discarded. Orowan noted it was possible for the tangential forces at the interface to exceed the yield stress of the material. This of course was impossible, as the material would undergo plastic shear leading to sticking rather than slipping friction. Due to this condition at the strip/roll interface homogeneous compression could no longer be assumed in flat rolling.

Following Orowan, Sims [4] synthesised that the hot rolling process was analogous to deformation between rough inclined plates. The work applied sticking friction over the entire length of contact and used a mean yield stress to account for strain and strain rate hardening. These assumptions were noted to satisfy conditions of rolling between rough, dry rolls with relatively soft materials. Sims' model can be shown for practical purposes in the form: -

$$P = w\sigma\sqrt{R\Delta h}\,Q \qquad (2.1)$$

Where $\boldsymbol{P}$ is the rolling load, $\boldsymbol{w}$ is the width of the strip and $\boldsymbol{(R\Delta h)^{0.5}}$ is the projected arc of contact. $\boldsymbol{Q}$ is a complex function of roll radius, final thickness and the reduction in the pass. Within this calculation, the value of the mean plane strain flow stress, σ,

represented the largest calculations. In practice, these calculations were only required for the range of values likely to be encountered during commercial rolling. Sims provided a significant development when the application of equation 2.1 took a graphical form [5] which provided a more rapid method to estimate rolling loads. Values for Q for different reductions are given by Larke [6] and reproduced below in Table 2.1.

	Values of Q for % reduction						
R / h_f	5%	10%	20%	30%	40%	50%	60%
2	0.857	0.880	0.905	0.912	0.904	0.881	0.838
5	0.904	0.948	1.003	1.037	1.055	1.055	1.040
10	0.956	1.022	1.111	1.173	1.216	1.242	1.249
20	1.029	1.127	1.264	1.362	1.439	1.496	1.501
30	1.086	1.208	1.379	1.505	1.608	1.689	1.747
50	1.175	1.337	1.563	1.734	1.875	1.992	2.085

Table 2.1 Values for Q at different reductions Larke (1957) [6].

Cook and McCrum [7] used the theory of Sims to compile graphs and charts for the calculation of roll force and torque. The majority of the work focussed on improving the description of the yield strengths of different materials. This was achieved at elevated temperatures using a high rate compression-testing machine termed a cam plastometer. Rapid calculation of the flow stresses could now be achieved by interpolation of the graphical presentation of the results. The combination of Sims and Cook's work has been the standard used within the steel industry for the calculation of rolling loads and torque requirements for many years.

An improvement in calculating roll forces was achieved when the whole deformation process including the geometry of the tools, frictional contact and the constraint of surrounding material was taken into account. The improvement described the roll gap as a field of stress and strain which differs from point to point. This 'field' type theory improved on the traditional slab technique by providing a solution as to how material is deforming on a point-to-point basis. Limitations dictated that the material could only be rigid-plastic where elastic and work hardening effects are neglected. Unfortunately, no slip line or trace shape are known prior to the calculation for problems involving

Coulomb friction or curved boundaries which violate linear solution. Slip-line field solutions for plate rolling were therefore generally very complicated and laborious [8].

Alexander [9] created the first slip line field approach to find a solution to hot rolling problems. The major limitation with this work was that it could only be applied to a single geometrical situation with a 33.5% reduction carried out where the ratio of the roll radius to the exit gauge was 86.7. Alexander and Ford [10] have attempted to reduce the amount of work involved in finding solutions to the slip line field by constructing a simplified field in which the entry slip line is straight and the exit slip line is made into a circular arc. Further work from Crane and Alexander [11] and Denton and Crane [12] described the manner in which a material was flowing during various rolling deformation regimes.

The slip-line field method was shown to offer a complete numerical solution to a limited number of hot rolling scenarios [12]. Unfortunately, this method could only incorporate constant yield stress and sticking friction over the entire arc of contact. Perhaps more importantly, as mentioned by Gupta and Ford [13], complete definition of the temperature field is not possible with slip-line field solutions. Their work also assessed how far the values of yield stress obtained from compression tests could be applied to the hot rolling process. Gupta and Ford [13] illustrated the importance of accurate yield stress data in the calculation of rolling load and to a greater extent rolling torque. They concluded that the inclusion of roll flattening was important when considering the hot rolling of steel and that whilst a semi-empirical relationship between temperature and yield stress seemed to exist, accurate description of the temperature field during rolling is essential.

The previously described research illustrated the significant developments within the field of numerical modelling of flat rolling. However, the preceding numerical techniques could not completely satisfy all of the complexities during hot rolling such as temperature dependent yield stress and varying friction conditions along the arc of contact.

The numerical methods described above can estimate rolling loads, torques and roll pressures. However, the slab method cannot take into account how the material is deforming within the roll gap. The 'field' type solutions, such as the slip line technique, can take into account the heterogeneous deformation and so can offer some insight into the material flow during hot rolling. All the techniques described above cannot consider complex material properties and therefore assume constant yield stress within the roll-gap but perhaps more importantly all the methods described cannot include the significant effect of roll chilling and heating due to the plastic deformation on the hot deformation characteristics of the strip. Due to these limitations the application of these methods are only of historic importance when considering off-line models of hot rolling.

2.4 The Finite-Element / Finite Difference Techniques

Engineering, science and solid mechanics have been among the first fields to benefit from the development of the silicon chip and the digital computer. Numerical techniques for the analyses of highly complex structural systems have been devised with the enhanced power of computation. For the first time, the difficulties in obtaining an exact numerical solution of the governing differential equations experienced by Orowan, Sims and Cook [3, 4, 7] was no longer the major problem it had been.

Many numerical techniques have been used in the field of computational mechanics but by far the most widely adopted are the finite difference and Finite-Element methods due to their applicability to many different boundary value problems with little restriction on workpiece geometry. Argyris [14, 15] in the UK and Clough et al [16] in America first coined the term Finite-Element and put this method to practical use while developing systematic structural analyses for complex aeronautical structures.

Whilst these numerical techniques have been developed harmoniously, the characterisation of boundary conditions and material rheology is still a matter of debate. Given these challenges it is well understood that the Finite-Element and Finite Difference techniques can offer significant advantages over traditional methods as materials can be better expressed in terms of strain, strain rate and temperature so that they can consequently provide an insight into how the material behaves during rolling.

2.4.1 Reference Frames

One of the first considerations when using the Finite-Element technique is to decide on the type of reference frame best suited to the physical problem. Finite-Element codes have evolved with two basic methods of solution [17]: -

1. Eulerian reference frame.
2. Lagrangian reference frame.

The Eulerian reference frame refers to a control volume where conservation of mass is not conditional. Normally if the material is assumed incompressible, the conservation of mass can be dealt within the equations of motion through a penalty function or Lagrange multiplier.

In a Lagrangian frame, conservation of mass is automatically enforced as the mesh distorts with the material. Thus, there is no need for any additional conservation of mass equation for material models that included elastic solutions within a Lagrangian reference frame. In general, it appears that most codes using elasto-plastic and elasto-viscoplastic rheology adopt the Lagrangian coordinate frame. The majority of commercial codes like ABAQUS, MARC, ADINA and NIKE2D use the Updated Lagrangian formulation.

2.4.2 Rheology

Rheology is the science of deformation and flow of matter. The goal of rheology is the prediction of the force system necessary to cause a given deformation or flow in a body, or conversely, prediction of the deformation or flow resulting from the application of a given force system to a body [18]. In fact the main difference between the Finite-Element works that followed was the determination of the material behaviour. In the case of metal forming simulations using the Finite-Element method the material rheology can be described rigid-plastic, rigid-viscoplastic, elasto-plastic or elasto-viscoplastic as shown in figure 2.2.

2.4.2.1 Rigid-Plastic

There are a growing number of Finite-Element codes that can predict the forming characteristics of a material. Most have the common basic assumption that elastic effects can be ignored. In the analysis of metal forming, plastic strains usually outweigh elastic strains and the idealisation of rigid-plastic or rigid visco-plastic material behaviour can be justified.

Chen and Kobayashi [19] developed a "general matrix method" for rigid-plastic deformation and applied the method to a detailed analysis of rigid plastic ring compression assuming isothermal conditions. Shima et al [20] analysed several cases of rolling using a rigid perfectly plastic model whilst Li [21] investigated spread during three-dimensional rolling using this material definition. Li and Kobayashi [22] also applied rigid-plastic analyses to a comprehensive investigation into plane-strain rolling to study the effects of material properties and rolling geometries.

Mori and Osakada [23] simulated three-dimensional plate rolling and edge rolling using the steady-state rigid-plastic formulation. The work focussed on the development of element types where constant displacements and velocities were assumed through the gauge. Their work later expanded to modelling non-steady-state schemes that can be applied to the head and tail ends of complicated shape rolling [24].

Yamada et al [25] included work roll deflection in his three-dimensional rigid-plastic Finite-Element model of flat rolling by modifying the contact surface. Yanagimoto et al [26] furthered this work by coupling the rigid-plastic strip deformation with the elastic roll deflection in three-dimensions. The work showed the capability of the Finite-Element method to calculate cross width shape and gauge performance for the flat rolling process.

2.4.2.2 Rigid-Viscoplastic

Since rigid-viscoplastic Finite-Element analysis is an extension of the older rigid-plastic method many applications using the older method can easily be applied to this technique.

Cornfield and Johnson [27] were the first to investigate the plastic flow of materials during hot rolling using the rigid-viscoplastic approach. The model made use of a modified elastic code with a variable elastic modulus. Lee et al [28] and Zienkiewicz et al [29] furthered this approach with special attention to metal forming processes such as extrusion. Kumar et al [30] examined the application of the flow formulation Finite – Element method to predict roll forces for the industrial hot rolling of steel strip. Their work took into account roll chilling and frictional effects with roll flattening. Jin et al [31] used visco-plastic material behaviour combined within a Eulerian reference frame to model the deformation within the roll gap where the mechanical and thermal equations were solved separately and the results iterated between the solutions.

The rigid-plastic or rigid-viscoplastic *flow* formulation cannot calculate residual stresses but the stress and strain tensors are easier to code. In addition, with the relatively small elastic portion of the stress/strain curve omitted less stringent convergence criteria can be employed which requires much less computational expense.

2.4.2.3 Elasto-plastic

Problems where the spring back effect may be significant such as the calculation of residual stresses for cold forming after unloading, or for hot forming after unloading and cooling require phenomena associated with elastic as well as the plastic effects to be taken into account. As Finite-Element methods were first developed to analyse the elastic response of structures it can easily be envisaged why the earliest attempts of metal forming occurred where elasto-plastic equations replaced the Hookean one. Marcal and King [32], Yamada et al [33] and Zienkiewicz et al [34] used the elasto-plastic formulation to analyse flat punch indentation, upsetting of solid cylinders and extrusion respectively. Pillinger and Hartley [35] presented a detailed description of the elasto-plastic method for metal forming applications including forging, rolling, extrusion and sheet metal forming problems.

In the so-called *solid* formulation, the material is considered to behave as an elasto-plastic or elasto-viscoplastic solid. Elasto-plastic behaviour is probably the most recognisable of all material non-linearity. This type includes the linear elastic modulus

and linear hardening (see Figure 2.2). The computational expense is now significantly increased, as the total strain increment is now the sum of the elastic and plastic strain increments as described in equation 2.2. The underlying assumption being that the increment of total strain can be subdivided into elastic and plastic components that are recoverable and permanent respectively.

$$d\varepsilon_{ij} = d\varepsilon_{ij}^{el} + d\varepsilon_{ij}^{pl} \tag{2.2}$$

Before the onset of plastic yielding the relationship between stress and strain is given by the standard linear elastic expression: -

$$\sigma_{ij} = C_{ijkl}\varepsilon_{kl} \tag{2.3}$$

Where σ_{ij} and ε_{kl} are the stress and strain components respectively and $\boldsymbol{C_{ijkl}}$ is the tensor of elastic constants, which for an isotropic material has the explicit form: -

$$C_{ijkl} = \lambda\delta_{ij}\delta_{kl} + \mu\delta_{ik}\delta_{jl} + \mu\delta_{il\delta jk} \tag{2.4}$$

Where λ and μ are the Lamé constants and δ_{ij} is the Kronecker delta defined by :-

$$\delta_{ij} = \begin{Bmatrix} 1 & if & i = j \\ 0 & & i \neq j \end{Bmatrix} \tag{2.5}$$

The situation is further complicated by the fact that different classes of materials exhibit different types of yield criteria. Whereas the Tresca and Von Mises laws closely approximate metal plasticity behaviour the Mohr-Coulomb and Drucker-Prager criteria are applicable to concrete, rocks and soils. Owen and Hinton [36] provided detailed descriptions of various yield criteria. Whilst the yield criterion itself determines at which stress level plastic deformation is incurred most of the various yield criteria suggested for metals are now only of historic interest, since they conflict with experimental predictions. The yield criteria can be written: -

$$f(\sigma_{ij}) = K(k) \tag{2.6}$$

Where f is some function and k a material parameter to be determined experimentally. The yield criterion can be independent of any co-ordinate or orientation system by only employing the three stress invariants: -

$$\begin{aligned} J_1 &= \sigma_{ij} \\ J_2 &= \frac{1}{2}\sigma_{ij}\sigma_{ij} \\ J_3 &= \frac{1}{3}\sigma_{ij}\sigma_{jk}\sigma_{ki} \end{aligned} \tag{2.7}$$

It is observed experimentally, at least for metals, that the onset of yielding is unaffected by the magnitude of the mean or hydrostatic stress in the system [37]. Therefore the yield function takes the form: -

$$f(J_2', J_3') = K(k) \tag{2.8}$$

Where J_2' and J_3' are the second and third invariants of the deviatoric stresses. Von Mises suggested that when J_2 exceeded a constant, K, yielding would occur. A suitable value for K could be obtained by applying the criterion to the tensile test. In this case the maximum principle stress corresponds to the stress along the axis so that yielding $s_1 = s_y$, $s_2=0$, $s_3=0$. Von Mises' law closely fits the experimental data [36] for most metals and it is this criterion that will be discussed further. This yield criterion may be written in its equivalent form as: -

$$\sigma_y = \sqrt{\frac{(\sigma_1 - \sigma_2)^2 + (\sigma_2 - \sigma_3)^2 + (\sigma_3 - \sigma_1)^2}{2}} \tag{2.9}$$

Where σ_y is the effective yield stress, generalised stress or equivalent stress. There are some important points to note about this equation. It is quite symmetric in respect that no principle stress is more important than any other. Since it contains squared terms the signs of the principle stresses become irrelevant. The criterion acknowledges that it is the

shear stresses that drive the onset of plastic deformation, as the terms are all the differences between the principle stresses. The derivation of the von Mises equation did not rely on any physical argument except to notice the usefulness of invariants. For nearly all applications, it is more logical to deal with stresses directly and although the ideas of deviatoric stresses and stress invariants were used throughout the derivation of this yield function, the result can be expressed in real stress components, without reference to these special, reduced representations.

Amici et al [38] chose the elastic-plastic approach to investigate the rolling of flat and long products using the MARC general-purpose Finite-Element programme. The model included isotropic hardening and the Von Mises yielding criteria. Results compared well to experimental rolling schedules.

Lindgren et al [39] included work roll flattening in their plane strain roll gap model by representing the circumference of the roll with a single row of elements measuring 3mm deep into the roll cross section. It was assumed that only a small fraction of the roll surface needed to be modelled as elastic deformation of the roll only affects a small fraction of the roll cross section. Residual stresses were also considered although the temperature field was assumed to be uniform. The stresses were noted to increase in proportion to the Young's modulus. This resulted in residual longitudinal stresses doubling during cooling as the Young's modulus rises from 100GPa at 1000°C 210 GPa at room temperature. The residual stresses reported in the publication were about 80 MPa at the surface of the plate and –40 MPa in the middle of the plate as an upper limit. No stress relaxation was computed for the early part of cooling.

Fukumura [40] developed an elasto-plastic Finite-Element simulation of rolling. Initially the rheology was chosen to discuss the effects of perfectly plastic material deformation with respect to rolling force results from differing rolled lengths of material. Investigation into the effects of elastic recovery and residual stress problems showed a marked effect on the rolling forces due to the material just prior to roll gap entry. This 'peening' restricts the immediate deformation of the stock in the roll gap. Roll force is also affected by the elastic recovery of the material that lengthens the arc of contact.

These effects could only have been simulated using both the elastic and plastic components of the stress/strain curve.

Boër et al [41] compared the elasto-plastic and rigid-plastic formulations for cylinder upsetting. Comparison between the numerical and experimental results showed that the elasto-plastic solution was far more sensitive to the type of element chosen and integration order selected than the rigid-plastic solution.

2.4.2.4 Elasto-Viscoplastic

All plastic deformations incur some degree of time rate effects whilst metals at high temperature exhibit both creep and viscoplastic phenomena. The former essentially a redistribution of stress and/or strains with time and the latter is a time dependant inelastic deformation [36]. Thompson and Berman [42] investigated the application of the elasto-viscoplastic material definition within an Eulerian reference frame for rolling. The work showed that whilst the numerical capability was there to analyse both the elastic and plastic contributions further work was required to identify several boundary conditions including heat transfer and friction at the roll/strip interface.

Jin [31] et al modelled the deformation that occurs in the roll bite using three different Finite-Element models. The main differences between the codes were that one used the Eulerian reference frame with visco-plastic material behaviour, whilst the other two used Lagrangian and Updated Lagrangian reference frames with visco-plastic and elasto-viscoplastic material behaviour respectively. In comparison with industrial measurements it was found that the Lagrangian and Updated Lagrangian models compared favourably to the Eulerian model. The work concludes that results between the Lagrangian models were more sensitive to the method of calculating the friction at the roll/strip interface than the actual method of computation.

Under conditions of high temperature and/or low forming speeds metals behave, as described in the previous sections, much as a viscous fluid. However, at lower temperatures and/or faster speeds the elastic behaviour begins to influence the flow further complicating any analysis [42]. Elasto-plastic and elasto-viscoplastic behaviour

are of course non-linear. Nevertheless, this method assumes that the relationship between force and displacement is piecewise linear over any small increment of time. During small total deformation analyses this strategy works extremely well but for high levels of accuracy, when the increment times need to be small, excessive computer run times can be incurred.

The Finite-Difference and Finite-Element techniques represent the current level of technology for numerical thermal and mechanical solutions. One of the major advances has been the accurate description of the metal flow, deformation dependant material properties and the mechanical interactions at the roll/strip interface. However, accurate descriptions of the mechanical and thermal boundary conditions have mostly been inversely calculated with few empirical studies for hot rolling.

2.5 Thermal Modelling

Temperature is perhaps the most important variable governing the hot deformation characteristics of metals. During metal forming processes, heat generation usually occurs. If the dies are at a considerably lower working temperature than the workpiece, heat is lost by conduction to the dies and by radiation and convection to the environment resulting in severe temperature gradients within the workpiece [43].

The original modelling techniques such as slab and slip line theorems did not calculate the temperature distribution within the material. The temperature was normally taken into account by using an appropriate average parameter. It was soon realised that assuming an average value to determine the temperature dependent variables would inevitably lead to erroneous results.

This section first describes finite difference and Finite-Element thermal modelling for metal forming processes. Advances in coupling temperature models to deformation models are then discussed. Finally each heat transfer phenomenon is discussed in some detail.

2.5.1 Thermal models

Pioneering researchers in this field reduced the complexity of industrial heat transfer within the hot strip mill by employing the following assumptions: -

1. Heat transfer in the width direction could be ignored, as temperature was uniform across the width of the strip.
2. Heat transfer in the rolling direction could be neglected, as it was insignificant compared to heat transfer by bulk motion.

Analytical approaches to solving the thermal calculations within the hot strip mill could then be based on the one-dimensional Fourier equation: -

$$\rho\, C_p \frac{\partial T}{\partial t} = \nabla(k \nabla T) + Q \qquad (2.10)$$

Where k is the conductivity of the material, T is the temperature of the strip, Q is the rate of heat generation due to plastic work, ρ is density, t is the time, C_p is the specific heat and ∇ is the gradient operator.

Hollander [44] applied the Fourier equation and developed a complete heat-transfer model for the hot rolling of steel strip including five roughing passes and six finishing stands using the finite-difference approach. Seredynski [45] attempted to estimate the temperatures during roughing and finishing for the commercial rolling of plates at Scunthorpe works, UK. He explained some of the difficulties in obtaining plant measurements and detailed some statistical models that used plant data to determine one-dimensional heat transfer coefficients. Yanagi [46] developed a finite difference algorithm to calculate the thermal evolution from furnace to the coiler on a one-dimensional transient heat flow basis. This work took account of radiation, natural and forced convection to air, boiling heat transfer to water sprays, conduction to the work rolls, heating due to deformation, heating due to friction at the roll/strip interface and water cooling on the runout table.

It can be seen that the above models assume a rather simplistic view of the total heat transfer within a hot strip mill and lack temperature-time data required for microstructural modelling. They are therefore of little use for calculating thermal aspects within the roll gap but do present the current level of understanding for heat transfer occurring at the interstand areas.

Increasing computing resources have allowed subsequent researchers to dispense with many assumptions employed by their predecessors. By considering a more complex two-dimensional condition where transportation occurs in the rolling direction in addition to that of the thickness direction, equation (2.10) becomes: -

$$\frac{\partial^2 T}{\partial X^2} + \frac{\partial^2 T}{\partial Y^2} + \frac{Q}{k} = \frac{1}{D}\frac{\partial T}{\partial t} \tag{2.11}$$

Where $\boldsymbol{D}$ is the thermal diffusivity of the material defined as a function of temperature and material grade: -

$$D = \frac{k}{\rho C_p} \tag{2.12}$$

Tseng [47] solved the thermal equations for the strip and the roll simultaneously increasing the accuracy of any predicted heat transfer occurring at the roll/strip interface. Devadas and Samarasekera [48] also used a combined strip and work roll finite difference model to further understand the interface heat transfer coefficients by investigating the effects of lubrication during strip rolling. Results showed that the interface heat transfer coefficient could vary between 50 and 200 $kWm^{-1}K^{-1}$ for water and lubricating oils respectively. The work did conclude however, that a variation in the heat transfer coefficient of 25% resulted in a 2% change in the surface temperature with the chilling penetrating to a depth of approximately $1/10^{th}$ of the thickness. Colas et al [49] added surface scale growth predictions to modify the heat transfer calculations within a two-dimensional finite difference model. The work also included natural and forced convection to air with water boiling during descaling operations. Although the

convection coefficients were not completely defined this type of modified convection coefficient model obtained accurate thermal predictions for several roughing simulations.

More recently, Pietrzyk and Lenard [50] used Finite-Element models to describe the thermal evolution during laboratory flat rolling of low carbon and aluminium samples. The interface heat transfer coefficient was specified at $50kWm^{-2}K^{-1}$ and was quoted as adequate for water cooled rolls with the numerical results comparing well to the temperature fields measured during hot rolling of slabs on a laboratory scale mill.

2.5.2 Combined Thermal-Mechanical Methods

As described above early work in this area was based on procedures that uncouple the problems of mechanical deformation and heat transfer. During metal forming a coupled deformation model with a thermal analysis will obtain a more realistic simulation of the process.

Johnson and Kudo [51] uncoupled temperature from deformation by calculating the velocity field using Finite-Element techniques prior to calculating any heat generation for extrusion. Tay et al used the technique for machining [52]. A modification of this approach was used by Altan and Kobayashi [53] for extrusion where heat generation and transportation are considered to occur instantaneously for each time step. Conduction then takes place during the time step as described by Bishop [54]. Lahoti and Atlan [55] applied this methodology to compression and torsion whilst Nagpal [56] investigated forging.

When the process becomes dependent on the thermal field and the thermal field is a function of the strain and strain rate of the stock material, realistic simulations can only be achieved by coupling the mechanical and thermal solutions. The coupling is achieved through the material constitutive relationship for the workpiece. The problem then includes through the consideration of the interface boundary condition both the thermal analysis of the workpiece and the die.

Cornfield and Johnson [27] were first to investigate the plastic flow of materials during hot rolling using the coupled thermal-displacement approach. Three different thermal profiles were investigated by including a finite difference model within the analysis to investigate temperature effects on the strain and strain rate distributions.

Lahoti et al [55] reviewed the application of finite-difference techniques to describe the thermal fields during metal forming processes. The processes included the compression of cylinders and rings, radial forging of tubes, impression die forging, temperature distributions for tubes inductively heated for end forming, metal flow in nosing of tubular products, temperature distribution in hydrostatically extruded rods and tubes, ironing of cups and deformations and temperatures during strip rolling. The slab method and the upper bound analyses were used to determine the theoretical flow patterns.

More recently Culling [57] investigated commercial hot rolling with a coupled rigid-viscoplastic Finite-Element roll gap model and a Finite-Difference temperature approximation. Although no roll flattening was allowed and the temperature of the work roll was assumed constant results did compare well to roll force measurements from a seven stand semi-continuous finishing mill.

The first attempt at a fully coupled thermomechanical Finite-Element analysis was carried out by Oden et al [58]. The work analysed the transient, non-linear, coupled thermovisco-elastoplasticity behaviour of a three-dimensional rectangular aluminium bar whilst it was constrained in one direction and heated in a corner. Hsu [59] used the Finite-Element technique for both the thermal and mechanical aspects of hot rolling because of its inherent superiority in metal flow problems with complicated geometry. His model included heat conduction to and within the work rolls, black body radiation and convection and heating due to plastic deformation and friction at the roll/strip interface.

Pietrzyk and Lenard [60] developed steady-state and non steady-state Finite-Element thermal models based on the rigid-plastic formulation for flat rolling processes. These laboratory validated thermal-mechanical Finite-Element models were used to simulate heat transfer during rolling in a seven-stand industrial strip mill.

Chen, Samarasekera, Kumar and Hawbolt [61] developed a complete heat flow and deformation model of rough rolling. Heat transfer phenomena including conduction, convection, radiation and scale growth were considered with the hot deformation behaviour calculated by the flow formulation Finite-Element model [30]. This collaborated work, perhaps represented the most complete thermal-mechanical investigation of hot rolling processes.

Bertrand et al [62] analysed the rolling process with a coupled three-dimensional steady state model for a four pass bar rolling schedule of plain carbon steel. The thermal problem was simplified by assuming steady state effects where the conduction terms were neglected in the roll gap model. However, they were included for the interstand analysis. The thermal fields were then mapped from roll gap models to the interstand thermal models and vice versa.

A visco-plastic transient, coupled thermomechanical model was also developed by Too and Barnes [63] to investigate rough rolling. Their work simulated and helped solve practical manufacturing problems such as turn up and turn down during rough rolling.

The preceding authors readily understand that most of the processing parameters and the quality of the rolled product in hot rolling are influenced by the temperature history of the material. Many fundamental heat transfer phenomena of the various cooling systems that have been employed in steel mills are still however not fully understood [64]. It is recognised that the accuracy of any numerical model is dominated by boundary conditions yet the accurate quantification of temperature in strip rolling has been hampered by the complexity of the mechanisms responsible for change in temperature. This is compounded by the difficulty in making reliable measurements on both experimental testing apparatus and operating finishing mills [65].

The development of coupled thermal and mechanical solutions where the thermal and mechanical calculations are solved simultaneously represent the current technology for numerical solution of metal forming analyses. Although coupled analyses have been carried out, realistic boundary conditions were not normally available. As a result they

were not incorporated for the heat transfer calculations. The following sections will attempt to explain the different heat transfer phenomena occurring within a hot strip-finishing mill.

In the proceeding sections, the five main components that constitute the majority of effort to determine heat transfer within hot strip rolling will be discussed individually: -

1. Heat conduction inside the work piece
2. Radiation loss to the surrounding medium
3. Heat conduction to the rolls
4. Heat losses due to water descaling jets
5. Heat gained by work done in mechanical deformation.

The scope of the published work ranges from simplified laboratory approaches with multiple assumptions to full scale commercial trials with complex numerical models giving more accurate predictions of heat transfer coefficients and their consequential effects.

2.5.3 Heat Conduction within the work piece

During rolling the strip loses heat by radiation and convection to the surroundings, by convection to water descalers and by conduction to the rolls. To calculate the temperature distribution within the strip the governing heat equation must be solved.

Employing the assumptions outlined in section 2.5.1, that heat transfer in the transverse direction can be ignored due to the width being far greater then the gauge. Heat transfer in the longitudinal direction is negligible compared to the heat transfer by bulk motion. Therefore, heat flow can be described: -

$$\frac{\partial}{\partial y}\left(k\frac{\partial T_s}{\partial y}\right)+Q=\rho\ C_p\frac{\partial T}{\partial t} \qquad (2.13)$$

where the symbols have their usual meanings. Heat conduction inside the stock material depends on the initial temperature distribution and on the thermal properties of the material. The uncertainty of thermal properties can lead to erroneous temperature predictions. Thermal conductivity generally increases from 25 to 30 $Jm^{-1}K^{-1}s^{-1}$ for steels with Carbon contents between 0.23 and 0.4% at temperatures between 900 and 1200°C [45]. Temperature gradients then become a function of time and can be solved using dimensional heat flow equations.

2.5.4 Surface Radiation

The strip loses heat by radiation and convection to the surrounding environment between descaling sprays and roll stands. In hot rolling problems no significant convection or radiation is assumed at the head, tail or the edges of the strip due to their relatively small surface areas. Early research found radiation to be the most significant heat transfer mechanism within the hot strip mill [45]. Thermal losses due to radiation can be described using the classical Stefan-Boltzmann equation: -

$$\frac{dT}{dt} = -\frac{AES}{C_p V \rho}\left(T^4 - T_a^4\right) \tag{2.14}$$

Where T and Ta are the surface and ambient temperatures respectively, A is the area of radiating surface, E the emissivity factor, S the Stefan-Boltzmann constant, C_p the specific heat of steel, ρ the density of steel and V the volume of the plate.

Yanagi [46] used various emissivities for the roughing operation with an optimum of 0.6 for the best fit of results although it was recognised that emissivity is in fact inversely proportional to temperature. Devadas and Samarasekera [48] defined the temperature dependent emissivity by: -

$$\varepsilon(T) = \frac{(T-273)}{1000}\left[0.125\frac{(T-273}{1000} - 0.38\right] + 1.1 \tag{2.15}$$

Chen et al [61] investigated the effect of oxide scale on the emissivity of the steel substrate. The accurate estimate of the emissivity was recognised and the model assigned emissivities of 0.65 and 0.8 for primary and secondary scale respectively. Although the thermal model was based on a one-dimensional transient heat flow equation by transforming the rolling direction coordinate into a time coordinate the thermal predictions compared well with measured temperatures for a nine pass commercial rolling schedule.

2.5.5 Surface Convection

Convection is the process by which heat is transferred by movement of a heated fluid. In hot rolling studies two types of convection exist: -

1. Natural convection.
2. Forced convection.

Yanagi [46] included both natural and forced convection as a function of strip speed. For roughing operations a constant 7.5 $kcalm^{-2}hr^{o}C$ was calculated from $Nu= 0.14\ (Gr.Pr)^{1/3}$ for natural convection. When the coefficient increased above 7.5 the surface heat transfer coefficient was then given by: -

$$\alpha_{FC} = \frac{\lambda_a}{L} 0.036\left(L.V/_{\omega}\right)^{0.8} \mathrm{Pr}^{1.3} \tag{2.16}$$

Where α_{FC} is the surface heat transfer coefficient for forced convection, λ_a is the thermal conductivity of air, L is a characteristic dimension given as 1.5 m in the publication, ν_a is the kinematic viscosity of air, V is the speed of the strip and Pr is the Prandtl number of air.

Lenard and Pietrzyk [60] defined convection and radiation within the same heat transfer coefficient. They calculated the transition from natural to forced convection by the ratio of the Grashof number and the square of the Reynolds number (Gr/Re^2). Free convection exists when (Gr/Re^2) >> 1 while forced convection prevails for (Gr/Re^2) << 1. The coefficient of convective heat transfer was then calculated according to: -

$$h_c = N_u \frac{k}{L} \tag{2.17}$$

Where Nu is Nusselt number dependent on the mode of convection, k is the strip conductivity and L is the characteristic length. Thermal results for a seven stand industrial strip mill compared well to measured surface temperatures.

2.5.6 Heat transfer at the Roll/Strip Interface

While a uniform temperature may exist in a homogeneous material, any junction creates a temperature difference between them. This difference depends on the mechanical and thermophysical properties of the contacting materials and overall environment of the junction [66]. Whilst many researchers now regard conduction to the rolls as one of the most significant modes of heat transfer it is undoubtedly the most difficult to measure and the most complicated to calculate [46].

In recent years, there have been significant advances in theoretical and analytical models used to predict the thermal contact resistance at an interface. Progressive experimentation and correlation with mill data has increased the understanding and knowledge of this phenomenon. Models for selected conditions and geometries have been developed and refined with remarkable success [66].

Early work in this area focussed on the heat balance equation where heat supplied to the rolls is proportional to the heat lost by the strip [45, 46]. The proportionality constant or heat-transfer coefficient then becomes a function of the temperature difference between the strip and the roll and a function of the time of contact. It can then be seen that the temperature drop due to conduction at the roll/strip interface is then proportional to the draft taken and inversely proportional to the rolling speed and rolled initial thickness of the stock.

Murata et al [67] performed laboratory experiments to determine this heat transfer coefficient by measuring the thermal response of high temperature specimens (780°C) in contact with low temperature specimens. The inversely calculated interface heat transfer values ranged from 7 to 0.5 $Wm^{-2}°C$ for 1-3 seconds contact with varying lubricants or interface chemicals shown in table 2.2. It is difficult to know how pressure affects these coefficients as no contact pressures were given.

Condition	Heat Transfer Coefficient (W/m°C)	
	No Scale	Scale @ 10μm
No lubricant	29.1	7-10.6
Water	23.3-81.4	10.6
Hot-rolling oil	200-460	5.8
Hot-rolling oil + (20%CaCO3)	69.8-175	12.8-23.3
Hot-rolling oil + (40%CaCO3)	12.79-17.4	---
KPO3	5.8	---

Table 2.2 Heat transfer coefficients for different interface conditions [67].

Yuen [68] considered the strip as a composite consisting of a steel substrate and a scale coating. The scale coating was given a conductivity of 2.5 W/m°C with the conductivity of the roll and strip at 31 and 28 W/m°C respectively. From this work it could be seen that the scale layer has a dominant effect on the heat transfer process and can reduce conduction to the rolls by as much as 50%.

Sellars [69] simulated three passes at 30% reductions at roll surface speeds of about 200mms^{-1} and used the finite difference scheme to model heat transfer during laboratory rolling of 304 stainless steel. A heat conduction coefficient of 200kW m^{-2} K^{-1} at the strip/roll interface was found to give the best results to measured thermocouple responses.

A more complex rolling schedule was investigated by Pietrzyk and Lenard [70] for low carbon steel slabs, fitted with thermocouples, at various temperatures, speeds and reductions. Coefficients at the roll/strip interface were optimised at 4800$Wm^{-2}K$ for the experimental range. It was acknowledged however, that the sampling time during the laboratory work was far too high and the sampling rate was much too low. These shortcomings effectively resulted in a coefficient that the authors recognised may be too low to account for conduction to the rolls alone.

Samarasekera [65] furthered understanding of the roll/strip interface by combining aspects of tribology and heat transfer to describe the condition between the strip and work rolls is a function of the real area of contact.

$$p = \frac{m_c ck}{\mu} \tag{2.18}$$

This difference between the apparent and the real area of contact being a function of an empirical constant (m_c) and the contact pressure (p) where (c) is the fraction between the real and apparent area of contact with material shear strength of (k) and μ is the coefficient of friction. A more detailed explanation of the mechanical interaction at the roll/strip interface is given in section 2.6.

The development of a Finite-Element model to compare experimentally derived heat transfer coefficients with the computed interface pressure, further enhanced this interdisciplinary approach of boundary lubrication and heat transfer.

Burt et al [71] investigated both the heat transfer and the friction between flat steel dies heated to different temperatures and brought together under varying pressures. Results of the measured heat conducted between the dies showed that the heat transfer coefficient did increase with increasing pressure with a maximum for dry interface conditions of 14MPa. The heat transfer was greater at all pressure levels for the lubricated conditions (see Figure 2.3.). Devadas et al [72] also performed some experimental rolling of various steels surmising that: -

1. Lubrication reduced the heat transfer coefficient from 51 $kWm^{-2}°C$ to 31 where only water was present.
2. With a higher rolling speed the heat transfer coefficient rises more rapidly but reaches the same maximum as when rolled at slower speeds.
3. The steady state heat transfer coefficient increases from 50 $kWm^{-2}°C$ to 57 $kWm^{-2}°C$ with increasing reductions of 35 and 50%. This was noted as a function of the increased rolling pressure.
4. During the first pass the interface heat transfer coefficient reaches a plateau. Subsequent passes show the increase of IHTC is linear with pressure and, for the conditions investigated, cannot be seen to reach a plateau.

Chen et al [61] included scale growth between deformations and a work roll thermal model to calculate average interfacial heat transfer coefficients of 28.2, 25.1, 36.5, 28.9, 40.4, 36.5, 48.6, 58.5 and 79.8$kWm^{-2}K^{-1}$ for a nine pass rolling schedule where the values were inversely calculated to give the best fit from mean roll force measurements [73]. The work demonstrated that the heat transfer coefficient rises to a maximum, coincident with the peak in pressure at the interface and can remain almost constant until exit.

Hlady et al [74] furthered the work by developing an equation for the interfacial heat transfer coefficients for high strength low alloy steel, stainless steel and aluminium: -

$$\frac{hC}{k} = \left(\frac{P_r}{\sigma\left(T_s, \bar{\dot{\varepsilon}}\right)} \right)^{1.7} \tag{2.19}$$

Where $\boldsymbol{h}$ is the heat transfer coefficient, $\boldsymbol{C}$ is a roughness parameter ($35E^{-6}$ for steels and $30\ E^{-6}$ for aluminium), $\boldsymbol{P}$ is the mean rolling pressure, σ is the bulk flow stress, $\boldsymbol{T_s}$ is the surface temperature, $\bar{\dot{\varepsilon}}$ is the mean strain rate, $\boldsymbol{k}$ is the combined conductivities of the roll ($\boldsymbol{k_r}$) and workpiece ($\boldsymbol{k_{wr}}$) defined as: -

$$k = \frac{k_r k_{wp}}{k_r + k_{wp}} \tag{2.20}$$

It was noted that a single definition of the heat transfer coefficient would suffice in the case of high strength steel where the asperities were not completely flattened. Due to the surface changes, the aluminium samples required a first stand and subsequent stand definitions to accurately predict the thermal evolution over multiple passes.

Li and Sellars [75] performed a comprehensive set of experiments using stainless steel samples to estimate the heat transfer as a function of thickness, pressure, reduction and evolving scale thickness. The interfacial heat transfer coefficients were then calculated using a 2-D finite difference thermal model. This work showed the importance of characterising the oxide scale layer at the interface due to its significant effect on the heat transfer [76].

Detailed investigation of the heat transfer analysis during hot forging of steel cylinders and hot rolling of slabs were combined with experimental measurements of workpiece temperatures to further evaluate the effective interfacial heat transfer coefficient for different scaling degrees and reduction/pressure conditions [77]. Investigations showed that the brittle scale is elongated and breaks during rolling which results in two contact regimes. Firstly, contact between the roll and the scale and the scale and the strip. Secondly, the roll directly onto the strip. This results in high conductance that leads to a very high effective interfacial heat transfer value for rolling compared with forging. Li and Sellars [78] also considered the effect of the deformation and the interfacial heat transfer coefficient on the kinetics of secondary scale growth. The work showed that the deformation mode of the oxide scale has a considerable influence on the mean thickness of the secondary oxide layer formed during multipass rolling. The work assumed that each descaling operation completely removed all the accumulated scale and the thermophysical properties were for F_eO only. Scale thickness varied from 180 to 360μm in their tests.

Fletcher and Beynon [79] investigated the influence of this scale layer and the effects of lubricant at the interface. They reported that the fluid pressure at the interface, between asperities, could alter the stress distribution and the immediate sub layer plasticity. Their work concluded that for high pressures the contact area ratio is decreased with the application of lubricant leading to decreased total heat transfer.

2.5.7 Water cooling

Interstand water-cooling is normally used within a finishing mill to remove and deter scale growth. The result of header geometry and flow rate is a high kinetic energy spray that impacts on the strip and removes the surface oxide. Due to the water flow and the surface temperature of the strip the reduction in temperature is due to film boiling.

While Tseng et al [80] focused on work roll cooling their work did present some data on water cooling. They concluded that a coefficient for a jet with water-head pressure between 0.3 and 0.7m was found to be 6000 $Wm^{-2}K$ directly under impingement and about 1000-2000 $Wm^{-2}K$ away from the impingement region. They also commented on the disparity between different researchers quoting heat transfer coefficients between 6.5 to 34 $kWm^{-2}°C$ for water cooling. Devedas and Samarasekera [48] took the finite difference modelling approach to spray cooling within the finishing mill. The publication states varying coefficients from 21 to 25 $kWm^{-2}K^{-1}$ while they actually used a coefficient of 19.2$kWm^{-2}K^{-1}$ for the descaler sprays.

When considering water-cooling Colas and Sellars [49] analysed the impingement zone using two separate coefficients. The first accounted for the heat transfer directly under the water curtain. Coefficients of about 17 $kWm^{-2}K^{-1}$ were used for two to three times the impingement width whereas a coefficient of 150$Wm^{-2}°C$ appeared reasonable for the area under still water. Chen et al [81] conducted experimentation of a water jet projected on to a moving plate. Although the operating temperatures were between 85 and 122°C and the effects of different velocities were not investigated, the work did further understanding with regard to how the impingement region extends in the direction of rolling. This is due to the friction between the moving surface and the water layer. Maximum heat transfer for the range of the experimentation showed heat transfer

coefficients of 95kWm^{-2}C and 59kWm^{-2}C for initial strip temperatures of 122°C (with boiling) and 85°C (without boiling) respectively.

Zumbrunnen et al [82] considered the effects of film boiling arising adjacent to a planar jet on a stationary plate. The work broke down the strip/water contact area into five different regimes each having different heat transfer characteristics: -

1. Single phase forced convection
2. Nucleate / transition boiling
3. Forced convection film boiling
4. Agglomerate pools
5. Radiation and convection to surroundings.

Further conclusions show that at temperatures above 900°C the relative velocities of the plate and water significantly influence heat transfer during film boiling whilst radiation becomes less important at higher plate velocities and can even be neglected if the plate temperatures are below 900°C.

Packo et al [83] investigated both spray cooling and quenching of low carbon steels containing 0.2% C and 2% Mn measuring 10 x 50 x 200mm and heated to 850°C. Heat transfer coefficients were derived using a Finite-Element model and thermal recordings taken from thermocouples embedded in the side of the samples. Published results indicated values of 10 kWm^{-2}K^{-1} for quenching and 6 kWm^{-2}K^{-1} and 4 kWm^{-2}K^{-1} for top and bottom sprays respectively.

The cooling characteristics of long products up to a temperature of 300°C were investigated by Horsky et al [84]. Heat transfer coefficients were then back calculated from temperature logs using a heat conduction algorithm. The general conclusion from the work showed that the peak heat transfer coefficient decreased from 50 kWm^{-2}k^{-1} to 25 kWm^{-2}k^{-1} as the relative velocities of the sample and the spray increased from 1ms^{-1} to 3ms^{-1}.

2.5.8 Heat Generation

Heat generation is caused during rolling by two phenomena. Most of the deformation energy during rolling is converted to heat due to the additional effort in excess of the energy required for homogeneous deformation. The frictional forces between the sliding metal at the roll/strip interface also cause heat to be generated at the roll strip interface.

With regard to the first of these phenomena the heat generation by plastic deformation can be described as a function of the yield stress of the stock material and the reduction within the roll pass. Seredynski [45] quoted Pavlov's formula referring to the estimation of work done on the mechanical homogeneous deformation with a uniform rise in temperature to: -

$$t_{wd} = \frac{K}{\rho C_p} \ln_e \frac{h_1}{h_2} \tag{2.21}$$

Where K is the mean yield stress, h_1 and h_2 are the entry and exit thickness. Hsu [59] suggested that 86.5% of the work for steels appeared as heat energy and could therefore be considerable during large deformation processes such as rolling.

Heating due to the friction at the strip/roll interface is the other source of heat generation during hot rolling. Although many attempts have been made to calculate the coefficient of friction there is currently no clear understanding of the extent of sliding between the rolls and the strip. Early work [3, 4, 12, 55] assumed sticking friction along the entire arc of contact resulting in zero heat generation at the roll/strip interface. Later work assumed that heat generation due to friction occurred uniformly along the length of the interface [46, 59]. Yanagi [46] surmised that some (66%) of the frictional work was converted to heat uniformly along the length of the arc of contact.

Review of the quoted publications shows that there is no consistent information on heat transfer to the rolls, water sprays or heat generation due to friction at the roll strip interface and most numerical models assume that the frictional heat is seldom, if ever, sufficient to offset the heat losses by conduction to the work rolls [85].

Calculation of the interface heat transfer coefficient has been most problematic due to the mechanical and thermal mechanisms involved. Empirical investigation of the interface heat transfer within the laboratory has returned a range of coefficients between 28W/m°C [73] to 51 W/m°C [72] depending on the initial temperatures and testing procedure. Numerical definition of this boundary condition has ranged from highly simplified approaches based on general steady state heat balance equations [45,46] to the more sophisticated Finite-Element solutions including primary and secondary scale effects [78].

2.6 Friction in Hot Metal Forming

Friction is necessary to convert the kinetic energy from the drive to the deformation energy within the strip. The shearing forces acting between the surfaces of the work rolls and strip achieve this conversion and pull the material into the roll gap. Pressures and forces generated during rolling are the subject of voluminous literature which show that friction not only effects the total roll force but also the power and torque requirements of the mill. Thus, the flat rolling process itself cannot be accurately analysed numerically unless a realistic account of the friction between the rolls and the workpiece is taken into account.

The interfaces between the work rolls and the strip are extremely complicated. The mathematical treatment of friction only becomes possible if a number of simplifying assumptions is made. Thus, calculations of friction and heat transfer are treated separately since the coupling between the heat transfer from tool to workpiece and the frictional stresses are not clearly understood or defined. Thus rolling is generally considered a problem of plane strain with sliding friction along the arc of contact except at the neutral point.

2.6.1 Engineering Friction

The engineering description of friction refers to three distinct categories. Firstly, quasi-static dry friction usually applies when two metallic surfaces are pressed slowly together and are in static equilibrium or are slowly displaced relative to one another. No penetration takes place, as the normal forces are small, although plastic deformation may

occur. The second category refers to dynamic sliding for problems that include dynamic motion, sliding, slip sticking and intermittent contact described as chattering. Frictional forces may vary with relative motions but again no penetration occurs. Thirdly wear or ploughing friction refers to cases where substantial penetration or damage occurs. There may be phase changes at the interface or portions of material may be removed [86].

Leonardo da Vinci (1452-1519) [87] discovered two basic friction laws which perhaps best fit the condition experienced during hot rolling: -

1. The friction between two solids in contact is independent of the apparent area of contact.
2. Friction and normal stress are proportional.

The most common and quantitative form of friction is the Coulomb-Amonton law of constant friction [88]. It states that the magnitude of the friction force is proportional to the magnitude of the normal force or the friction stress is proportional to the normal stress or pressure.

$$\begin{aligned} \tau &= \mu \sigma_N \\ \tau &= \mu p \end{aligned} \tag{2.22}$$

However, while Coulomb's law has the proper form suggested by simple friction experiments for non-deforming bodies, it drastically overestimates friction at high contact pressures. Experimentation has shown that friction at the interface cannot exceed the shear strength of the material, as the material can slide at this shear strength even if the interface is bound tightly. This extreme is called sticking friction and is shown as: -

$$\tau_F = \tau_{\max} \tag{2.23}$$

Where τ_{max} is the shear strength of the material alone. For a von Mises material this can be shown as: -

$$\tau_{max} = \frac{\overline{\sigma_y}}{\sqrt{3}} \tag{2.24}$$

$\overline{\sigma_y}$ is the equivalent yield stress. A modification to the sticking friction is often introduced to account for the fact that frictional forces are seldom as high as the shear strength of a material. In high pressure, contact regimes they are only weakly dependent on pressure. This generalisation may be written as: -

$$\tau_F = m\tau_{max} \tag{2.25}$$

m is known as the friction factor and is required as input in most finite element programs involving friction. Wanheim and Bay [89] suggested a new friction model that combined the two friction laws: -

$$\tau = f\alpha k \tag{2.26}$$

Where ***f*** is the friction factor and α is the ratio between the real and apparent area of contact. In practical terms the model assumes friction to be proportional to the normal stresses at low pressures, but tending towards a constant value at high normal pressure. This work showed that at low pressures a rough surface results in the real contact area being proportional to the low pressures, which therefore confirmed Amonton's law (see Equation 2.2), whilst at high normal pressures α approaches, but never reaches unity where the law of constant friction is valid.

2.6.2 Experimentation

Two of the most quoted tests for estimating friction in hot metal forming are the ring and the spike tests. Both tests incorporate the notion of reversed slip directions analogous to rolling. An alternative for the estimating of friction factors within hot rolling is the compression of small cylinders etched with grids. More recent investigations take friction measurements from laboratory rolling apparatus or directly from commercial mills. These types of experimental studies of friction are scarce, therefore making direct

comparisons difficult. Only the most recent and relevant publications are included here as more comprehensive friction reviews are provided elsewhere [90].

Munther and Lenard [91] performed comprehensive laboratory rolling on mild Carbon steel and high strength low alloy steel where the coefficients were back calculated using the commercial Finite-Element code, Elroll. Results confirmed the suggestions by Ekelund [92] where: -

1. The coefficient of friction increases as temperature decreases.
2. Increasing velocity decreases the coefficient of friction.
3. Greater reduction increases the coefficient of friction.
4. Thicker scale reduces the friction as it provides a certain degree of lubrication.

They described the change in the coefficient of friction by two phenomena. The first concerns the adhesive bonds that form between the sample and the rolls upon contact, which are harder to separate as the temperature decreases. The required shear stresses increase, thereby increasing the frictional forces. Furthermore the material's flow stress augments with decreasing temperature as a result of the strengthening mechanisms, described earlier. The asperities on the surface become harder to deform, resulting in an increased friction. The greater the velocity the less time there is available to form adhesive bonds. The greater the reduction the longer the contact times and the greater the contact pressure.

Rudkins et al [93] conducted dry ring compression tests on a low Carbon steel and a lead free cutting steel at various temperatures and reduction patterns analogous to those experienced in commercial finishing rolling. Results showed that increasing the temperature from 800 to 1000°C increased the friction factor for both materials from 0.75 to 0.9.

Forward slip measurements were made by Li, Beynon and Sellars [94] to determine friction coefficients during laboratory rolling of plain carbon steel at temperatures between 900, 1000 and 1100°C at constant roll speed. From the work they concluded that whilst forward and backward slips are always present the neutral angles derived from

backward slip are significantly larger than those derived from forward slip. This suggests a neutral zone, instead of a neutral plane in the roll gap. From the simplified numerical analysis of the friction, resulting coefficients were very close to sticking friction. According to the von Mises yield criterion, the maximum coefficient of friction is 0.577. The work does accept the need for more detailed analyses of the friction coefficients by the Finite-Element method including the detailed distribution of contact pressure.

2.6.3 Modelling Friction

Early theorists assumed sticking friction to act over the entire arc of contact [4,7,8]. More recently Finite-Element models have been applied to derive friction coefficients. In general Finite-Element models take a simplified vision of friction where the dynamic effects are neglected due to the relatively small contact times.

Chun [95] presented a comprehensive review of the subject describing several approaches by researchers in this field. Starting with the simplest where interfacial frictional stress can be represented by a nodal force or surface shear stress within the Finite-Element program. The second approach described the introduction of a thin layer of interface elements with yield strength assumed to depend on the product of the coefficient of friction and the mean stress. The third approach described by Chun [95] was to consider the boundary as a nodal force and velocity constraint problem, taking account of slipping and sticking from Coulomb's model.

Chen and Kobayashi [19] developed an arc tangent velocity function to deal with the plane strain rigid-plastic Finite-Element simulation of rolling. Chun [95] developed a friction model that combined the conventional Amanton law with an exponential velocity dependent expression. This work notably accounted for the effect of the sticking zone rather than a point of sticking friction. The work concluded that the combined models of Wanheim and Bay [96] and the exponential velocity dependent expressions are numerically suitable for rolling.

Empirical studies of friction in hot rolling are significantly less numerous than in cold rolling due to the added complexities of temperature dependent material properties and

oxide layers at the interface. There also seems to be no collective decision on a dependable testing technique that does not have some form of limitation with regard to its applicability to hot rolling. Numerical description of friction has not been made without some uncertainty in either its application or theory with perhaps the maximum shear stress law [89] lending itself more to metal forming applications than earlier theories [88]. All but the very simplest theories now recognise that one of the most important controlling factors during rolling, besides the yield properties of the rolled material and the geometry of the roll pass, is friction.

2.7 Material Considerations

2.7.1 Introduction

An ideal analysis of any metal forming process will include a detailed description of the elastic and inelastic material behaviour. This material module within all Finite-Element programmes contains the constitutive equation, which designates the inelastic, non-linear, rate dependent behaviour of metals and their alloys. These flow stress predictions can then be employed to calculate the resistance to hot deformation and therefore the loads and power requirements.

It is now also possible to take the results from Finite-Element calculations with constitutive relationships based on plasticity and include microstructural effects due to the processing parameters. Quantitative descriptions of these material models are required principally for two purposes. Firstly, to enable predictions of the flow behaviour of the material during working and secondly to further understanding and optimisation of the mechanical properties of the material. Such calculations show how advances are being made in linking numerical techniques together to simulate entire processes. This focus on the application of mathematical models to predict material properties is key to meeting the era of heightened environmental awareness and competitive drive to enhance material quality [97].

This chapter is not designed to deliver the history of the theory of plasticity. Its aim is to aid the reader, who is perhaps unfamiliar with Finite-Element modelling and deliver a basic description of the concepts involved when considering material modelling of metal forming processes. A review of recent Finite-Element metal forming analyses reveals that the determination of a material's behaviour with plasticity and creep constitutive descriptions is frequently the oldest part of any stress analysis.

2.7.2 Modelling Dynamic Effects

Dynamic effects are those microstructural changes, which occur during the deformation. During uninterrupted straining of metals at constant strain rate, stress/strain curves exhibit several generic components. These are commonly termed: -

- Elastic deformation
- Yield stress
- Work hardening
- Maximum stress
- Dynamic recovery and/or recrystallisation

An elastic stage followed by a work hardening stage and finally a softening stage [98] (see Figure 2.4). The elastic region is considered linear up to the yield stress. Modelling elastic behaviour is relatively simple, as the only requirements are the elastic modulus and Poisson's ratio. Koster [99] carried out the first study of the temperature dependent elastic modulus. Here it can be seen that whilst elasticity is temperature dependent, strain rate and chemical composition effects can be neglected.

As the dislocation density rises, metals begin to work harden. Due to the considerable ease of self-diffusion at high temperatures, dynamic recovery processes are active as soon as dislocations appear during plastic deformation. This softening process reduces the rate of work hardening until a maximum or peak stress is reached. At this point work hardening is in equilibrium with the softening process. This peak stress occurs after some low fraction of recrystallisation has taken place. Therefore, the strain at peak stress is always greater than the critical strain to cause the onset of the dynamic softening processes.

The predominant microstructural feature of dynamically recovering metals is a well-defined sub grain structure [100]. As the strain increases from the strain at which maximum stress occurred the flow stress could either maintain the maximum stress or decrease due to the softening mechanisms. Various types of intragranular substructures exist in dynamically recrystallised grains at strains beyond the steady state strain, which correspond to the various stages of the restoration process. During dynamic recrystallisation nucleation as well as grain growth (grain boundary migration) take place. Flow curves of materials that exhibit dynamic recrystallisation can be cyclic or single peak [101] (See Figure 2.4b).

The constant evolution of the austenite structure during deformation means the stress-strain behaviour can be described using empirically derived equations where the flow stress is described as a function of strain ε, strain rate $\dot{\varepsilon}$, temperature T and austenite structure S_t [102]: -

$$\sigma = f\left(\varepsilon, \dot{\varepsilon}, T, S_t\right) \tag{2.27}$$

2.7.3 Flow Stress, Strain Rate and Temperature Effects

Softening due to diffusion processes counteracts the hardening and depends heavily on temperature. One way to define this influence is to take a ratio of the operating temperature over the melting temperature of the material measured in °K.

When the material temperature is < 0.4 T_m the dislocation interactions dominate the diffusion. Therefore recovery is small and the modulus is usually positive. This region is normally termed 'cold working' of metals during forming processes. Between 0.6 T_m and 0.4, diffusion competes with the hardening effects as in cold forming where several factors dictate which mechanism prevails over the other. A balance can be reached where hardening and softening are equal such as the state of creep where a constant strain-rate can be observed. The tangent modulus is normally positive and this region is normally termed 'warm working'. Where the stock temperature is greater than 0.6 T_m the diffusion-controlled recovery is dominant and very little hardening is observed. This region of 'hot working' is where the majority of metals and their alloys are formed.

Sellars et al [98] accounted for strain rate and temperature effects on the flow stress by the power law when the temperatures are high and the stresses are low: -

$$\dot{\varepsilon} = A'(\alpha\sigma)^n \exp\left(\frac{-Q}{RT}\right) \tag{2.28}$$

Where A, α and n are material dependant constants. However, when the stresses are high the equation takes the exponential form: -

$$\dot{\varepsilon} = A'' \exp\left(\beta\sigma - \frac{Q}{RT}\right) \tag{2.29}$$

Where $\beta = \alpha\sigma$. From the hyperbolic sine law and various experimentations it can be observed that decreasing temperature and increasing strain rate increases flow stress.

2.7.4 Flow Stress and Strain Effects

The hyperbolic sine law predicts a particular stress at a particular temperature and strain rate. In order to complete a material module, changes of stress with strain must be taken into account. The method used to model the stress-strain curve in the work-hardening region is based on the analysis of experimental data using Avrami type laws without the use of a critical strain [103]. Therefore at lower strains a rate dependent constant and a hardening exponent can describe a satisfactory relationship. Laasraoui et al [104] took account of the decrease in work hardening to steady state by calculating peak stress from the hyperbolic sine law to give: -

$$\sigma = C\sigma_p \varepsilon^n \tag{2.30}$$

Where C is a material dependant constant, σ_p is the peak stress and n is the hardening exponent. Such equations are rather simplistic and as such can be erroneous. Due to the increase in computing power more complex curve fitting procedures have been employed. Anderson and Evans [105] successfully modelled the dynamic behaviour of two commercial low Carbon steels using the theory of the hyperbolic sine law rearranged to yield flow stress in terms of strain rate and temperature: -

$$\sigma = \frac{1}{\alpha}\sinh^{-1}\left(\left\{\frac{\dot{\varepsilon}}{A} EXP\left(\frac{Q}{RT}\right)\right\}^{\frac{1}{n}}\right) \tag{2.31}$$

The constants were derived from axisymmetric testing at temperatures between 1123 and 1372 °K, total strain of 50% and strain rates up to $40s^{-1}$.

Later Anderson [106] modelled the complete stress/strain curves for varying temperatures and strain rates by calculating three critical stresses using the hyperbolic sine law: -

1. Yield stress
2. Peak stress
3. Stress at large strain

The strain at which peak stress occurred was described by: -

$$\varepsilon_p = A' \dot{\varepsilon}^{n'} EXP\left[\frac{Q_p}{RT}\right] \tag{2.32}$$

Complete stress/strain curves were then calculated by interpolating between these three points using binomial and linear curves (see Figure 2.5).

2.7.5 Multipass Modelling

Including static phenomena

After deformation at high temperature and high strain rates the resulting microstructures are unstable, and upon holding at temperature at the end of deformation, will undergo further structural changes by static recovery, recrystallisation, metadynamic recrystallisation and grain growth [102]. If any comprehensive numerical model is to be developed for metal deformation processes that involve multiple deformations with intervals between, such as those experienced within a semi-continuous finishing mill, static effects upon the microstructure must be taken into account.

Post dynamic recovery and/or recrystallisation is followed by a combination of static recrystallisation and metadynamic recrystallisation depending on the deformation conditions (see Figure 2.6). The latter mechanism differs from static recrystallisation in a

number of significant ways. The first relates to the kinetics. The rate of metadynamic recrystallisation is sensitive to the strain and the temperature. Conversely, the rate of conventional recrystallisation depends on the initial strain and temperature, but only slightly on the strain rate [101].

On holding a deformed structure at temperature, softening is calculated as a function of time and the rate for 50% recrystallisation with the Avrami equation: -

$$X = 1 - EXP\left(-C\left(\frac{t}{t_F}\right)^k\right) \tag{2.33}$$

Where X is the fraction recrystallised or softened in time t after deformation, k is an a material dependent exponent, t is the time to some fraction softened F, and C = -ln (1-F).

Sellars and Tegart [98] discussed the complicated interactions between dynamic and static softening processes under interrupted, non-isothermal deformation conditions. The consideration of deformation conditions and grain growth was increased by the work of Sellars and Whiteman [107] where the static recrystallisation was considered as a function of time. The time to 95% recrystallisation, $t_{0.95}$, can be expressed as: -

$$t_{0.95} = A' Z^{-3/8} \varepsilon^{-4} d_0^2 \exp\left(\frac{Q_{rex}}{RT}\right) \qquad (\varepsilon < \varepsilon_c) \tag{2.34}$$

Values for the constants A' and Q_{rex} were determined from hot compression experiments where Z is the Zener-Hollomon parameter , d_o is the original grain size, Q_{rex} is the recrystallisation energy, R is the gas molar constant and T is the temperature. The recrystallised grain size was then expressed as: -

$$d_{rex} = A''\left(\frac{1}{\beta}\ln\frac{Z}{A}\right)^{-\frac{2}{3}} \varepsilon^{-1} d_0^{\frac{1}{2}} \qquad (\varepsilon < \varepsilon_c) \tag{2.35}$$

Where the strain, ε, is described for plane strain conditions in rolling converted to equivalent strain using the von Mises relationship: -

$$\varepsilon = \frac{1.155V}{\left(R\left(h_o - h_f\right)\right)^{\frac{1}{2}}} \ln \frac{h_o}{h_f} \tag{2.36}$$

Where h_o and h_f are the plate thickness before and after a pass. R is the roll radius in metres and V is the peripheral roll speed measured in ms^{-1}. Once recrystallisation is complete or has reached 95%, further grain growth takes place as a function of time and temperature and was found by: -

$$d^{10} = d_o^{10} + A'''t\exp-\left(\frac{Q_{gg}}{RT}\right) \tag{2.37}$$

Where the values of Q_{gg} and the constant A''' are determined experimentally through metallographic techniques.

The measurement of dynamic and static recrystallisation and recovery kinetics by metallographic studies is very time consuming. Alternative solutions include the analysis of experimental stress-strain curves by assuming the equivalence between the softening and the recrystallisation kinetics that imposes that the softened fraction at entry to the mechanical steady state domain is close to 100% [103].

The investigation of these restoration processes in austenite with the aim of relating them to the rolling mill performance has been carried out by Djaic and Jonas [108]. The work employed double hit compression testing to a total strain of 0.8 of three hypo-eutectoid steels. In order to determine the value of the field stress, an offset method, with a strain offset of 0.001 to a strain rate of $1s^{-1}$ was employed (see Figure 2.7). The drop in yield stress on restraining was taken as a measure of the progress of static softening according to: -

$$X = \left[\frac{1-(\sigma_2 - \sigma_1)}{(\sigma_m - \sigma_1)}\right] \times 100 \tag{2.38}$$

Here X represents the fraction softened, σ_2 the yield stress on restraining, σ_1 the initial yield stress and σ_m the flow stress immediately before unloading. Their work also showed that the mechanisms for static softening were dependent upon the magnitude of strain, temperature and chemical composition of the steel.

Further work by Sun and Hawbolt [109] concentrated on calculations for the onset of static recrystallisation. This work showed that the static recovery does not have an incubation time. As a result, nuclei of the new grains, which are relatively free from dislocations, are formed in the deformed matrix. During subsequent static recrystallisation these nuclei grow and thus the material is further softened. It is this which dictates that it is static rather than dynamic or metadynamic recrystallisation that plays the dominant role in the softening process during finishing rolling of plain Carbon steel strips because of the high strain rates involved.

Grain growth occurring after static softening was investigated for plain Carbon steel within the temperature range of 900 to 1150°C by Militzer et al [110]. Investigation into grain growth within an A36 stainless steel depended strongly on the pre-heated microstructure. The general applicability of the grain growth model was subject to some scepticism.

A complete analysis of modelling austenite grain refinement and grain growth was also carried out for plain Carbon steels by Sun et al [111]. The work demonstrated the final austenite microstructure was mainly determined by the recrystallised grain size that can be linked to mill processing parameters, such as the applied strain, strain rate and temperature. The recrystallised grain size was shown to increase with either initial grain size or deformation temperature or decrease with applied strain.

Medina [112] calculated the static recrystallisation kinetics with respect to the chemical composition. Each element within plain Carbon and High Strength Low Alloy steels, in the most usual percentages, except Carbon, tend to increase the activation energy and

therefore delay the recrystallisation kinetics. Results showed correlations for the elements: -

$$Q(Jmol^{-1}) = 124714 + 28385.68[Mn] + 64716.68[Si] + 72775.4[Mo] + 76830.32[Ti]^{0.213} + 121100.37[Nb]^{0.1} \quad (2.39)$$

Where each square bracket indicates the percentage by weight of the element indicated. From further examination of the softening constants included within equations 1.34 and 1.35 it can be shown the static softening kinetics have the following dependencies: -

- Initial grain size only has a slight influence
- Exponent ***n*** within the Avrami equation diminishes with temperature
- Strain rate has less influence than strain, initial grain size and temperature.

Grain growth was included in the work by Colas et al [113]. The most important mechanism controlling Austenitic grain refinement was shown to be grain growth that occurs when the interpass durations are large enough to accomplish full recrystallisation. As the roll gap was modelled assuming uniform deformation, heterogeneity of the computed grain growth was purely a function of temperature and not deformation conditions. Bianchi and Petrone [114] have implemented static softening algorithms into their elasto-plastic and elasto-viscoplastic rolling Finite-Element models using the commercial code MARC. Their simulations compared reasonably well to laboratory rolling schedules of 100mm x 200mm wide samples processed at 1200°C with a roll of 0.47m diameter rotating at a constant angular speed of 2.68 s^{-1}. Although non-complete softening was calculated for the latter passes no accumulated strain was included within the model.

The effect of through-thickness strain distribution on the static recrystallisation of hot rolled austenitic steel strip was investigated by Zhang et al. [115]. Conclusions through the use of Finite-Element modelling included that the accumulated strain is dependent only on the amount of straining and not the strain path.

Pietrzyk et al [116] coupled a thermal-mechanical Finite-Element model of the hot rolling process with the closed form equations describing recrystallisation and grain growth phenomena. The approach assumes that the recrystallisation time can be determined by adding partial times calculated for the temperatures. Grain sizes were also calculated and compared well to commercial rolling schedules of 2mm gauge low Carbon strip.

The change of a material's internal structure by dislocation movement, generation and annihilation changes its internal structure. Thus, materials with the same chemical composition through deformation may exhibit different thermomechanical properties. This is taken account in modelling terms by calculating any accumulated strain resulting from incomplete restoration during the interstand periods (see Figure 2.8). Anderson [106] quoted the effective strain technique was appropriate for a number of steels: -

$$\varepsilon_{eff} = \varepsilon_n + \lambda\left(1 - X_{n^{-1}}\right)\varepsilon_n \tag{2.40}$$

Where ε_n is the strain by pass n and X is the fractional softening from the previous pass n^{-1} where λ is unity for C-Mn and low carbon steels.

2.7.6 Experimental Techniques

In order to obtain the necessary stress/strain curves to determine various material characteristics various methods of deformation have been devised. The most frequent quoted techniques within the literature are tensile, axisymmetric, plane strain compression, torsion and laboratory rolling techniques. Each method has its inherent strengths and limitations. Problems have arisen in all these techniques where experimental strain rates cannot achieve those experienced within a commercial hot finishing mill. In order to apply laboratory data constitutive methods are employed to extrapolate the data to those conditions experienced during rolling.

Different methods of testing will produce various values for the yield stress. The yield stress obtained by uniaxial compression tests will (apart from small effects associated with the Bauschinger effect) be numerically the same as that obtained in tension.

However if deformation is conducted by means of the torsion test and the resulting shear stress is plotted against shear strain, the end of elastic deformation occurs at the shear stress limit known as the yield stress in shear k_y. Most notably the Bauschinger effect loses significance when the strain paths are nearly proportional, as they are for many forming operations such as rolling.

Dunstan [117] and Evans [118] investigated both the axisymmetric and the plane strain compression apparatus (see Figure 2.9) to describe the dynamic behaviour of metals at varying temperatures and strain rates. This has enabled quantitative relationships that give satisfactory description of the structural changes. However if large strains are required torsion testing is normally preferred due to the lack of frictional problems.

Heating of the sample for hot deformation studies is usually achieved through a resistive heating furnace. Hot deformation studies carried out by Anderson and Evans [105] showed that during axisymmetric compression temperature non-uniformities within a test piece 6mm in diameter and 8mm in length can be ignored. Analysis of each testing procedure has found that for reductions of around 50% true strain, uniaxial compression appears to give the most consistent results in perhaps the simplest manner [106]

2.8 Summary

Rolling has been the subject of numerical analysis since the first part of the 20th Century. These numerical methods began with the Slab technique incorporating several simplifying assumptions. The Slab method can estimate rolling loads, torques and roll pressures but is now rarely applied to the hot rolling process due to the techniques inability to calculate how the material flows during deformation and the failure to consider temperature evolution within the roll gap.

The first 'field' type solution of rolling was conceived with the Slip-Line technique. This technique provided the first clarification of the heterogeneous deformation in the roll gap and offered some insight into the definition of the neutral plane during rolling. Limitations of this technique dictated that the material could only be considered perfectly plastic with a constant yield stress and neglects any temperature effects. Sticking friction was also assumed along the entire roll/strip interface for rolling analyses. Due to the laborious nature of this method evidence of its application to strip rolling have been rare.

Advances in computer software and hardware have enabled more complex numerical methods to be developed. The Finite Difference and Finite-Element techniques discard many of the assumptions required by the above 'traditional' techniques. The user can now define any material rheology and the roll/strip interface can be accurately described with both sliding and sticking friction conditions along the arc of contact. Moreover, geometry within the roll gap no longer imposes any limitations on the numerical solution with these techniques. The Finite-Element technique represents the current level of technology for metal forming analyses and provides detailed solutions of strains, strain rates, stresses and temperatures during the deformation.

Accurate prediction of the strip temperature is now regarded as essential during the analysis of hot forming processes. Whereas the classical techniques required constant temperature during deformation, it is now recognised that the rolling power for modern hot strip finishing mills can only be determined with the accurate calculation of temperature during the deformation phase.

From the previous chapter it can be seen that thermal aspects can be calculated with both the Finite Difference and the Finite-Element techniques. However, the latest development in hot deformation process modelling has been where the displacements and the thermal calculations are processed simultaneously. With this methodology the rolling process can now be simulated with non-linear, process dependent thermal boundary conditions. Unfortunately, studies of hot rolling using these latest techniques are still not commonplace due to the difficulties incurred when characterising the thermal and mechanical boundary conditions within a commercial hot strip-finishing mill.

Several research groups have investigated the thermal boundary conditions in the laboratory using rolling equipment and compression apparatus analogous to rolling. Whilst there does not seem to be any exact solution to the heat transfer phenomena occurring within hot strip finishing mills, many researchers have derived heat transfer coefficients that satisfy the thermal aspects of the finishing mill by employing the Finite-Element and Finite Difference models.

The mechanical boundaries are dominated by the friction between the rolls and the strip. Friction is widely accepted as one of the most difficult variables to investigate and numerically define within any hot rolling analysis. The two most common friction theories are the Coulomb-Amonton constant friction law and the friction law of maximum shear. In hot rolling, where the contact pressures high, only a maximum shear stress friction model can account for friction at the interface.

The fact that estimations of friction at the roll/strip interface have significant effects on the roll force and to a greater extent on the torque results has provided the motivation to investigate friction through experimentation. There are several techniques available for the determination of friction coefficients although each technique is only applicable to a limited number of conditions. Each contact situation is different and detailed knowledge of the contact condition and the material properties have proven to be essential.

Detailed description of the hot deformation characteristics for each grade of material is required for the flow stress calculations during hot strip rolling. The hyperbolic sine equation can provide accurate description of the flow stress development during

uninterrupted straining for carbon steels. Dynamic recrystallisation further complicates flow stress models but it has been shown that calculations, which include the strain at peak stress, can account for this phenomenon. Dynamic softening events have been shown to be more difficult to predict and there seems to be some uncertainty regarding whether or not materials dynamically recrystallised at strains greater than 50%.

Any complete model of a semi-continuous process should include the static microstructural effects. With respect to roll-gap models, detailed description of the material behaviour after the deformation phase should be defined and included within any simulation of commercial hot strip finishing mills. These static-softening processes may be studied by the changes in flow stress during a second deformation given after different holding times and temperatures.

Understanding roll-gap deformation is important because it facilitates a measure of control over the rolling process. From the literature it can be seen that whilst the roll gap has been extensively researched there is a distinct lack of understanding concerning the interstand areas including the thermal and microstructural effects. Review of microstructural understanding at the interstand areas has shown that the phenomenon of static recrystallisation has rarely been considered in any general roll-gap analysis. This is regarded as an area for significant research as it will contribute significantly to any rolling simulation.

It can now be said that the theoretical investigation of commercial hot rolling has consumed multiple disciplines from numerical, metallurgical, topological and thermal faculties and has therefore truly become a multidisciplinary subject of research.

In conclusion the literature has shown there is a need to develop coupled temperature-displacement Finite-Element models and to combine them with metallurgical algorithms to complete thermal-mechanical simulations of commercial semi-continuous hot finishing rolling.

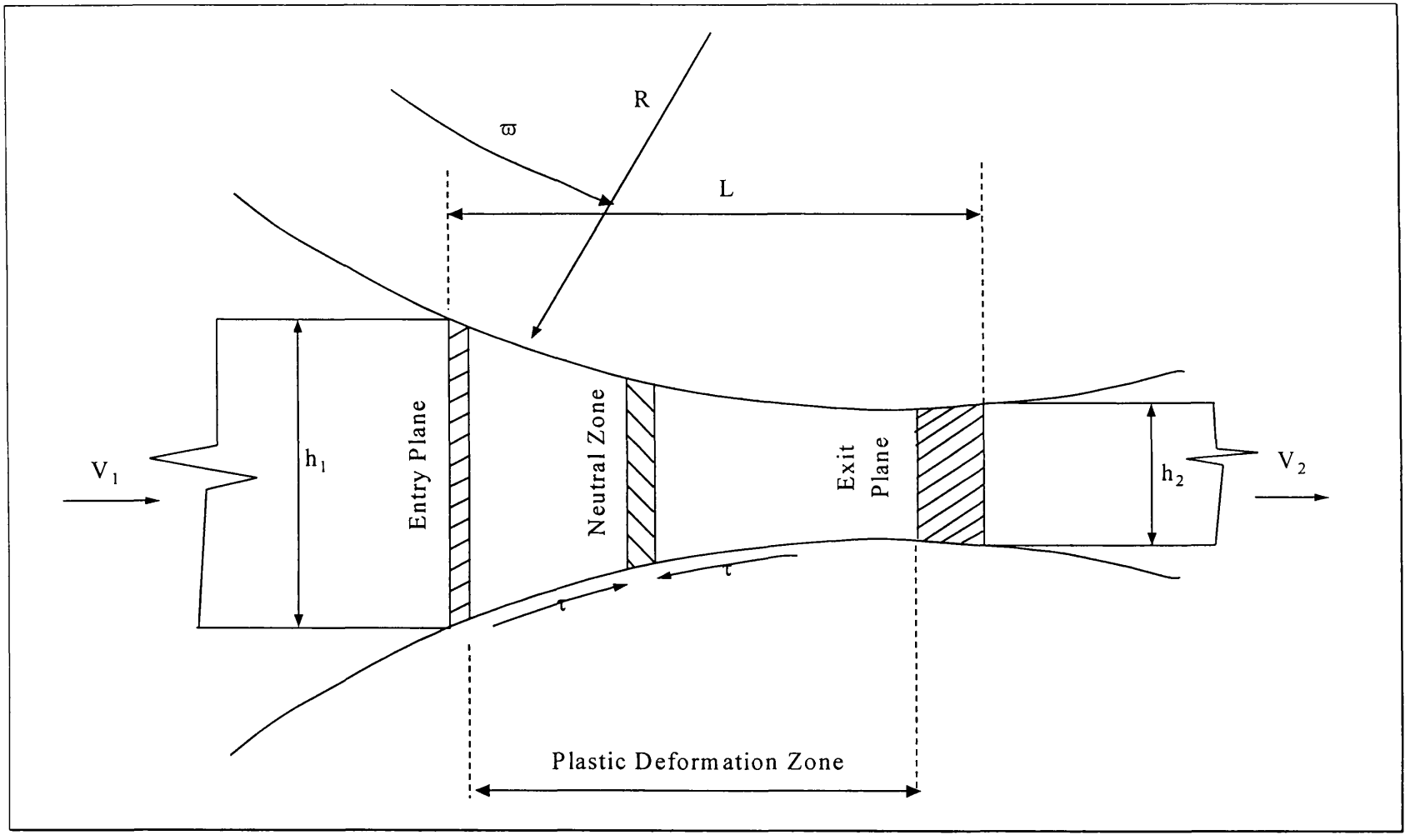

Figure 2.1 Roll Gap Geometry

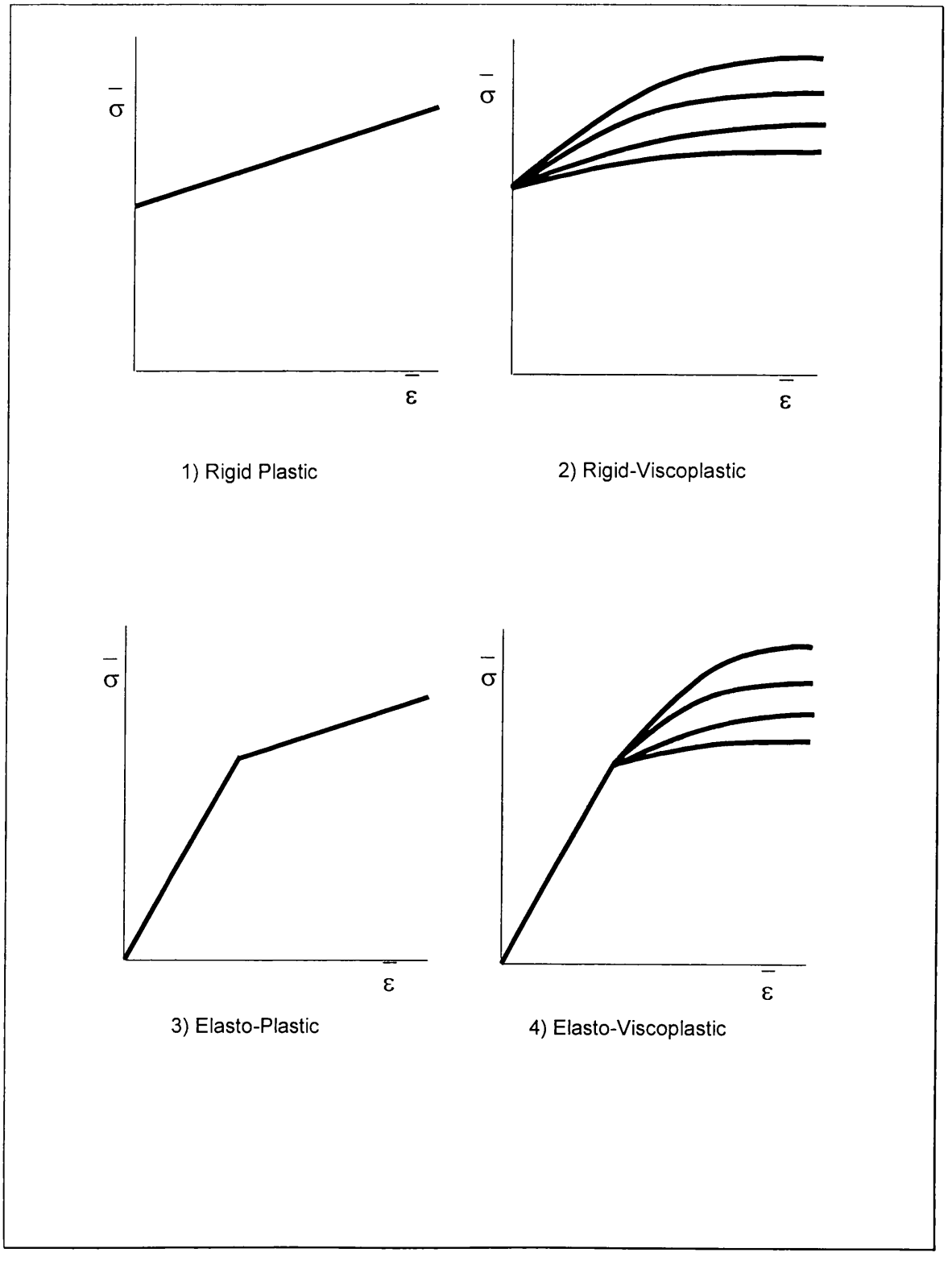

Figure 2.2 Different Types of Material Rheology

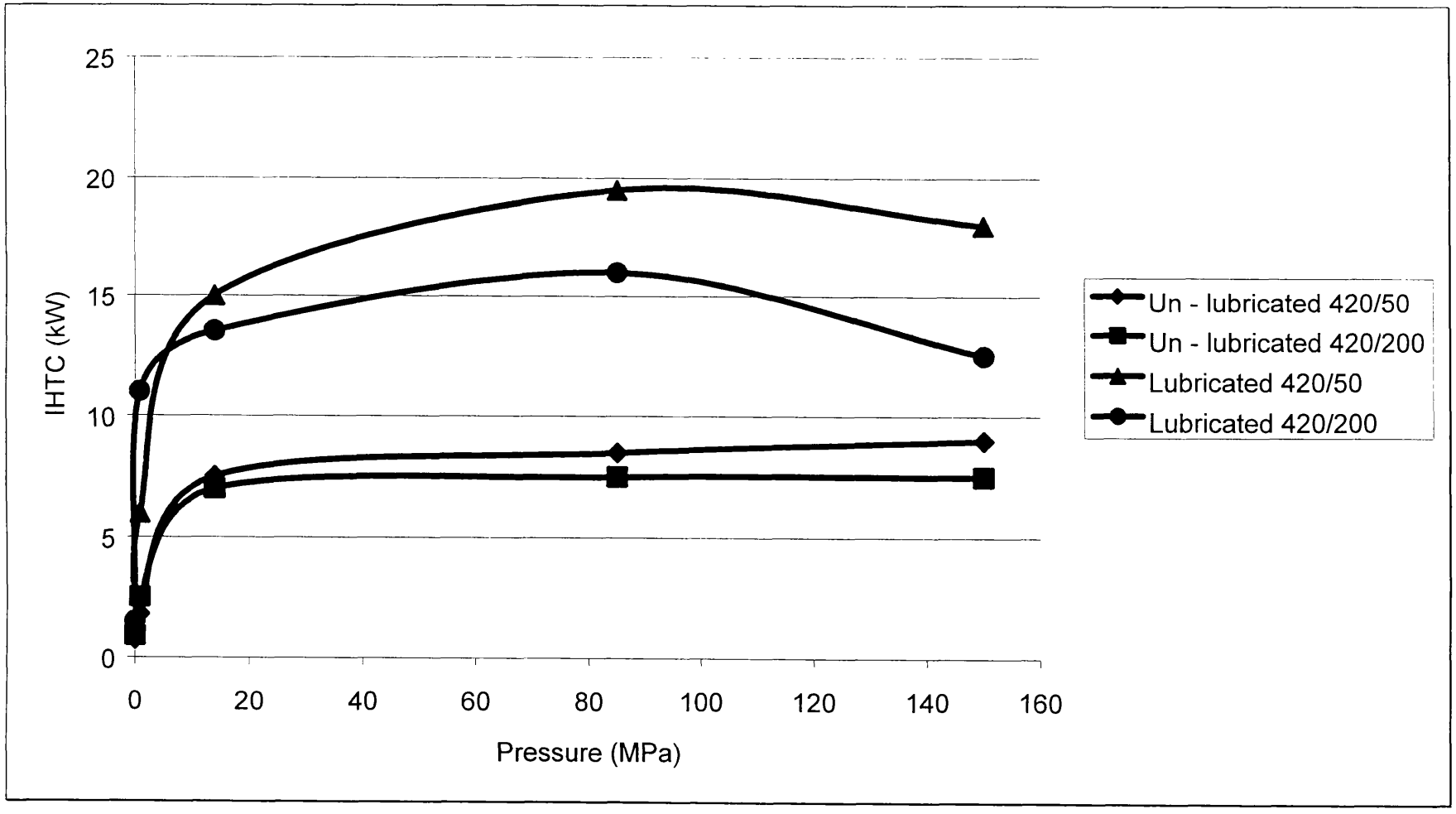

Figure 2.3 Pressure Dependent Conductance [71]

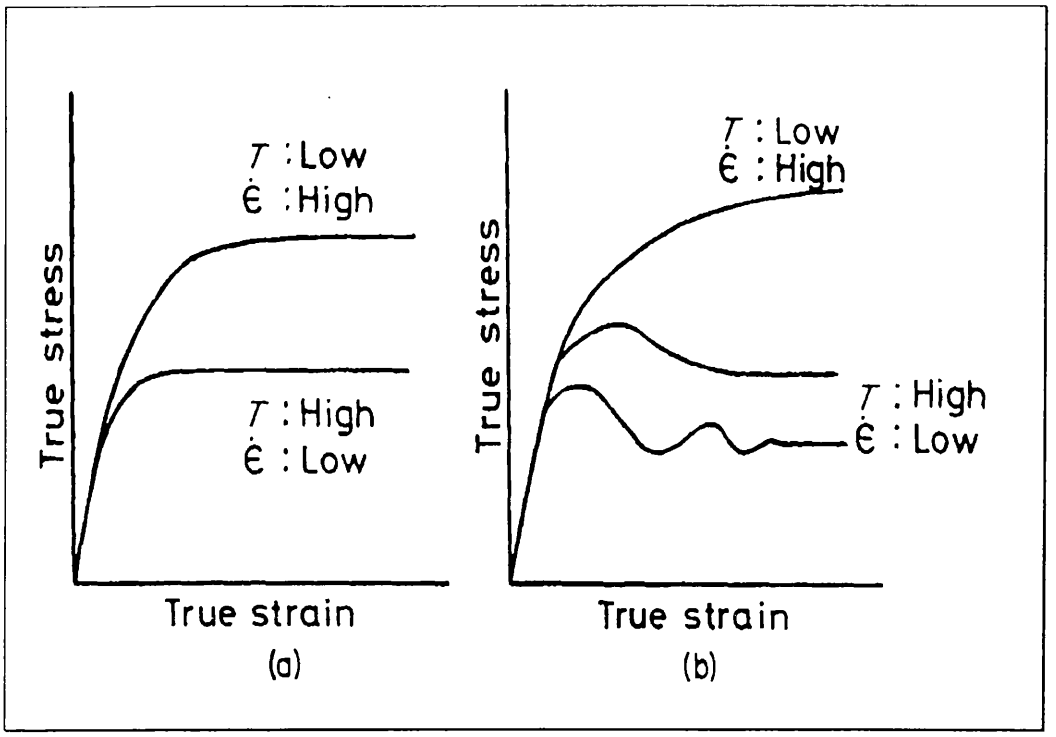

Figure 2.4 Schematic Representations of Stress/Strain Curves for Dynamic restoration Processes : a) Dynamic recovery; b) Dynamic Recrystallisation

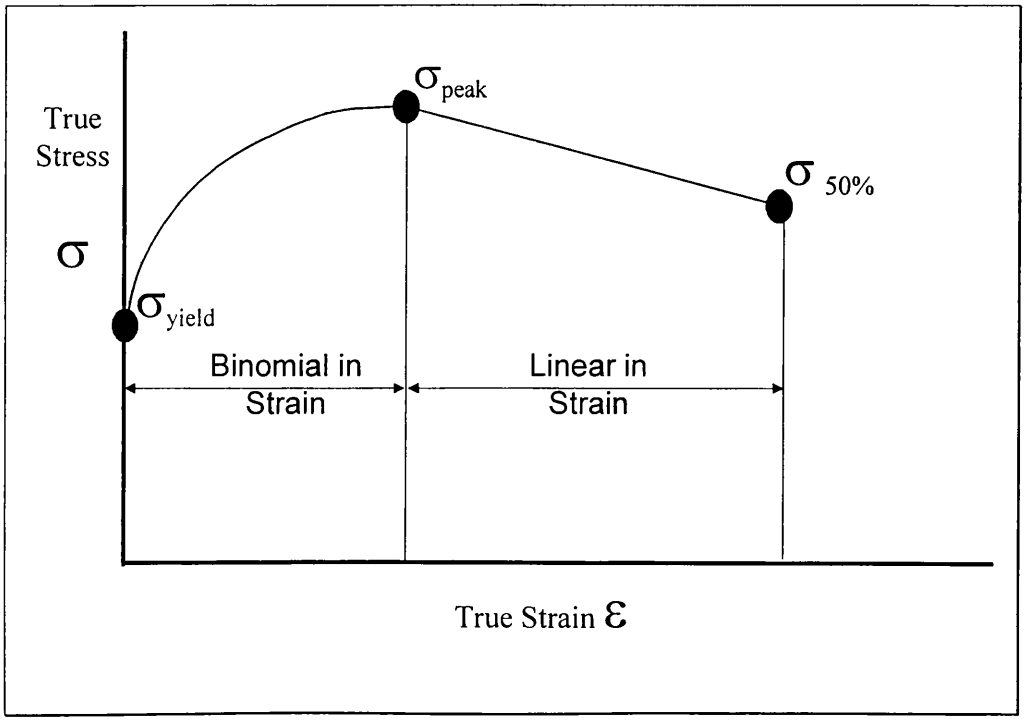

Figure 2.5 Modelling Flow Stress with Strain by Numerical Methods [106]

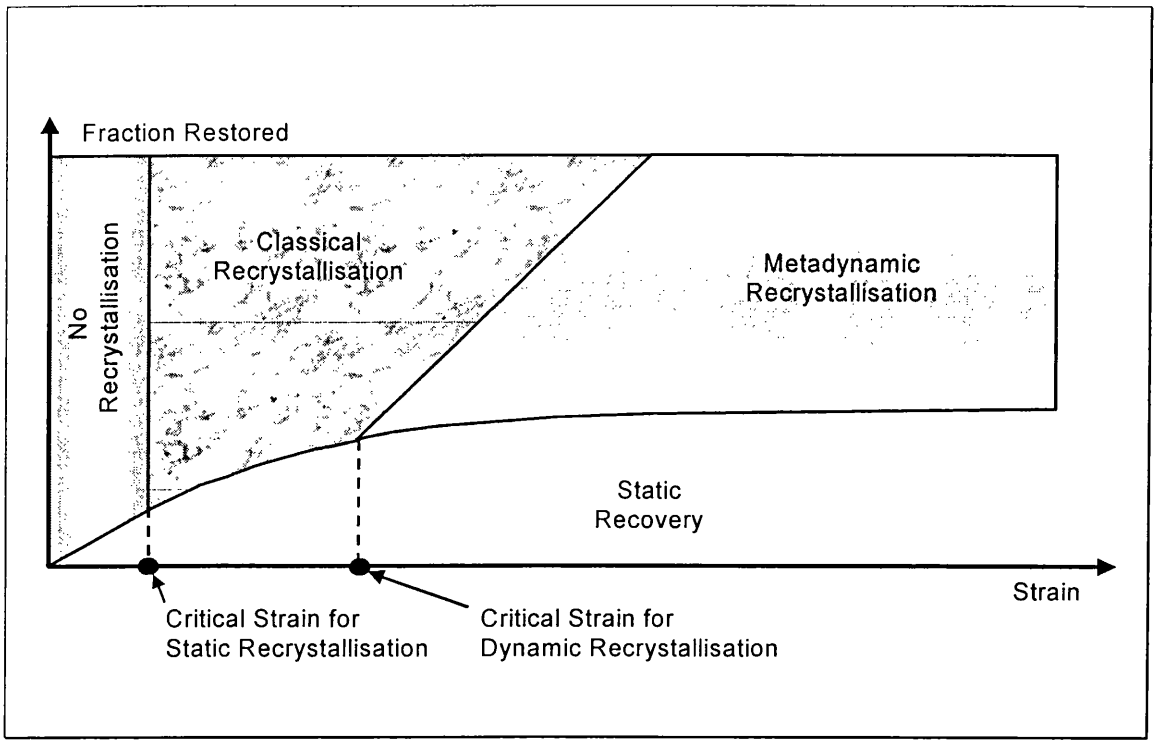

Figure 2.6 Schematic Illustration of Softening Phenomena Attributed to Restoration

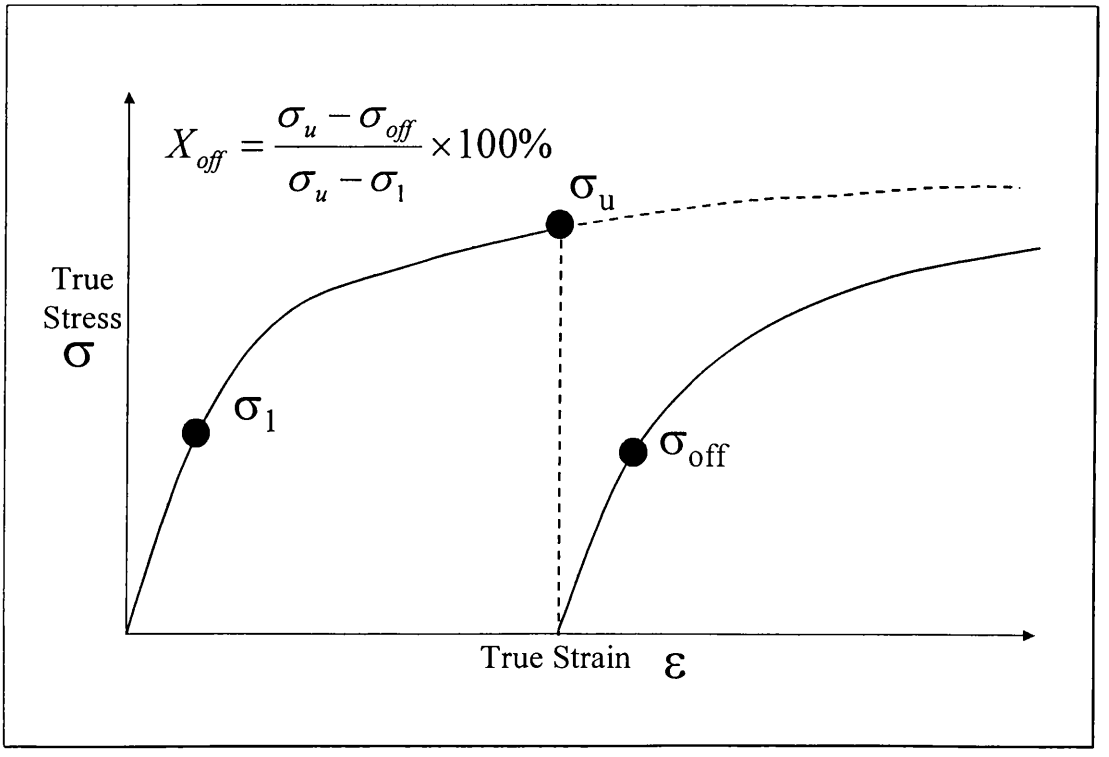

Figure 2.7 Fraction Softened Calculations by the Offset Method

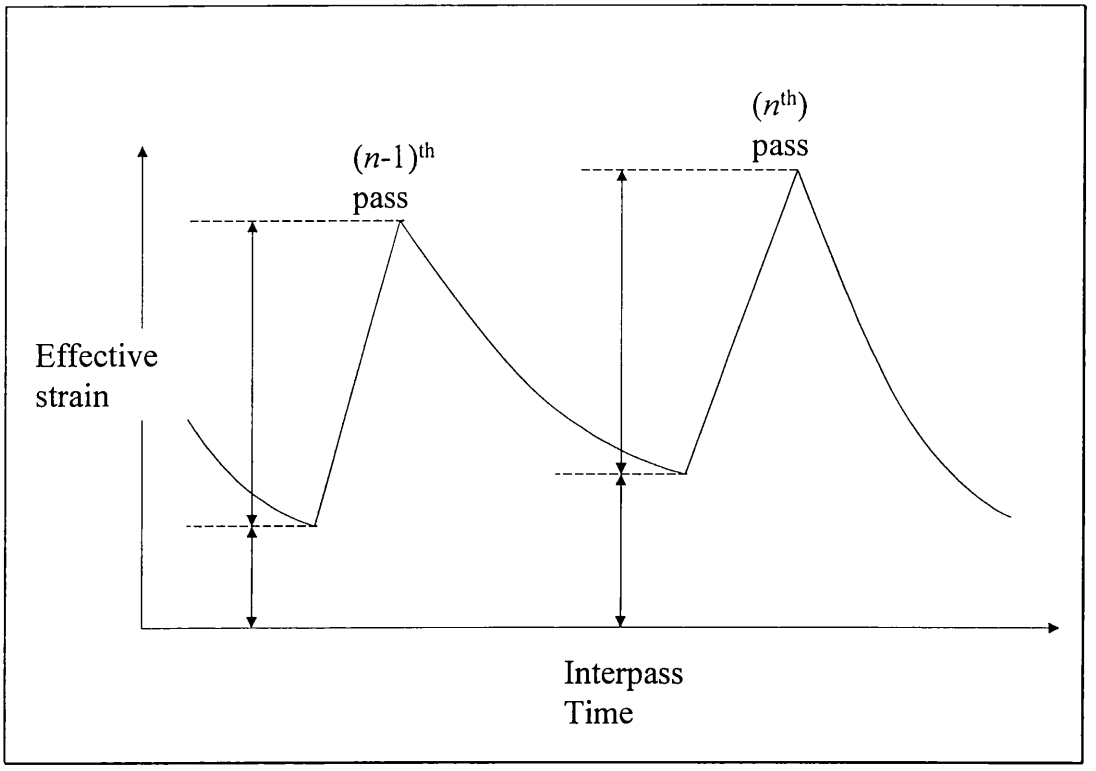

Figure 2.8 Schematic of Strain Accumulation

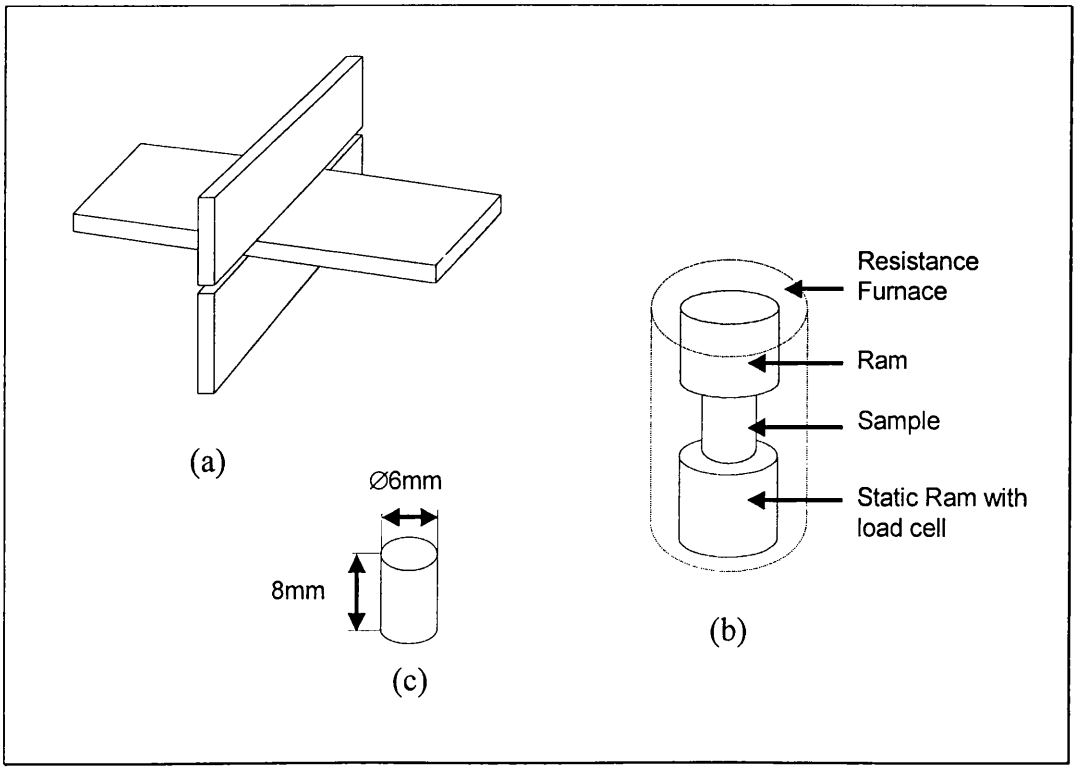

Figure 2.9 Schematic Representation of: a) Plane Strain Compression; b) Axisymmetric Compression; c) Typical Sample Dimensions

3 Commercial Aspects

3.1 Introduction

This chapter is intended to give the reader some insight into the motivation behind the development of such complex numerical models as described in section 2.4. It is also intended to give the reader, who perhaps is not familiar with the hot rolling process, an introduction into the hot strip process routes. Brief descriptions of these processes within a typical hot strip mill are given in section 3.3.

The production of steel strip from ore and coal is an energy intensive, large-scale industrial process where the economic background for this whole industry has been linked to the hot strip mill. Hot rolling itself is the highest tonnage industrial forming process and as such all industrialised nations will want to have a hot strip mill as part of their infrastructure. It is worthwhile noting that the steel industry is a highly competitive international activity that consumes enormous quantities of raw materials. The continual pursuit of economic and technical advantage within the steel industry provides the motivation to research and develop complete solutions for design and control of both plant and process. Several advantages of numerically modelling the hot strip finishing mill are discussed below: -

1. Reduce the number of expensive mill trials for product and process development.
2. Evaluate control system hardware and software.
3. Investigate different mill configurations.
4. Predict variables, which cannot be easily measured.
5. Perform sensitivity analyses to determine which process variables should be measured and controlled to achieve the required final product properties.

1. Historically mill operators have investigated how a new product or process pattern behaves by conducting expensive mill trials. These normally result in products being processed outside the normal quality specifications. Computer simulations of the hot rolling process can represent an important software tool to compliment or even replace the expensive experimental procedures associated with innovative developments.

2. Once off-line models have been validated they provide useful controls to evaluate any modifications to on-line control systems. Predicted variables from off-line numerical simulations can also provide useful benchmarks for any on-line control system.

3. Off-line simulations also enable relatively inexpensive investigation into new finishing mill configurations. These may include rapid acceleration of the mill with greater mill velocities and reduction patterns. It may also include the analysis of processing steels at lower temperatures, perhaps within the ferrite region, in contrast to current mill practices.

4. One of the most quantifiable advantages of numerical analyses of the hot rolling process has been the ability to predict parameters that are difficult or impossible to measure during normal operations. These include recrystallisation rates of different grades within the finishing mill and predicting the austenite grain size exiting the finishing mill.

5. Computational models of the finishing mill have been used to calculate the parameters which have the greatest effect on internal and external product properties. These parameters can then be given any extra effort required to monitor and control them.

3.2 Project Brief

The primary objective of this research is to address the modelling of commercial hot strip finishing mills. Numerical modelling of any manufacturing processes offers researchers at academic institutions tools to find new insights into the physical behaviour of materials and processes. Industrial organisations can use these techniques to develop and optimise operating practices to maximise output and improve the product quality.

It is envisaged that a software tool should be able to quantitatively link the processing parameters to the behaviour of the product and would therefore involve a multi-disciplined approach. Although many modern numerical techniques have been employed to calculate the mechanical and thermal events within a hot strip mill the static recrystallisation algorithms have rarely been included to calculate the metallurgical

issues that occur between successive deformations. Microstructural effects are currently being investigated within the steel industry and are current topics of interest within the aluminium industry. The inclusion of these microstructural effects within a process model is seen as key to developing a complete finishing mill simulation.

3.2.1 Objectives

1. Complete thermomechanical testing to generate fundamental data for the definition of the hot deformation characteristics for a material regarded as a high value product and challenging to roll.
2. Further develop Finite-Element models of the roll gap.
3. Couple predictions of roll-gap models with microstructural algorithms that can predict the evolution of microstructure and assess their accuracy.
4. Develop algorithms to couple roll-gap and interstand models to complete a seven-stand finishing mill simulation.

3.2.2 Deliverables

A complete multi-stand finishing mill simulation that can be used to investigate existing and future mill practices.

3.3 The Hot Strip Mill – Process Overview

The hot strip mill is the name given to the complete process yielding the first major reduction step in the production of steel strip. Steel strip is used for a vast number of applications including automobile, construction, tube manufacture, consumer white goods and packaging solutions. Hot rolled steel is also the core component of many other steel processing operations. The strip must therefore meet all the challenging dimensional specifications and have the ability to retain any deformed shape with surface properties that allow it to be coated.

Hot strip mills at different sites, even within Corus, have different sub-processes so generic description of the hot mill is difficult. Nevertheless, a brief introduction to these sub-processes is given below with reference to Port Talbot and Llanwern hot strip mills (see Figures 3.1 & 3.2), Corus UK.

3.3.1 Hot slab delivery

Steel slabs from a basic arc furnace or electric arc furnace are either cast into ingots or, more recently, directly cast into 43 tonne slabs. Delivery to the hot strip mill is either directly from the casting shop or via the reheat furnaces. Allowing the slabs to cool allows visual surface inspection and machine scarfing to remove any slab defects whereas direct scheduling from the casting shop has the economical benefit of not requiring any energy for reheating. Port Talbot has 2 walking beam furnaces and Llanwern has 5 pusher furnaces that can deliver 350 and 180 tonnes/hour/furnace respectively. In both cases the slabs are delivered 7-12m long, approximately 0.25m thick and at 1250°C to the descaling and roughing processes.

3.3.2 Descaling and roughing

Due to the high affinity of carbon with air and rapid surface cooling, surface scale appears immediately after discharge from the reheat furnaces. Minor reductions in the range of 10% then take place in both the gauge and width directions by two high mills. This usually fractures any surface oxide scale allowing hydraulic sprays to wash away any scale before roughing.

Slabs are further reduced in thickness in either a sequence of five, four high single stand roughing mills or a reversing rougher. These powerful four high mills consist of two work and two backup rolls positioned in a vertical stack. In the case of the reversing rougher there are usually three forward passes and two reversing passes. Therefore as the slab progresses through each mill reduction the thickness is being reduced and the slab is getting continually longer. Some effort may be made during the roughing operation to control the width of the slab but during finishing rolling the width remains largely unaltered. On departure from the descaling and rough rolling operations the slab is now at a temperature of about 1250°C, a thickness of about 0.035m and approximately 100-120m long. Further details of the scale breakers and roughing stands are given in table 3.1.

	Diameter (Max)

Detail	No. of rolls	Roll length (m)	Work roll (m)	Back-up (m)
Vertical scale breaker	2	0.23	1.07	-
Horizontal scale breaker	2	1.96	0.91	-
Reversing rougher	4	2.03	1.2	1.58

Table 3.1 Scale breakers and Roughing Roll Data

3.3.3 Finishing mill

At entry to the finishing mill the slab, now termed the transfer bar, is beginning to assume the shape and dimensions of the steel strip. However there may be slight delays at entry to the finishing mill if the mill is still processing the previous slab or if there are any finishing mill set-up problems. During the interim it is necessary to delay the incoming transfer bar without heat loss. Solutions to this problem have been either to install a linear bank of heat retention shields between the roughing and finishing operations or alternatively coil the incoming slab in a heat retaining coil box. The heat retention screens or Enco panels extend the overall length of the hot strip mill whereas the coil box is an extremely compact device. The coil box has the added advantage of reversing the direction of the strip. This further homogenises the temperature along the transfer bar as the tail end now becomes the head end entering the finishing mill. Eventually the finishing mill is ready to accept the incoming bar and suitable entry temperatures and speeds must be correctly attained. Both mills operate hydraulic descalers at entry to the finishing mills to remove any surface oxide which may damage the work rolls and crop shears to square the head and tail sections to ensure optimum threading.

Entry temperature to the finishing mill is grade dependant, although an average temperature is circa 1050°C. In contrast to the roughing operations the finishing mill consists of seven four high mills positioned close enough to process the strip in tandem. Between each pair of stands is a device called a looper that is designed to control strip

tension and the mill speed. Thus the sequence of roll stands is being used to achieve a successive reduction in strip gauge and the looper device is part of the mechanism to control tension and mass flow through the finishing mill. Both finishing mills at Port Talbot and Llanwern have roll bending on all the stands and roll shifting on the latter 4 stands. However whilst the mill at Port Talbot can process material widths between 675 – 1880mm Llanwern can only process strip to a maximum width of 1580mm. In both cases the strip normally leaves the mill at gauges between 0.0015m - 0.003m, at a temperature range of 850 - 900°C and length approaching 1000m.

3.4 Finishing mill measurements and actuators

Automatic control systems for hot strip mills have been in use since the 1960's. The rolling, actuating and sensing equipment have made significant advances since then, but the control principles and methods applied have remained relatively unchanged. Given the complexity of the process dynamics and operations it is quite surprising that there are so few measurements and actuators available for the control of the finishing mill. A typical list is given below with reference to figure 3.3.

3.4.1 Measurements

Strip temperature: This is usually measured at the entry to the mill (before stand 1) and at the exit of the mill (after the last stand).

Gauge: An x-ray gauge monitor is positioned after the last stand. Strip profile (namely, the gauge across the width of the strip) is available at the same location.

Roll-force: Load cells on each stand give the stand roll force measurement.

Interstand tension: The interstand tension depending on grade of material may or may not be available.

3.4.2 Actuators

Stand screw positions and Capsules: The screw position on a roll stand relates to the vertical movement of the back up rolls and thereby changes the roll force being applied. Capsules have more recently been introduced to set the roll gaps. Capsules are preferred to stand screws due to their rapid reaction times.

Stand drive motor speeds: The drive motor speed on each stand affects the mass flow rate through the finishing mill and is available for all grades.

3.5 Cooling and coiling

Beyond the finishing mill is the runout table where computer controlled cooling of the strip takes place. This is the last area of the hot mill where the final metallurgy of the product may be influenced. Depending on the required material microstructure laminar sprays above the strip and pressure sprays below the strip are used to bring the strip down to a uniform temperature between 450 and 650°C. Interrupted cooling, where the water-cooling is interrupted with air-cooling, can be used to promote the transformation to ferrite for some grades of steel. After cooling the strip it is coiled on either one of 2 down-coilers at Port Talbot or one of 3 down-coilers at Llanwern. Here the strip is labelled, strapped, sometimes wrapped and dispatched to the customer or transported directly to further processing centres.

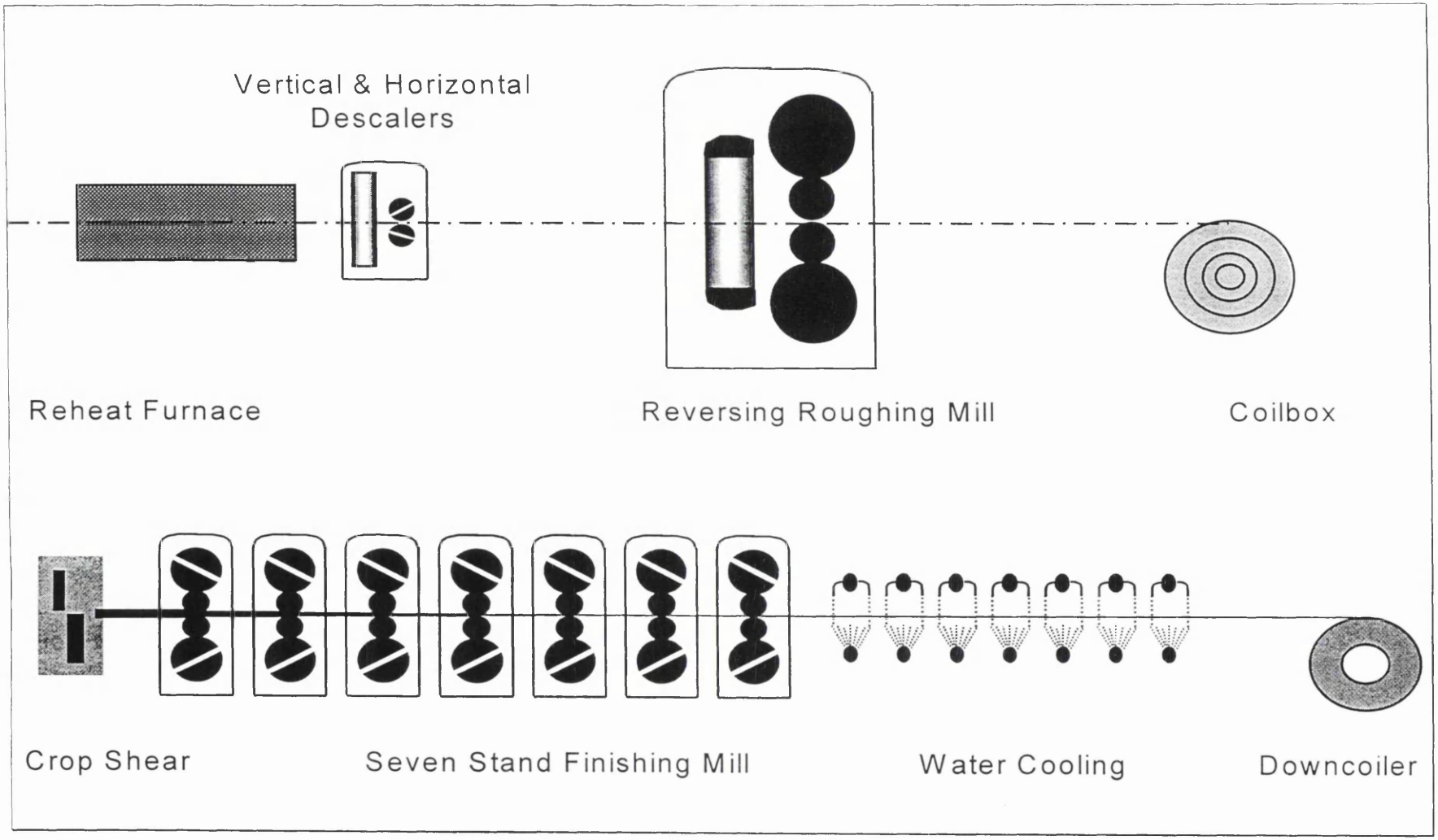

Figure 3.1 Schematic of Port Talbot Hot Mill

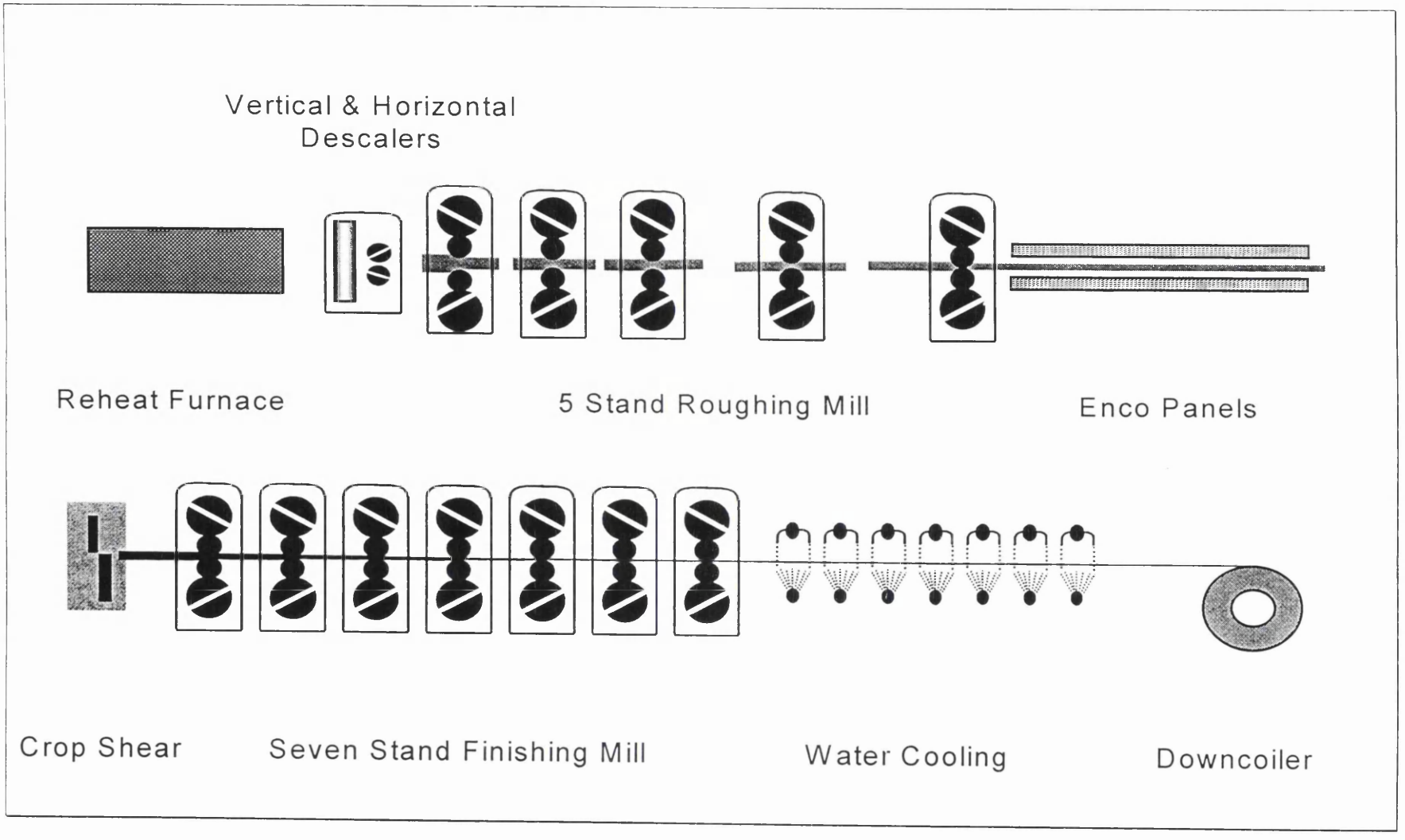

Figure 3.2 Schematic of Llanwern Hot Strip Mill

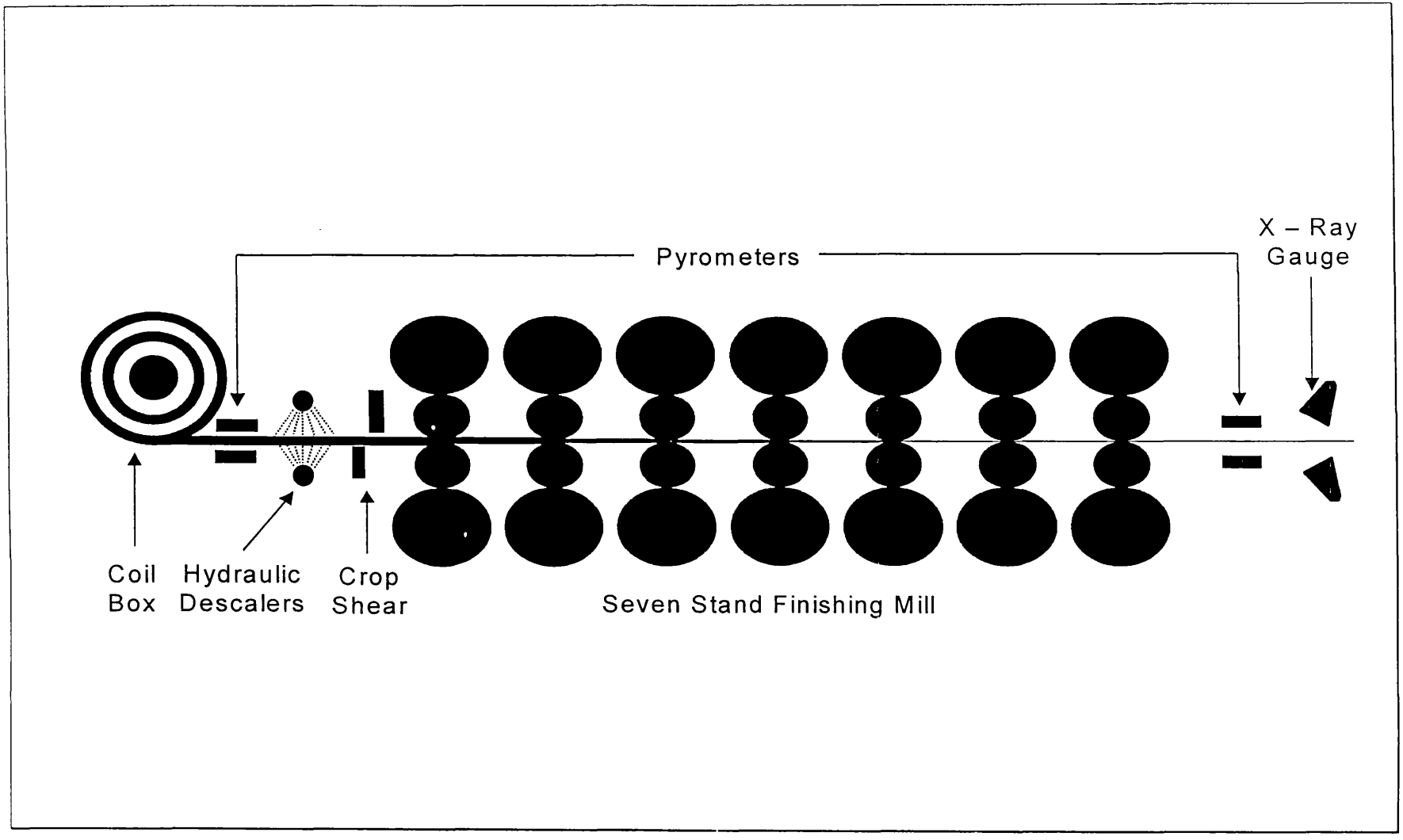

Figure 3.3 Schematic of the Actuators and Sensors within the

4 Finishing Mill Model Overview

4.1 Introduction

This chapter introduces the concepts and procedures that are discussed in depth within subsequent chapters. The overall project methodology is described first with section 4.3 providing an introduction to the Finite-Element method. Following this brief overview the detailed definitions of the material behaviour, roll-gap and interstand models are given in chapters 5, 6 and 7.

4.2 Project Methodology

As described in chapter 1, the overall aim of this work is to enhance understanding of the mechanical, thermal and microstructural evolution during the production of steel strip through the application of numerical techniques.

The methodology adopted to complete this task has been to separate the finishing mill into two distinct areas. Firstly, the roll gap has been considered using the Finite-Element method with coupled temperature-displacement techniques. This numerical model can predict the effects of process variables such as strain, strain rate and temperature with their consequential effects on mechanical behaviour during rolling. Secondly, the Finite-Element technique has also been applied to describe the interstand areas. During this analysis heat transfer and microstructural parameters are calculated for single-phase austenitic Carbon steels.

Whilst the methodology has been to separate the areas of the finishing mill into roll-gap and interstand problems, both areas have been described using the commercial ABAQUS Finite-Element software. The roll-gap and interstand models are sequentially linked to provide vital information regarding both the geometry and material characteristics during rolling with the calculations of the transient cooling and microstructural evolution during the periods between deformations to complete a seven stand finishing mill simulation.

The advantage of the Finite-Element method is its inherent capability to provide detailed stress, strain and temperature fields with realistic boundary conditions to define the finishing mill. Justification for using commercial software originates from the desire of Corus UK to be operating the industry standard software where constant development by international organisations can be readily understood and incorporated within any existing off-line model by Corus staff.

4.3 Introduction to the Finite-Element Method

The Finite-Element method has been the engineer's most powerful numerical tool of the 20th Century. The rapid increase in computational power and the equally rapid decrease in the cost of computers has extended the availability of this method to students and engineers even within small to medium enterprises.

The Finite-Element method is a technique of acquiring an approximate numerical solution to a specific 'field' type of problem. The approximate solution in a stress analysis is the displacement or stress field whereas in a thermal analysis it is the heat flux or temperature field. In order to calculate this 'field' the method must first simplify and break down the area of interest. Discretisation involves dividing the area into a number of Finite-Elements where shared nodes connect each element and the behaviour of each element is then described in some simple way. The collection of all the connected elements is called the *mesh*. The field quantity is then interpolated over the entire area of interest in a piecewise fashion. The set of simultaneous algebraic equations are then assembled and solved. For a stress analysis these equations are equilibrium equations.

A more sophisticated description of the FE method regards it as a piecewise polynomial interpolation. There being as many polynomial equations as there are elements. Finite-Element analyses, particularly when using the ABAQUS programme suite, consists of three distinct stages shown in figure 4.1 [119]: -

1. Pre-processing
2. Simulation
3. Post-processing

These stages will be discussed in the following sections with particular reference to finishing mill models described in section 2.4.

4.3.1 Pre-processing

This initial phase requires the greatest amount of user interaction with the Finite-Element analysis programme. For any particular analysis several parameters must be defined: -

1. Workpiece Geometry
2. Tooling Geometry
3. Element Types
4. Material Behaviour
5. Loads and Boundary Conditions
6. Analysis type
7. Output Required

4.3.1.1 Geometry

Workpiece and tooling geometry are defined with Finite-Elements and nodes in three-dimensional (x, y, z) space. If a two-dimensional analysis is required then all z co-ordinates are zero.

4.3.1.2 Element Type

There are many families of elements that can be used within a particular Finite-Element analysis. However many limitations exist with all these elements and correct selection is essential for any accurate Finite-Element solution. For simplicity only continuum elements are described here. The main distinction between the continuum or solid elements is the geometry which they assume. In most stress analyses two or three-dimensional solid elements are used. The variables associated with these elements are characterised by their degrees of freedom. For both two-dimensional and three-dimensional elements the degrees of freedom are the translations and rotations at each node. The mesh design is also of critical importance for accurate Finite-Element

solutions. Quadrilateral elements should be kept as square as possible over the region of interest to allow correct interpolation of the results across the element boundaries. These elements should also be as numerous as possible over any region where the magnitude of the results changes significantly over any specific area. As the number of elements increases the computational expense increases and the analysis results converge to unique solution. The user must therefore reach some compromise between computational expense and model accuracy.

4.3.1.3 Materials

A wide variety of materials are encountered during stress analysis problems. For any one of these materials, several models are available to describe their behaviour, each suitable to a particular type of application. Finite-Element analyses usually accommodate both flow and solid material formulations and it is in the pre-processing phase that the material rheology is determined. The constitutive library provided by ABAQUS contains a range of linear and non-linear material models for all categories of materials including metals, rubbers, polymers, composites, reinforced concrete, crushable and resilient foams and geotechnical materials such as soils and rocks [119].

4.3.1.4 Loads and Boundary Conditions

Accurate description of the loads and boundary conditions are essential for the correct interpretation of the physical problem. Loads distort the physical structure and create stress within it. Loads can be point loads, pressure loads, body forces such as gravity loads or even thermal loads. Conversely, boundary conditions are normally used to constrain the model or to move it by a prescribed amount. Boundary conditions are normally prescribed for nodes rather than elements within the pre-processing phase. Nodes that define lines of symmetry require both translation and rotational degrees of freedom to be restricted.

Contact between two bodies is one of the most difficult and computationally expensive to simulate using Finite-Element techniques. Within a Finite-Element analysis contact conditions are described as discontinuous constraints [119]. The constraint being discontinuous as any forces are only transmitted when the surfaces are in contact. In

these problems a force normal to the surface is generated upon the two surfaces. Many contact situations also consist of interactions between the two surfaces. If there is friction between these surfaces there is also a shear force that resists the sliding or tangential motion of the two bodies. The aim of any contact simulation is normally the quantification of the areas in contact and the contact pressures that are generated [119].

4.3.1.5 Type of Analysis

There are many different types of Finite-Element analyses. Stress-displacement is the most popular for metal forming analyses. However, when the material is at a high temperature either a sequential heat transfer and stress analysis or a fully coupled temperature-displacement analysis is required. Sequential analyses are preferred to fully coupled analyses as the computational expense is more than doubled when both the displacement and thermal calculations have to be computed simultaneously.

4.3.1.6 Output

Finally the type and frequency of the output must be defined within the pre-processing phase. Output files are normally written at a specified increment frequency for nodes or elements with specified internal variables such as stress, strain, strain rate and temperature.

4.3.2 Simulation

During the calculation stages the nodal displacements are calculated from which the strain rates can be determined. The stresses are derived from the material rheology definitions. The material behaviour is decided within the input phase and only considered here through interpolation of these defined stress/strain relationships. Elasto-plastic behaviour is characterised by the yield stress from which permanent plastic strain takes place together with the elastic strain associated with the stress (see section 2.4.2.3). The plastic flow is then an irreversible process described in terms of the deformation history and a group of internal variables, known as hardening parameters.

4.3.2.1 Non-linear Analysis

Due to the material and boundary conditions during rolling the analysis is obviously non-linear. The Finite-Element solution cannot therefore be calculated by solving a single system of linear equations. Instead the solution is found by specifying the loading as a function of time and incrementing time to obtain the non-linear response. ABAQUS breaks the simulation into a number of time increments and finds the approximate equilibrium configuration at the end of each time increment. Using the Newton method [120], it often takes several iterations to determine an acceptable solution for each time increment.

4.3.2.2 Consequences of non-linear analyses.

Good engineering analysis of any non-linear system requires skilful approximation and in many instances the assumption of linear behaviour leads to a reasonable idealisation of structural behaviour. However, there are situations where non-linear effects must be incorporated for a realistic assessment of structural response.

The advantages of linear analyses are fairly obvious: simple direct solutions may be obtained with no need for costly load incrementation and iterative schemes. Furthermore, solutions for various load cases may be superimposed and the number of material constants required to describe the constitutive behaviour is kept to a minimum in a linear analysis.

Two major areas where non-linear analysis are used include: -

1. Research (a) to help understanding of 'code – based' mathematics of analysis and design, (b) to help understand basic structural behaviour, and (c) to test the validity of proposed 'material models'.
2. Simulation of materials processing and manufacturing, e.g. forging, casting, extruding and rolling.

The major limitations with non-linear analysis are numerous but with the new generation of powerful yet inexpensive computers, solution cost is no longer the obstacle it has been. One major consideration when contemplating a non-linear analysis is the principle of superposition cannot be applied. Thus, for example, the results of several ' load cases' cannot be scaled, factored or combined as in linear analyses. Below is a list of some of the more costly consequences of non-linear analyses: -

1. Only one load can be computed at a time.
2. The loading history may be of importance e.g. the response where material is heated then stressed may be different from one where it is stressed then heated.
3. The structural response can be markedly non-proportional to the applied loading.
4. The initial state of stress (e.g. residual stress from welding, pre-stressing etc.) may be important.

4.3.3 Output Stage

The output stage concerns the presentation of the results from the Finite-Element calculation stage. This can take the form of contour plots, x-y plots and x-y tables. Although the output from a complete Finite-Element solution may be unique, it is generally an approximation to the physical problem being simulated. The extent of the approximations made for the geometry, material behaviour, boundary conditions, loading and quality of the output determines how well the numerical solution matches the physical problem.

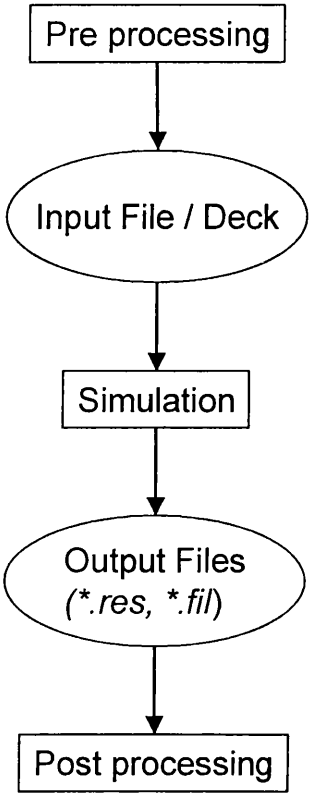

Figure 4.1 Overview of the Finite-Element method

5 Material Modelling

5.1 Introduction

A wide variety of materials are processed within the finishing mill. Any one of these materials consist of constitutive relationships between the temperature, strain, strain rate and initial austenitic structure. Constitutive models are only required when considering the plastic response of a material and they define the hot deformation characteristics for each particular material grade with respect to the deformation conditions.

Much of the metallurgy of hot working is now well understood and can be described in sound physical terms. However, the motivation to develop numerical models of microstructural evolution during thermomechanical processing requires empiricism to relieve the limitations of this physical understanding. From the literature review it can be seen that the hyperbolic sine law (equation 2.28) in conjunction with the required constants can accurately predict the dynamic behaviour of the strip during rolling. Avrami equations (equation 2.33) with the required constants, can also determine any static phenomena occurring within the finishing mill.

This chapter describes the experimental procedure and apparatus used to derive the hot deformation and static characteristics of a high Carbon material. These characteristics described using equations presented within chapter 2 can then predict the dynamic and static events during multiple hot deformations at different strains, strain rates, holding times and temperatures.

5.2 Experimental Procedure

This section describes the method to simulate the hot deformation of high carbon steel with the chemical composition give in Table 5.1.

C	S	P	Mn	Al	N	Si	Cr
0.82	0.007	0.016	0.72	0.041	0.0028	0.22	0.027

Table 5.1 Chemical Composition of the High Carbon Steel (Wt%)

The selected deformation conditions were analogous to the conditions commonly encountered during hot finishing rolling and the experimentation of the material consisted of three distinct components.

1. Single deformation at various temperatures and strain rates to 50% true strain.
2. Interrupted deformation testing at varying delay times. Total deformation is equal to (1) where softening rates are assumed to be strain rate independent.
3. Single deformations equal to the initial deformation of (2) followed by varying hold times also equal to (2) with quenching.

5.2.1 Material Selection

The high carbon steel was selected due to the large production demand for this grade with the associated high added premium value of the product. The High Carbon grades are very rarely used in their hot rolled condition but are normally cold rolled and annealed before being pressed or formed into their design and re-austenised to reveal their superior mechanical properties. Most uses for this grade of steel come from engineering applications such as tooling and high strength structural components.

The steels were acquired by double crop shearing the transfer bar at entry to the finishing mill. This ensured that the mass flow through the finishing mill was not affected by sampling. The head crops were allowed to cool to ambient in the pit before being retrieved.

5.2.2 Specimen Geometry and Preparation

Uniaxial testing requires homogeneous deformation. Therefore, friction resulting in barrelling of the sample during deformation must be minimised. Specimen geometry is critical, as it is known that a low height to diameter ratio reduces barrelling. For this exercise the dimensions of the cylindrical samples machined from the transfer bar crop ends had a height of 8mm and a diameter of 6mm, resulting in a height to diameter ratio of 1.33 (See Figure 2.9).

Prior to testing each sample was coated in a glass-based lubricant to reduce the friction between the sample and the dies. This coating also provided some protection against decarburisation whilst in the furnace. Further measures included applying boron nitride suspension in water to the dies during the interrupt compression testing to ensure the lubricant did not adhere to the ram. The suspension liquid would obviously flash off during soaking to the test temperature. The lubricant residue after each test severely reduced the number of tests that could be completed before the platens had to be reground.

5.3 Experimental Apparatus

The ESH manufactured servo hydraulic test machine located at the University of Wales-Swansea was employed for all the experimentation. The machine has a load capacity of ±100kN with ram rates between 0.008 and 500mms^{-1}(see Figure 5.1) with the furnace capable of temperatures up to 1373K. The upper ram moves at a constant rate with the fixed lower die being connected to a load cell.

5.3.1 Temperature Control

The cylindrical resistance furnace surrounds both the specimen and the dies. The furnace has two thermocouples. The first 'factory fitted' thermocouple was part of the control system. Whereas the second thermocouple, positioned at the centre of the deformation chamber at a height corresponding to the specimen was coupled to a digital ampmeter to provide test piece temperature readings to the operator. The electrical current to the furnace could then be adjusted consequently adjusting the sample temperature. The resistance furnace heated the samples by convection up to temperatures of 1373K

A circular port at the front of the furnace allowed the manual positioning of the samples onto the static ram. This port was sealed during soaking and testing using a ceramic refractory. Each specimen was soaked at the deformation temperature for 600 seconds. It is assumed that due to the relatively small sample size isothermal conditions would then exist throughout the experimentation

5.3.2 Test Data Capture

The load and displacement readings were captured on a personal computer. Software developed by the Interdisciplinary Research Centre-Swansea combining the test limits such as load and stroke on the compression apparatus with data from the control software converted the test data into true stress/strain curves. The software used the common expressions: -

$$\varepsilon = \ln \frac{h_i}{h_o}$$
$$\sigma = \frac{F}{A_i} \qquad (5.1)$$

Where h_i is the instantaneous height of the specimen, h_o is the original speimen height and F is the force at an instantaneous area A_i. The peak loads were also noted for each test. These readings could then be used to enable accurate load scaling for subsequent tests.

5.4 Single Deformation

To determine the hot deformation characteristics of the material single hit deformation tests were carried out at various strain rates and temperatures to a total strain of 0.5 (see Figure 5.2 a). Whilst soaking the specimen at temperature a small load was placed on the sample to ensure it did not lose its position on the platens. This then allowed the ram position to be zeroed permitting the correct stroke to be calculated.

5.4.1 Strain Rates

The strain rate test matrix varied from ram rates between 0.008 and 500 mms^{-1}. These ram rates resulted in strain rates between 0.0001 and $40s^{-1}$ when considering the sample geometry. For the faster deformation rates an initial back off dimension was set to 1mm to ensure the ram had reached the correct velocity before it came into contact with the specimen.

5.4.2 Temperatures

The electric resistance cylinder furnace provided both the soaking and deformation temperatures. The maximum operating temperature for the furnace was 1373K and was therfore used as the maximum deformation temperature for this research. The lowest temperature was taken to be 1123K corresponding with the lowest temperatures experienced during finishing rolling of this grade of material. Each specimen was loaded into the furnace and soaked for 600 seconds at the deformation temperatures to completely re-austenise the test pieces and create an equiaxed homogeneous microstructure. After deformation each specimen was then immediately quenched in water in an attempt to retain the deformed austenite microstructure.

5.5 Double Deformation Testing

Double deformation testing required new and more complex control software. The sequence of testing can be seen in figure 5.2 (b). It can be seen that the test consists of both constants and variables. The variables notably consisting of pre-strain and interrupt time where the constants were the total strain and the ramp rate. The interrupt time was set as a real number opposed to an integer within the control software to allow fractions of one second to be set. The 0.5mm back off before the second part of the test was traversed during the interrupt time to allow direct specification of the time between the tests. The back off was calculated as a function of the maximum ramp rate and the distance required to reach this rate.

5.5.1 Strains and Temperatures

The total strains were set to those used within the single deformation tests. The initial strains were set to those encountered within the latter stands of the finishing mill. These pre-strains were deliberately kept as small as possible to enable partial softening at the minimum interrupt time. The pre-strains selected were 15% and 25%. The temperatures chosen for the double hit test were from 850, 875 and 900°C. These temperatures represent typical latter stand strip temperatures where incomplete softening within commercial hot strip finishing mills is expected.

5.5.2 Strain Rate

A constant ram rate of $0.8mms^{-1}$ was maintained for the entire double hit deformation testing procedure for the investigation into pre-strain and temperature effects. Due to the specimen geometry this resulted in a strain rate of $0.1s^{-1}$. From the design of the Avrami type equations it can be assumed that strain rate effects can be ignored when investigating static softening kinetics [106].

5.6 Microstructural Investigation

Direct optical analysis of the evolving structure during the experimentation offers a complimentary technique to obtaining quantitative data regarding the softening kinetics of single-phase austenitic steels. To investigate any effects of grain size on the softening kinetics the samples were quenched after the single and double hit deformation experimental procedures.

5.6.1 Optical Investigation

The specimens were prepared for optical investigation according to standard metallographic techniques employed by Corus Research, Development and Technology departments. Samples were sectioned along the length of the specimen, parallel to the compression axis. The samples were then mounted under pressure in Bakelite and polished using four grades of wet silicon carbide paper followed with mechanically operated 6 and 1μm diamond suspension polishing apparatus. A 5% Nital solution was used to reveal the prior austenite grain boundaries. The analysis of the grain boundaries was carried out on an optical microscope. Unfortunately due to the high carbon and low alloy content even when annealing the sample and applying longer etching times the prior austenite grain boundaries could not be revealed.

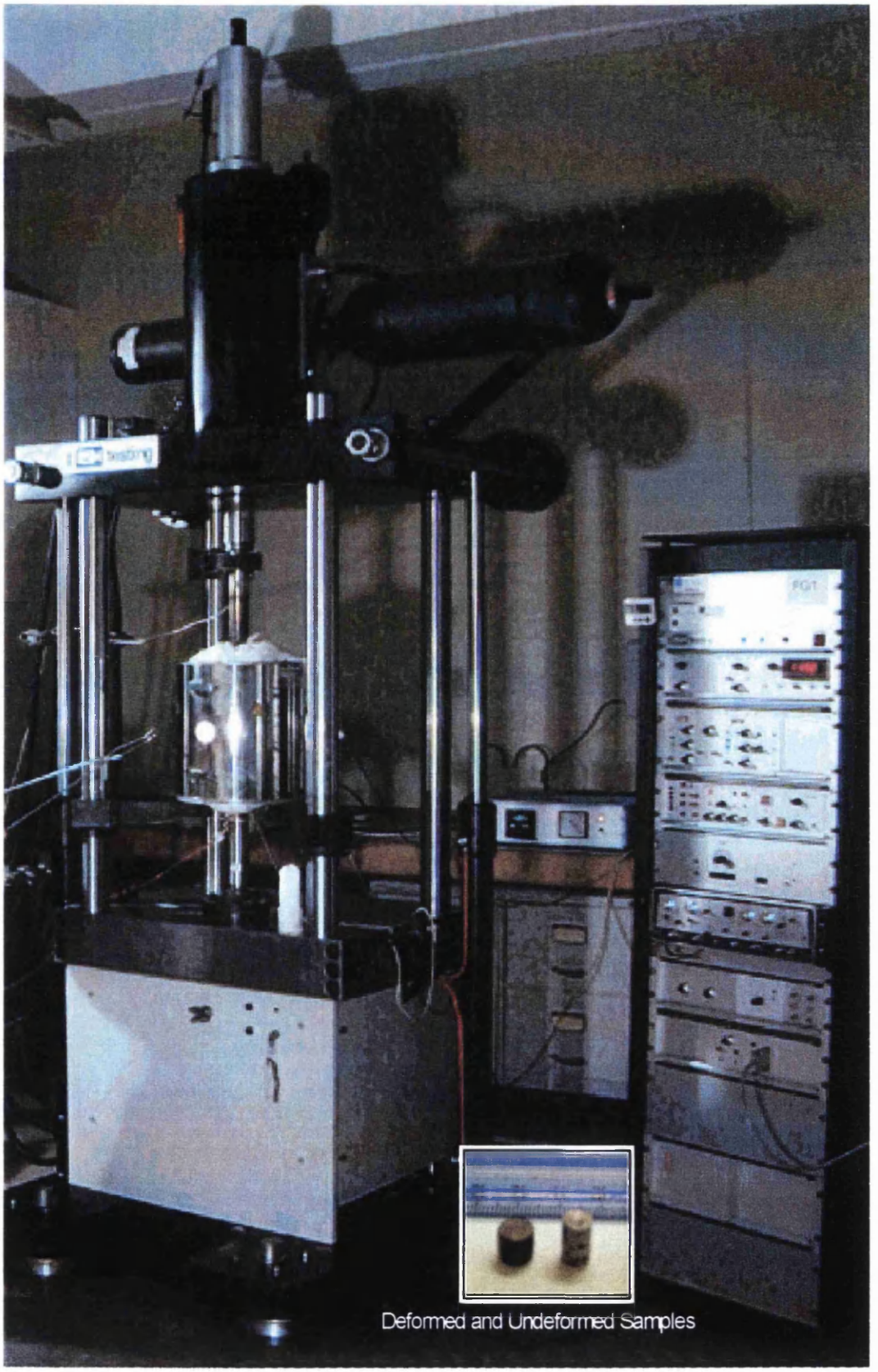

Figure 5.1 Image of the Hot Compression Simulator

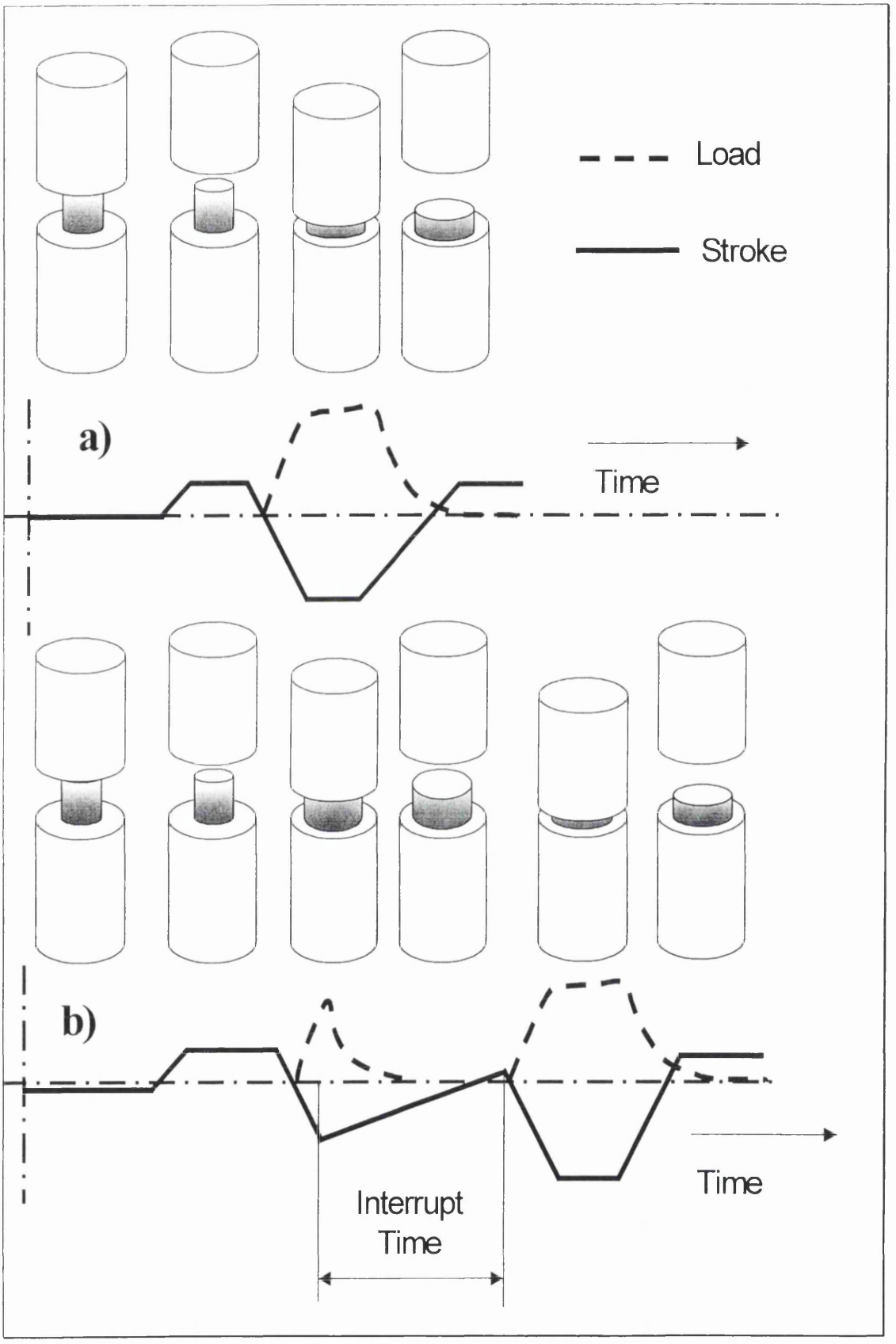

Figure 5.2 Schematic of Stroke and Loads for a) Single and b) Interrupt Compression testing

6 Roll-Gap Model Development

6.1 Introduction

The fundamental development of a roll-gap model was required to assess and improve off-line models of the finishing mill. This improved model would then provide a software tool for the investigation into the mechanical behaviour of the strip during rolling and the heat transfer that occurs during finishing rolling.

The roll-gap model was initially based on existing Finite-Element models used within the Welsh Technology Centre. These primarily consisted of the commercial code called ABAQUS (supplied by HKS) although there were some in house codes available. All the rolling ABAQUS models were based on the two dimensional scheme with several limitations including rigid rolls with no heat transfer at the roll/strip interface.

The roll gap was considered a plane strain problem, as changes in the width are negligible compared to the elongation during finish rolling. As the stress analysis was strongly dependent on the thermal analysis the system was thermo-mechanically coupled. Thus the thermal and mechanical solutions were obtained simultaneously.

Two approaches to modelling the roll-gap material have been completed: -

1. A model based on the original material properties, where the flow stress is independent of any deformation history. This model will obviously be correct for any material that fully recrystallised during the interpass time. The flow stress is therefore dependent on temperature, strain and strain rate.

2. A model based on updated material properties, where the flow stress at pass (p+1) is dependant on the previous amount of recrystallisation after pass (p). The flow stress here is a more complex function of temperature, strain rate, strain and initial strain from recrystallisation calculations.

Initially, with the assumption of uniform cooling on both the top and bottom of the strip, a half symmetry model has been developed. This roll-gap model comprised a single roll and half gauge of the workpiece. This model was seen as a fundamental tool for calibrating these types of models to measured data from an operating finishing mill due to their relatively short run times. A model accounting for asymmetric cooling during the interstand regions was later developed. This model required both top and bottom work rolls and the full material gauge to be taken into account.

The following sections describe the three phases of the roll-gap model developments from pre-processing through simulation and the resulting output. The pre-processing phase for all ABAQUS analyses results in an input file commonly termed the input deck. This input deck contains information regarding the '***model data***' and the '***history data***'. Model data mainly consists of user-defined input such as the geometry, elements, materials, loads and constraints. History data normally refers to the sequence of events that affect this Finite-Element model. The contributions to creating the model data, history data and output files used for interrogating the results from the roll-gap analysis are described below.

6.2 Geometry

The elements and their nodes define the geometry of the tooling and workpiece. Whilst it may be assumed that the external shapes of the tooling and workpiece are regular shapes many assumptions can be included to simplify their geometry and minimise any computational expense.

With the assumption that rolling is a steady state process only a representative volume of the workpiece was described. This also meant that only a small projected length of the work roll required representation. Only a small fraction of the roll through thickness would also be required as any roll flattening was considered to only effect the surface of the roll. The workpiece was represented as a perfect rectangle where the gauge and the test length of the material were described. The work roll was represented using a quarter circle. All the dimensions for the work roll and the workpiece were parametised using a Fortran code to enable rapid generation of the roll gap geometry for multiple analyses.

It was noted that due to the type of geometrical representation of the workpiece only a single node would initially be in contact with the roll. Thus, some artificial system would be required to ensure complete roll bite engagement during the early stages of rolling.

6.3 Discretisation

As described in section 4.3.1.2 many families of elements exist and the correct choice for a particular simulation is critical for the accurate solution of physical problems. As continuum elements were the obvious choice for stress-displacement analyses the factors affecting the particular element type revolved around the capability to model the contact and heat transfer aspects of the finishing mill. For contact situations with large mesh displacements, linear, reduced integration elements obtained the most accurate results at reasonable cost.

With the added functionality of the simultaneous calculation of the temperatures and displacements, a fully coupled temperature-displacement, linear continuum element was chosen to describe the workpiece and work roll. Continuum elements use the Lagrangian formulation where the elements deform with the workpiece. These elements use linear interpolation for temperature and displacement in order to obtain a compatible variation of thermal and mechanical strain. Both the heat conduction and the plastic dissipation terms are integrated at the Gauss points. However, whilst the plastic dissipation term is integrated at each Gauss point, the heat generated by the mechanical deformation at a Gauss point is applied to the nearest node.

The work-roll was discretised with the same elements as the workpiece. The length of the arc of the work-roll was equal to the length of the rolled workpiece. A single row of elements represented a depth of 10mm into the roll diameter. In order to determine whether a suitably refined mesh was used for the work-roll and the workpiece a series of tests were carried out with sequentially increased mesh densities until a particular result from the model tended towards a unique value indicating mesh convergence.

6.4 Material Considerations

Complete definition of the material behaviour for the roll-gap Finite-Element analysis required the mechanical elastic and inelastic behaviour with any thermal properties to be defined. The definition of the elastic response used one of the simplest types of stress-strain relationships. The elasticity was considered linear and isotropic with only temperature dependent behaviour. As the work roll only deforms elastically a modulus of 200 GPa with a Poisson's ratio of 0.3 were the only constants required.

The elastic and inelastic responses of the workpiece were distinguished by separating the deformation into recoverable (elastic) and non-recoverable (inelastic) parts. In its most general form this is written as: -

$$F = F^{el} \cdot F^{pl} \tag{6.1}$$

Where **F** is the total deformation gradient, $\mathbf{F}^{el}$ is the fully recoverable part of the deformation at the point under consideration and $\mathbf{F}^{pl}$ is defined by $\mathbf{F}^{pl} = [\mathbf{F}^{el}]^{-1} \bullet F$.

The Elasto-plastic material behaviour was characterised by the yield stress from which permanent plastic strain takes place together with the elastic strain associated with the stress. Both the elastic and plastic strains accumulate as the metal deforms in the post-yield region. ABAQUS uses the Von Mises yield criteria to calculate whether or not the material has passed this yield stress. The plastic flow is then an irreversible process described in terms of the deformation history and a group of internal variables, known as hardening parameters.

The departure from linear elasticity is a complex matter and the definition of the inelastic behaviour required more detailed consideration. Post-yield deformation required more parameters to be quantitatively researched and defined as the stress state was no longer uniquely defined by the strain. For the roll-gap this material model was required to be both temperature and strain rate dependent. This was achieved through the implementation of the Constitutive equations discussed in section 2.7. During a non-linear analysis the implementation of a constitutive model involves the integration of the state of the material at an integration point over a time increment.

The stress/strain behaviour was provided to the Finite-Element programme through a series of tables where the relationships were defined by the Cauchy stress (stress per current area) and the logarithmic strain. These tables were later written as a function of the independent field variable, temperature. Therefore the major assumptions of the material model included: -

1. Approximate linear elasticity. Only the Young's Modulus and Poisson's ratio were required and taken to be temperature dependent.
2. The material was assumed to be isotropic, elasto-viscoplastic obeying Von Mises' yield criterion.
3. The data deck for the ABAQUS material model was supplied in tabular form to describe the elastic plastic and thermal behaviour of the material.

6.4.1 Initial Strain

During the latter stands incomplete softening may occur during the interstand periods. To take account of this fraction of retained strain a level of strain could be prescribed to the workpiece as an initial condition. The equivalent plastic strain output during the analysis then contained the initial value of equivalent plastic strain plus any additional equivalent plastic strain due to the straining during the analysis. With reference to figure 6.1 a roll-gap analysis with a material with retained strain $\varepsilon^{pl}{}_1$ would modify the original material stress/strain curve ABCD to EFCD. Thus, resulting in the yield stress being modified from σ_A to σ_B due to some work hardening. Furthermore, if any strain is calculated greater than the specified stress/strain relationships, the roll-gap model assumes perfect-plastic behaviour.

6.5 Loads and Boundary conditions

The roll-gap model requires a number of loads and boundary constraints to accurately simulate the physical problem. These include artificial loads and constraints to stabilise the model and simulate roll-gap threading.

6.5.1 Loads

Due to the discretised work-roll and workpiece only a single node was actually on the arc of contact. In order to thread the strip into the roll-gap an initial velocity was given to the strip. This initial velocity was prescribed equal to the surface speed of the work-roll and was only present until there was enough contact to ensure friction could effectively pull the strip through the roll-gap. A number of sensitivity analyses were carried out to ensure this condition had no effect on the final results.

6.5.2 Contact Constraints

ABAQUS uses a pure master/slave penalty algorithm where any nodes on the slave surface cannot penetrate elements on the master surface. However this algorithm places no restrictions on the master surface nodes, which can penetrate between slave nodes. As a consequence of these restrictions the harder surfaces (the rolls) were chosen as the master surfaces and the slave surfaces (the strip) were given an equal or more refined mesh than the master surface (see figure 6.2). The contact logic itself is built around the Newton-Raphson technique [120] and a schematic can be seen in Figure 6.3 Where $\boldsymbol{p}$ is pressure and $\boldsymbol{h}$ is clearance.

The finite-sliding formulation was selected which allowed for arbitrary separation, sliding and rotation of the surfaces. Finite-sliding formulations where both surfaces are deformable was only available for 2-dimensional analyses. The contact formulation also required linear elements to be chosen for the slave surface.

6.5.3 Multi Point Constraints

The internal row of nodes on the work-roll were linked using linear constraints to a node defining the center of the work-roll. This permitted one rotational velocity to be defined within the input deck, at the center of the work-roll. These linear constraints have no internal degrees of freedom resulting in the internal nodes of the work-roll having a rigid constraint to the roll radius. The nodes defining the center of the rolls were then fixed from any translations with only a rotational freedom in the xy plane.

6.5.4 Friction

The friction model defines the force resisting the tangential motion of the strip and the work-rolls. From section 2.6.3 it can be seen that a contact pressure-clearance relationship that governs the motion of the surfaces is adequate to simulate hot rolling.
An extended Coulomb friction model is used within the roll-gap model where an additional limit on the allowable shear stress was defined: -

$$\tau_{crit} = \min(\mu p, \tau_{\max}) \tag{6.2}$$

Where τ_{max} was specified during the pre-processing phase. In this investigation the friction was isotropic so that the direction of the slip and frictional stress were equal: -

$$\frac{\tau_i}{\tau_{eq}} = \frac{\dot{\gamma}_i}{\dot{\gamma}_{eq}} \tag{6.3}$$

Where $\dot{\gamma}_i$ is the slip rate in the direction i and $\dot{\gamma}_{eq}$ is the equivalent slip rate. The Coulomb friction coefficient was selected within the range 0.2 to 0.4 for the roll-gap models as described by the literature (see figure 6.4) and τ_{max} was defined as $\sigma_y/\sqrt{3}$ where σ_y is the Von Mises yield stress of the workpiece.

6.6 Heat Transfer

The original modelling methods such as slab, slip line and the upper bound theorems were developed several years ago and generally did not calculate the temperature distribution within the material. The temperature was normally taken into account by using an appropriate average parameter, which obviously affects the material properties. It was soon realised that assuming an average value to determine the temperature dependent variables of rolling would invariably lead to erroneous results. Therefore it is necessary to develop models, which are thermally and mechanically coupled.

The heat transfer considered within the roll-gap includes: -

1. Heat generation due to the work of plastic dissipation.
2. Conduction to the work-rolls that are at a much lower temperature.
3. Heat conduction within the strip.

All these types of heat transfer have been accommodated within the Finite-Element analysis using the ABAQUS programme. General thermal properties of the material were also required for the coupled temperature-displacement analysis of the roll-gap. Firstly, in order to calculate the heat transfer within the material the density was required. Density was specified as a function of temperature for the initial conditions of the workpiece. However, this dependency was not applied during the analysis as mass cannot be created or destroyed.

Isotropic thermal conductivity was selected from the literature and prescribed as mildly temperature dependant. The specific heat was prescribe for the work-roll and workpiece and assumed constant. Thermal expansion coefficients were also required for the thermal strain calculations. A complete description of the thermal properties can be seen in table 6.1 [121].

Property	Work-Roll	Workpiece
Emissivity	-	0.85
Thermal Conductivity, k ($Wm^{-1}K^{-1}$)	25	(28.5 @ 800°C) (27.6 @ 1000°C)
Specific Heat Capacity, C_p ($kJ\ kg^{-1}K^{-1}$)	550	525
Density, ρ (kgm^{-3})	7408	7680
Property	**Work-Roll**	**Workpiece**
Stefan-Boltzmann Constant	$5.67E^{-8}$	$5.67E^{-8}$

Thermal Expansion Coefficients (mm K^{-1})	$12.5E^{-6}$	$1.0\ E^{-5}$

Table 6.1 Material properties for the roll-gap and interstand models.

6.6.1 Heat Generation

The thermo-mechanical coupling of the model allows heat to be generated through the associated plastic straining. The model assumed plastic straining gives rise to a heat flux per unit volume where the heat flux is added to the thermal energy balance according to: -

$$r^{pl} = \eta\sigma : \dot{\varepsilon}^{pl} \tag{6.4}$$

Where r^{pl} is the heat flux added into the thermal energy balance, η is the factor defined by the user, σ is the stress and $\dot{\varepsilon}^{pl}$ is the rate of plastic straining. All the roll-gap models assumed 86.5% of the inelastic work was converted to heat. This value is generally reasonable for metals [59].

6.6.2 Conduction

Within the roll-gap heat transfer occurs through losses to the rolls and heating due to the plastic deformation. In the current work the general heat transfer equation to calculate the thermal transport was solved by the iterative process in Newton's method via a Fourier law (Eq. 2.10) until convergence was achieved. A reasonably accurate solution was described as: -

1. The largest component of the residual flux vector is less than 0.005 of an "average flux" accumulated over the entire body.
2. The size correction to the appropriate solution was less than a small fraction of the incremental change to the solution for the current increment. This value was taken as 1%.

When these criterions are satisfied, the solution to this increment is accepted and the analysis proceeds to the next increment.

6.6.3 Interface Conduction

Conduction depends on the conductivity of the material within the interface as well as the temperatures of the respective surfaces: -

$$q = k_b(\theta_W - \theta_R) \tag{6.5}$$

Where q is the heat flux across the interface, k_b is the conductivity of the material within the interface, θ_W and θ_R are the temperatures of the workpiece and roll respectively. The temperature of the work rolls was initially set to 80°C and then allowed to heat during contact with the workpiece. The conductance across the interface for all the roll-gap models was described as a function of the pressure transmitted across the gap.

6.7 Analysis

A basic concept within ABAQUS is the dissection of the problem history into steps. Each step is broken down into increments. In a non-linear problem ABAQUS will increment and iterate as necessary to analyse the step, depending on the severity of the non-linearity. The coupled temperature-displacement analysis is non-linear because of the temperature dependent material properties and the boundary conditions although temperature dependent thermal properties are usually mild except when latent heat effects are included.

6.7.1 Steps, Increments, and Iterations.

The time history for a simulation consists of one or more steps. The user defines these steps, which generally consist of an analysis procedure option, loading options, and output request options within the input deck. Different loads, boundary conditions, analysis procedures and output request options dictate how many steps are required for

each analysis. Non-linear analysis steps consider the end of an increment represents the last non-linear step provides the initial conditions for the next.

In any non-linear analyses each step is broken into increments so that the non-linear solution path can be followed. The user suggests the size of the first increment and ABAQUS can then automatically control the size of subsequent increments. At the end of an increment the solution is in approximate equilibrium and the results can then be saved to file or read immediately.

An iteration is an attempt at finding an equilibrium solution within an increment. If the model is not in equilibrium at the end of iteration, ABAQUS tries another iteration. With every iteration the solution that ABAQUS obtains should be closer to equilibrium; however, sometimes the iteration process may diverge – subsequent iterations may move away from the equilibrium state. In that case ABAQUS may terminate the iteration process and attempt to find a solution with a smaller time increment size.

6.8 Output

The ABAQUS program generates several files during the calculation or simulation phase. Some are utilised to evaluate the rate of convergence and help troubleshooting when analyses fail. Others are purely for post-processing of the results and these will be discussed below.

The '***Data***' file displays any warnings or errors that may have been detected within the input deck. The '***status***' file reports on the number of equilibrium calculations during an analysis and the time increment size. This text file is useful for investigating how an analysis is progressing. The '***message***' file is essential for debugging purposes as it reports on step, increment and iteration calculations.

The '***Restart***' file is probably the most common output file and can provide data for contour plots and/or x-y plots for the variables specified for each analysis type. All output is defined at the element integration points, nodes or the element centroid. Whilst this file is extremely useful it can get extremely large and was therefore rarely used for

output purposes. The '***Results***' file is a binary file that can only produce x-y plots of the variables specified within the input deck. This file is normally much smaller than the Restart file and can therefore be written to disk much more frequently. There also exists the opportunity to develop algorithms that can interrogate results from the calculation stage and write text files defined by the user. These are termed '***user subroutines***' and provide a great deal of functionality within ABAQUS analyses. Such a subroutine was written to interrogate the results file and output time, temperature, strain and strain rate in tabular form to a data file. This would then allow any calculations during the interstand model to take place where the data can be easily accessed.

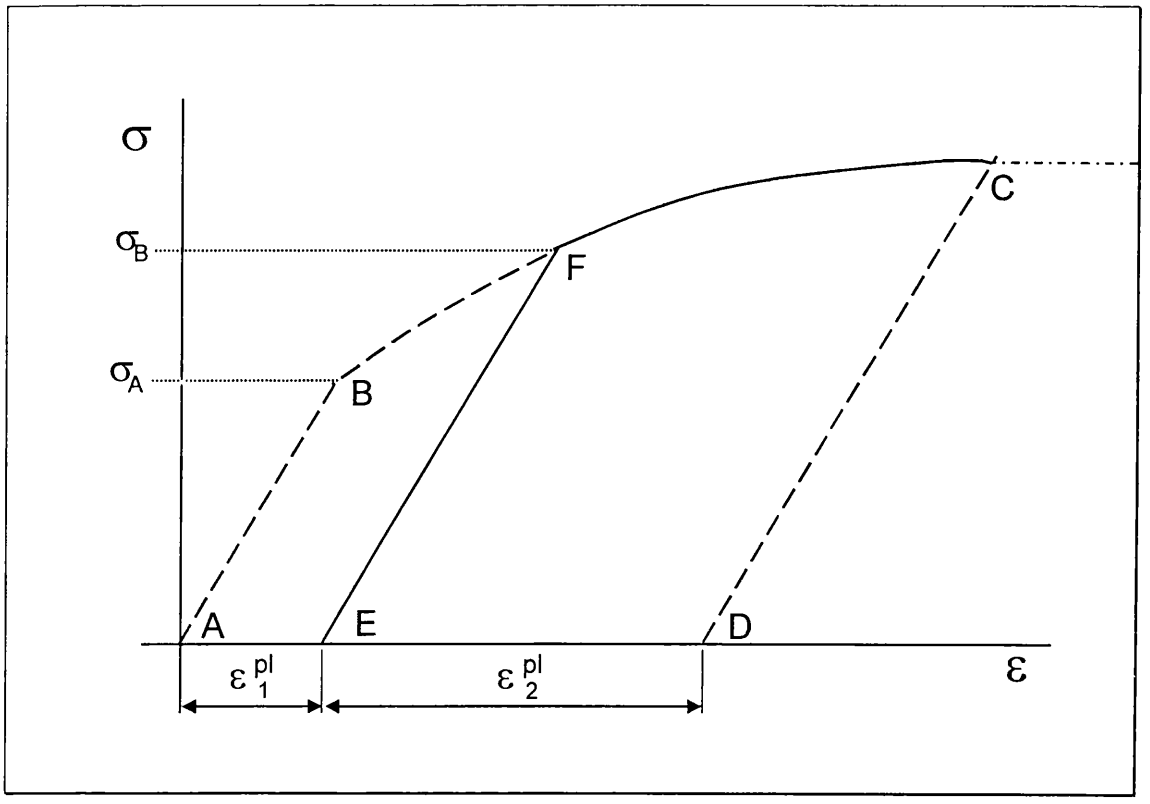

Figure 6.1 Effect of Initial Strain

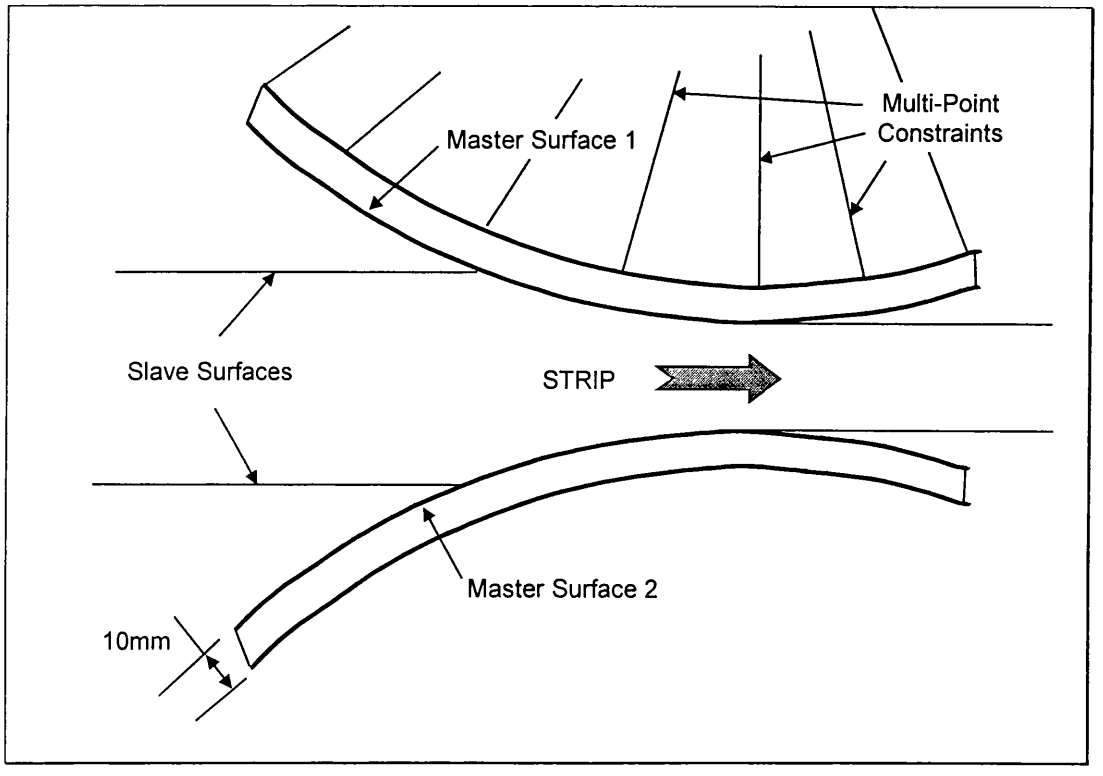

Figure 6.2 Geometry of Roll-gap Model with Master/Slave Surfaces

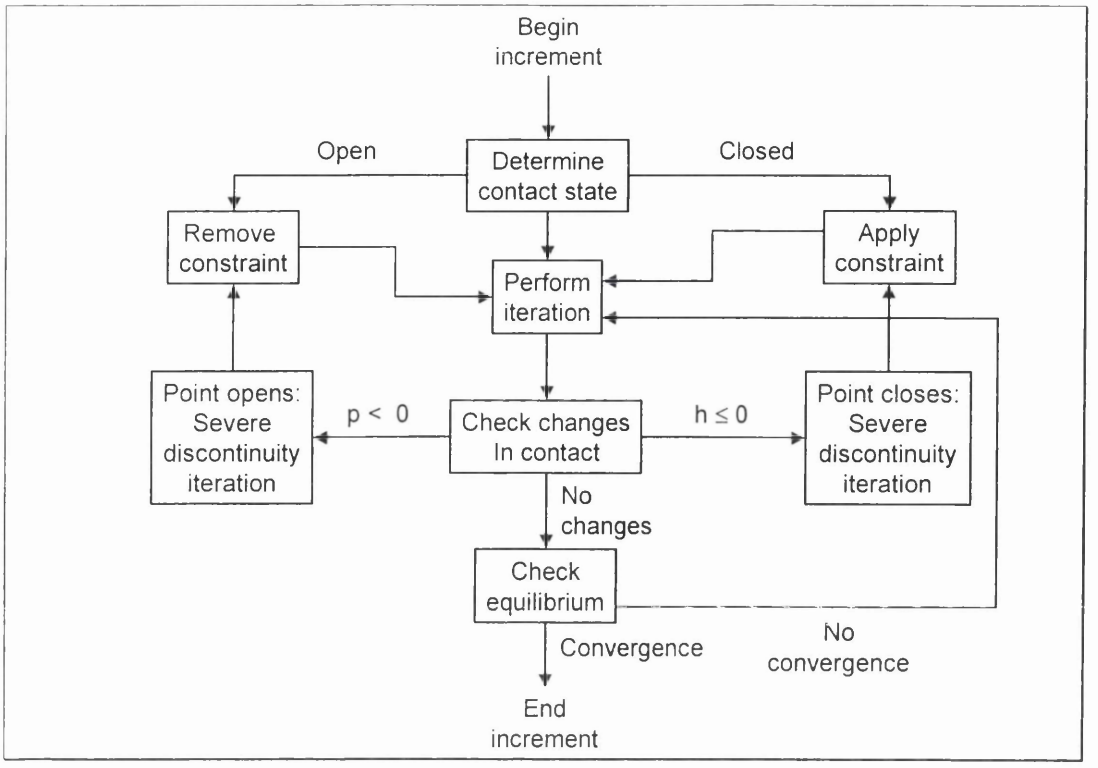

Figure 6.3 Contact Logic

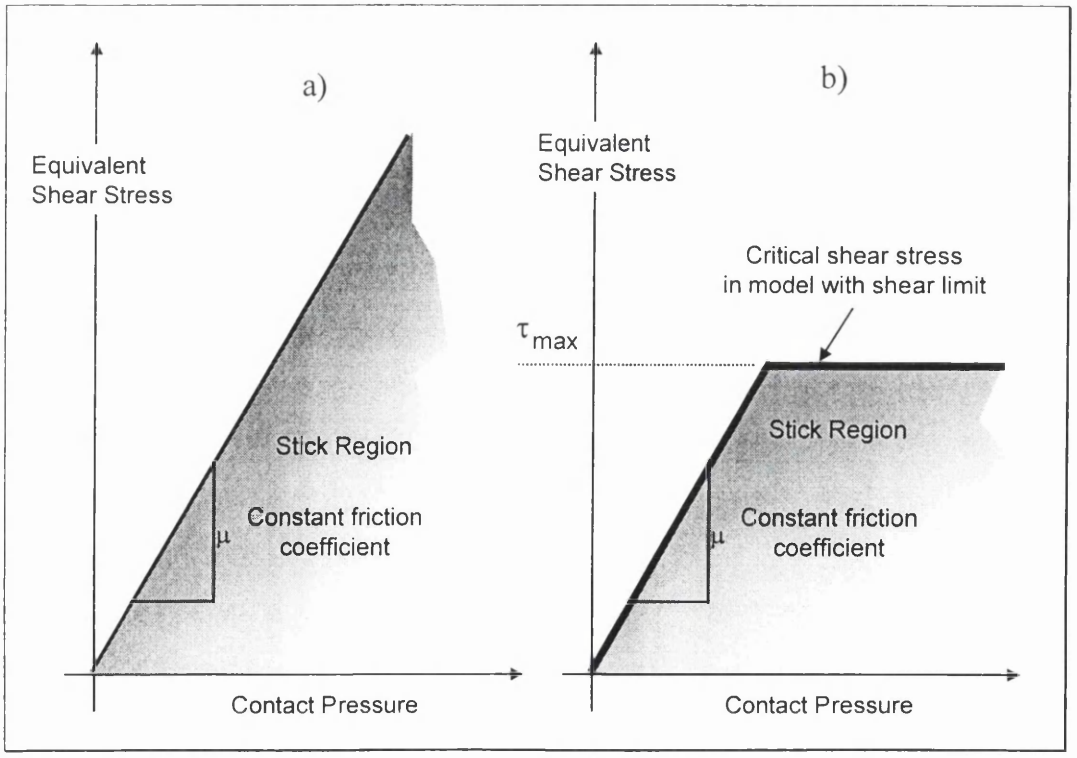

Figure 6.4 a) Coulomb-Amonton Friction law b) Shear Stress Limit

7 Interstand Model Development

7.1 Introduction

The development of an interstand model to take account of both the heat transfer and microstructural evolution during the periods between deformations was seen as fundamental to the development of a complete finishing mill simulation tool. This chapter describes the efforts to create such a program with both the practical and numerical considerations illustrated in figures 7.1 and 7.2.

7.2 Interstand Thermal Model

The first practical function of the interstand model was to record the temperature variations through the strip gauge during any roll-gap model and link the results to a subsequent interstand model. This was achieved from the development of various Fortran 90 routines that import the temperature results from the previous roll-gap analysis onto the interstand mesh. For convenience the same number of elements were used through the gauge for both the interstand and the deformation models. Once all the required nodal temperatures had been imported from the roll-gap model the interstand thermal model could solve the heat transfer equations for the prescribed time period.

The interstand thermal model considered the time period between two deformations as a two-dimensional heat transfer problem and included the bulk heat flow due to high speed motion but ignores heat conduction in the rolling direction. This model design was justified from the assumptions that heat transfer in the width direction was uniform and conduction in the rolling direction was negligible compared to the heat transfer by bulk motion [45,61]. Due to the nature of the Finite-Element technique only a single column of elements would therefore be required to calculate the temperature distribution through the gauge in a discretised manner as shown in figure 7.1. The heat transfer elements chosen for the interstand model required boundary conditions to be defined for the radiation to the surroundings and any convection to the interstand cooling sprays.

To simulate the water-cooling a convection or *film* routine was developed to create a heat flux on the surface of the material to simulate this transient cooling effect. However, the hostile environment within the finishing mill (including large amounts of water spray and water vapour) led to the unreliability of any quantitative study of the impingement areas of the interstand sprays unreliable. This difficulty led to the assumptions that the water from the cooling headers impacted the lower surface of the strip and fell away immediately due to gravity and the water that impacted the top surface was assumed to only cover the strip up to the maximum height of the looper as shown in figure 7.2. In practical terms this meant that the convection routine would only be active over half the total time period for the interstand model with the convective coefficient considerably reduced for the lower strip surface. Due to the rapid effect of the water-cooling it was necessary to prescribe a maximum time step of 0.15s to capture this transient cooling effect.

Radiation effects were taken into account using equation 2.14 and convection coefficients for water-cooling were based upon Hodgson et al [122] with their investigations into water quenching of hot plates. Coefficients between 800 and 600 $Wm^{-2}K^{-1}$ were applied to the top and bottom surfaces respectively to simulate water-cooling during hot finishing rolling.

7.3 Interstand Microstructural Algorithm

Until recently empirical algorithms to describe the microstructural evolution were only used with analytical models. Therefore bulk data was used as input to these models and any metallurgical calculations such as fraction statically recrystallised or prediction of the recrystallised austenitic grain size could only be performed globally. With the development of new computational techniques coupled thermal-microstructural algorithms are now able to predict these variables in a discretised manner. Such algorithms, based on the Avrami equation (Equation 2.33), have been developed within the interstand Finite-Element model using Fortran 90 routines. These routines interrogate the interstand thermal model results for each increment of time and create tabular output of the fraction softened, resulting accumulated strain and recrystallised austenite grain size if applicable.

7.3.1 Fractional Softening

Static recrystallisation is the predominant softening process after hot deformation. During hot rolling the material is deformed under interrupted, non-isothermal conditions where the dislocation density is increased within the material during the deformation stages. This stored energy makes the microstructure unstable and if the material is subsequently held at temperature further structural changes occur by static recrystallisation. The kinetics of static recrystallisation can be well described by the Avrami equation as described in chapter 2.7.

Empirical equations of state reflecting the fraction statically recrystallised with an activation energy and time to 50% softened can be expressed as a function of strain, strain rate, temperature and initial microstructure [106]: -

$$t_{0.5} = A'' \varepsilon^{p} \dot{\varepsilon}^{q} d_o^{r} \mathrm{Exp}\left(\frac{Q_{sof}}{RT}\right) \tag{7.1}$$

Where A, p, q, r, Q_{sof} are material specific constants. Most notably within this equation the temperature dominates the time to 50% softened. After deformation, in the majority of commercial applications, the stock temperature changes with respect to time. A reduction in temperature will therefore cause a change in the restoration kinetics within the deformed material. Non-isothermal conditions are taken into account during the interpass period by calculating the temperature for each increment of time according to section 7.2 and allowing the resultant rate of softening to be calculated according to [106]: -

$$\frac{dX}{dt} = (1-X)\left(\frac{0.639k}{t_{0.5}}\right)\left(\frac{-\log_e(1-X)}{0.639}\right)^{\left(1-\frac{1}{k}\right)} \tag{7.2}$$

Multiplication of **dX/dt** by the time increment will give the fraction recrystallised in that particular time period according to the previous deformation conditions and current

material characteristics. Summation of the individual softening calculations will then give the total softening occurring between passes.

7.3.2 Accumulated Strain

Incomplete restoration of the microstructure between passes is possible especially between the latter stands where the temperature of the strip is lower and the interpass periods smaller. The effect of incomplete softening must be taken into account to enable the accurate calculation of the hot deformation characteristics of a material that has retained strain from a previous deformation. Due to the condition of equation 2.33, **X** will never reach one or zero and so for computational purposes upper and lower limits for the calculation of the fraction softened were set to 0.95 and 0.05 respectively. Therefore, when the fractional softening calculation is less than 95% complete during the interpass period the steel has retained strain from the previous deformation. On entering any subsequent roll-gap model the strain will now be a function of the strain during the deformation and the retained strain from the previous pass according to: -

$$\varepsilon = \varepsilon_n + (1 - X)_{n^{-1}} \tag{7.3}$$

Where n is the current roll-gap and **X** is the fraction restored for pass n^{-1}. The finishing mill model takes account of this 'retained strain' within the microstructural algorithm by calculating the initial strain (ε_I) that can be applied to any subsequent deformation (**n**). It is important to note that the flow stress for the next deformation is calculated using the normal hyperbolic sine law as if the material was fully restored. However, the initial flow stress will be at a strain of ε_I . The strains from the roll-gap deformation will therefore be greater than if the material was fully restored resulting in higher flow stresses and faster softening kinetics during the next interpass period.

7.3.3 Recrystallised Austenite Grain Size

After static recrystallisation is complete the recrystallised austenite grain size can be calculated. Due to the incremental nature of the interstand model the calculation of the recrystallised grain size only takes place once the fraction softened has exceeded 0.95.

During hot rolling the significant factors on the recrystallised austenite grain size are the initial grain size and the magnitude of strain. For a low carbon steel the austenite grain size can be calculated according to [106]: -

$$d_{rex} = A\varepsilon^{-a} d_o^b \tag{7.4}$$

Where d_o is the initial austenite grain size. From the above equation it can be seen that the recrystallised grain size increases with initial grain size and decreases with applied strain.

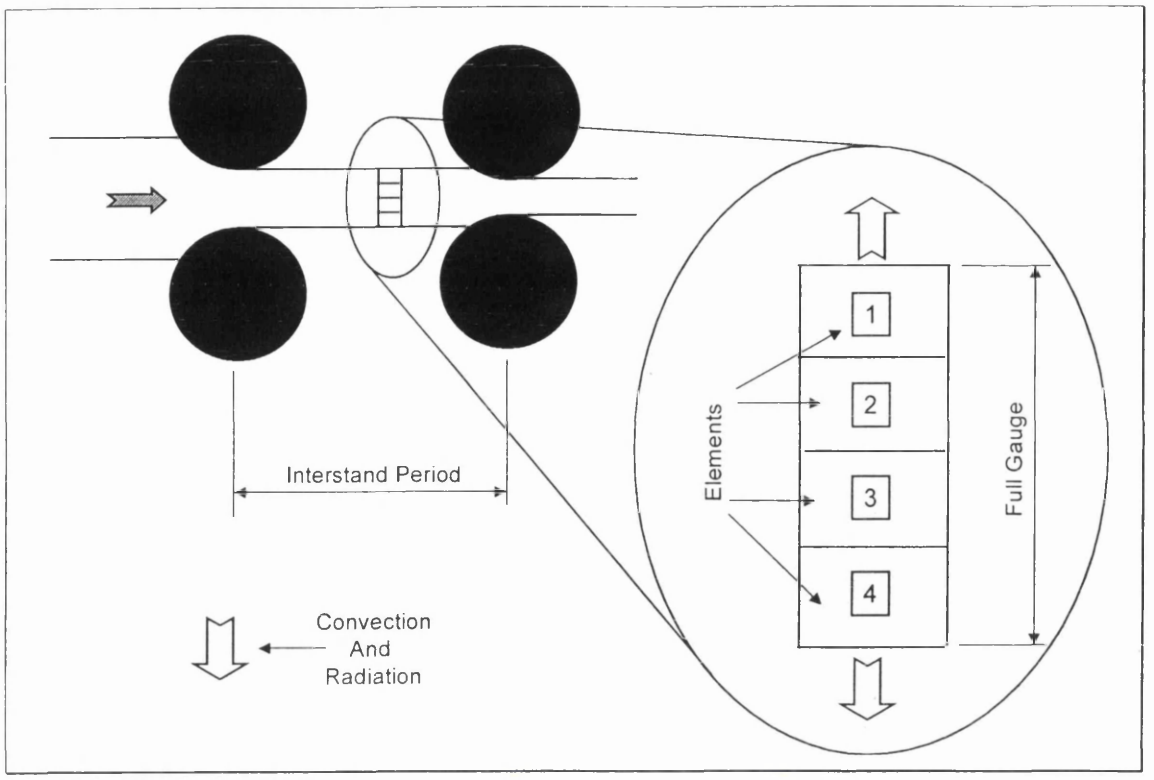

Figure 7.1 Schematic of the Interstand Model

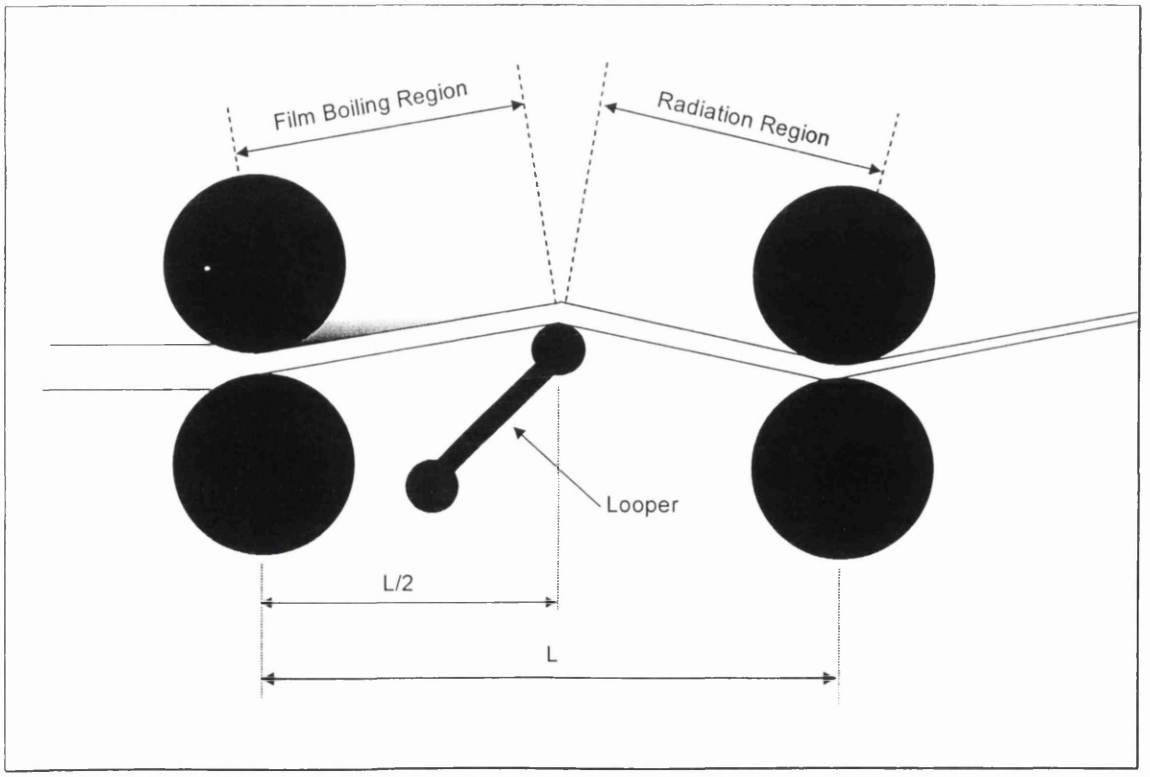

Figure 7.2 Practical Interstand Considerations

8 Results and Discussion

This chapter describes all the results from the work completed. It includes experimental results of the material testing and its implementation within a complete finishing mill simulation. It also shows individual calculations for roll force, temperatures and fractional softening calculations compared to those measured from an industrial finishing mill when possible.

8.1 Material Model

One of the most important components of the finishing mill model is the characterisation of the material being deformed. The following sections describe some of the results from uniaxial compression tests and how these laboratory results can be extrapolated to those conditions experienced within a commercial hot strip finishing mill.

The ESH uniaxial compression apparatus described in chapter 5.3 provided all the necessary data required for the development of the empirical relationships described in chapters 2.7. These empirical relationships for both the dynamic and static behaviour permitted this experimental data to be extrapolated to predict the hot deformation characteristics of the high Carbon steel for conditions experienced during commercial finishing rolling.

8.1.1 Single Deformation Flow Stress Curves

The single deformation test matrix can be seen in table 8.1. The true stress/strain results for these tests are shown for temperatures 1123K to 1323K with increments of 50K in figures 8.1 to 8.6.

Temperature (K)	1123	1173	1223	1273	1323	1373
ε	0.5	0.5	0.5	0.5	0.5	0.5
$\dot{\varepsilon}$	0.0001	0.001	0.01	0.1	1.0	5.0	10.0	20.0	40.0

Table 8.1 Test Matrix for the Single Hit Compression Tests

It must be noted that the legends from these figures display the actual strain rate achieved during the test and not those prescribed by the operator. It can therefore be seen that the test apparatus found the hot strength of the material great enough to slow the hydraulic ram at the faster deformation rates of 20 and $40s^{-1}$. This indicated some of the limitations of this type of testing procedure for laboratory investigations into high strain rate deformations.

Although all the curves were unique several generic stages could be seen. All the test results display smooth curves that undergo yield and some work hardening. The true stress/strain curves then reach steady state with a minor amount of softening at larger strains. Only the tests carried out at the maximum deformation rate do not exhibit this definite steady state.

Some of the tests show a well-defined yield point where the linear increase in stress with strain was lost. This was most prevalent in figures 8.3 and 8.4 for the temperatures 1223K and 1272K respectively. All the flow curves above the deformation rate of $0.001s^{-1}$ display a smooth transition form this yield point to the maximum stress which in most cases also approximated the true stress at large strain.

The increase in flow stress for all the figures seemed fairly uniform with a decrease in temperature of 50K and an increase in strain rate of one order of magnitude. Some flow stress curves did however produce unexpected results. All the tests carried out at rates of 0.0001 and $0.001s^{-1}$ displayed similar results and indicated the lowest strain rate that required testing. Figure 8.1 shows the tests carried out at 1123K. Here the curves at a strain rate of around $20s^{-1}$ resulted in a flow stress less than the test carried out at a strain rate of $10s^{-1}$. On further inspection, all the tests carried out at a strain rate of $20s^{-1}$ deviated from their expected path. Through re-examination of the raw load/displacement test data it was found that the load sensors and data acquisition software were unable to capture the early part of the deformation. This problem was rectified by increasing the test data sampling rate for the faster strain rate of $40s^{-1}$.

By far the most significant variable during testing was the deformation temperature. Figures 8.7 shows that a temperature decrease of 200K more than doubled the maximum true stress at equivalent strain rates of $40s^{-1}$. A secondary effect on the maximum true stress was also identified as the strain rate. Figure 8.1 shows that an increase in the strain rate from 0.001 to $40s^{-1}$ increased the flow stress from 50MPa to approximately 300 MPa at 1123K. However, at 1373K (Fig 8.6) this increase was markedly reduced.

All the tests were prescribed a total deformation of 50% true strain. From the true stress/strain results it can be seen that this total deformation was only achieved at the faster deformation rates. This was due to the safety mechanisms within the experimental apparatus that decelerate the ram when approaching the maximum stroke according to the maximum ram rate of $500mms^{-1}$. When slower ram rates were chosen the ram failed to reach the total extent of the required stroke due to the resistance of the material. This was the reason for selecting a total deformation of 50% when only 40% would be required for the constitutive analysis. Furthermore, this also demonstrates that the material had reached steady state at 40% true strain for all of the tests.

8.1.2 Double Deformation Flow Curves

The matrix for the double deformation tests can be seen in table 8.2. Figures 8.8 to 8.13 show the true stress/strain deformation curves for the interrupt deformation tests.

Temperature (K)	**1123**		**1148**		**1173**	
Initial Strain (%)	**15**	**25**	**15**	**25**	**15**	**25**
Interrupt Time (s)	1	0.5	0.5	0.25	0.5	0.25
	2	1	1	0.5	1	0.5
	4	4	2	1	4	1
	6	8	4	2	8	2
	10		16		16	4
	16					

Table 8.2 Test Matrix for the Interrupt Compression Tests

To optimise the number of tests the initial strains were taken as 15 and 25%. This was the minimum number of tests required to accurately quantify the effect that deformation prior to holding at temperature has on the softening kinetics of the material. The strain rate was set to $0.1s^{-1}$ for all the interrupt compression tests. This strain rate was seen as a compromise between minimising the time required for each test whilst providing ramp rates that were slow enough to be captured using the ESH compression apparatus and associated software. The double deformation curves show the stress relative to both the initial strain and to the final true strain of 50%. Whilst the softening kinetics for each test were calculated on the complete flow curve the differences between the initial parts of the stress/strain curves for all the interrupt compression tests were found to be negligible.

Figure 8.8 shows the first double deformation test at 1123K with a 15% pre-strain. The initial flow curve can be seen to work harden up to 15% true strain whereas figure 8.9 shows that after an initial strain of 25% the flow curve has reached steady state. For comparison figure 8.1 shows the complete true stress/strain curve for this temperature where a strain rate of $0.1s^{-1}$ results in a fairly flat flow curve with a maximum stress of about 120MPa attained between 0.2 and 0.3 true strain. The second deformation flow curves in figure 8.8 starts with an interrupt time of 1 second. For clarity not all the secondary flow curves are shown, however softening can be seen after an interrupt time of 6 seconds. From figure 8.9, at the same temperature with an initial strain of 0.25, softening becomes apparent after an interrupt time of only 4 seconds. For this particular test the minimum interrupt time was reduced to 0.5s to capture the onset of softening.

Figures 8.10 and 8.11 show the interrupt compression tests at the intermediate temperature of 1148K. Softening can be seen in figure 8.10 after an interrupt time of 4 seconds compared to 6 seconds for the corresponding test at 1123K. For the tests carried out at this temperature with an initial strain of 25% the time period to incur significant softening was reduced to 2 seconds with almost complete softening at 4 seconds. This trend of increasing softening kinetics with increasing temperature is further emphasised in figures 8.12 and 8.13. Although there is a degree of experimental scatter for both these tests the maximum interrupt period required to capture almost complete softening was

reduced to 8 and 2 seconds for the interrupt compression tests with 15% and 25% initial strains respectively.

8.1.3 Softening Calculations

The calculation of the fraction softened was completed using the offset method described in chapter 2.7.5 where the ratio of the 0.2% proof stress from the first and second parts of the flow stress curve compared to the maximum stress of the first curve gives the fraction softened (see Equation 2.74). Software was developed within the laboratory to run on a personal computer to display the true stress/strain curves and perform this analysis.

The restoration indexes for the material at 1123K at 15% initial strain gave a fraction softened of 8% at the interrupt time of 1 second. This was seen as the minimum amount of softening that could be expected using this type of apparatus. For the 25% initial strain the minimum time increment was reduced to half a second to capture the onset of softening. This time increment still represented a 16% softening and was the minimum fraction restored that could be achieved at this temperature. The maximum time increment for this test was set at 16 and 8 seconds for the 15% and 25% initial strain tests respectively. Whilst the testing at this temperature produced some experimental scatter the sigmoidal nature of the curves can still be seen in Figure 8.14.

An increase in temperature of 25K for the interrupt compression test is shown in figure 8.15. Again the increase of 15% to 25% true strain for the first part of the deformation produced a significant increase in the rate of softening. Both the series of tests experienced the minimum softening at smaller interrupt times than seen previously in figure 8.14. In order to account for this a test at 25% initial strain was carried out with an interrupt time 0. 25 seconds. The result was still above the 10% softened marker.

As expected, a further rise in temperature of 25K to 1173K increased the softening kinetics for the both the 15% and 25% initial strain tests. From an overall perspective the 25% initial strain tests softened faster than the 15% tests for all the temperatures. The 25% initial strain tests for both the 1148K and 1173K showed very little difference between their softening characteristics whereas the differences between 1148K and

1123K were more significant. The three tests at 15% initial strain resulted in a fairly regular decrease in the rate of softening with the decrease in temperature.

8.2 Constitutive Development

The conditions experienced during commercial hot rolling are rarely simulated within the laboratory. In order to extrapolate the results achieved during the thermomechanical simulations the hyperbolic sine law has been used. The mechanical constitutive relationship between stress (σ), strain rate ($\dot{\varepsilon}$) and temperature (T) is: -

$$\sigma = \frac{1}{\alpha}\sinh^{-1}\left[\left\{\frac{\dot{\varepsilon}}{A}\exp\left(\frac{Q}{T}\right)\right\}^{\frac{1}{n}}\right] \qquad (8.1)$$

The three critical stresses from each flow stress curve can then be described using Equation 8.1 combined with the required constants for: -

1. Yield Stress
2. Maximum stress during hot deformation
3. Stress at large strain e.g. 50%

To predict these three stresses using equation 8.1 the constants ***A, α, n*** and ***Q*** are required for each stress condition and the methods employed to calculate these values will be discussed in the following sections.

8.2.1 Determination of n

The development of the hyperbolic began with the estimation of the exponent ***n***. At low stresses the hyperbolic sine law can be broken down to a power relationship: -

$$\sigma = \frac{1}{\alpha}\left[\frac{\dot{\varepsilon}}{A}\exp\left(\frac{Q}{RT}\right)\right]^{\frac{1}{n}} \qquad (8.2)$$

or: -

$$\dot{\varepsilon} = A[\sinh(\alpha\sigma)]^n \exp\left(-\frac{Q}{T}\right) \tag{8.3}$$

At low stresses, a plot of $Log_{10}\sigma$ vs. $Log_{10}\dot{\varepsilon}$ will give a line of slope ***n***. This is done at the highest testing temperature where the flow stresses are the lowest and ($\alpha\sigma$) is the smallest. The maximum deformation temperature during this study was 1373K. Figures 8.17 to 8.19 show initial estimates for ***n*** according to yield stress, maximum stress and stress at large strain. On initial examination of the data a general trend could be seen where the stress increases with increasing strain rate. The trend is also linear especially for Figures 8.18 and 8.19 corresponding to the maximum stress and stress at large strain. These curves help validate the application of the above assumptions and equation 8.2. The greatest deviation form this exponential approximation occurred for yield stress values in figure 8.17. This was a direct consequence of some flow stress curves not providing a definite point of yielding. From these trends it can be seen, even when considering the scatter observed for yield stress, increasing strain results in a decreasing value of ***n***.

8.2.2 Determination of the α value

The second phase of the development of the hyperbolic sine law required derivation of the constant α (MPa^{-1}) for the high Carbon steel. At the high stresses the hyperbolic sine law reduces to an exponential relationship: -

$$\sigma = \frac{1}{\beta}\left[\frac{Q}{RT} + Ln\frac{\dot{\varepsilon}}{A}\right] \tag{8.4}$$

$$\beta = \alpha n$$

Hence at the lowest temperature of 1123K i.e. the highest stresses a semi-logarithmic plot of σ vs. $Log_e\dot{\varepsilon}$ gives a line of slope αn. Since ***n*** is already known, the value of α

can be found. Figures 8.20 to 8.22 show that as the rate of reduction increases the flow stress increases. The linear nature of these results shows equation 8.4 to be a good representation of the change in flow stress with deformation rate and temperature.

8.2.3 Q and A values

Since α and n are now known, **Q** and **A** were found by rearranging the hyperbolic sine law as: -

$$\ln\left\{\dot{\varepsilon}[\sinh(\alpha\sigma)]^{-n}\right\} = \ln A - \left(\frac{Q}{T}\right) \qquad (8.5)$$

For each strain rate and stress combination at each temperature the left-hand side of equation 8.5 can be plotted against the inverse of the deformation temperature (1/**T** x 100,000). The slope of this line will give the value of **–Q/R**, and the intercept gives Ln**A**. Experimental scatter can easily be seen for each of the figures 8.23 to 8.25 although the sinh term can be seen to decrease with increasing as temperature. Regression analysis reveals initial estimates of Q/R of 54377, 43273 and 45620 for the yield stress, maximum stress and stress at large strain respectively. The estimates for Ln**A** are 46.842, 35.519 and 35.997 for the yield stress, maximum stress and stress at large strain respectively. Table 8.3 gives the initial estimates of the constants. The inverse of the temperature and the natural logarithm of **A** are maintained to avoid either small numbers where rounding up errors may occur or excessively large numbers where exponentials would be required.

Variable	Yield Stress	Maximum Stress	Stress at 40% Strain
α (m^2MN^{-1})	0.01199	0.00673	0.00831
N	8.9855	6.1380	5.8011
Q ($kJ\ mol^{-1}$)	452	360	379
ln A	46.842	35.5190	35.9970

Table 8.3 Initial values for constants of the Hyperbolic Sine Law.

8.2.4 Final constants for the Hyperbolic sine law.

Least squares regression was then carried out on all the constants for the hyperbolic sine law. Table 8.4 presents the final values for A, α, n and Q respectively.

Variable	Yield Stress	Maximum Stress	Stress at 40% Strain
α (m^2MN^{-1})	0.00433	0.00431	0.00545
N	7.3072	5.3985	5.0452
Q (kJ mol^{-1})	311	281	272
ln A	40.5262	30.5818	28.3339

Table 8.4 Final values for constants of the Hyperbolic Sine Law.

Figures 8.26 to 8.28 show how the final constants give the predicted flow stresses for yield stress, maximum stress and stress at large strain with their associated measured values over the entire test matrix. The greatest experimental scatter was associated with the prediction and selection of the yield stress as mentioned earlier. Due to this difficulty not all the estimated yield points were included during this stage of the analysis. Improved correlations can be seen in figure 8.27 and 8.28 for the prediction of maximum stress and stress at large strain. Some data points were also omitted from these analyses due to the fact some curves did not have a definite point where maximum stress occurred. Over the entire data set the increase in flow stress with increasing strain rate and decreasing temperature can easily be seen.

8.2.5 Strain at Peak Stress

One of the most important variables when calculating flow stresses by the hyperbolic sine law is the strain at which maximum stress occurs. For each of the deformation curves the strain at which maximum or peak stress occurred was noted. The best fit of the experimental data was given by: -

$$\varepsilon_p = A'\dot{\varepsilon}^{n'} \exp\left[\frac{Q_p}{RT}\right] \qquad (8.6)$$

The best-fit constants are given in table 8.5 and the measured vs. predicted strains at which maximum stress occurred are shown in figure 8.29.

Variable	Strain at Peak Stress
Ln A'	1.939
n'	7.356 E-02
Q_p (kJ mol^{-1})	5.166

Table 8.5 Final Constants for the Strain at Maximum Stress.

Whilst all the constants have been derived directly from experimental data, any physical association with any or all of the constants has been discouraged due to the statistical methods employed during the regression of these values.

8.2.6 Modelling Flow Stress Evolution with Strain

Whilst the hyperbolic sine law combined with the equation to predict the strain at maximum stress predicts the three critical flow stresses with changing temperature and strain rate it cannot define the path of the flow stress with increasing strain.

This is accomplished by a series of linear and non-linear equations that define the change in stress with strain between the three critical stress defined by equations 8.1 and 8.6.
The change in stress with strain is assumed linear until the yield point. After yield the rate of increase in stress with strain reduces until $\delta\sigma/\delta\varepsilon$ becomes zero. The material is now at the peak or maximum stress. Between zero plastic strain and the strain at peak stress the binomial equation 8.7 is used: -

$$\sigma_{(0,\varepsilon_p)} = \left[\frac{\sigma_y - \sigma_p}{\varepsilon_p^2}\right]\varepsilon^2 + 2\left[\frac{\sigma_p - \sigma_y}{\varepsilon_p}\right]\varepsilon + \sigma_y \qquad (8.7)$$

Further straining will take the material past the maximum stress and depending on the deformation conditions and the internal structure, the material will either maintain this stress or the softening mechanisms will overcome the work hardening and the flow stress

will drop and reach steady state. This part of the flow stress curve can be effectively modelled with the linear equation: -

$$\sigma_{(\varepsilon_p,0.5)} = (\varepsilon - \varepsilon_p)\left[\frac{\sigma_{0.5} - \sigma_p}{0.5 - \varepsilon_p}\right] + \sigma_p \qquad (8.8)$$

If the true strain becomes larger than 0.5 it is assumed that the flow stress maintains the stress determined by the stress at large strain solution (See Figure 2.5).

8.3 Avrami Development

The Avrami type equation was used to describe the static softening. To model the softening after an initial deformation and holding time, t, the material would be restored by fraction **X** as described by: -

$$X = 1 - \exp\left(-0.639\left[\frac{t}{t_{0.5}}\right]^k\right) \qquad (8.9)$$

Where $t_{0.5}$ is the time to 50% restored. Interrupt compression testing provided the data to derive the Avrami exponent, k. Figures 8.30 to 8.32 show the double logarithmic curves for the fraction softened against the interrupt time. All the figures show a linear relationship for both the initial strains of 15% and 25% true strain. The softening also shows a general distribution with similar softening gradients for all the tests with increasing temperature resulting in accelerated softening.

Least squares regression was carried out over the entire double compression experimental matrix to derive the best fit value for the exponent k. The best fit value was found to be 0.973.

8.3.1 Time to 50% Softened

To complete the Avrami equation the time to 50% softened also required development. From the final measurement of k the time at which 50% softening had occurred could be found. The equation for 50% softened was taken as: -

$$t_{0.5} = A''\varepsilon^{p}\dot{\varepsilon}^{q}\exp\left(\frac{Q_{sof}}{RT}\right) \tag{8.10}$$

Statistical regression using the least squares method was again applied to the entire double hit testing data to remove as much experimental scatter as possible. Figure 8.33 illustrates that raising the temperature from 1123 to 1173K decreased the time to 50% softening and therefore increased the rate of the softening kinetics. The relevant activation energy (Q_{sof}) was derived by employing the common expression: -

$$t_{0.5} \propto \mathrm{EXP}\left(\frac{Q_{sof}}{RT}\right) \tag{8.11}$$

Regression analysis was carried out on the entire set of results from figure 8.33 with a Q_{sof} result of 183.86 kJmol^{-1}. The effect of the initial strain can be seen in figure 8.34. Here increasing the initial strain reduces the time to 50% softened, thereby increasing the rate of softening. Regression analysis determined the best-fit constant p to be 2.8223. Strain rate and initial grain size were not determined for this steel as they were deemed to be minor considerations after chapter 2. The complete set of constants for the static softening calculations can be seen in table 8.6.

Steel	k	A''	P	Q_{sof} (kJmol^{-1})
High Carbon	0.973	7.78E^{-11}	-2.8223	183.86

Table 8.6 Final Constants for Fractional Softening

8.4 Discussion of the Hot Deformation Characteristics

8.4.1 Single Deformation

During the single deformation testing it became clear that changes in strain rate and temperature greatly affected the true stress/strain curves as shown in figures 8.1 to 8.7. This effect confirmed the sensitivity of the apparatus and software to the hot deformation characteristics of the material. The experimental matrix was designed to capture this behaviour whilst avoiding high strain rates that could overload the apparatus. One of the major considerations during testing was to avoid large contact areas between the tooling and the test piece that could result in nonhomogeneous deformation. However, as all the flow stress curves can be seen to have entered steady state, strains above 50% were unnecessary.

Further examination of the flow stress curves revealed that no significant drop in the flow stress occurred that would have indicated dynamic recrystallisation was taking place as shown in figure 2.4b. Any decrease in flow stress at the fastest rates of deformation was considered attributable to adiabatic heating as the lower temperature tests exhibited this phenomena to a greater degree. Therefore, the individual flow curve characteristics indicated the material was undergoing dynamic recovery [104] where subgrains began to form as the strain increased. In general subgrain size decreases with work hardening but this effect was ameliorated by dynamic recovery that tended to make the grains grow. At large strains the two processes achieved a balance so that the size of the subgrains remained constant with strain. This had the consequence of maintaining a constant or steady-state flow stress.

The lowest temperature during testing was 1123K and represented the minimum rolling temperature for this particular grade as any further reduction in temperature could represent a mixed microstructure of austenite and ferrite. Whilst it may have been useful to accurately determine the Ar_3 temperature through experimentation the scope of this project was deliberately limited as this grade was only to be processed within the austenite temperature range.

Analysis of the three critical stresses of Yield stress (σ_y), Maximum stress (σ_M) and Stress at large strain (σ_L) provided the raw data to derive the constants **A**, **n**, α and **Q** for the application of the Hyperbolic Sine Law. Whilst it was difficult to apply any real physical significance to these constants, due to the numerical techniques employed to find the best fit, **Q** provided the greatest reflection on the hot deformation characteristics of the high Carbon steel. Table 8.4 shows how **Q** decreased from 311 to 272 $kJmol^{-1}$ with increasing strain. It can therefore be deduced that resistance to hot deformation increased with increasing strain, which was revealed with decreasing values of **Q**. Previous studies have compared this value to that of self diffusion at approximately $300kJmol^{-1}$ which is in agreement with this study. However, an average **Q** value of $300kJmol^{-1}$ for the High Carbon Steel was significantly lower than that reported for both Carbon Manganese and Low Carbon steels [106].

Modelling the evolution of stress with strain was carried out according to section 8.2.6. Figure 8.35 shows the schematic of a cylinder-upsetting example that was used to verify the High Carbon material model. Due to symmetry only one quarter of the cylinder was represented with axisymmetric elements. Figure 8.36 shows how the Finite-Element results of the compression test carried out at 1323K and strain rate of $1s^{-1}$ compared with the experimental true stress/strain curves. As expected the greatest errors occurred around the yield stress where observations of the experimental yield stresses proved difficult. Prediction of the strain at which maximum stress occurred during the Finite-Element analysis proved much less problematic. The prediction of the stress at large strain (40%) was also satisfactory with the Finite-Element results being slightly greater than the measured flow stress.

The results from figure 8.36 show that the hyperbolic sine law can accurately predict the three critical stresses even without an initial austenite grain size term. The results also show that the method of calculating the evolution of stress with strain using binomial and linear relationships can also accurately predict the flow stress for the High Carbon material.

8.4.2 Interrupt Compression

The interrupt compression method is perhaps the simplest tool for the determining the softening kinetics of a material. Direct microstructural analysis through optical measurements was not carried out during this research due to the time consuming and laborious nature of the technique and difficulties experienced when attempting to reveal the prior austenite grain boundaries. The softening calculations for the interrupt tests were made with the offset method since at high temperature the yield strength is a sensitive measure of the microstructural state. This method also provides insensitivity to any dynamic recrystallisation that may occur during the initial or secondary strains. As zero softening was measured at the minimum interrupt times no back extrapolation was required, further simplifying the calculation of static softening.

To model the softening kinetics the Avrami equation was combined with the prediction for 50% softening. The time to 50% softened was preferred to the time to 95% softened as it was seen as more reliable with less sensitivity to experimental errors. The exponent k from the Avrami equation was determined from figures 8.30 to 8.32 and although this constant was probably a complex function of the deformation conditions and austenite structure, over the experimental conditions investigated k remained relatively constant.

Investigation into static softening confirmed that the driving force was determined by the amount internal energy within the material. The amount of initial strain was of critical importance to this internal energy and significantly affected the softening kinetics. Increasing the applied strain increased the dislocation density produced by the deformation and consequently increased the driving force for softening.

The dependence of strain on the time to 50% softening was investigated with initial strains of 15% and 25%, shown in figure 8.34. From [106,107,108,109] a power law relationship for strain exists (ε^p) where the parallel lines in figure 8.34 suggest a relatively constant value of p for the experimental conditions. One of the main considerations of the time to 50% softened was the insensitivity to strain path. However, as flat strip rolling was seen as a compressive metal forming process all the strains should actually be compressive. Sensitivity of the time to 50% softened with Strain rate was ignored during the testing as literature notes that this is by far the weakest of the

parameters of deformation with respect to static softening. Anderson [106] quoted strain rate exponents of -0.9 and -0.6 for low Carbon and Carbon Manganese steels (q) in equation 8.1. When taking into account the relatively limited strain rates encountered during finishing rolling with those experienced during wire extrusion for example this effect can be neglected.

The effect of temperature on the time to 50% softened was investigated in figure 8.33 where a function of the time to 50% softened was plotted against the reciprocal of the absolute temperature. As recrystallisation and recovery are diffusion-controlled processes the deformation temperature had a dominant effect on the rate of softening. Within this calculation Q_{sof} was seen as a function of both the recovery and recrystallisation kinetics and therefore represented 'pseudo' activation energy. The Q_{sof} result of 183 $kJmol^{-1}$ was low in comparison to other steels [106].

During the interrupt tests where the specimens were unloaded at strains less than the strain to maximum stress, as in the case of the 15% strain tests, classical static recrystallisation took place as shown in figure 2.6. The softening mechanisms were recovery followed by the nucleation of recrystallised grains that grow by grain boundary migration [107]. During interrupt testing where the flow stress had reached steady-state, as in the case of the 25% strain tests, various types of intragranular substructures exist which correspond to the various stages of the restoration processes. From Djaic and Jonas [108] softening then took place by metadynamic recrystallisation and static recovery.

Derivation of the Avrami equation permitted incremental calculation of the fraction softened with respect to strain and temperature where >0.95 and <0.05 represented fully restored and work hardened structures respectively. Figure 8.37 represents the test results for time to fraction softening versus the predicted values using the numerical techniques discussed earlier. It can be seen that both the Avrami equations and the time to 50% recrystallised equation model the physical phenomena well.

During hot rolling it is likely that partial static recrystallisation will occur in multipass deformation that will introduce a mixed microstructure prior to the next deformation.

Incorporating retained strain from a previous deformation through a *1-X* function as shown in equation 7.3 was in effect a simplification of the physical problem but did satisfy the numerical objective of increasing the total strain during any subsequent deformation.

One of the major shortcomings of the Finite - Element metallurgical approach is that it is developed from empirical metallurgical algorithms, based on Avrami equations and multiple microstructural analyses. Errors in predicting the recrystallisation kinetics can be present, owing to the type of method adopted for grain analysis, or to the choice of regression methods.

8.5 Rolling Simulations Results

The Finite-Element model of the finishing mill was used to simulate various rolling schedules for different grades of materials. One of the main advantages of describing the roll-gap using discretised techniques is that independent variables such as strain and strain rate can be analysed at any point during rolling. The first part of this section therefore covers some of the more important results from single roll gap analyses that are important to any subsequent microstructural analyses. Latter sections refer to the results from multi-pass simulations with special attention given to the thermal and microstructural evolution within the finishing mill.

8.5.1 Single Stand Results

Figure 8.38 shows the initial temperature distribution given to the transfer bar at entry to the finishing mill according to the pyrometer readings positioned at the entry to the finishing mill as shown in figure 3.3. The subsequent Finite-Element heat transfer analysis takes account of any thermal losses at the surface of the transfer bar during the period between either the coilbox or Enco heat retaining panels at Port Talbot and Llanwern respectively and the first finishing mill stand. From figure 8.39 the non-uniform thermal field at entry to the first finishing stand can clearly be seen.

The first 2-D, plane strain roll-gap analysis was programmed to represent a typical first stand reduction pattern of 50% at a linear velocity of $1.3ms^{-1}$ as shown in table 8.7.

Rolling Parameter	Stand 1	Stand 7
Entry Gauge (m)	0.035	0.003
Exit gauge (m)	0.0175	0.0025
Reduction (%)	50	16.7
Strip Width (m)	1.02	1.02
Linear Strip Velocity (ms^{-1})	1.3	11.0
Roll Radius (m)	0.350	0.370
Temperature - Top (°C)	1040	860
Temperature - Bottom (°C)	1030	860

Table 8.7 Typical Stands 1 and 7 Rolling Data.

Figure 8.40 illustrates the deformed mesh with the hot deformation characteristics of the material provided by the hyperbolic sine law for the high Carbon steel described within section 8.2. This deformed mesh plot illustrated the dramatic displacements that were incurred at the head end of the strip during threading into the roll-gap. These large displacements render this area unsuitable for microstructural analysis aimed at representing the main body of the material. The deformed mesh plot also identified how the material was pulled through the roll gap by the mechanical interactions between the work roll and the surface of the strip.

Figure 8.41 shows the total equivalent plastic strains generated during the first pass of the finishing mill. This plot also provides overwhelming evidence that plane sections do not remain plane during finishing rolling and therefore, inhomogeneous deformation is an important characteristic during hot finishing rolling. On further examination, if we take any vertical section through the gauge of the strip, the maximum plastic strains appear near the roll/strip interface with the minimum strains occurring along the centre line of the material.

Strain rates are also of interest as the hot deformation characteristics of the material are strain rate dependent. Figure 8.42 shows the *y-y* component of strain rate. The high strain

rates, shown as red in this contour plot, are initially seen at the surfaces near entry to the roll-gap. Conversely along the centre line of the strip the higher strain rates are identified further into the roll-gap with some elastic recovery taking place at exit of the deformation zone. Shear strain rates shown in figure 8.43 are predominantly seen at the surface of the strip with the lower and upper surfaces having opposite sign. These signs only represent the direction rather than the type of strain as strain rate, like strain, has no sign.

One of the most important parameters when attempting to model the deformation and microstructural behaviour of carbon steels is temperature. Figure 8.44 shows the temperature distribution for the first stand of the finishing mill. Although the surfaces are at a lower temperature than the body of the material at entry to the finishing mill this is exaggerated during the deformation due to conduction to the rolls which are at a much lower temperature and heating of the body of the strip due to the plastic deformation. Whilst the effect of roll chilling can be up to 300°C this plot illustrated the limited penetration of this roll chilling during the first stand of the finishing mill. Both the magnitude and distribution of the thermal results were similar to those reported by Lenard and Pietrzyk [60] for finishing stand thermal analyses. Finally, for the first stand, the Mises stress distribution is plotted in figure 8.45. As a combination of the strain, strain rate and strip temperature the greatest stresses are seen at the surface where the strip nears the roll-gap exit.

A single stand analysis was also carried out for the last stand of the finishing mill to investigate the sensitivity of the roll-gap model to changing deformation parameters such as speed, reduction and temperature. The complete listing of deformation conditions for the last stand of the finishing mill are given in table 8.7. Figure 8.46 shows the temperature distribution and although there is similar temperature contours to that given in figure 8.44 for the first finishing mill stand the magnitude of this distribution is around 40°C compared with 280°C for the first stand. Figure 8.47 shows the components of strain rate (A,B), total equivalent plastic strain (C) and the Von Mises stress distribution (D). All are similar to those seen for the first stand with magnitudes that represent the lower reduction and increased speed.

In order to validate the roll-gap model against measured rolling loads from commercial finishing mills it was first necessary to investigate the numerical sensitivity to the most important rolling parameters such as temperature. Figure 8.48 Shows the results for both the first and last finishing stands with respect to the reaction force at the centre of the work rolls, corresponding to rolling load, and initial temperatures ranging from 850 to 1050°C for stand 1 and 800 to 900°C for stand 7. Both curves illustrate how increasing temperature reduces the rolling load for each case. However, the sensitivity of force to temperature ($\delta P/\delta T$) was approximately -57 for finishing stand 1 and only -21 for stand 7.

Perhaps the most significant factor directly affecting the reaction force is friction. The roll-gap model sensitivity to friction coefficients was investigated, again for both the first and last finishing stands. Figure 8.49 shows the results from these trials and suggests as the friction coefficient is increased from 0.25 to 0.45 the reaction force increases at a linear rate. Again the gradients of the two curves are slightly different suggesting that stand 1 is more sensitive to friction coefficient than stand 7.

Further examination into this friction sensitivity is permitted with figure 8.50 giving evidence of the differing contact pressures and shear stresses encountered within stand 1 with varying coefficients of friction. Contact pressure is seen to increase to a peak coincidental with the reversal of the shear stresses with increasing friction tending to push the neutral plane or zone further into the roll-gap. Increasing friction also increases the maximum contact pressure and decreases the time period any discrete piece of material takes to exit the roll-gap.

Increasing friction has significant effects upon the shear stresses experienced within stand 1 with increasing friction increasing the maximum shear stress. From these shear stresses it can be seen that the higher friction coefficients incur shear stresses greater than the yield stress of the material at about 100MPa at this temperature and strain rate. Figure 8.51 shows the same simulation for stand 1, as described previously, but with the maximum shear stress friction law applied to the roll-gap model. With a maximum shear stress of 50MPa both the shear stress and the contact pressure curves are markedly different. Although the contact pressure has been reduced approximately 75MPa, the

contact times have increased effecting the total rolling force for stand 1. Examination of the effect of the maximum shear stress upon rolling load is given in figure 8.52. Here we can see directly how the maximum shear stress law has reduced sensitivity to the coefficient of friction within the first stand model. The same principles were also applied to the last stand model with rolling load results given in Figure 8.53.

8.5.2 Multipass Thermal Evolution

Modelling the thermal evolution during multi-pass rolling using coupled Finite-Element techniques was seen as one of the critical components for the completion of a complete finishing mill simulation. Within the finishing mill the strip would lose heat by radiation and convection to the surroundings and conduction to the rolls. Thermal results for the high Carbon steel according to the processing parameters within table 8.8 can be seen in figure 8.54. Both of Corus' hot strip mills in South Wales log set-up data on their respective hot mill computers. With the specification of the grade and coil identification number this data such as roll diameters, speeds and gauges could be downloaded and employed in the design for accurate simulations of the finishing mill for any particular coil.

Stand No.	Roll Speed (m/s)	Roll Radius (mm)	Stand Gauge (mm) (Entry = 33.88)	Interpass Time (s)
1	1.25	351.63	17.19	2.35
2	2.00	370.25	11.02	1.85
3	3.09	361.38	6.85	1.16
4	4.36	353.89	4.79	0.92
5	5.67	353.60	3.71	0.79
6	6.98	358.70	3.05	0.68
7	8.26	365.00	2.64	

Table 8.8 Mill Data for the Rolling of High Carbon Steel. Coil Id = 8334801

From figure 8.54 the non-uniform initial temperature distribution can be seen. In this particular case the surface temperatures were 1028 and 999°C for the top and bottom

surfaces respectively. The chilling of the surfaces due to contact with the rolls and the heating of the centre of the strip due to plastic deformation can be seen with each of the seven stands. However, when the strip emerges from the roll-gap the surface temperature of the strip can be seen to rebound due to the higher centre line temperature. Although at entry to the finishing mill there was a temperature gradient of 30 °C, at exit this was reduced to below 5°C. The amount of roll surface chilling can be seen to decrease in the latter stands until at exit of the finishing mill the final measured temperature of 850°C with 5% error bars can be seen in figure 8.55.

The thermal evolution for a Carbon Manganese material can be seen in figure 8.56 with the mill data shown in table 8.9.

Stand No.	Roll Speed (m/s)	Roll Radius (mm)	Stand Gauge (mm) (Entry = 34.76)	Interpass Time (s)
1	1.15	358.32	23.36	3.38
2	1.59	372.38	16.83	2.62
3	2.11	367.10	12.24	2.00
4	2.83	347.22	9.02	1.51
5	3.64	348.60	7.21	1.27
6	4.49	353.63	6.10	1.09
7	5.30	366.10	5.00	

Table 8.9 Mill Data for the Rolling of Carbon Manganese Steel. Coil Id = 6314003

Here both the entry and exit temperatures are slightly higher than that for the previous finishing mill simulation of the high Carbon steel. Again the thermal gradient through the gauge of the strip can be seen to be equalised by the fifth roll pass with the final temperature well within the 5% tolerance of the measured temperature shown in figure 8.57.

The thermal evolution of a low Carbon steel required interstand water cooling to be taken into account. The results shown in figure 8.58 illustrate this surface cooling according to the rolling conditions shown in table 8.10 and the assumptions described in chapter 7.

Stand No.	Roll Speed (m/s)	Roll Radius (mm)	Stand Gauge (mm) (Entry = 37.71)	Interpass Time (s)
1	1.20	353.20	23.16	2.96
2	1.67	373.85	16.49	2.47
3	2.26	367.80	11.54	1.79
4	3.20	355.25	8.02	1.25
5	4.26	351.45	6.18	1.05
6	5.41	360.43	4.97	0.86
7	6.47	373.18	4.21	

Table 8.10 Mill Data for the Rolling of low Carbon Steel. Coil Id = 3681301

The water cooling can be seen to hold the temperature near to the minimum temperature due to roll chilling, therefore absorbing all the heat flux from the hotter core of the strip. These results show that the temperature gradients through the gauge of the strip are greater than for the simulation of both the high Carbon and Carbon Manganese steels. In fact for the low Carbon steel the temperature only homogenises during interstand 6 where there is no water cooling present. The final temperature of the strip was predicted at 838°C at mid-gauge of the strip with on-line measurements taken at 840°C from figure 8.59.

8.5.3 Multipass Microstructural Evolution

Modelling the evolution of the austenite microstructure within the finishing mill was carried out as described in chapter 7 with the results of the fraction softened during the interpass periods for the high Carbon steel show in figures 8.60 to 8.65. For clarity these figures only show the total softening for the centre-line and the top and bottom surfaces of the strip. The difference between the rates of fractional softening between the surfaces

and the core of the strip can easily be seen for interpasses 1,2 and 3. However, for the latter passes 4,5 and 6 the difference between the surfaces and the centre become negligible. Incomplete softening takes place during interpasses 5 and 6 for the high Carbon simulation. Notably, the rate of softening for interpass 6 was greater than that for interpass 5 although the temperature, according to figure 8.54, was lower. Figure 8.66 illustrates how the strain from pass 5 in conjunction with the fraction softened during interpass 5 calculated the initial strain for pass 6.

Figure 8.67 illustrates the microstructural behaviour of the Carbon Manganese simulation during the multi-pass analysis described in table 8.9. Full softening was seen through the entire gauge during the first four interpasses. However, during interpass 5 only the centre of the strip achieves this amount of softening with the top and bottom surfaces only experiencing 23% and 24% respectively. This gradient was reversed for the final interpass with both the top and bottom surfaces achieving 7% softening whilst the centre of the strip was only 1% softened. Although the first four interpasses all achieved full restoration, figure 8.68 shows how the centre and the top surface softening kinetics were affected by the processing parameters. For the first interpass both the centre and top surface experienced rapid softening with the surface kinetics being significantly reduced during interpasses 2,3 and 4.

The low Carbon Steel completed 100% softening for all the interpasses. From the austenite grain size kinetics from [106] figure 8.69 illustrates the evolution of the austenite grain size throughout the finishing mill. With an initial grain size of 16 μm the grains decrease in average size until during interpasses 5 and 6 the grain sizes recover to final austenite grain sizes of 5.89μm and 5.37μm for the centre and top surface of the strip respectively.

Perhaps the most important of all the finishing mill parameters is rolling force. It is essential to know this variable to effectively utilise the mill to capacity without endangering any of the components to overload within the finishing mill. Prior knowledge of the rolling forces during finishing rolling also allows the calculation of rolling power requirements and mill stretch which effect external properties of the strip such as gauge and shape. Comparison of the measured rolling forces with the predictions

from the multi-stand model can be used as an indication of the accuracy of the hot deformation characteristics of the material and the thermal and microstructural algorithms initiated during the simulations. Rolling force during the two-dimensional, plane strain analysis of the roll-gaps is a complex function of the frictional shear loads, reaction forces, flow stress calculations from section 8.2 and similar work from Anderson [106] for the Carbon Manganese and low Carbon steels and their associated microstructural characteristics. Figure 8.70 shows the results for the seven stand multi-pass simulation of the high Carbon, Carbon Manganese and low Carbon steels. Of the 21 data sets it can be seen that only 4 rolling force results have an error greater than 10%. The average errors for all three materials tested were 73, -11 and 24 tonnes representing 3%, -2% and 2% errors for the high Carbon, Carbon Manganese and Low Carbon Steels respectively.

8.6 Discussion of Numerical Results

Results from the single stand analyses identify several important characteristics of finishing rolling. Firstly the fact that a non-uniform temperature exists at entry to the first finishing stand suggests nonhomogeneous deformation is inevitable during the early finishing stands as identified in figures 8.41 to 8.43. This non-uniform thermal profile was either a function of the inner and outer laps of the coilbox cooling at different rates or non-uniform cooling of the top and bottom surfaces of the transfer bar between the Enco panels and the roller tables as discussed in chapter 3.

Figure 8.40 identified the deformed mesh within the first stand of the finishing mill and illustrated how the actual material deformed during rolling. However, the shape of the deformed mesh would be highly dependent upon the mechanical contact constraints imposed at the strip/roll interface and some function of the non-uniform temperature field discussed above. The greater the adhesion between the rolls and the strip surfaces the greater the mesh would distort both before and after the neutral zone where a surface speed differential would exist.

The mechanical deformation parameters of strain and strain rate are also sensitive to adhesion between the roll and the strip as figures 8.41 and 8.42 show the majority of the

plastic deformation taking place at the surfaces where the mesh distortion is the greatest and the temperatures are the lowest as shown in figure 8.44. Strain rates in the y-y direction increase towards the exit of the roll-gap for the centre of the strip as temperature increases due to plastic deformation and the strip becomes less viscous.

Whilst the greatest strain and strain rate can be seen at the surface of the strip it must also be noted that the lowest temperatures are also at the surface. As temperature is the most significant factor within the constitutive relationship of the material it seems imperative to accurately account for initial temperature distribution prior to entry to the finishing mill and during rolling if accurate predictions of rolling loads and metallurgy are to be made.

Investigation into the roll-gap models sensitivities revealed several insights into the characteristics of Finite-Element modelling of finishing rolling. Firstly, temperature can be seen to have a significant effect on the predicted rolling loads. For the range of temperatures investigated stand 1 had the greatest sensitivity to this parameter. This is unsurprising since the first stand of the finishing mill performs a far greater gauge reduction than the last stand of the finishing mill resulting in greater bulk deformation as described in table 8.7. This fact is also reflected in figure 8.53 which investigated the friction coefficient sensitivity of the roll-gap model. Again as the strip is travelling faster and therefore the real time of contact between the strip and the roll is significantly reduced for stand 7 the results are perhaps unsurprising that rolling force is less sensitive to the interface conditions.

Figures 8.52 and 8.53 do indicate however, that to accurately predict rolling loads, stand 1 requires the greatest accuracy regarding mechanical contact constraints and temperature prediction even though the strip material is much harder within stand 7 due to the lower temperature and higher strain rates.

Investigation into the thermal profiles of the multipass simulations reveals how the differential surface temperatures become uniform after one or two interpass periods as the lower temperature will rebound faster to the near uniform temperature of the rolled stock. Although only the head end of the strip has been modelled identification of

thermal rundown can still be seen in figures 8.55, 8.57 and 8.59. This non-uniform thermal profile illustrates some of the difficulties when attempting to accurately model the thermal evolution within the finishing mill.

Fractional softening during the interpass periods is a complex function of strain, temperature and material characteristics. Figures 8.60 to 8.62 illustrate the balance between strain and temperature with their consequential effects upon the softening kinetics of the high Carbon material during interpass 1 and 2 for the high Carbon material respectively. During interpass 1 the strains are greater than those at the centre of the strip that would suggest the softening kinetics should be greater at the surface. However, due to roll surface chilling these kinetics are retarded with the surfaces taking much longer to achieve 100% softening. Figure 8.65 illustrates that when incomplete softening takes place, the softening kinetics after any subsequent deformation will be increased due to the extra straining incurred within the material during the deformation.

Prediction of the austenite grain size for the low Carbon during finishing rolling was taken as a function of strain and initial grain size from Anderson [106]. The results shown in figure 8.69 represent this calculation given in equation 7.4. Here we can see that when the equivalent plastic strain decreases during the latter stands the actual average grain size increases during the interstand period. This is extremely concerning if refinement of the austenite grain size was the aim of the thermally controlled rolling of this particular grade.

Care should also be taken when making comparisons between the measured forces and those predicted by multi-pass thermomechanical and microstructural algorithms. Whilst these measured values may give some insight into the model's accuracy, these readings are normally made at a prescribed frequency and therefore only represent an average value. Perhaps most importantly these readings are taken from load cells within each of the seven finishing stands and the accuracy of these load cells are unknown. The effects of the operators modifying process parameters such as speed or gauges during rolling are also unknown and may have a significant effect on the interaction between the product and process. These dynamic effects coupled with the accurate measurement of rolling loads and temperatures are still a matter for concern when attempting to quantify the

relationship between rolling parameters and rolling load. Table 8.11 illustrates how the average errors compare with the standard deviation of the errors to illustrate some of the difficulties when comparing measured versus predicted rolling loads.

Stand No.	Average % Error	Standard Deviation of the % Error
1	2	6.03
2	5	1.82
3	13	2.52
4	2	1.83
5	-5	3.20
6	-8	14.19
7	-3	6.77

Table 8.11 Standard Deviation of the Finishing Stand Simulations

From table 8.11 the scatter of results can be seen to be greatest for stand 6 although the percentage errors were dominant at stand 3. Errors at stand 3 are attributable to the combination of large reductions of approximately 30% whilst the material is rapidly cooling as shown in figures 8.54, 8.56 and 8.58 where the prescribed interface conditions have the greatest influence on rolling load. The large standard deviation at stand 6 is attributable to the varying quality of the measured data as described above and the erroneous result for the Carbon Manganese material at stand 6 as shown in figure 8.70.

One of the overall concerns when considering modelling a semi-continuous metal forming process such as finishing rolling is the coupling of results between roll-gap models and interstand analyses. Ideally all the subroutines would be written inside the Finite-Element programme.

However, during the development stage of the finishing mill model it became apparent that results from the roll-gap model would have to be exported to a neutral text file in order to be read in by the interstand analyses. This caused a number of problems during the development stage as variables required identical formats in order to be read at a later stage. Another shortcoming of this technique was the large amounts of data transfers

taking place during the roll-gap analysis. This method of recoding the various deformation parameters using I/O techniques increased the run time for the first finishing stand roll-gap analysis up to a factor of 3.

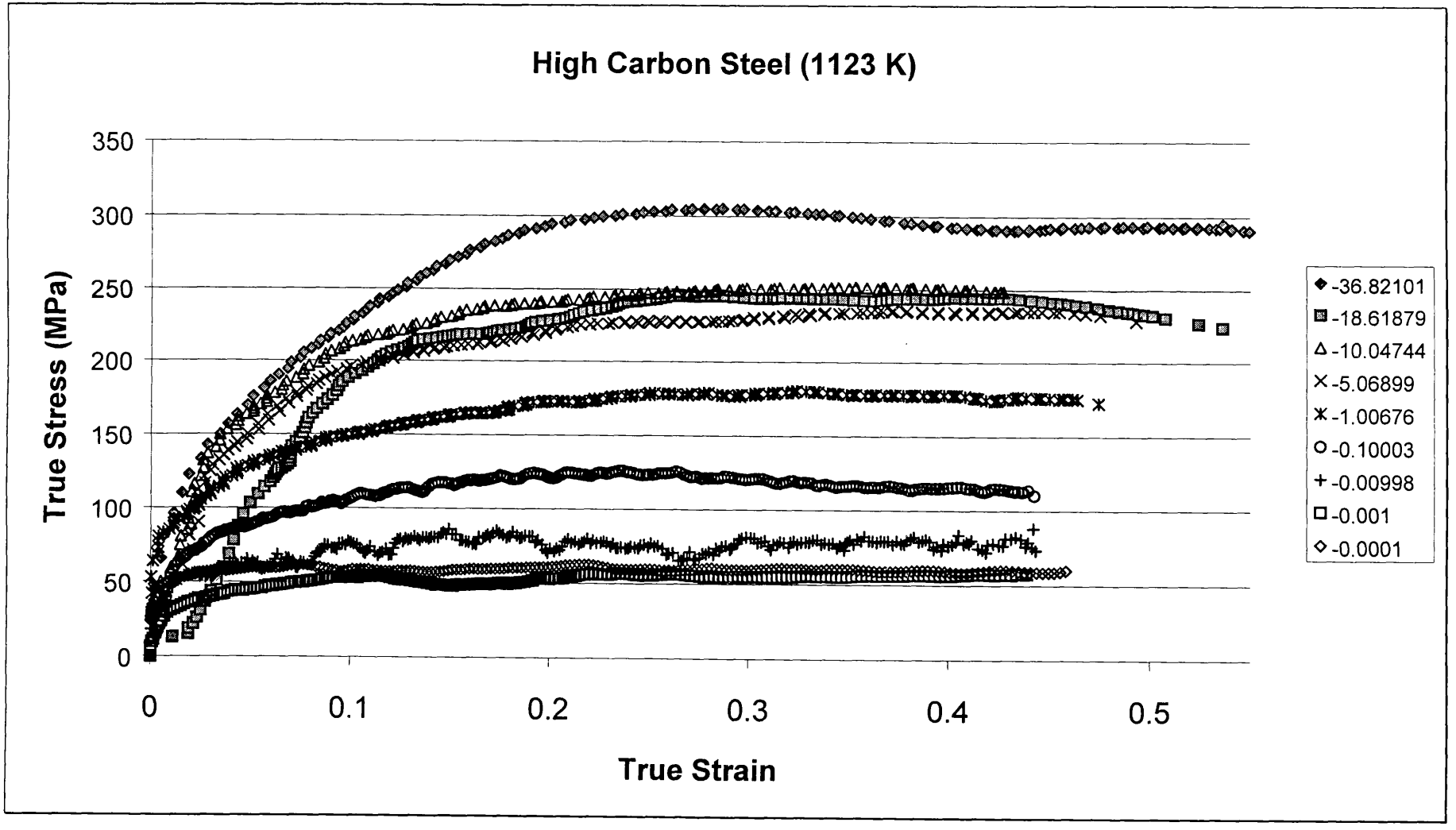

Figure 8.1 True Stress/Strain Curves for the Uniaxial Compression at 1123K

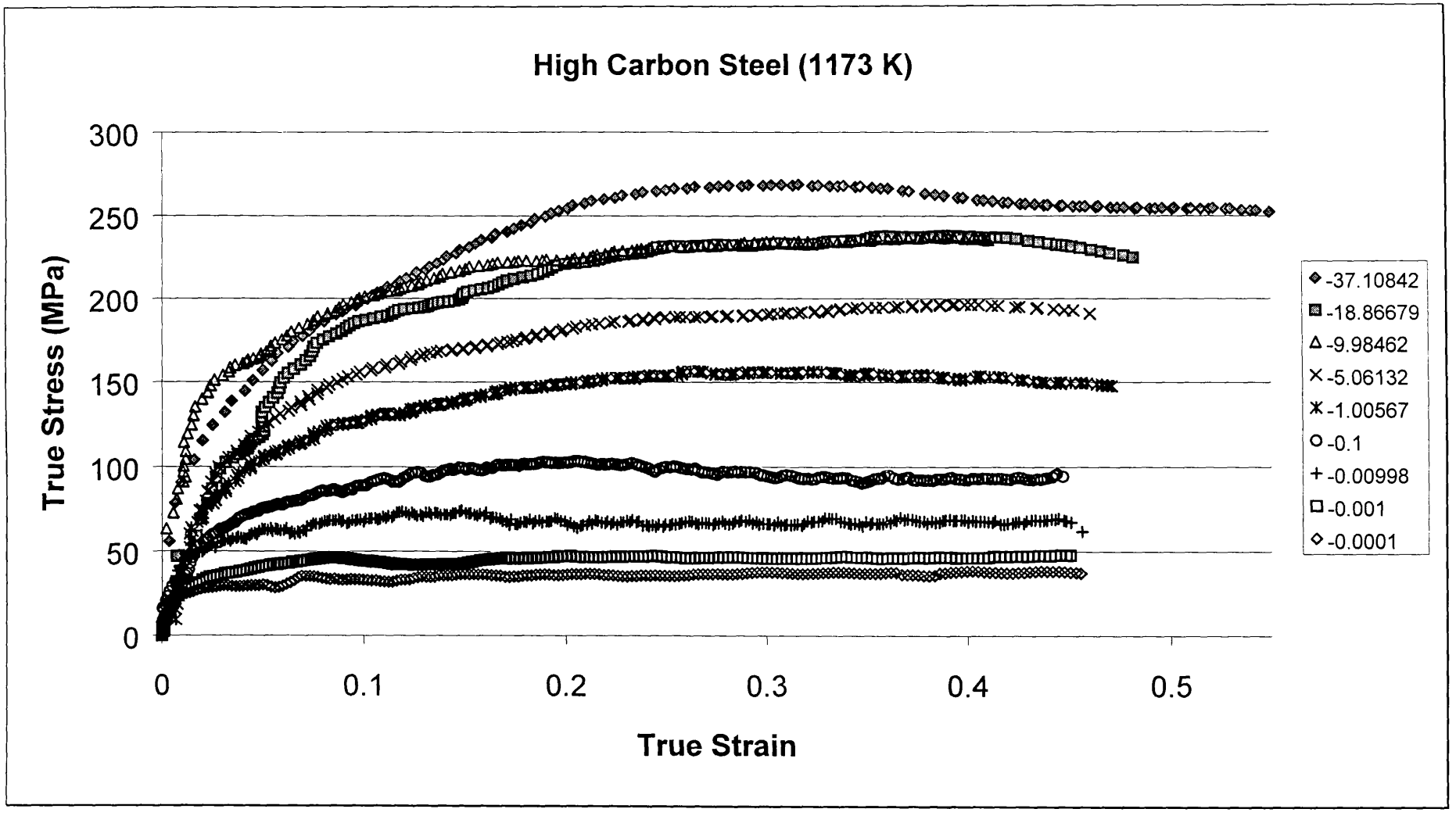

Figure 8.2 True Stress/Strain Curves for the Uniaxial Compression at 1173K

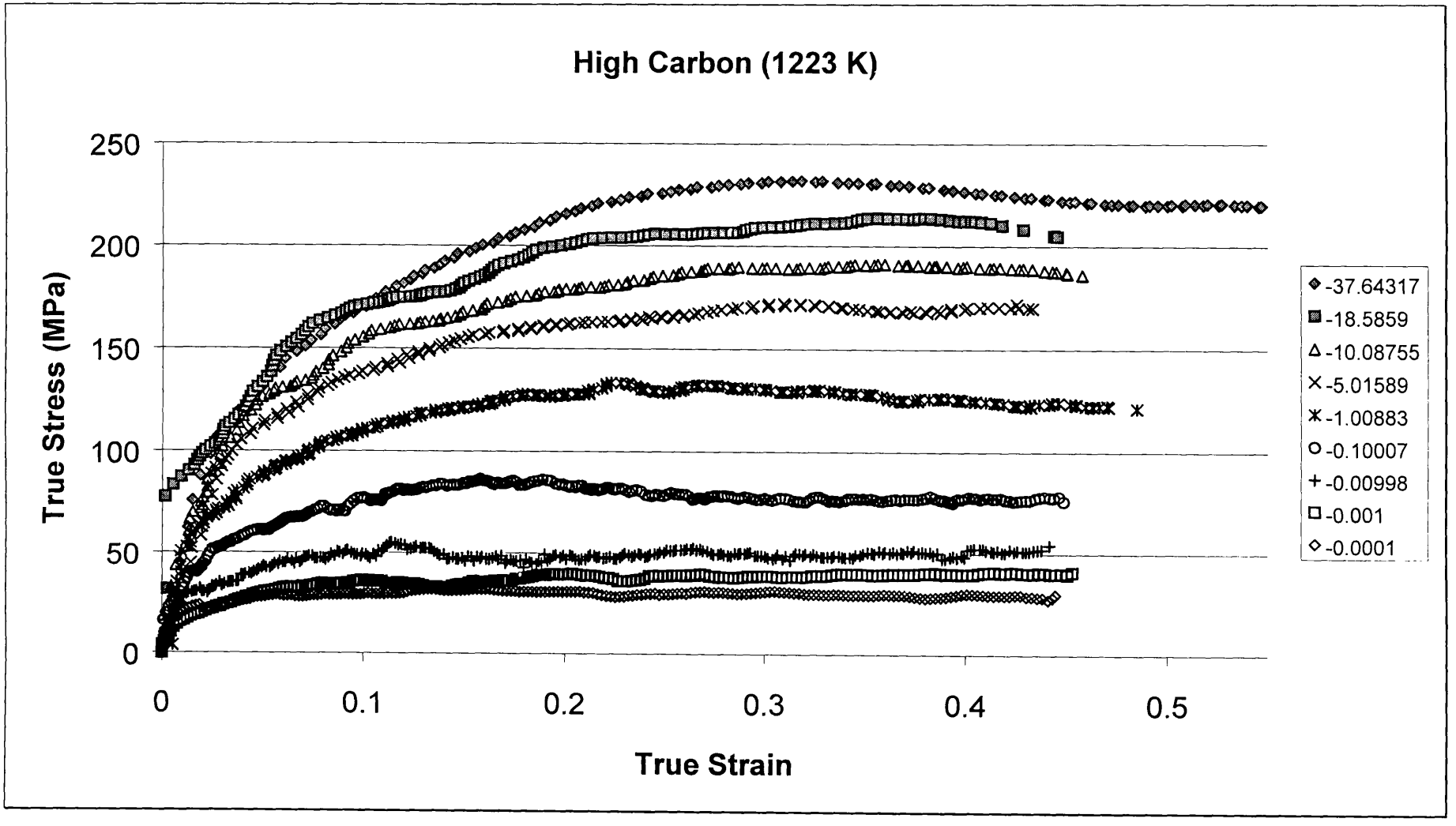

Figure 8.3 True Stress/Strain Curves for the Uniaxial Compression at 1223K

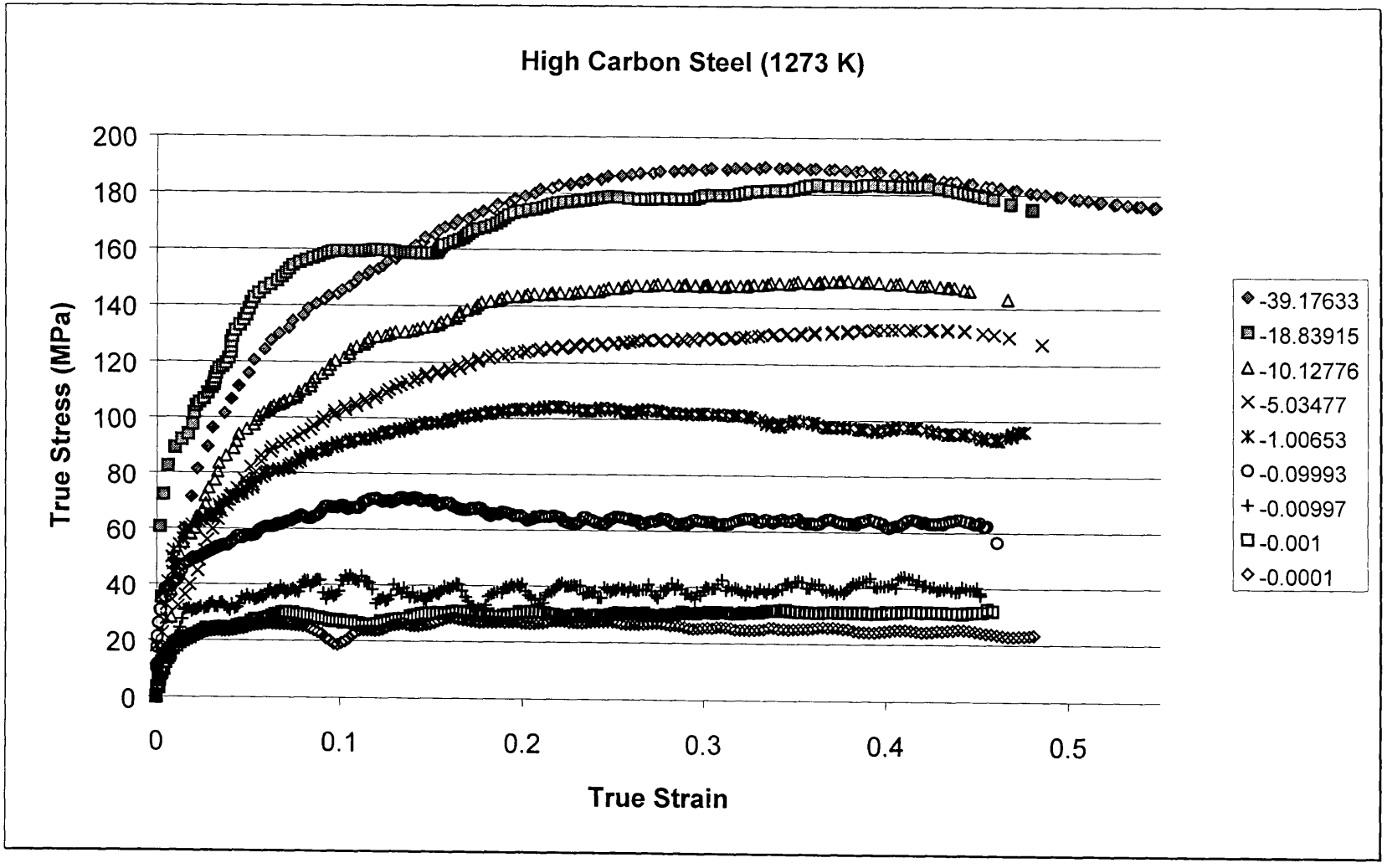

Figure 8.4 True Stress/Strain Curves for the Uniaxial Compression at 1273K

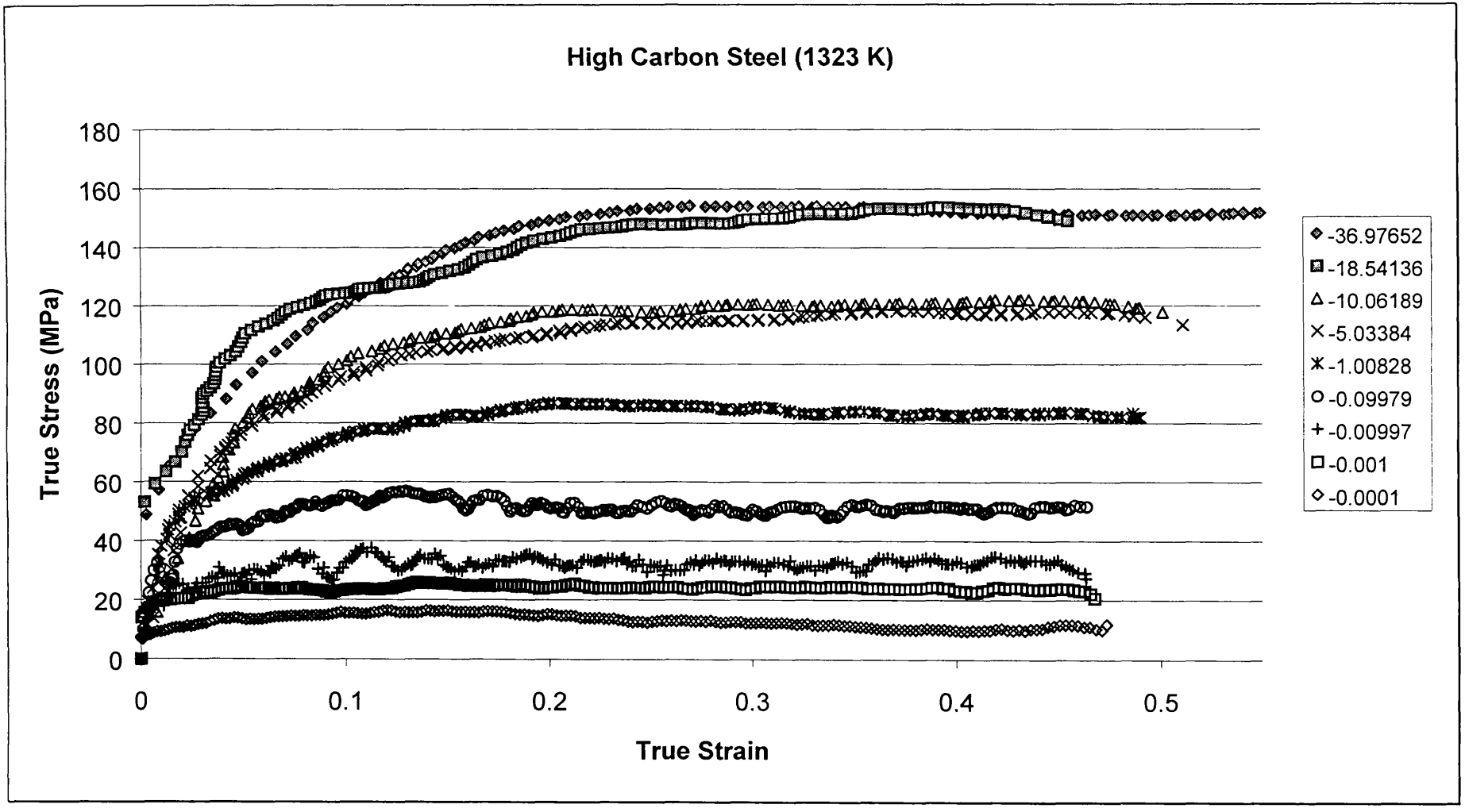

Figure 8.5 True Stress/Strain Curves for the Uniaxial Compression at 1323K

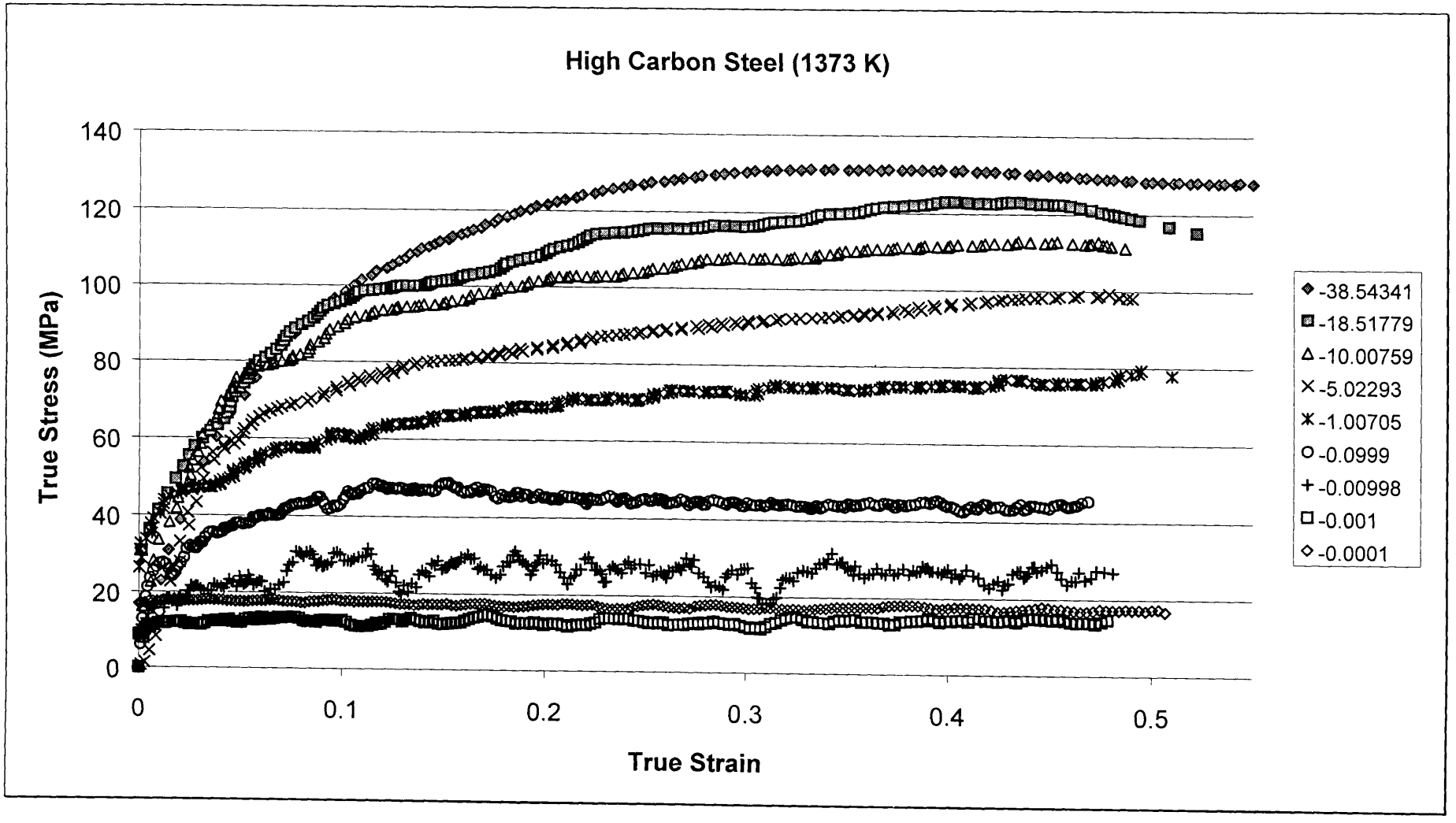

Figure 8.6 True Stress/Strain Curves for the Uniaxial Compression at 1373K

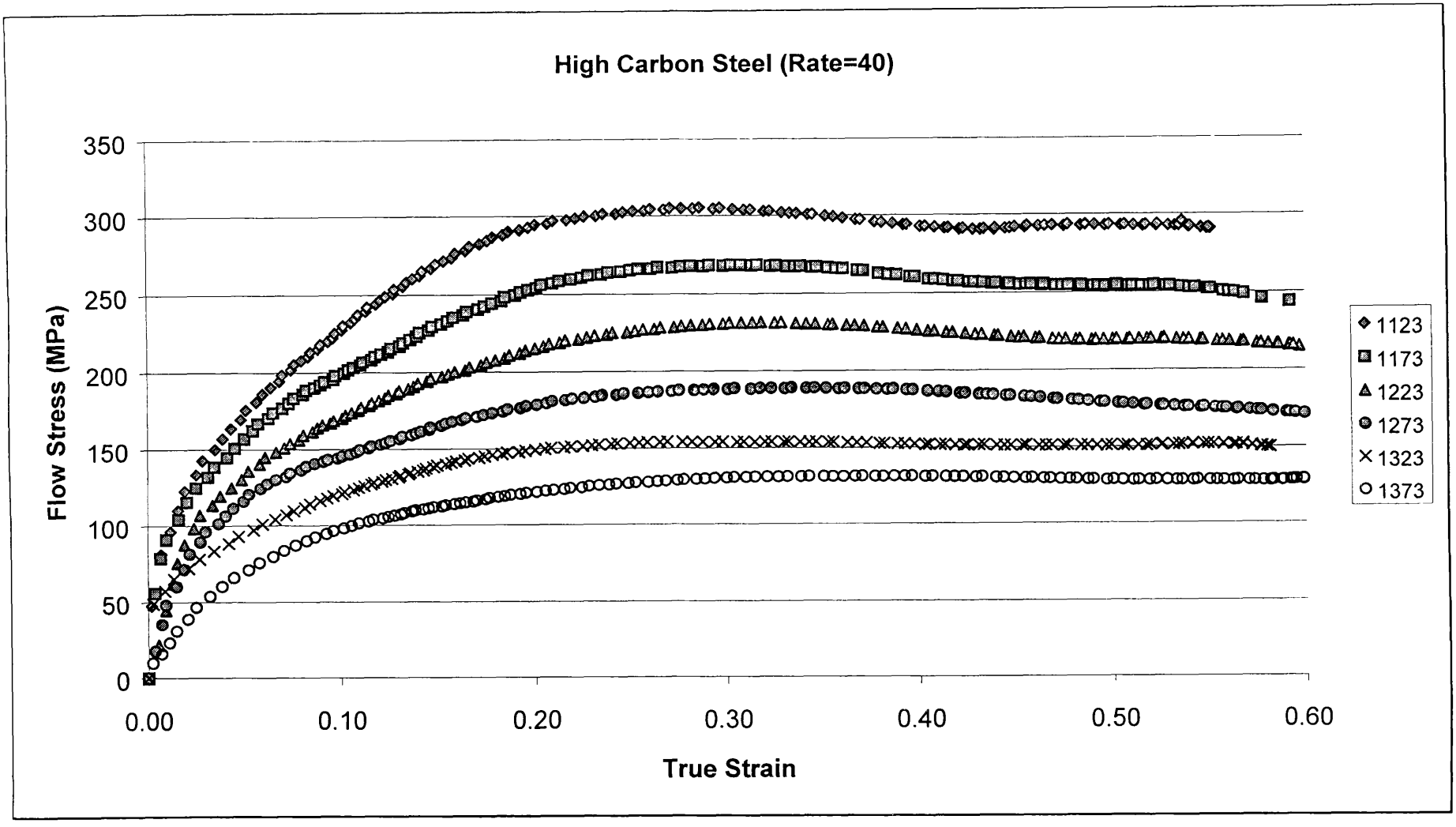

Figure 8.7 True Stress/Strain Curves for the Uniaxial Compression at a Rate of $40s^{-1}$

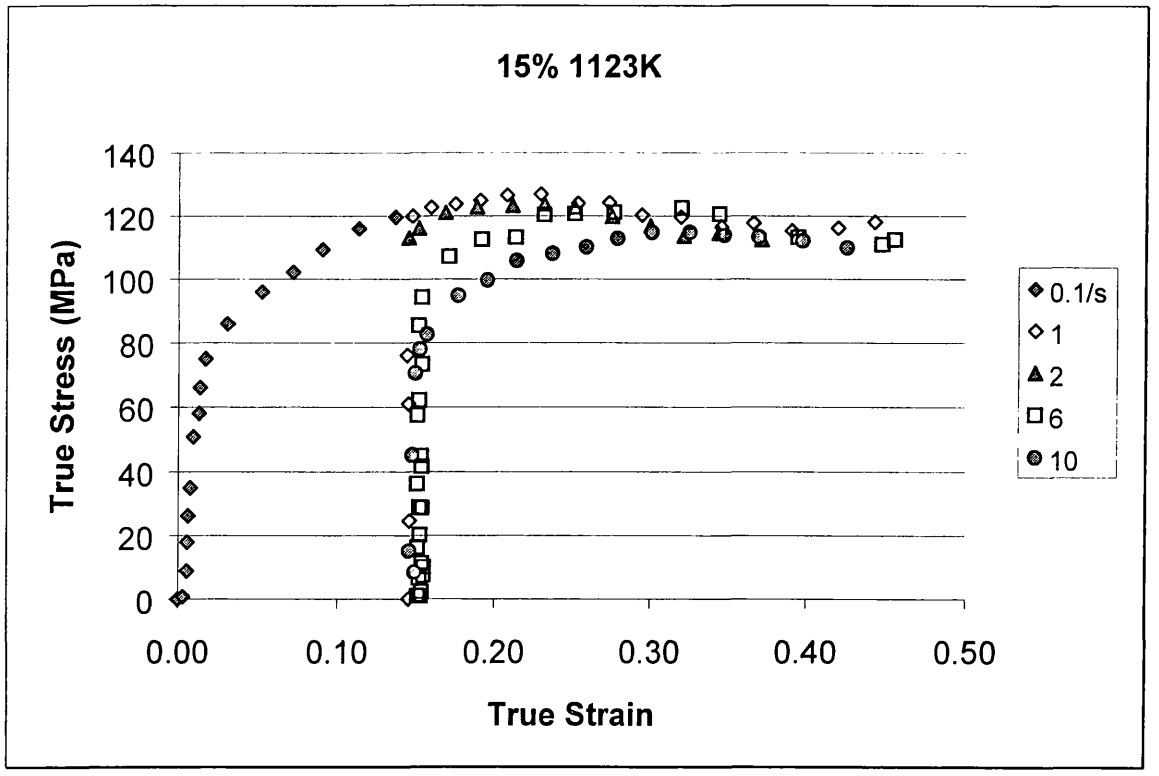

Figure 8.8 Interrupt Compression Test true Stress/Strain Curves at 1123K and 15% True Strain

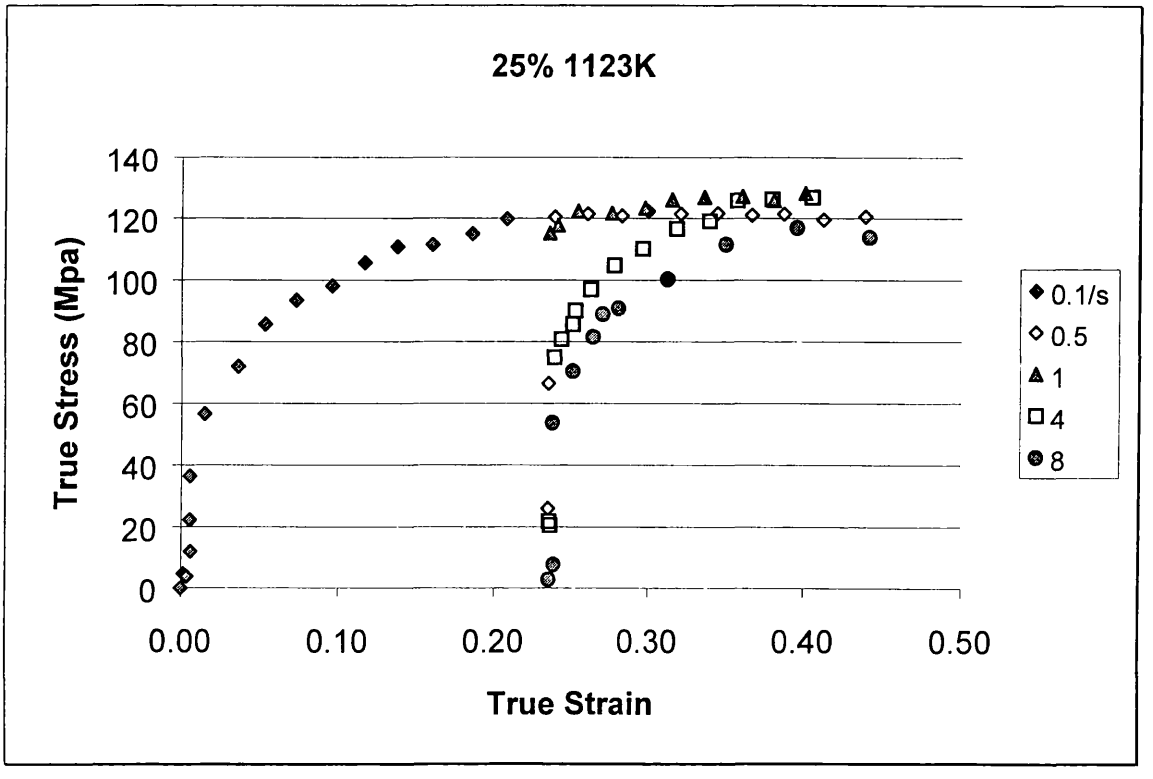

Figure 8.9 Interrupt Compression Test true Stress/Strain Curves at 1123K and 25% True Strain

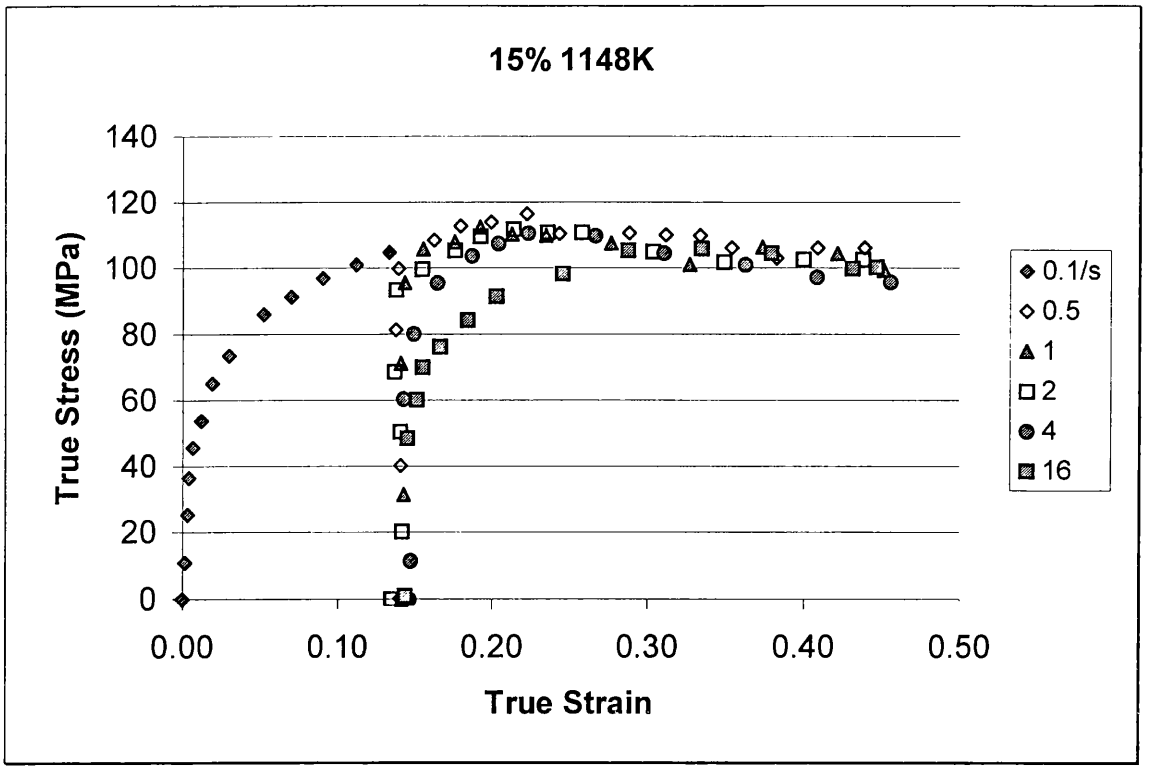

Figure 8.10 Interrupt Compression Test true Stress/Strain Curves at 1148K and 15% True Strain

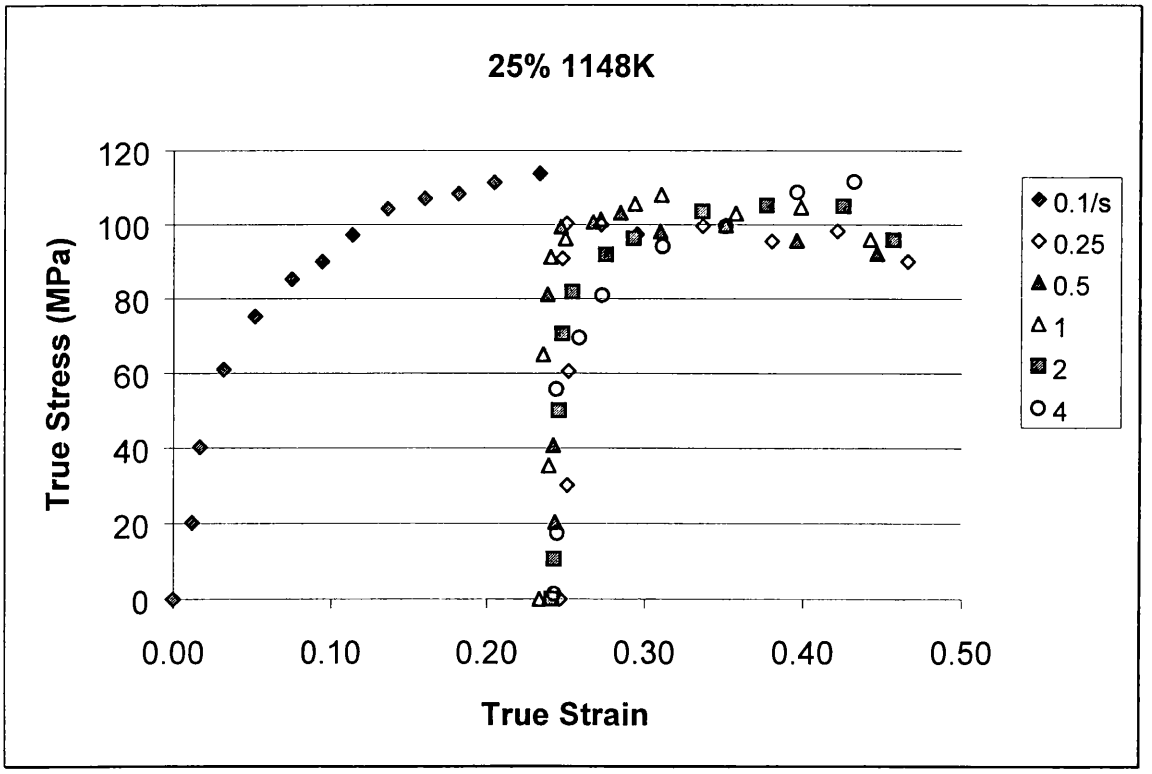

Figure 8.11 Interrupt Compression Test true Stress/Strain Curves at 1148K and 25% True Strain

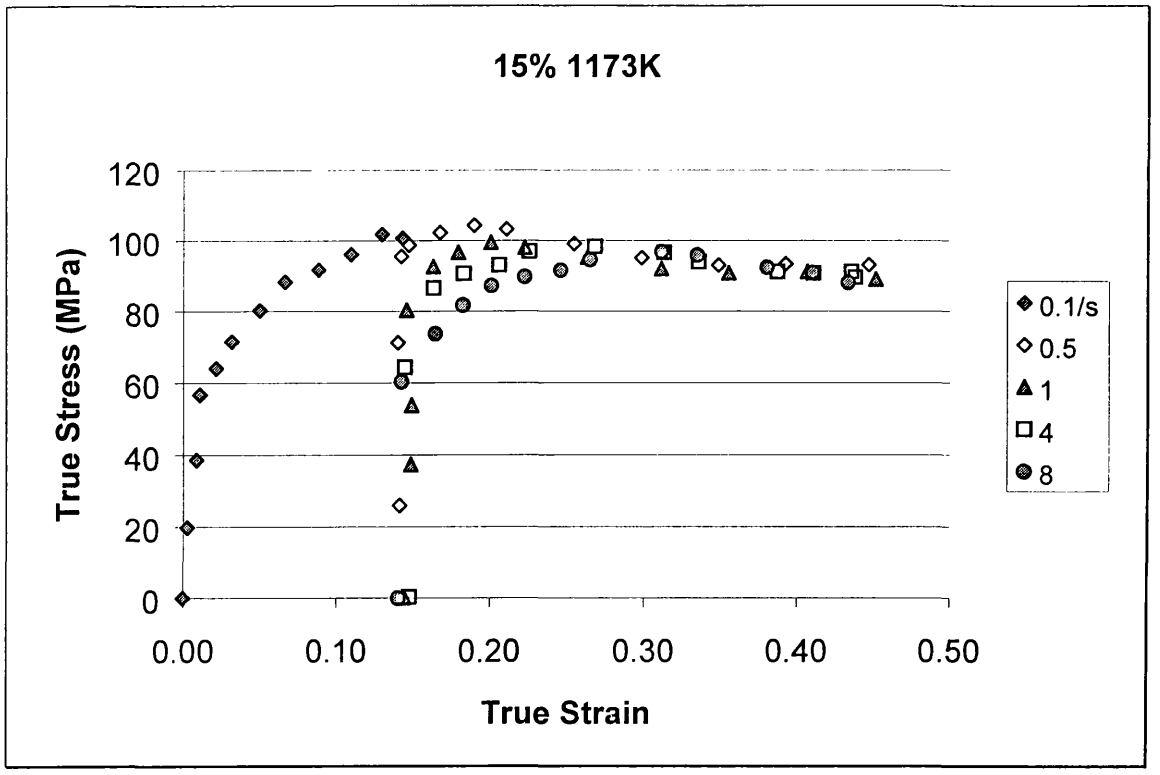

Figure 8.12 Interrupt Compression Test true Stress/Strain Curves at 1173K and 15% True Strain

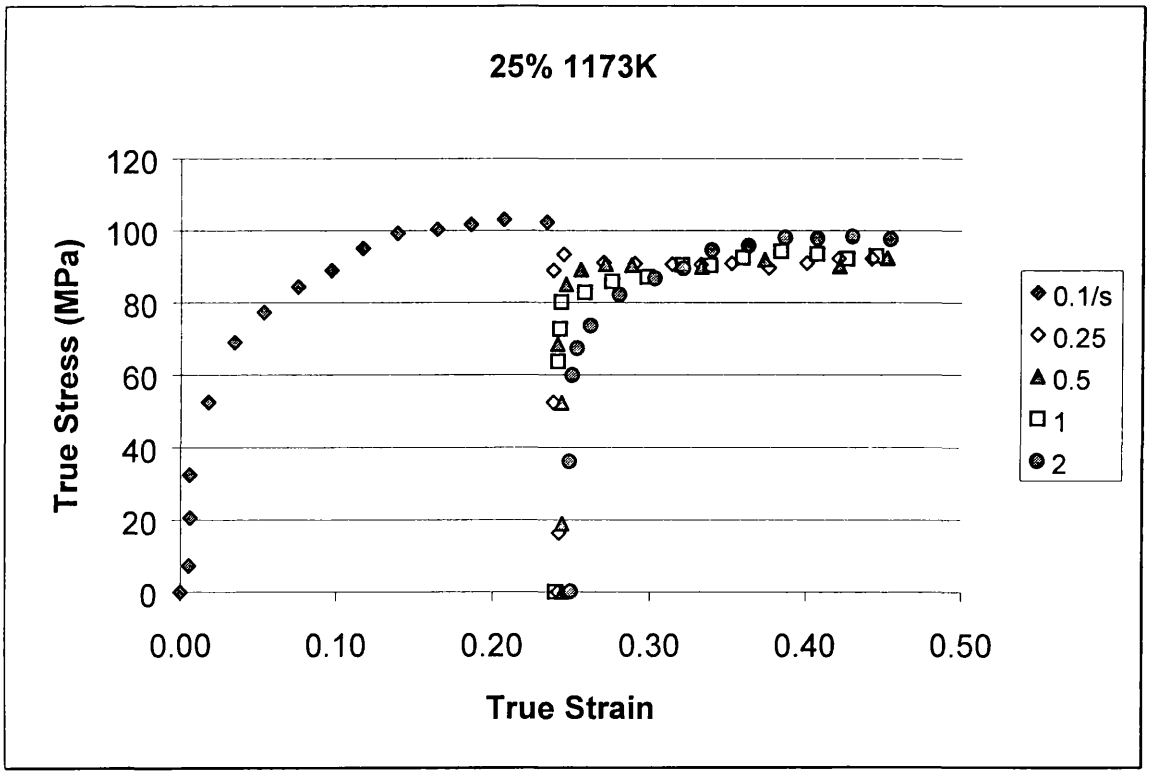

Figure 8.13 Interrupt Compression Test true Stress/Strain Curves at 1173K and 25% True Strain

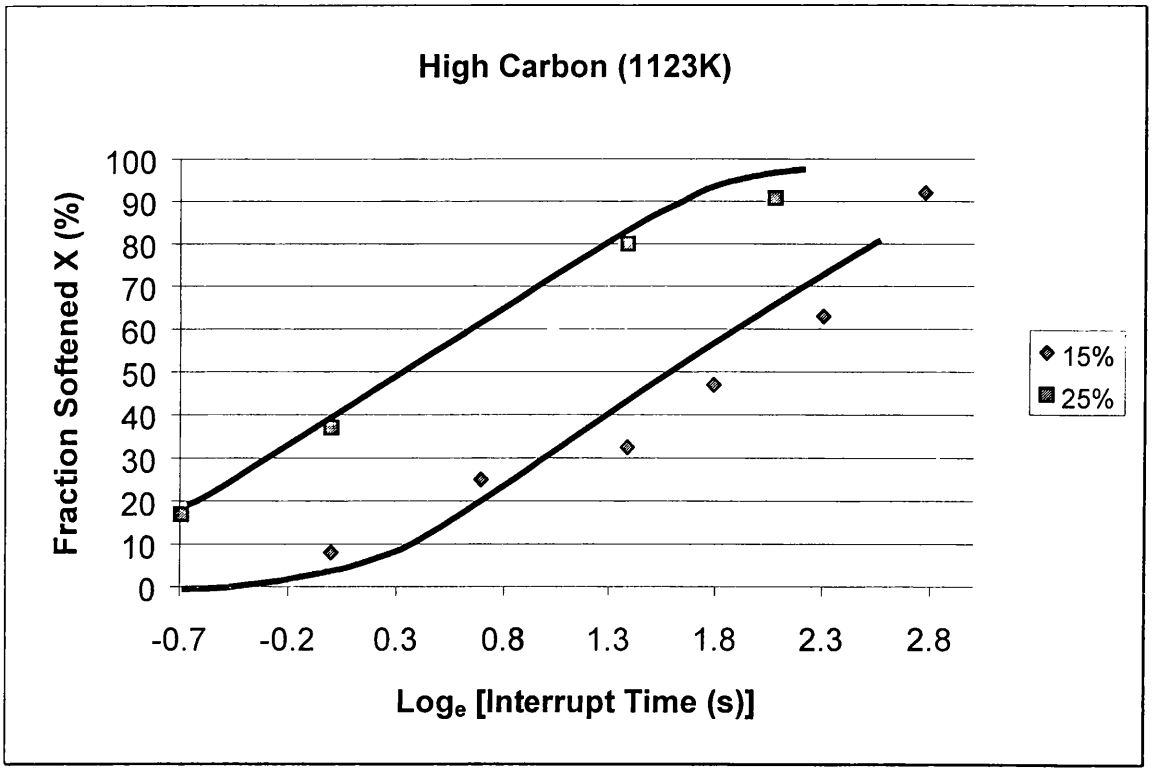

Figure 8.14 Fractional Softening for the Interrupt Compression Testing at $0.1s^{-1}$

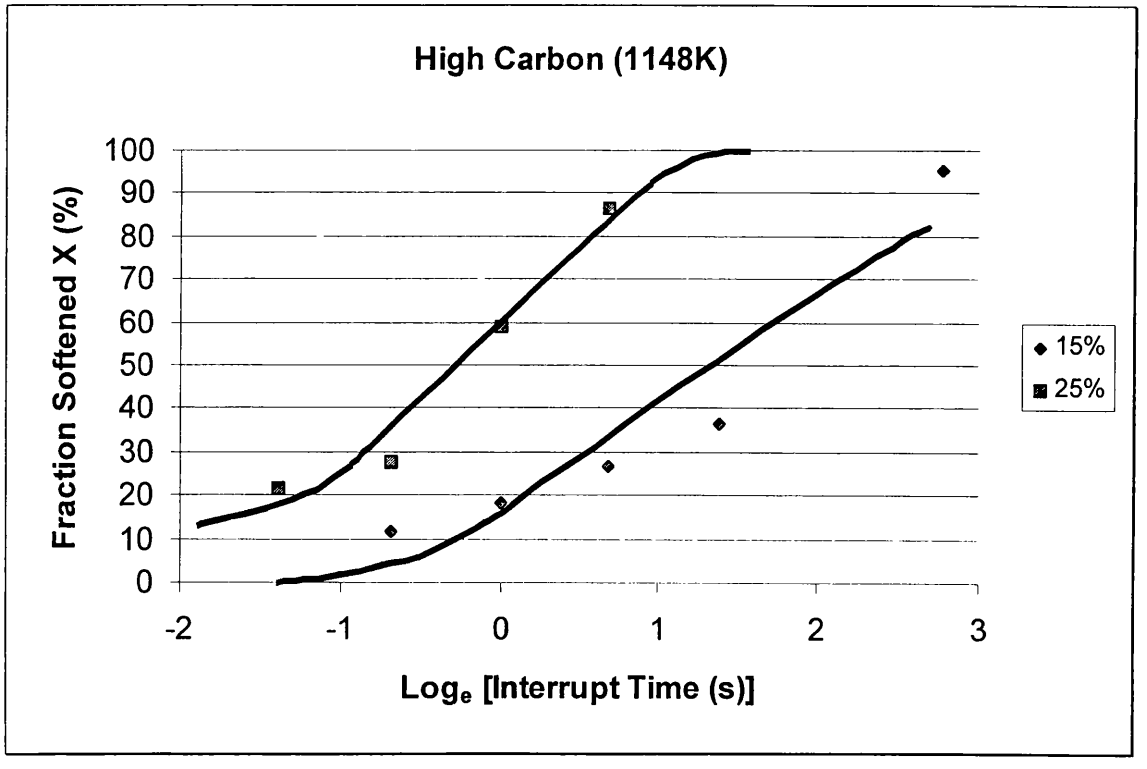

Figure 8.15 Fractional Softening for the Interrupt Compression Testing at $0.1s^{-1}$

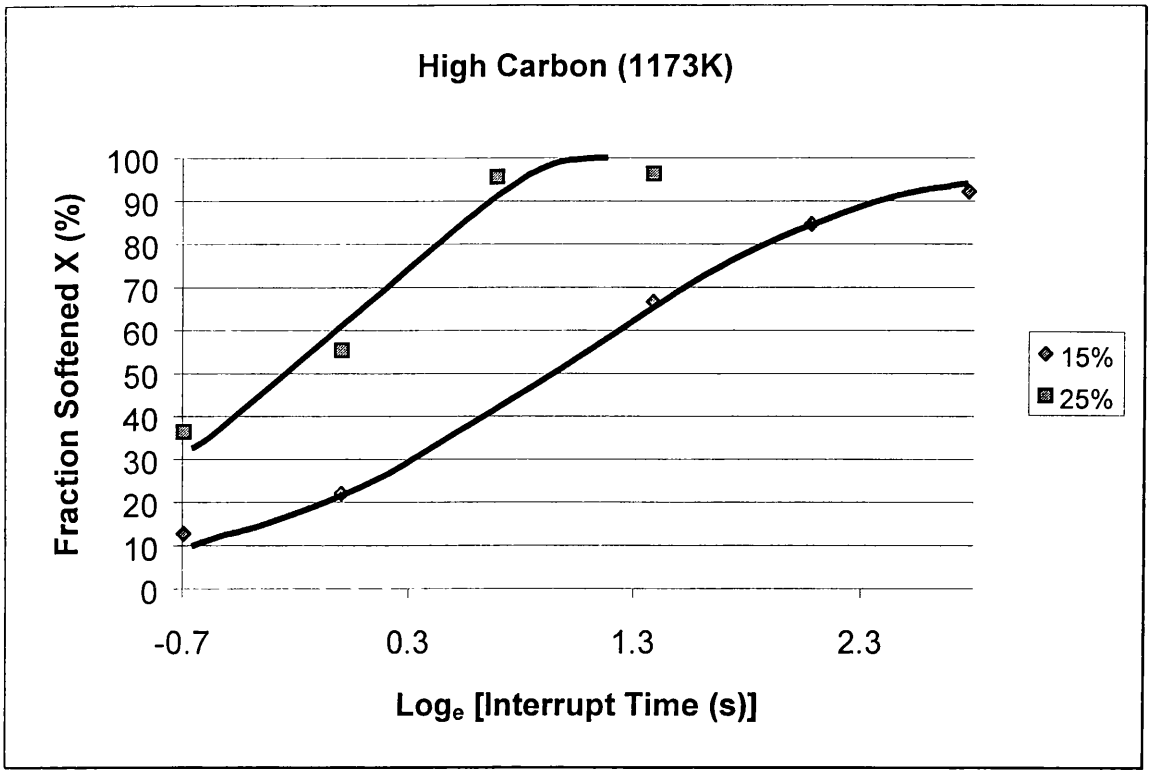

Figure 8.16 Fractional Softening for the Interrupt Compression Testing at $0.1s^{-1}$

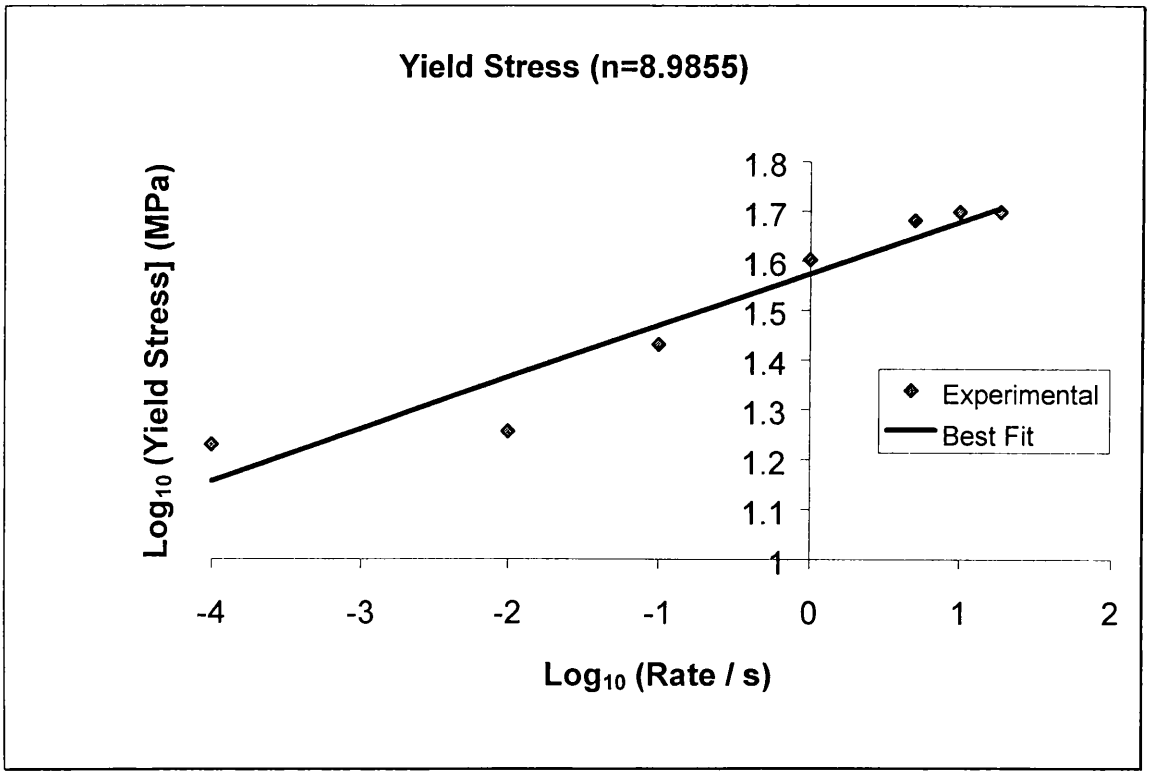

Figure 8.17 Yield Stress Values at 1373K

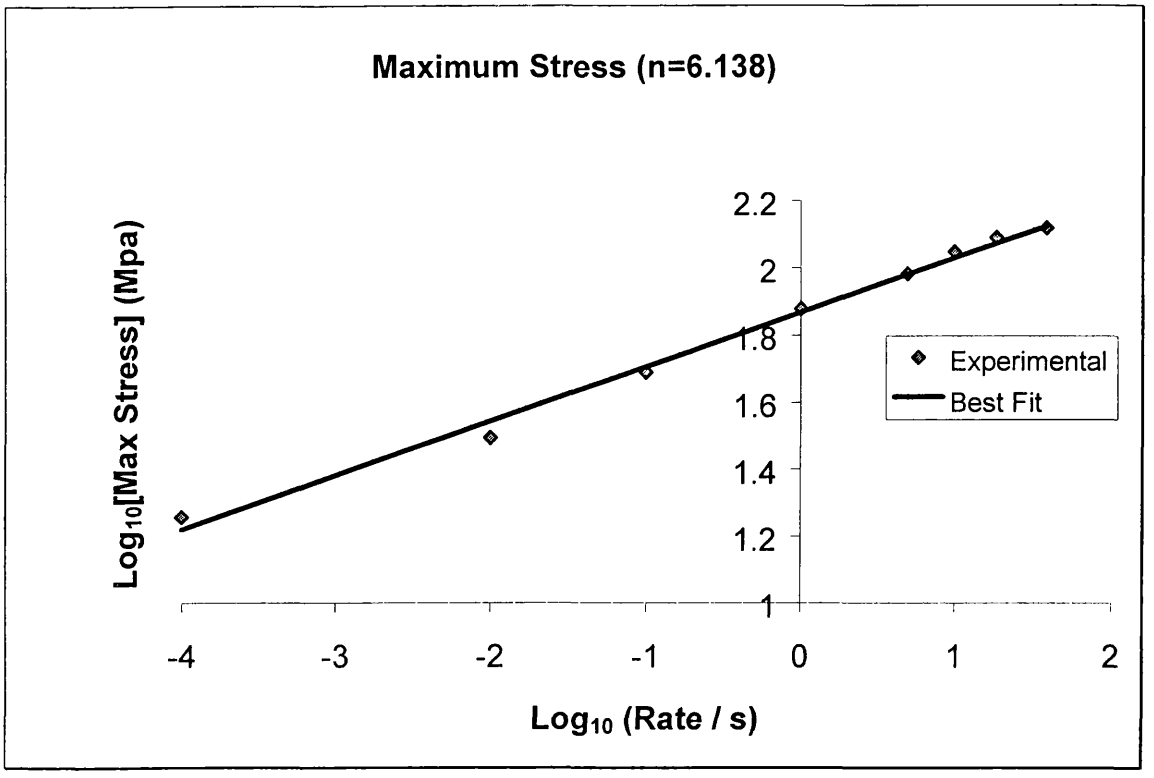

Figure 8.18 Maximum Stress Values at 1373K.

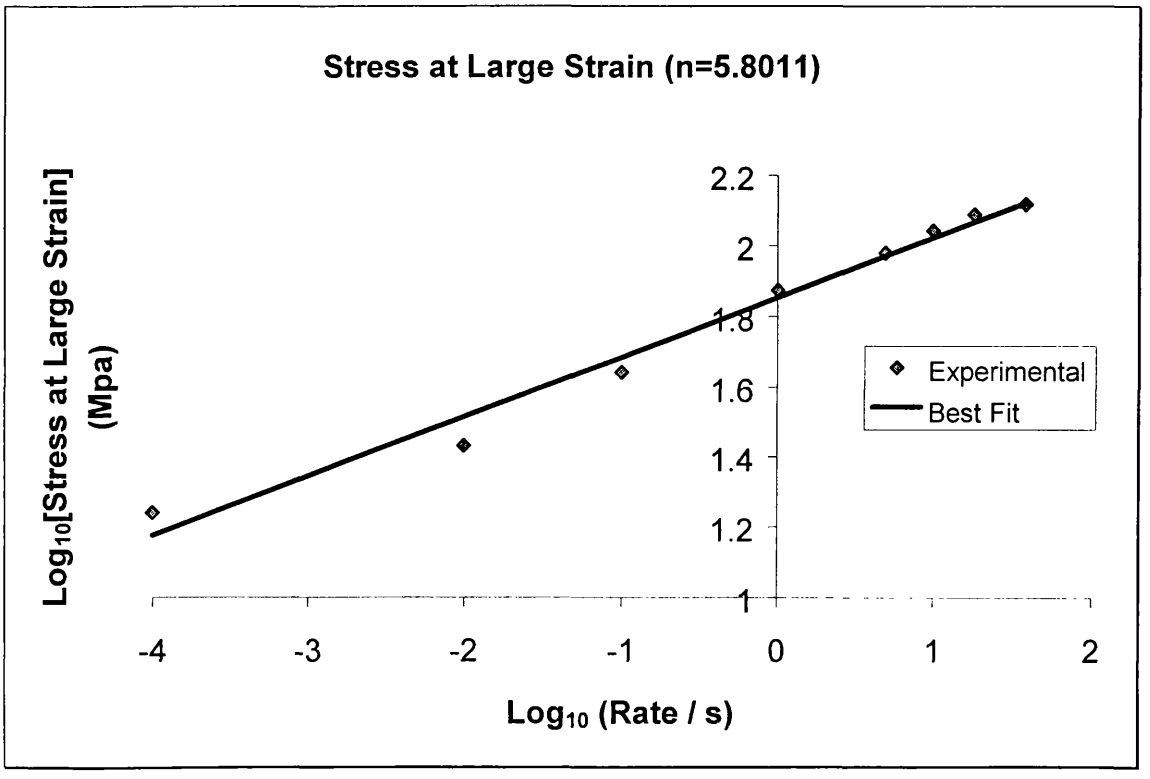

Figure 8.19 Stress at Large Strain at 1373K

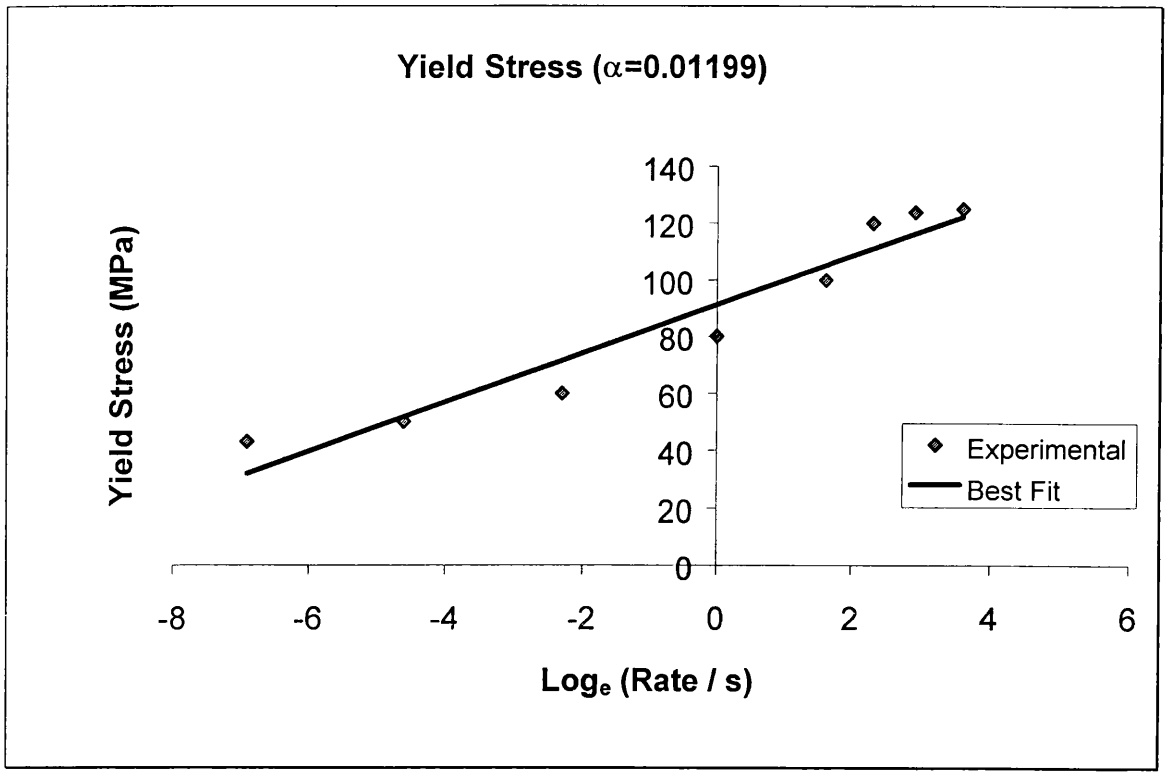

Figure 8.20 Yield Stress Values at 1123K

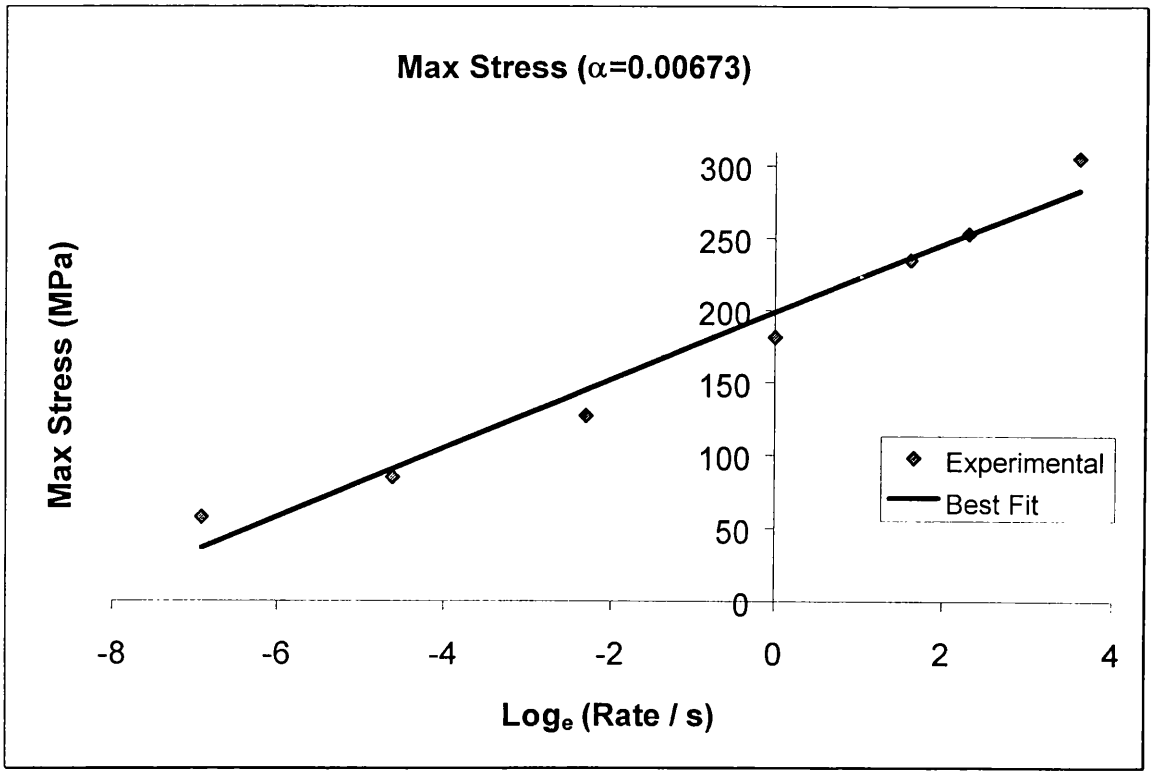

Figure 8.21 Maximum Stress Values at 1123K

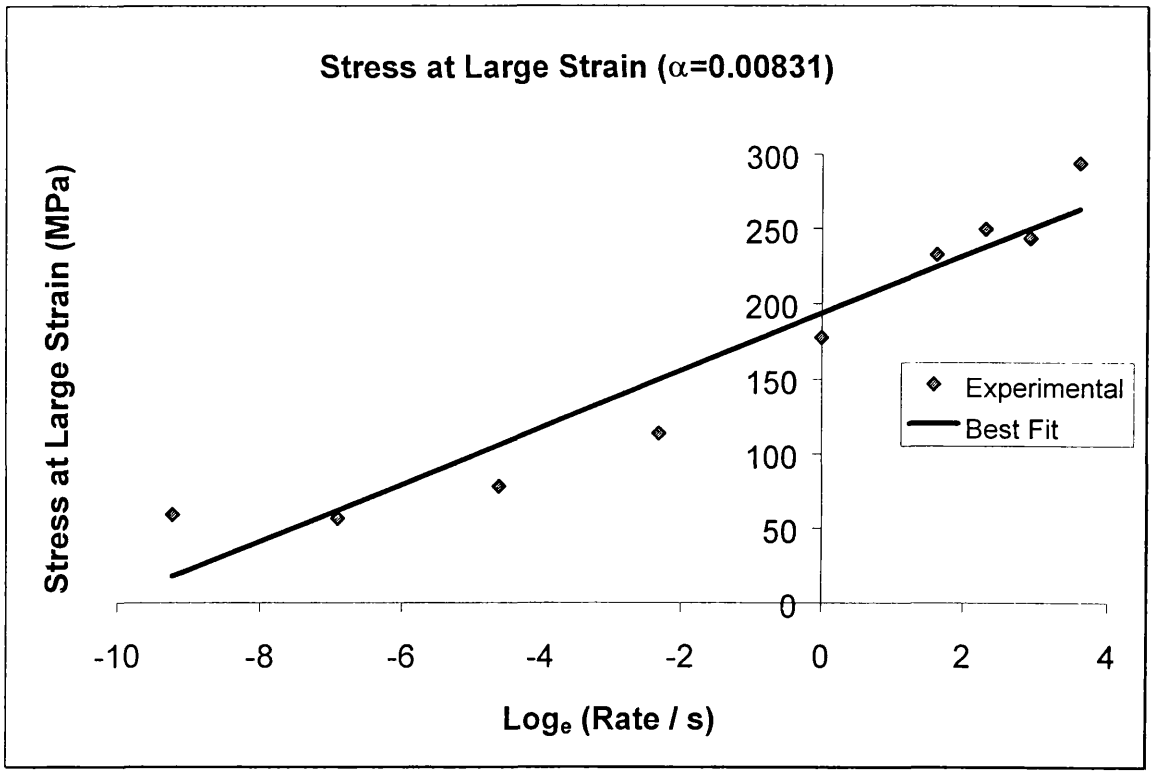

Figure 8.22 Stress at Large Strain at 1123K

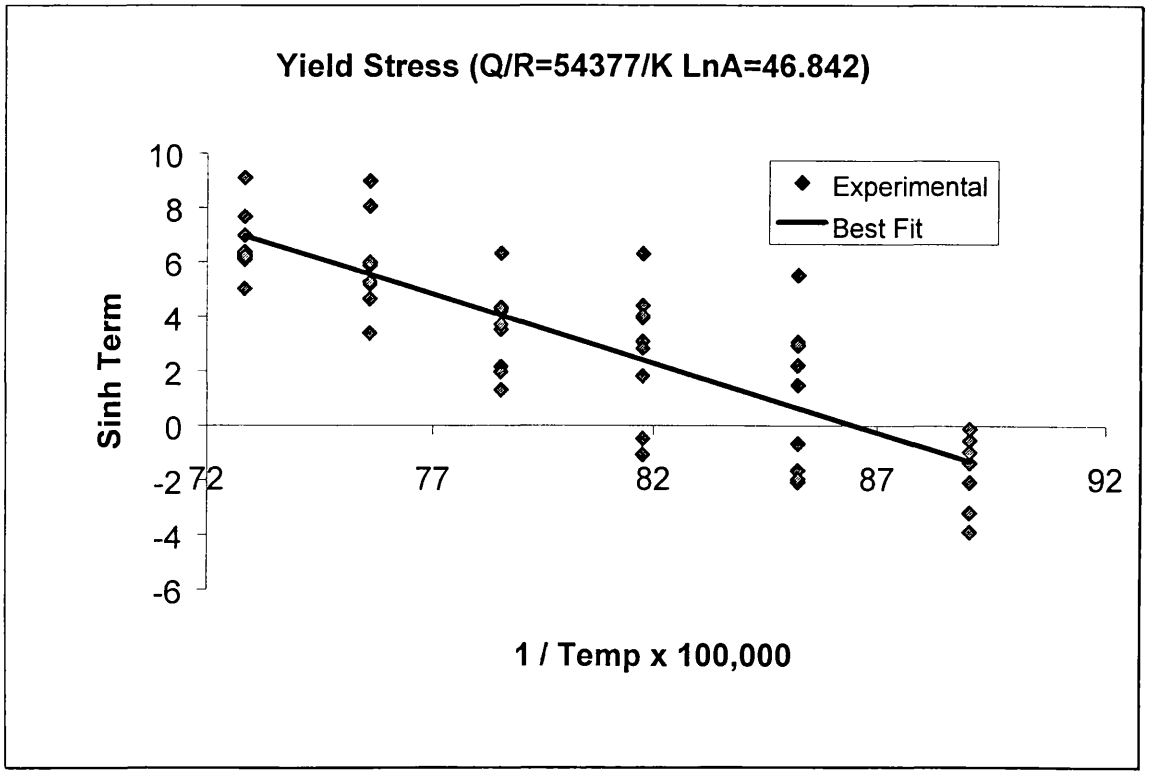

Figure 8.23 Equation (8.5) Values at Yield Stress from1123 to 1373K

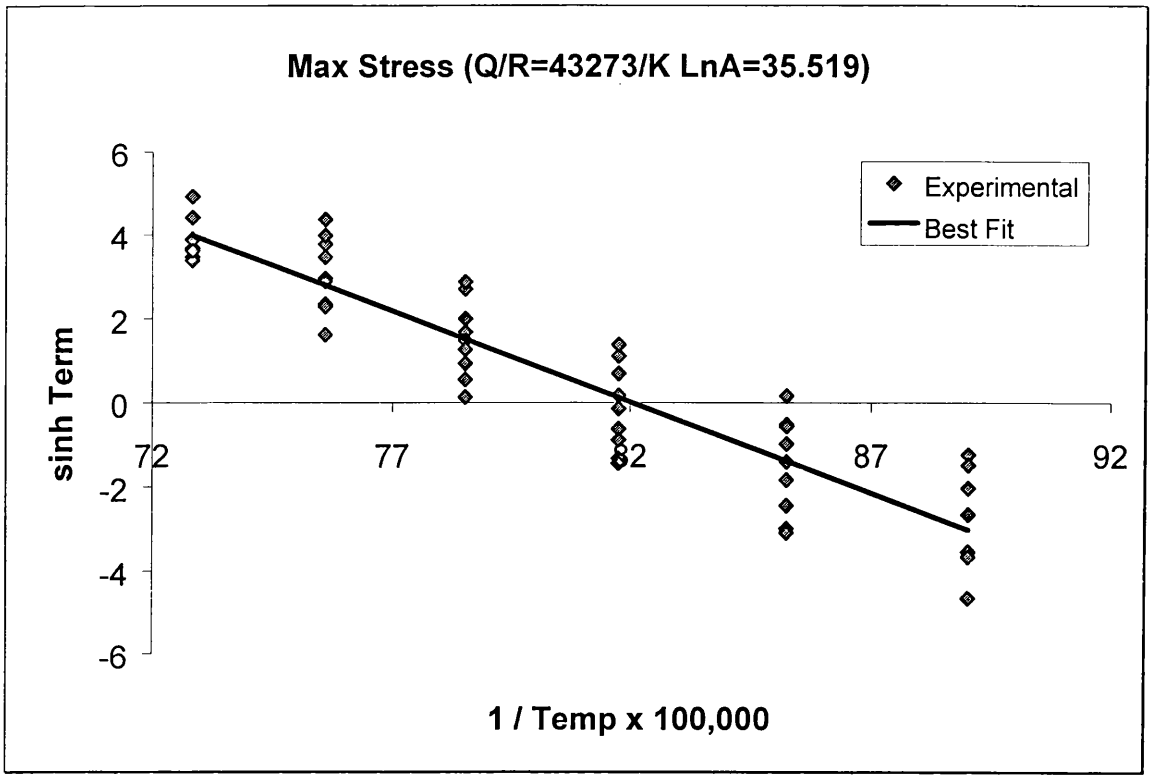

Figure 8.24 Equation (8.5) Values at Maximum Stress from1123 to 1373K

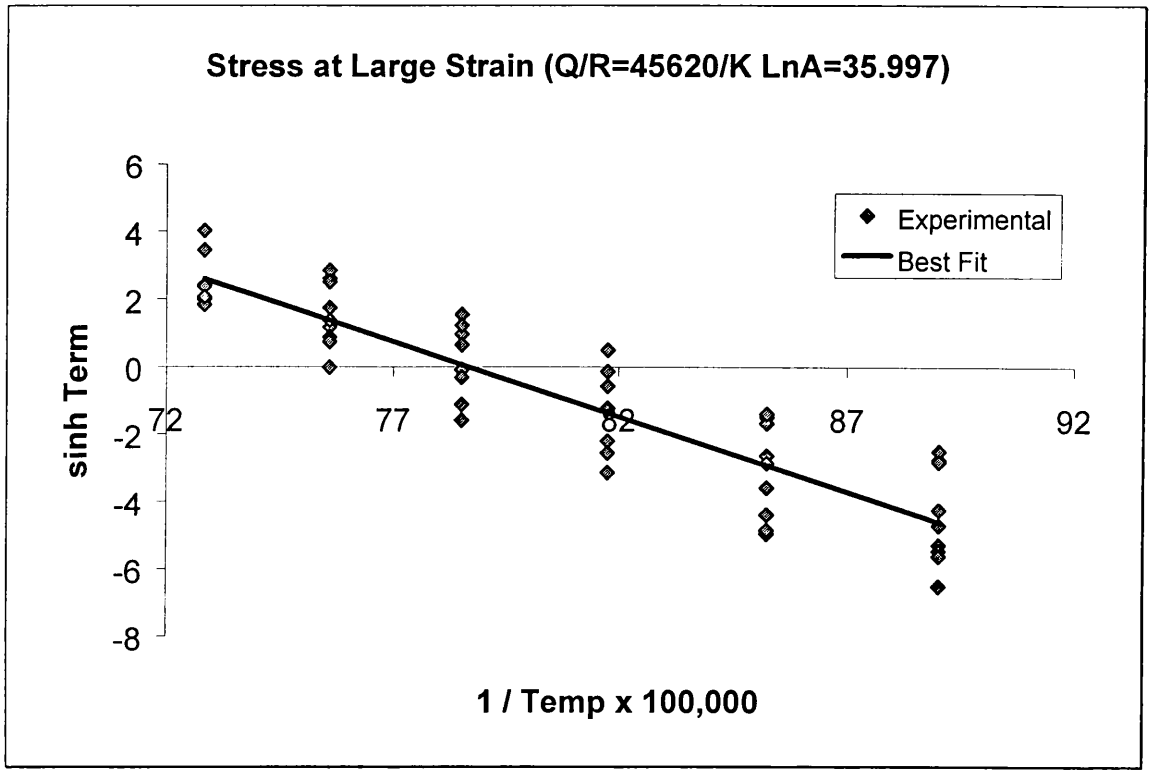

Figure 8.25 Equation (8.5) Values at Stress at Large Strain from 1123 to 1373K

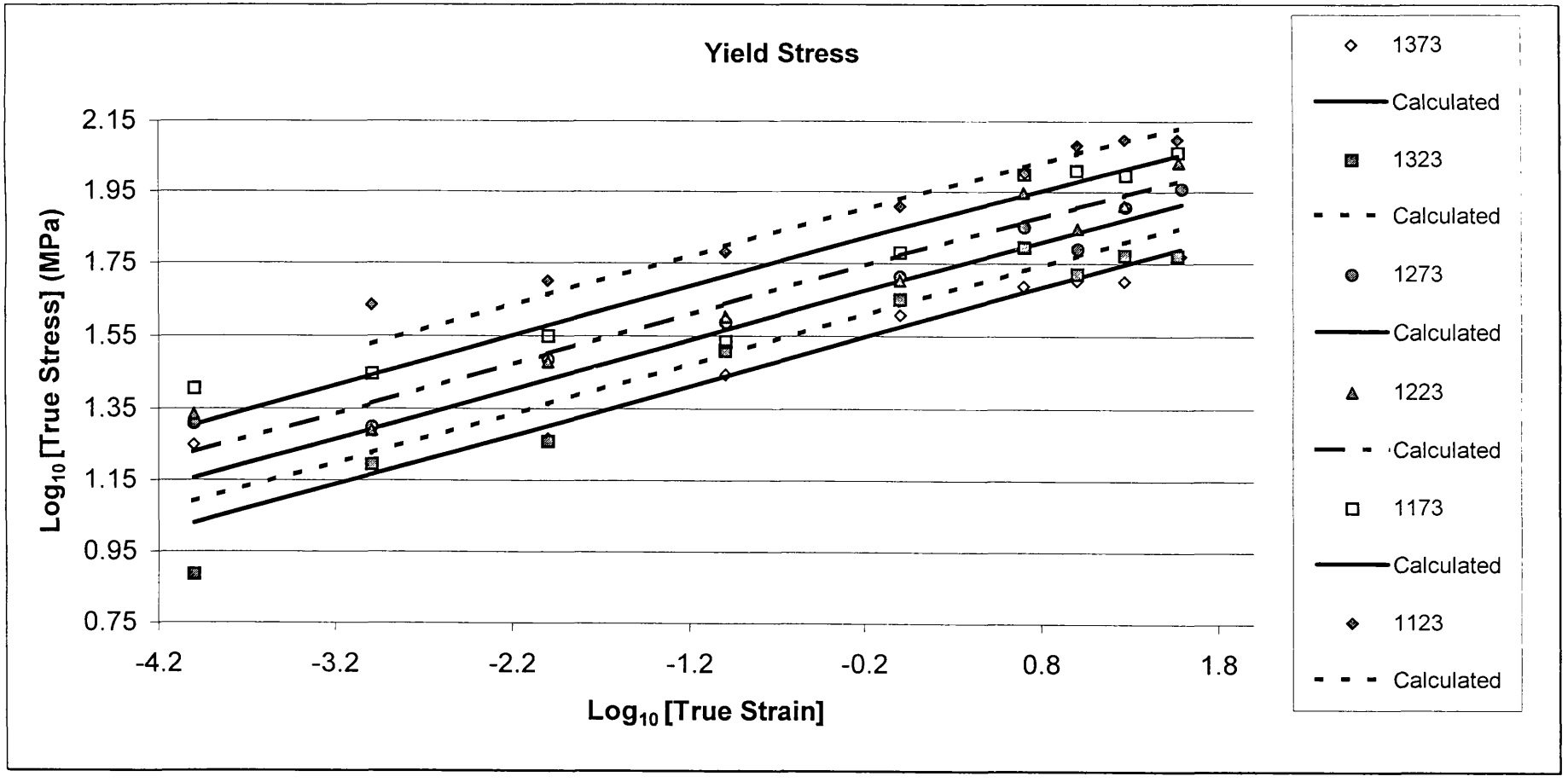

Figure 8.26 Final Hyperbolic Sine Law Predictions for Yield Stress

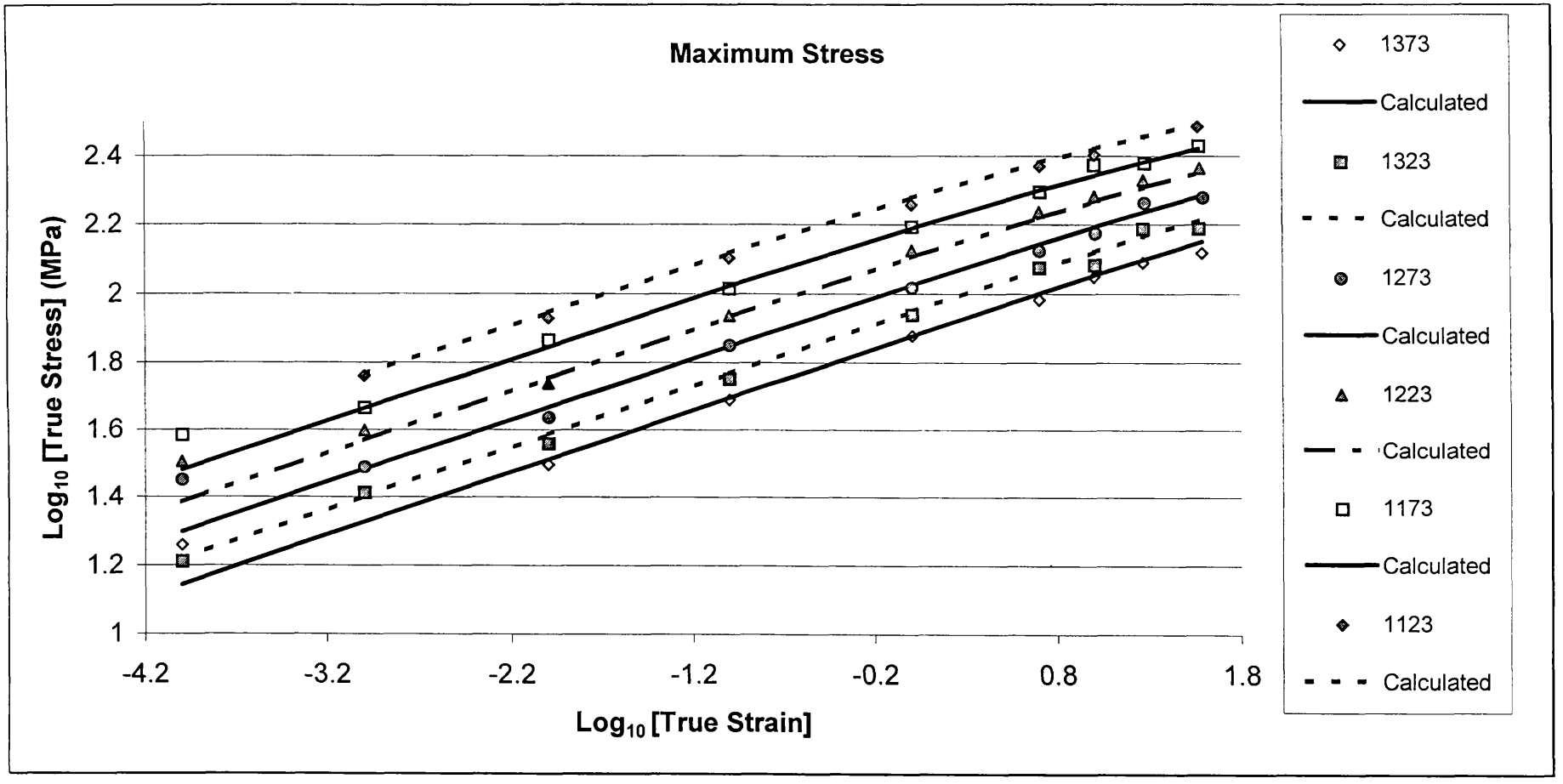

Figure 8.27 Final Hyperbolic Sine Law Predictions for Maximum Stress

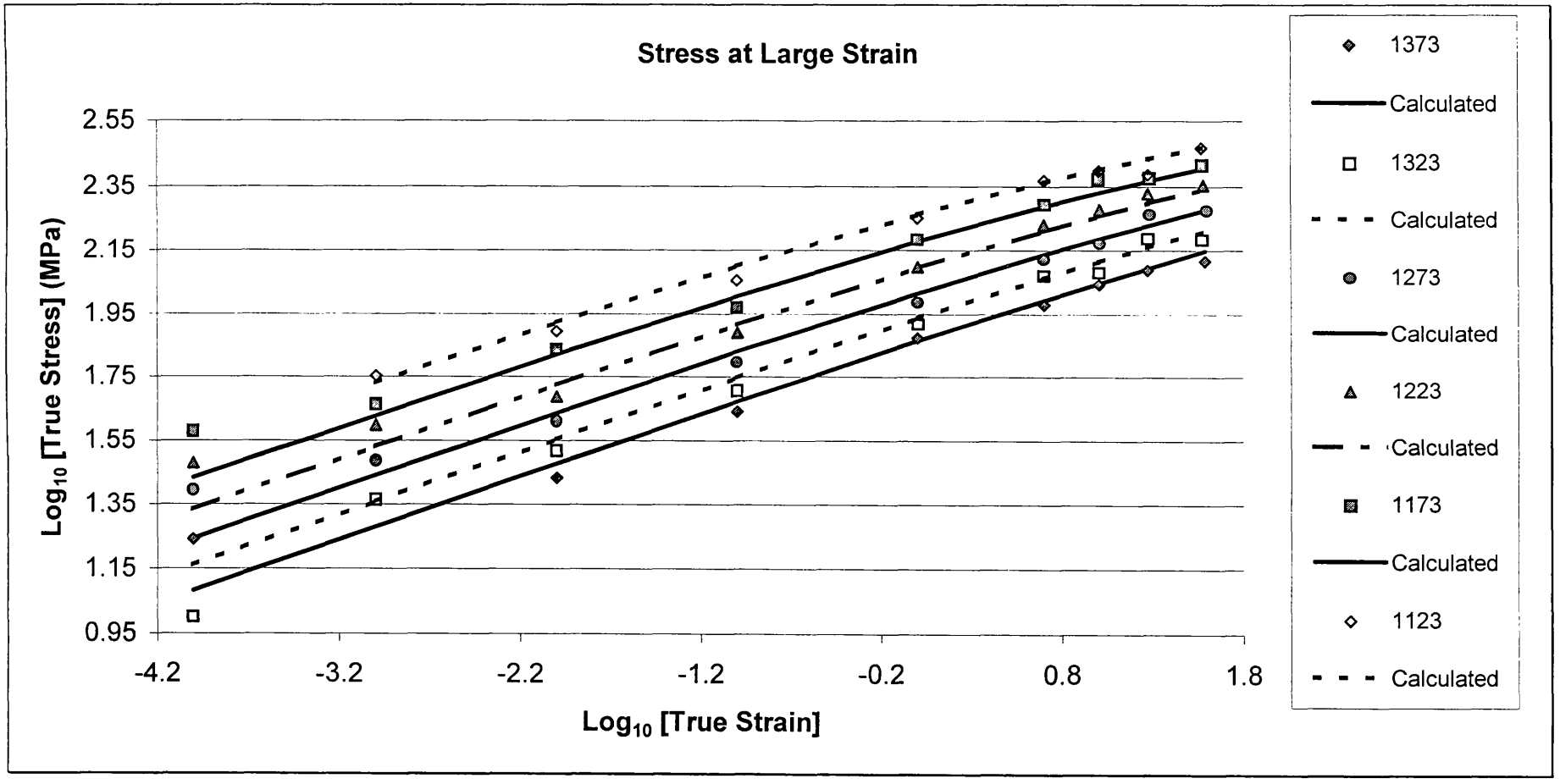

Figure 8.28 Final Hyperbolic Sine Law Predictions for Stress at Large Strain

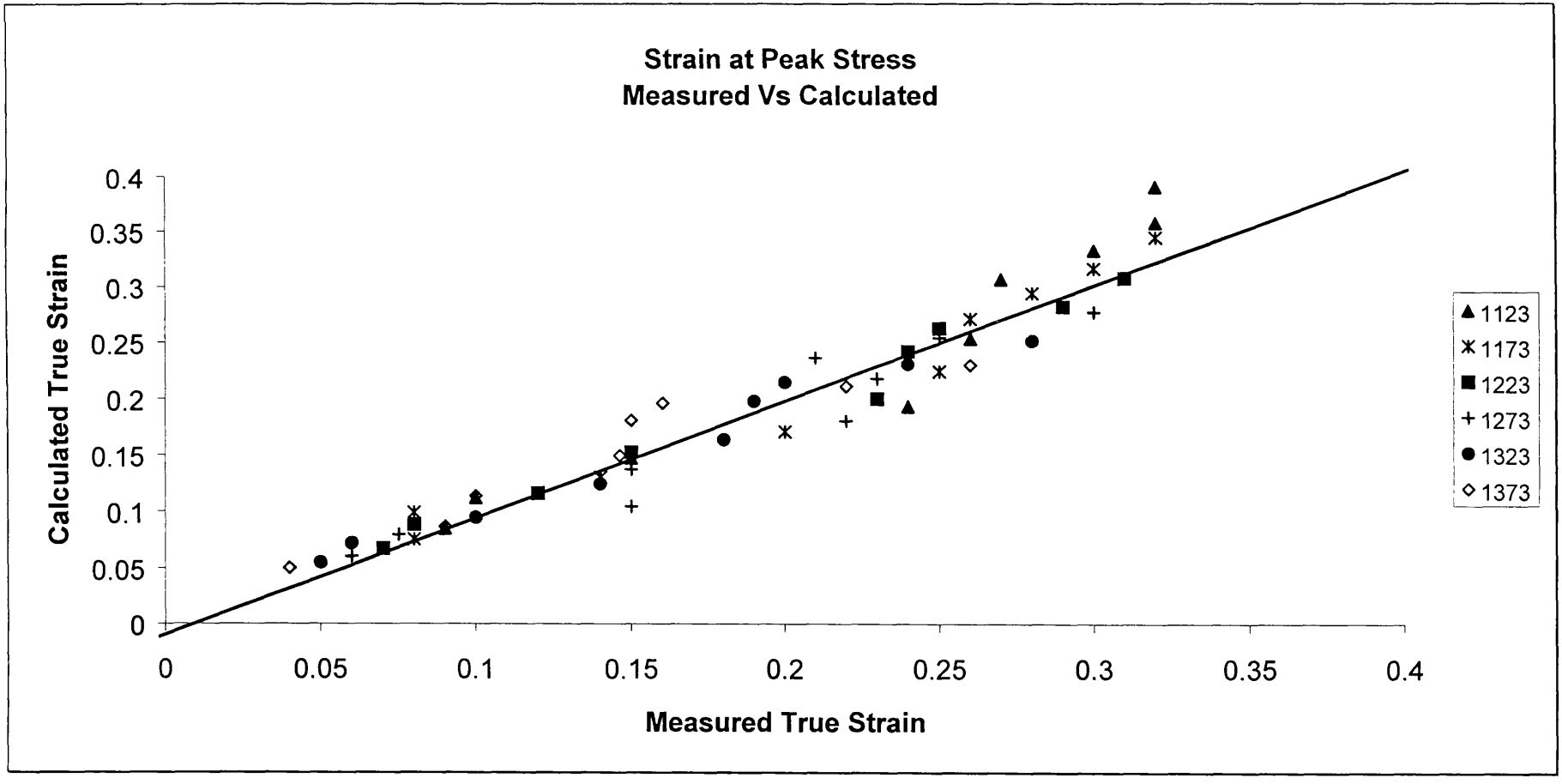

Figure 8.29 Measured and Calculated Strain at Peak Stress for the High Carbon Steel

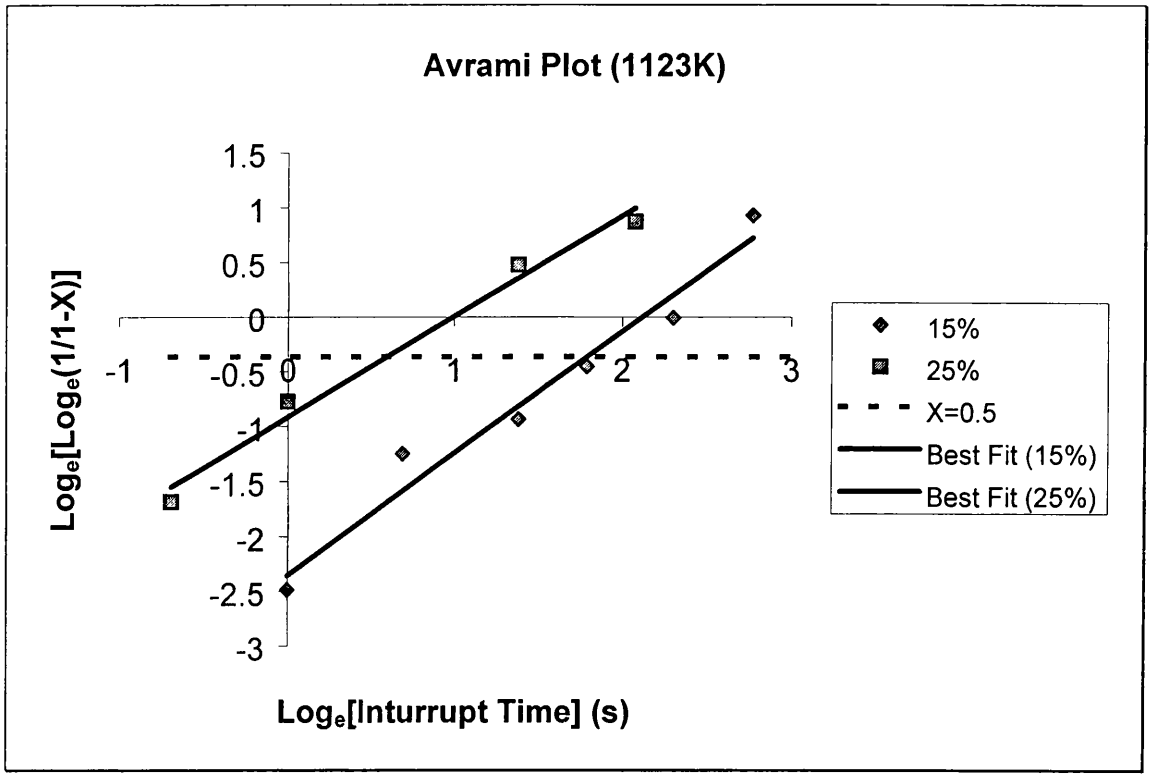

Figure 8.30 Avrami Plot for Interrupt Compression Testing at 1123K

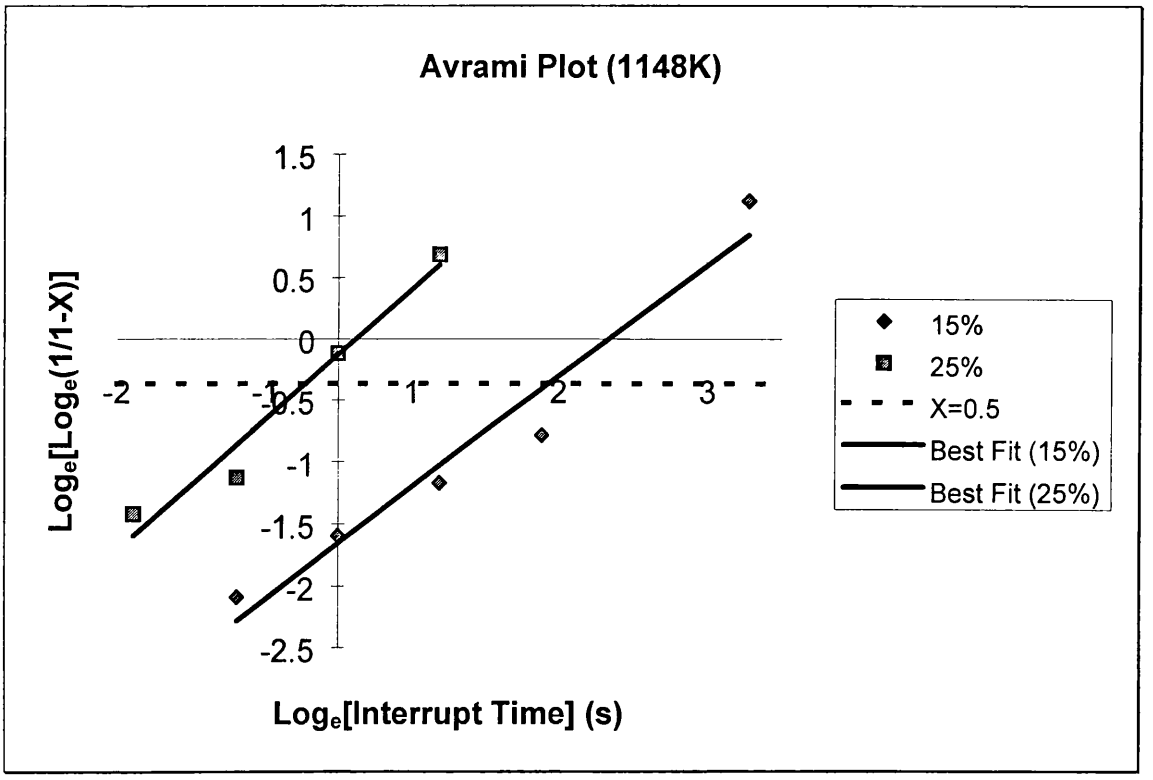

Figure 8.31 Avrami Plot for Interrupt Compression Testing at 1148K

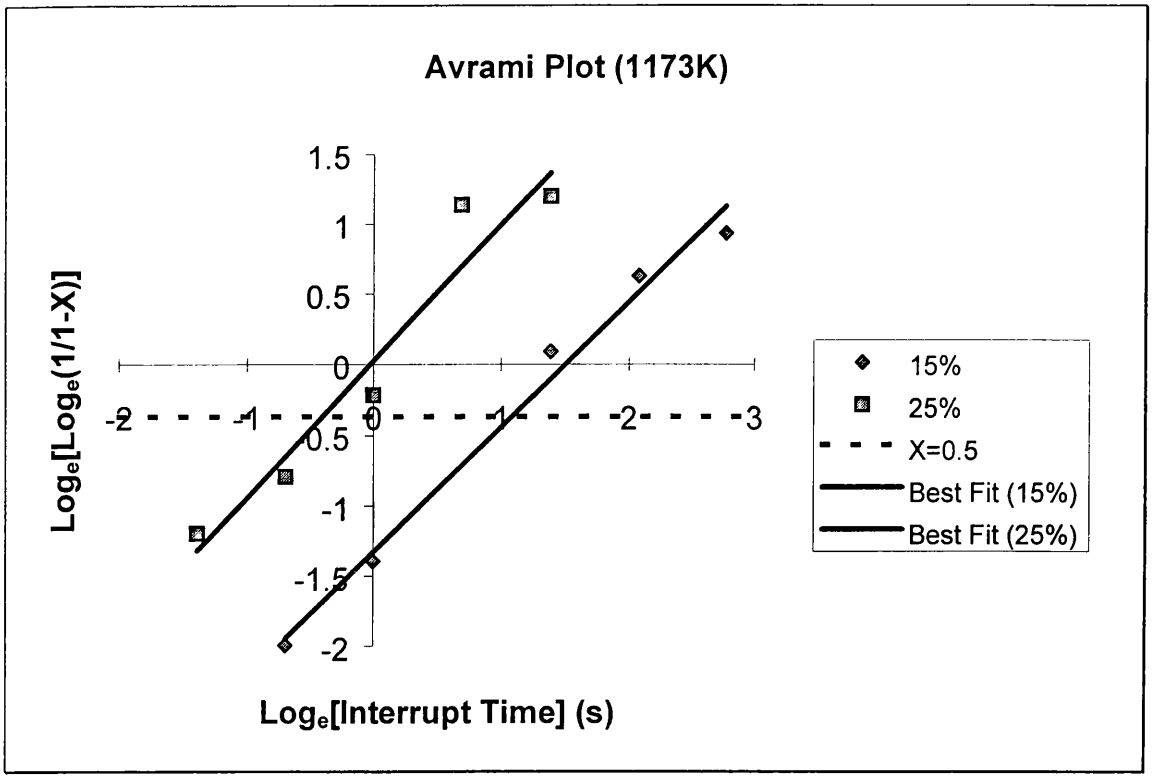

Figure 8.32 Avrami Plot for Interrupt Compression Testing at 1173K

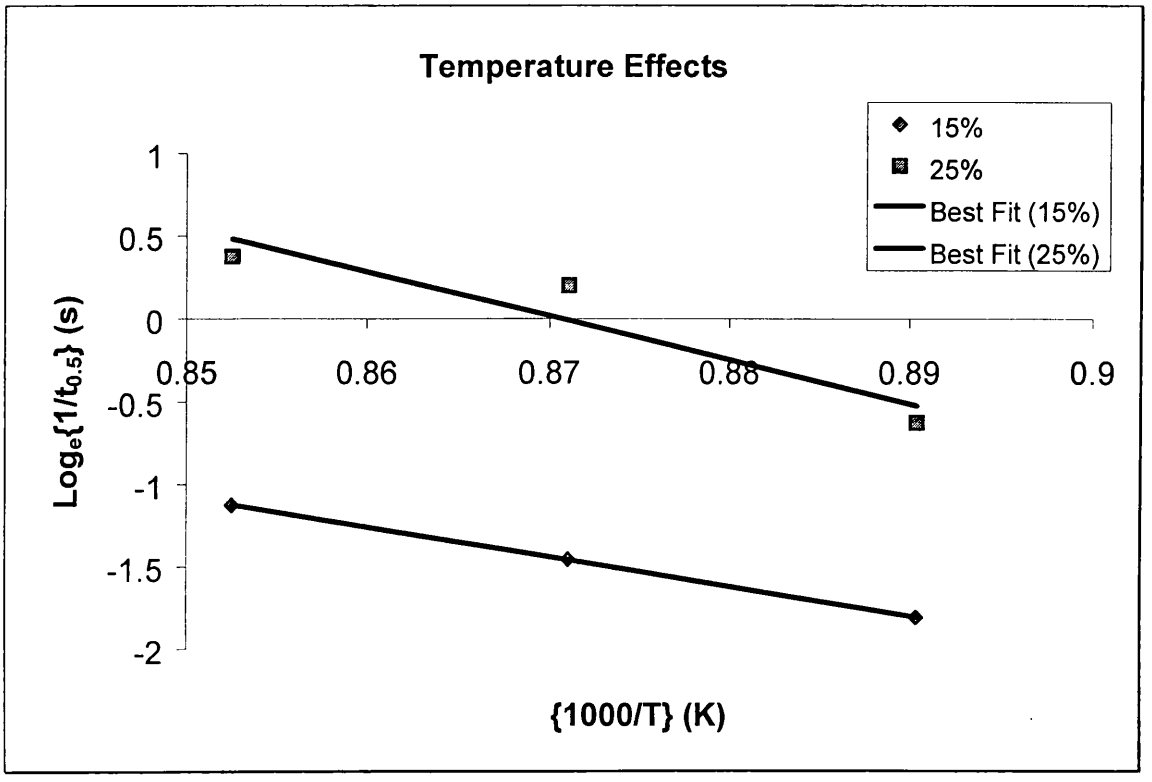

Figure 8.33 Effect of Temperature on Time to 50% Softened

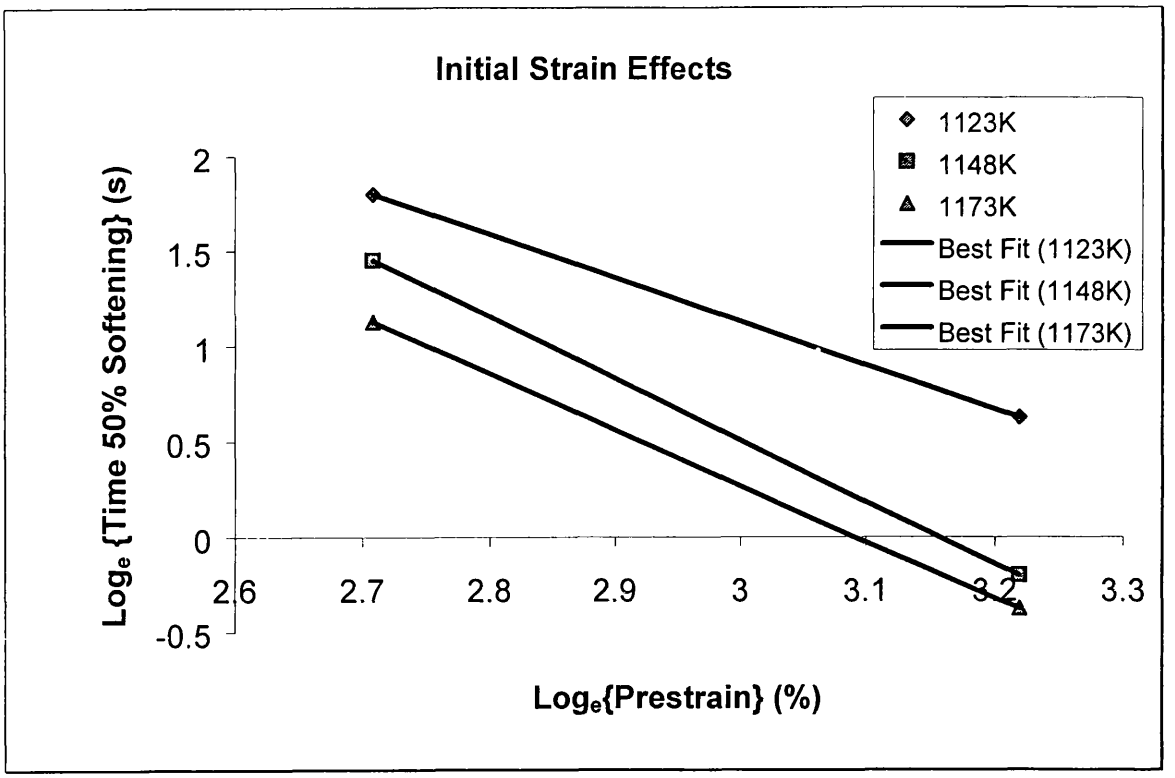

Figure 8.34 Effect of Initial Strain on the time to 50% Softened

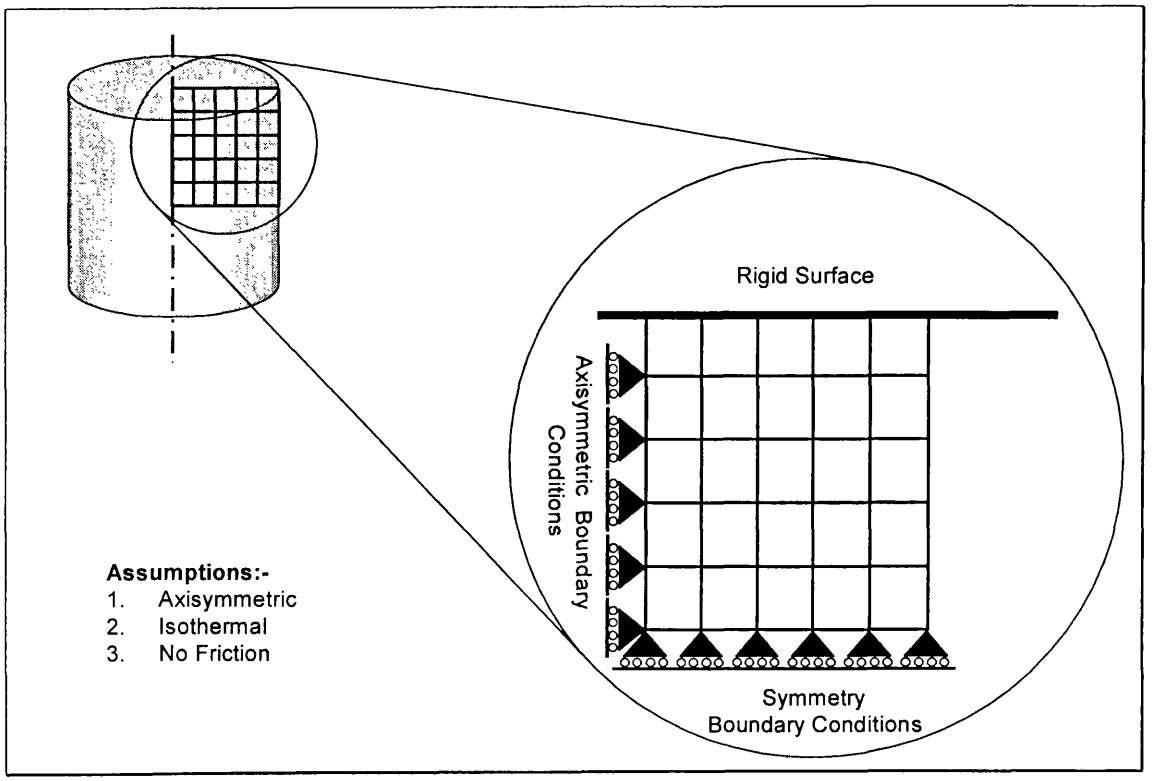

Figure 8.35 Schematic of the Cylinder Upsetting Problem.

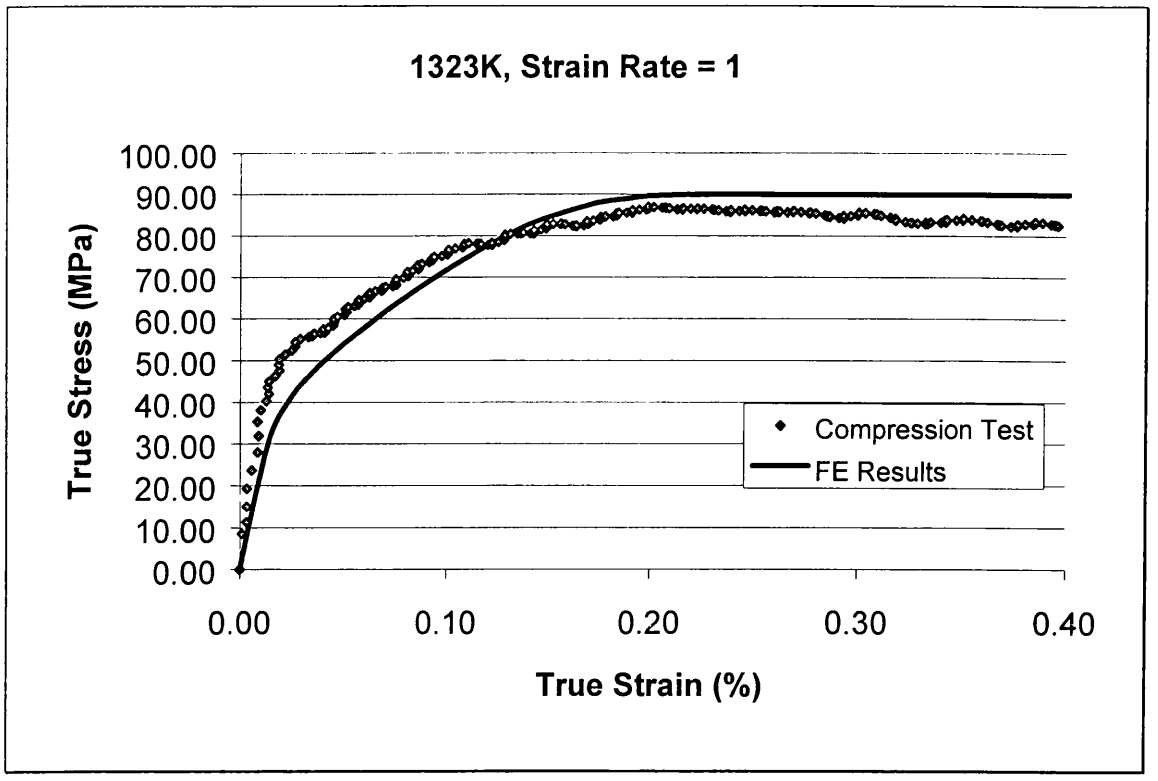

Figure 8.36 True Stress/Strain Results for the Cylinder Upsetting Example.

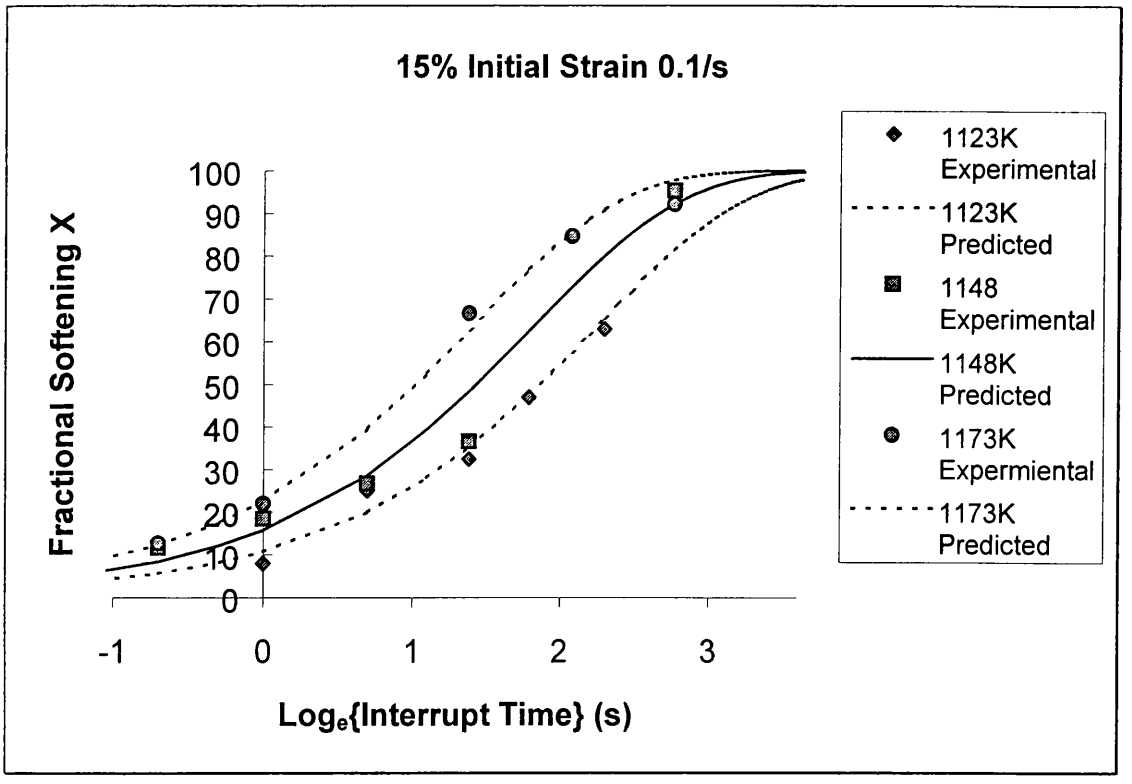

Figure 8.37 Experimental and Predicted Time for Fractional Softening

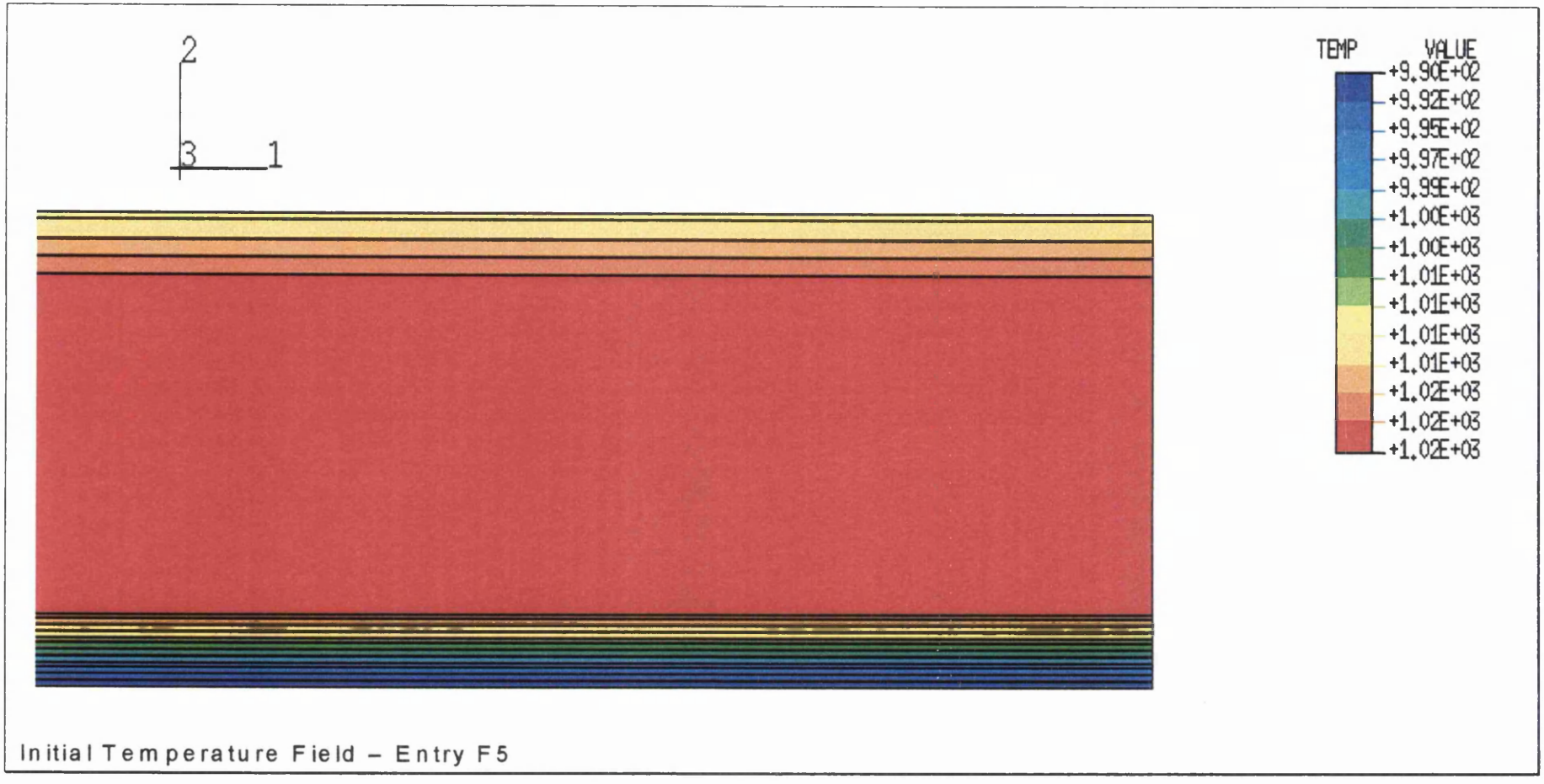

Figure 8.38 Temperature distribution at Entry to the Finishing Mill.

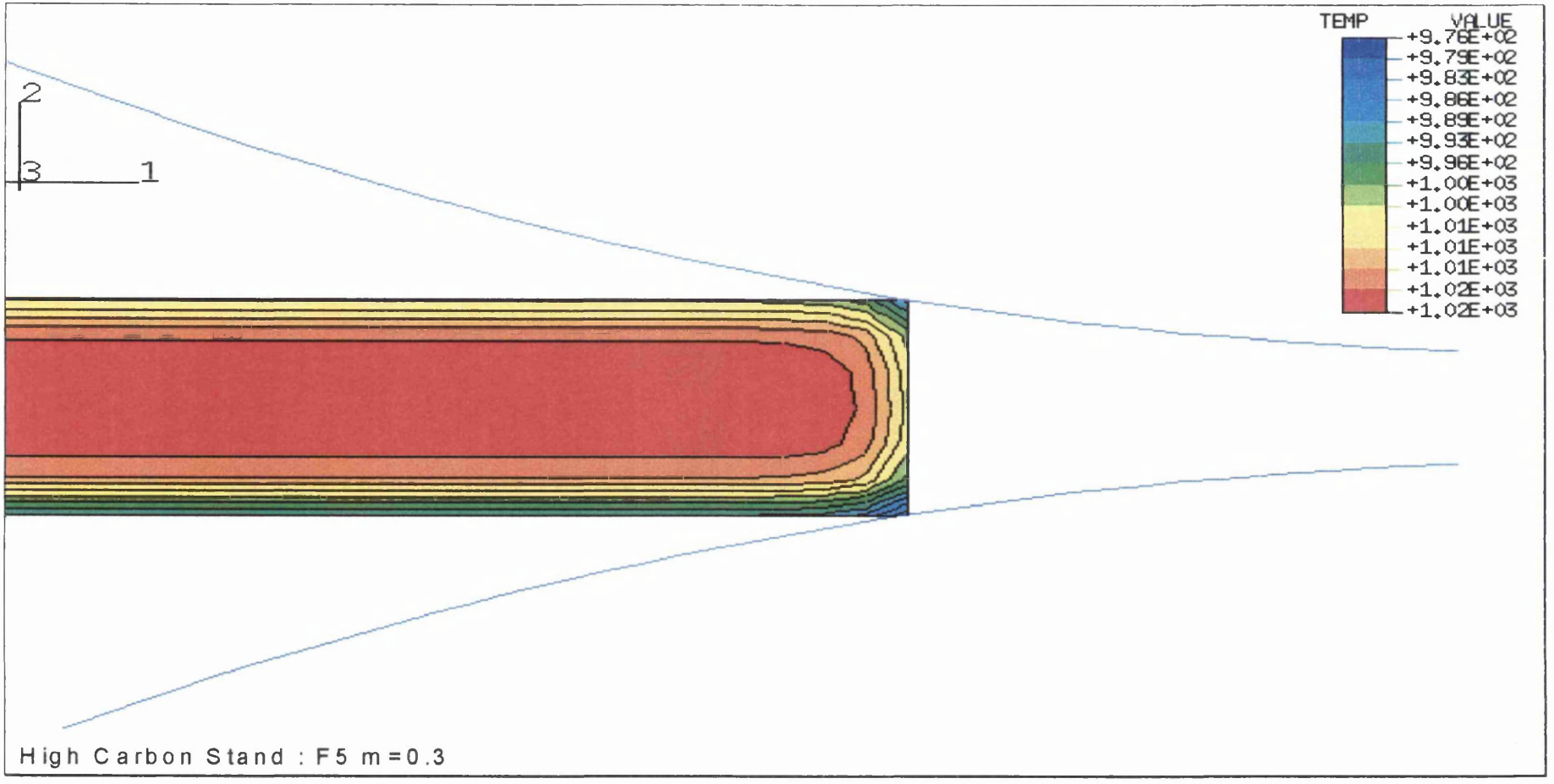

Figure 8.39 Temperature Distribution at Entry to the First Finishing Stand

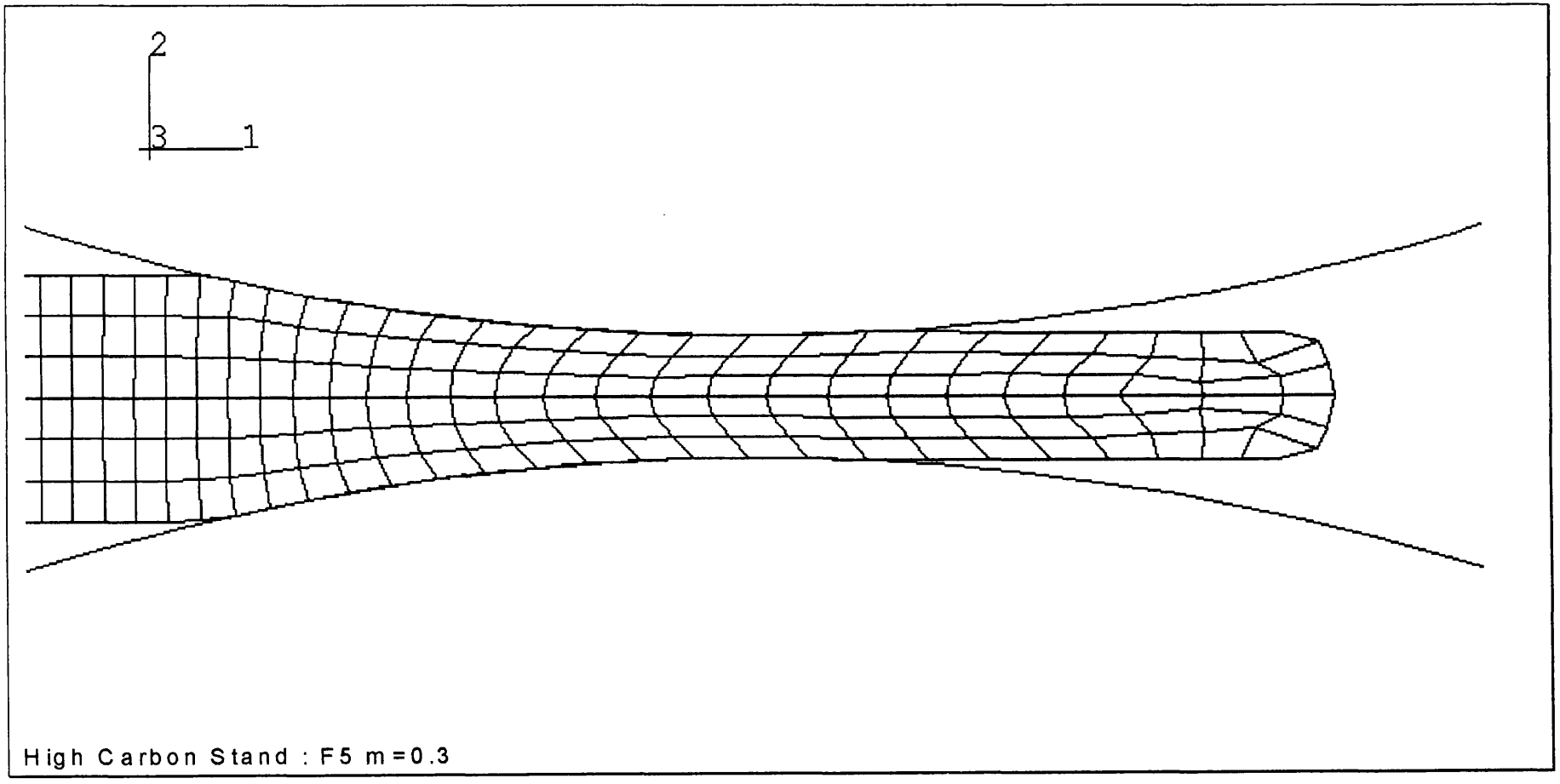

Figure 8.40 Displaced Mesh for Stand 1 (table 8.7)

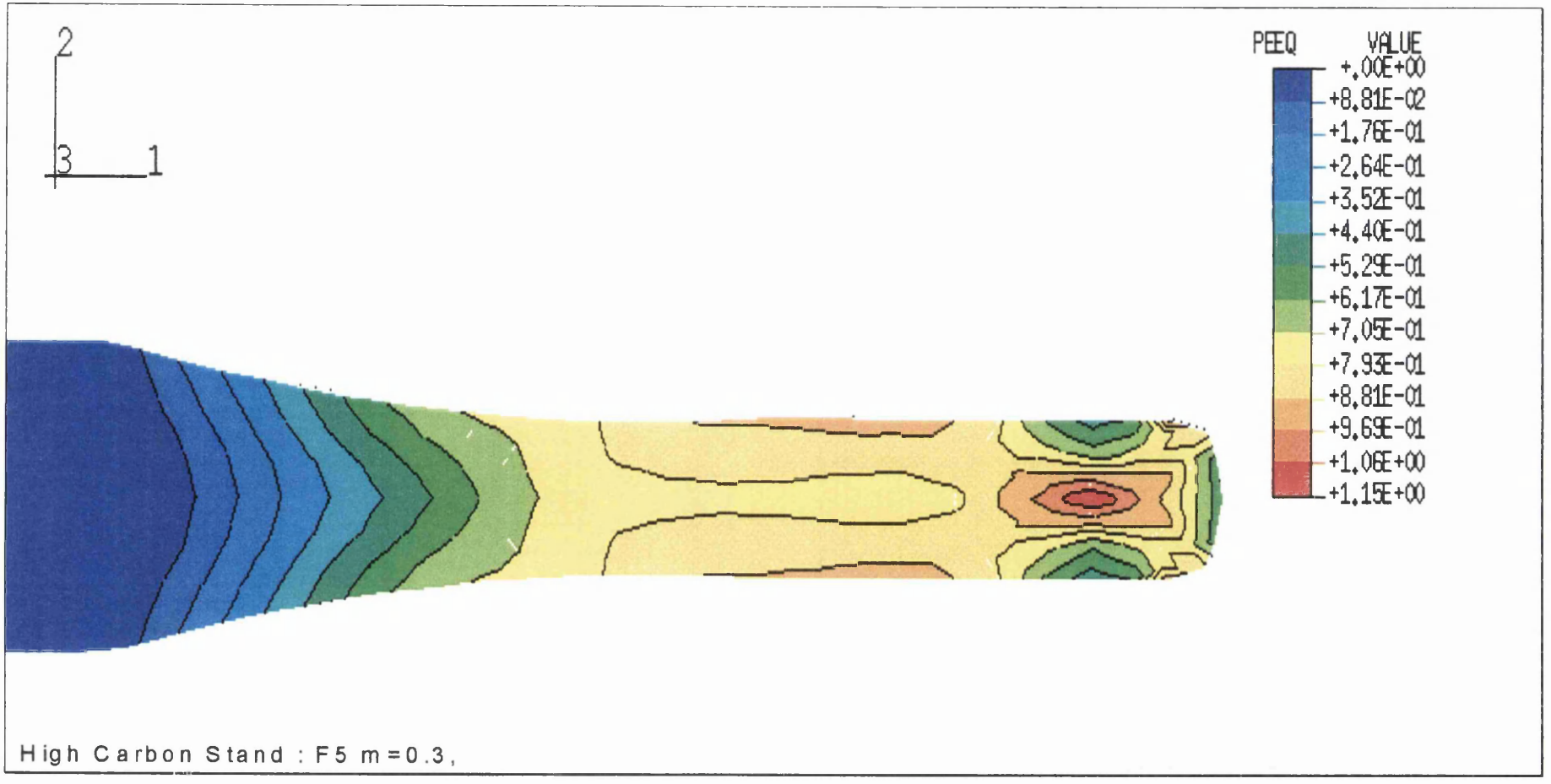

Figure 8.41 Plastic Effective Strain Distribution for Stand 1 (Table 8.7)

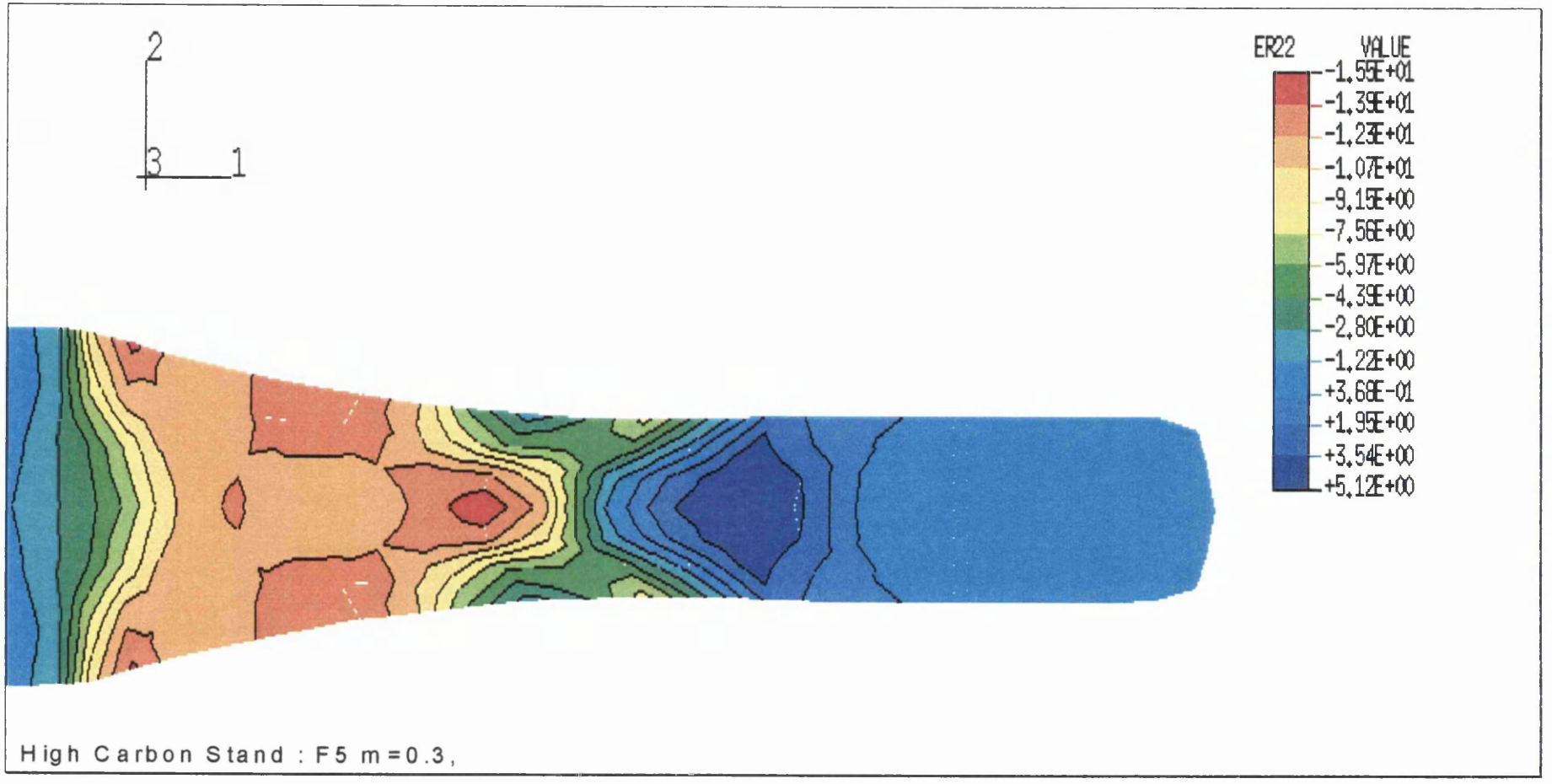

Figure 8.42 Strain Rate in the y-y Direction for Stand 1 (table 8.7)

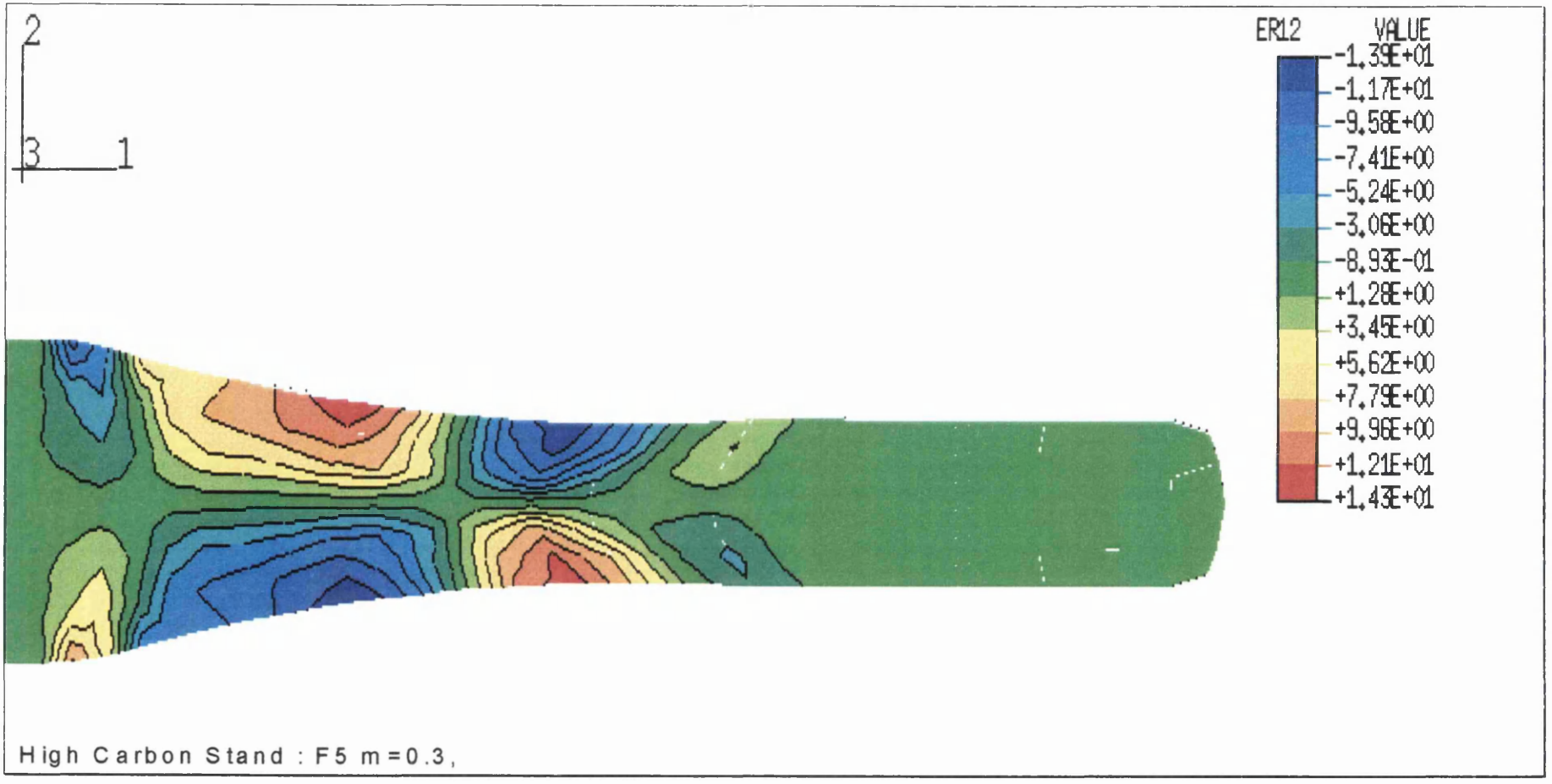

Figure 8.43 Shear Strain Rate in the x-y Direction for Stand 5 (table 8.7)

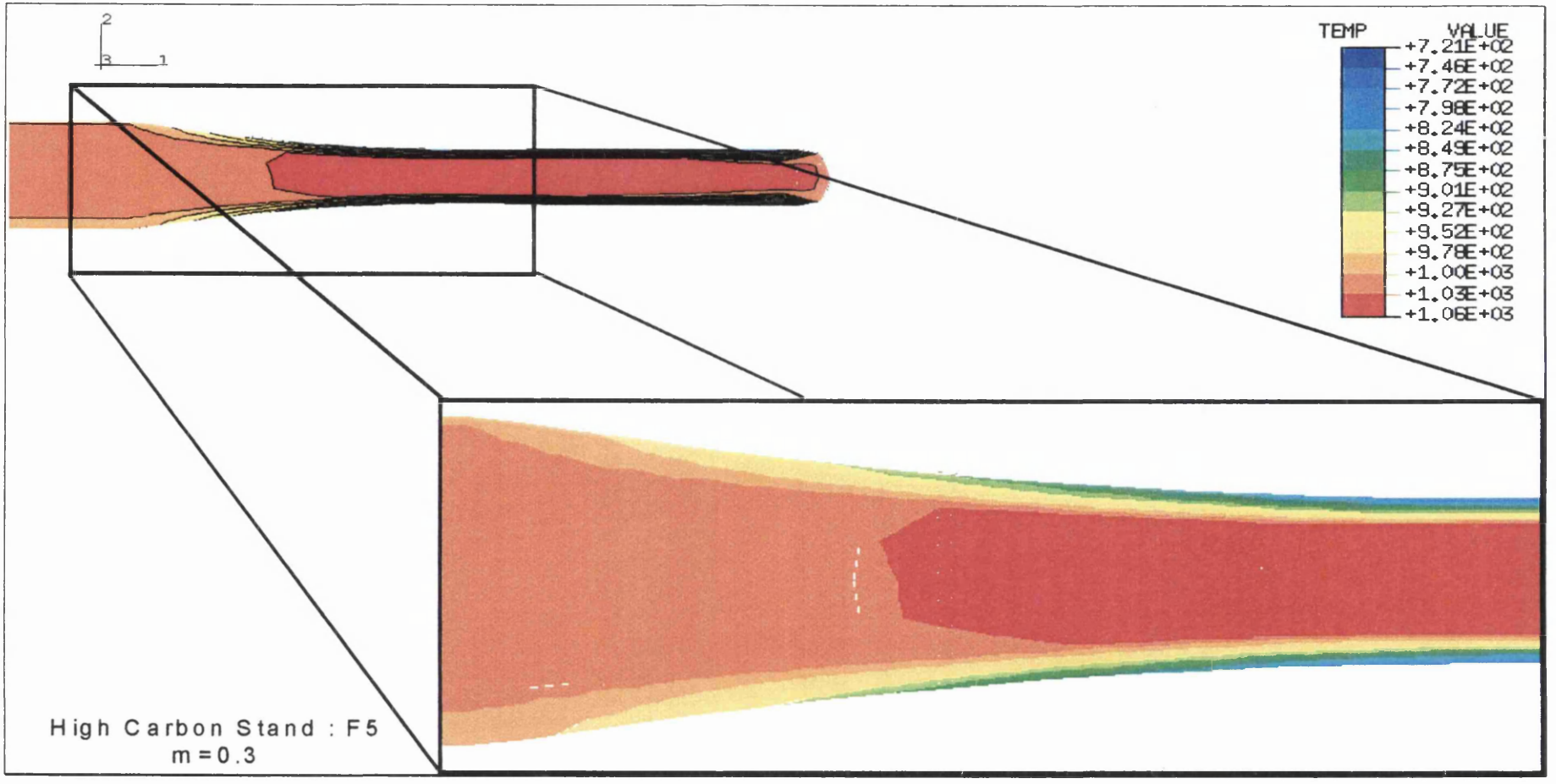

Figure 8.44 Temperature Distribution for Stand F5 (Table 8.7)

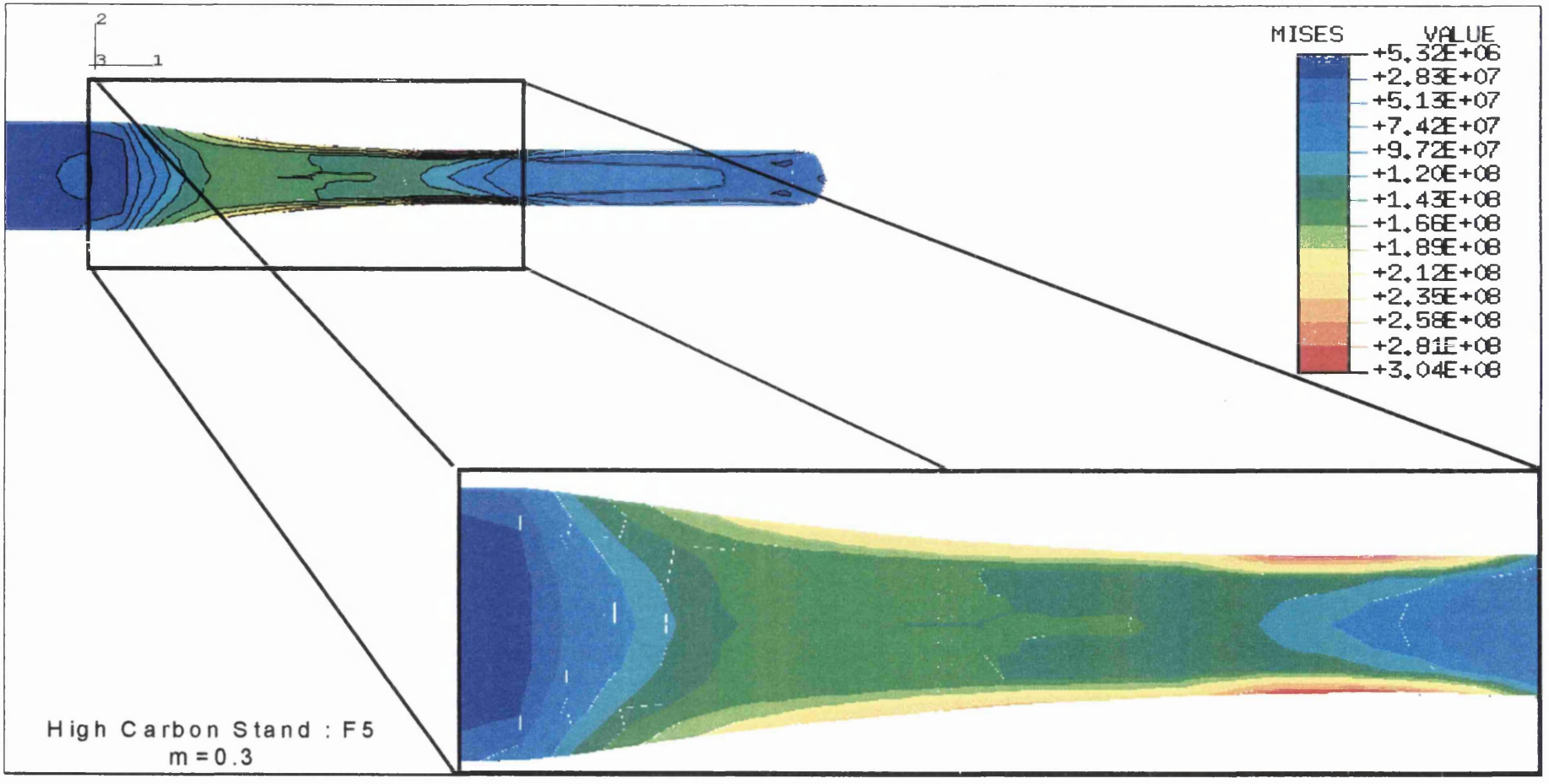

Figure 8.45 Mises Stress Distribution for Stand 1 (table 8.7)

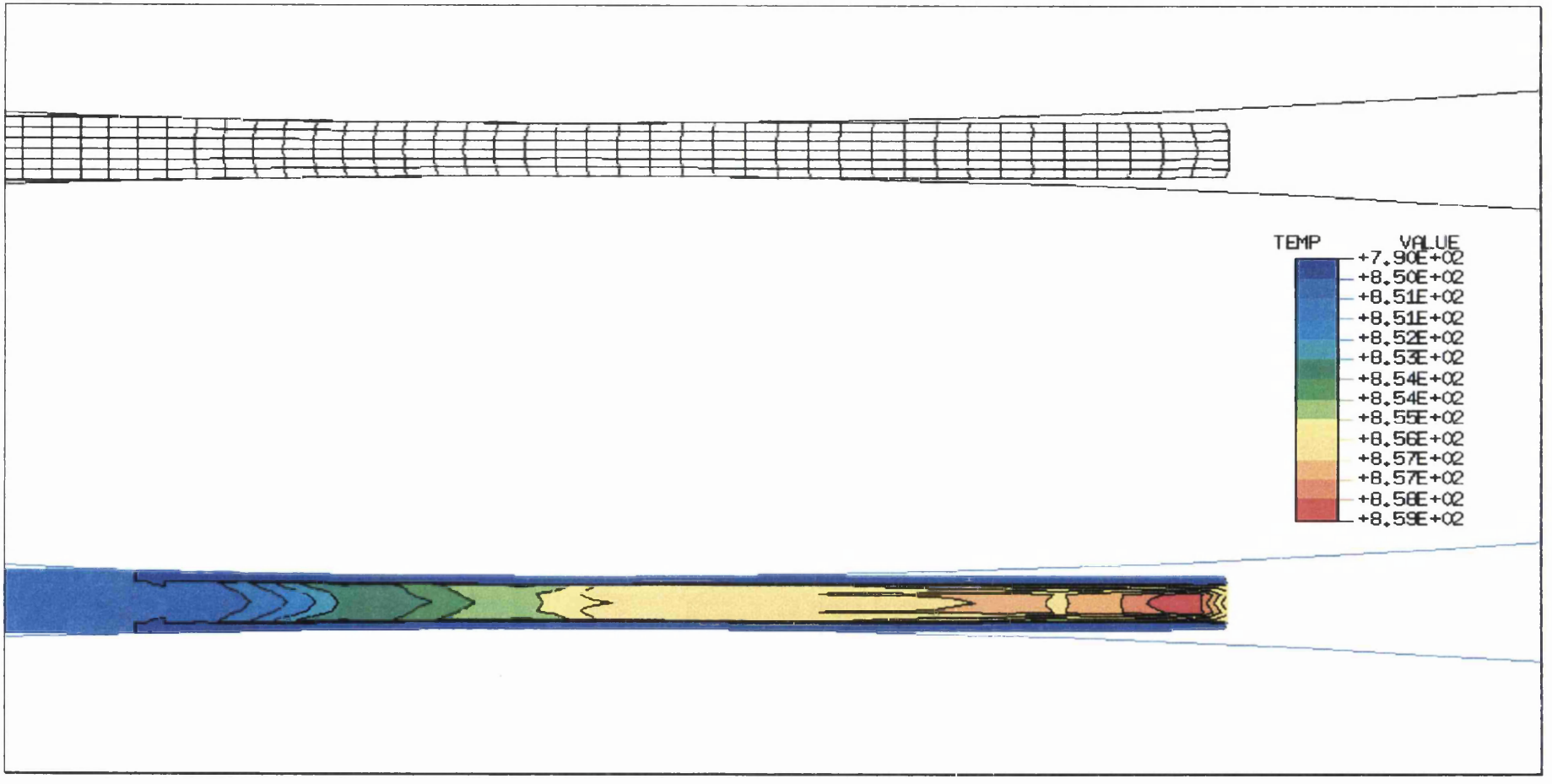

Figure 8.46 Displaced Mesh and Temperature Distribution for Stand 7 (table 8.7)

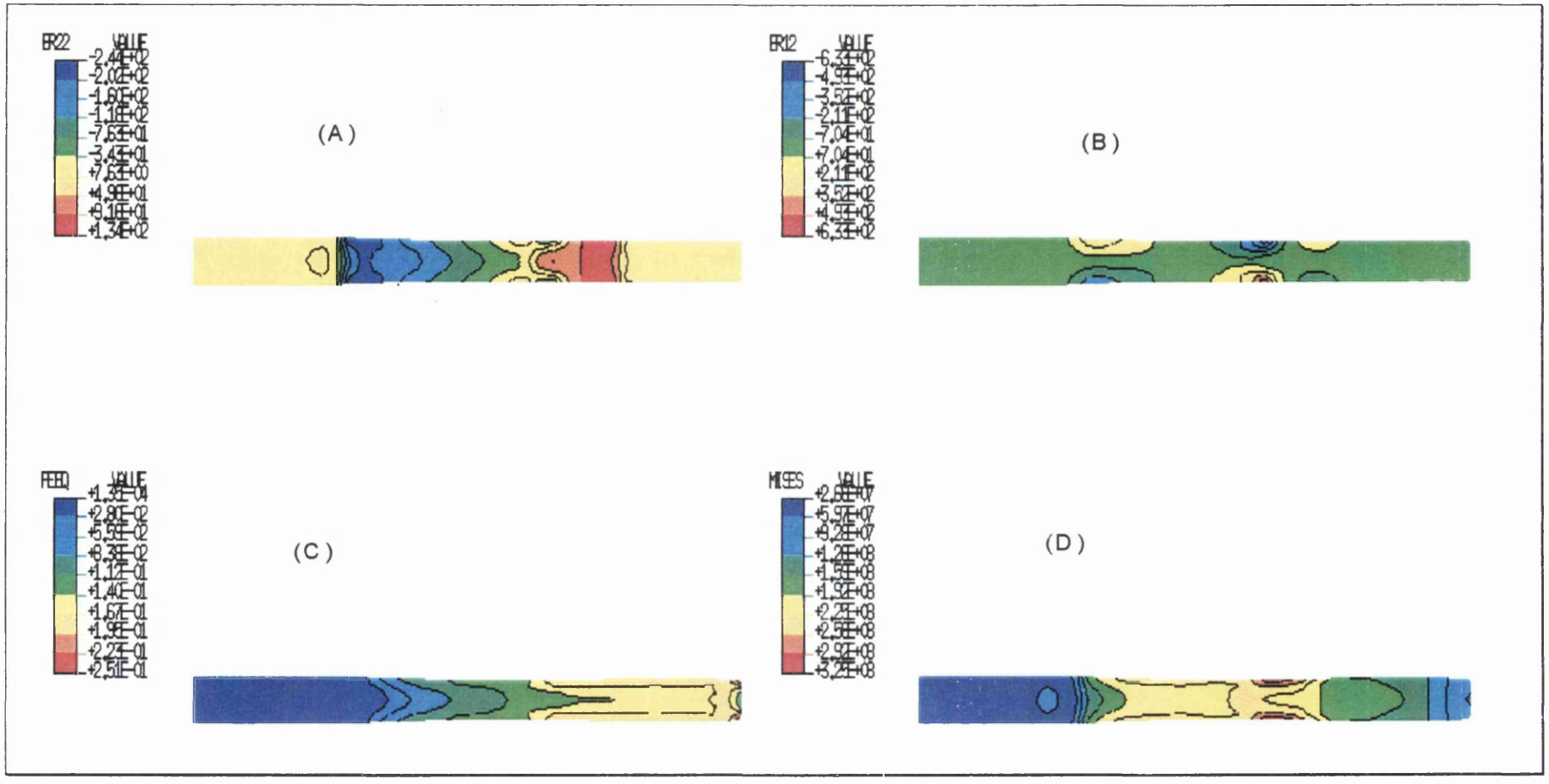

Figure 8.47 A) Strain Rate B) Shear Strain Rate C) Plastic Equivalent Strain D) Mises Stress Distributions for Stand 7 (table 8.7)

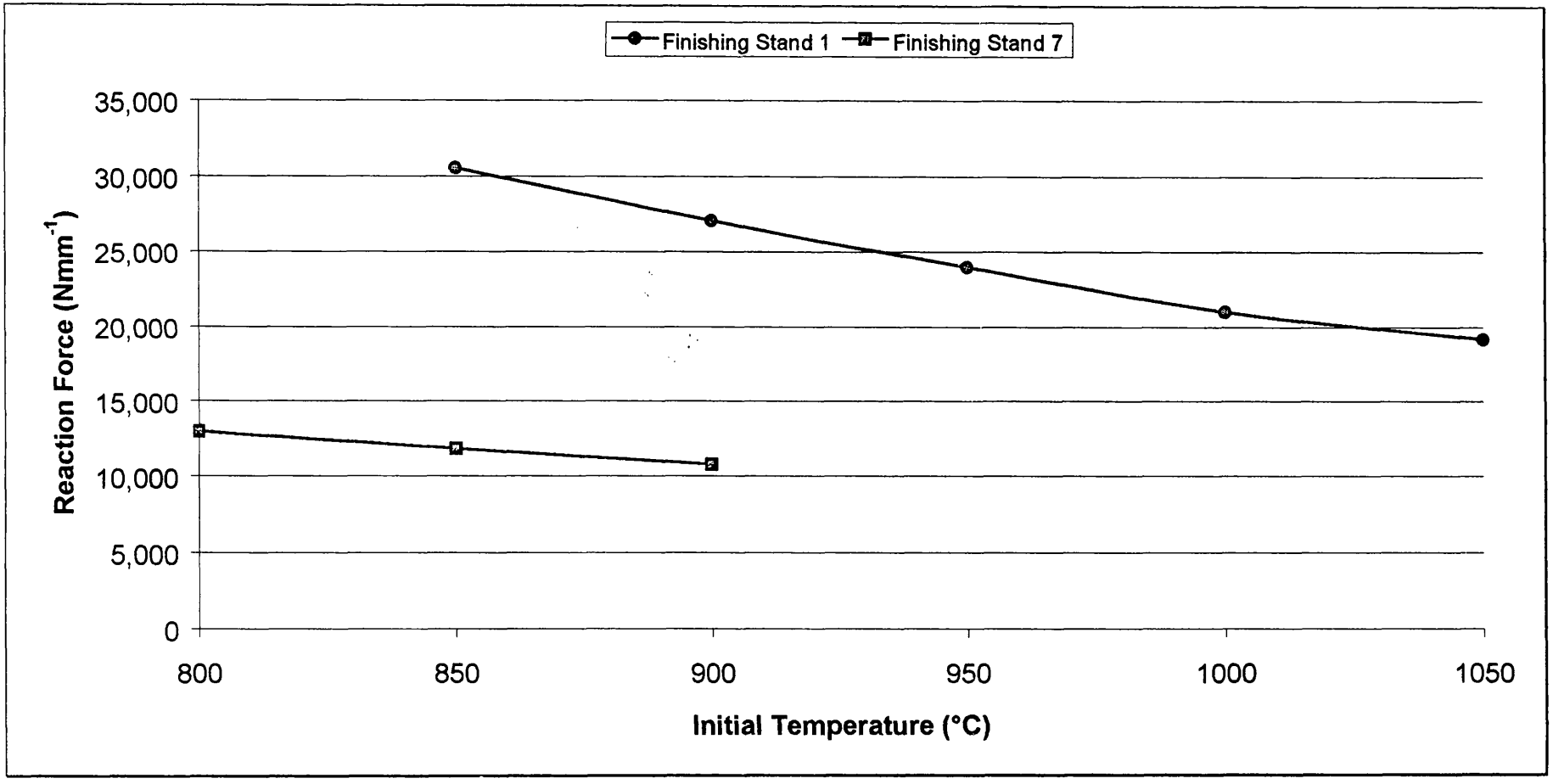

Figure 8.48 Rolling Loads for Stands 1 and 7 With Varying Initial Temperature

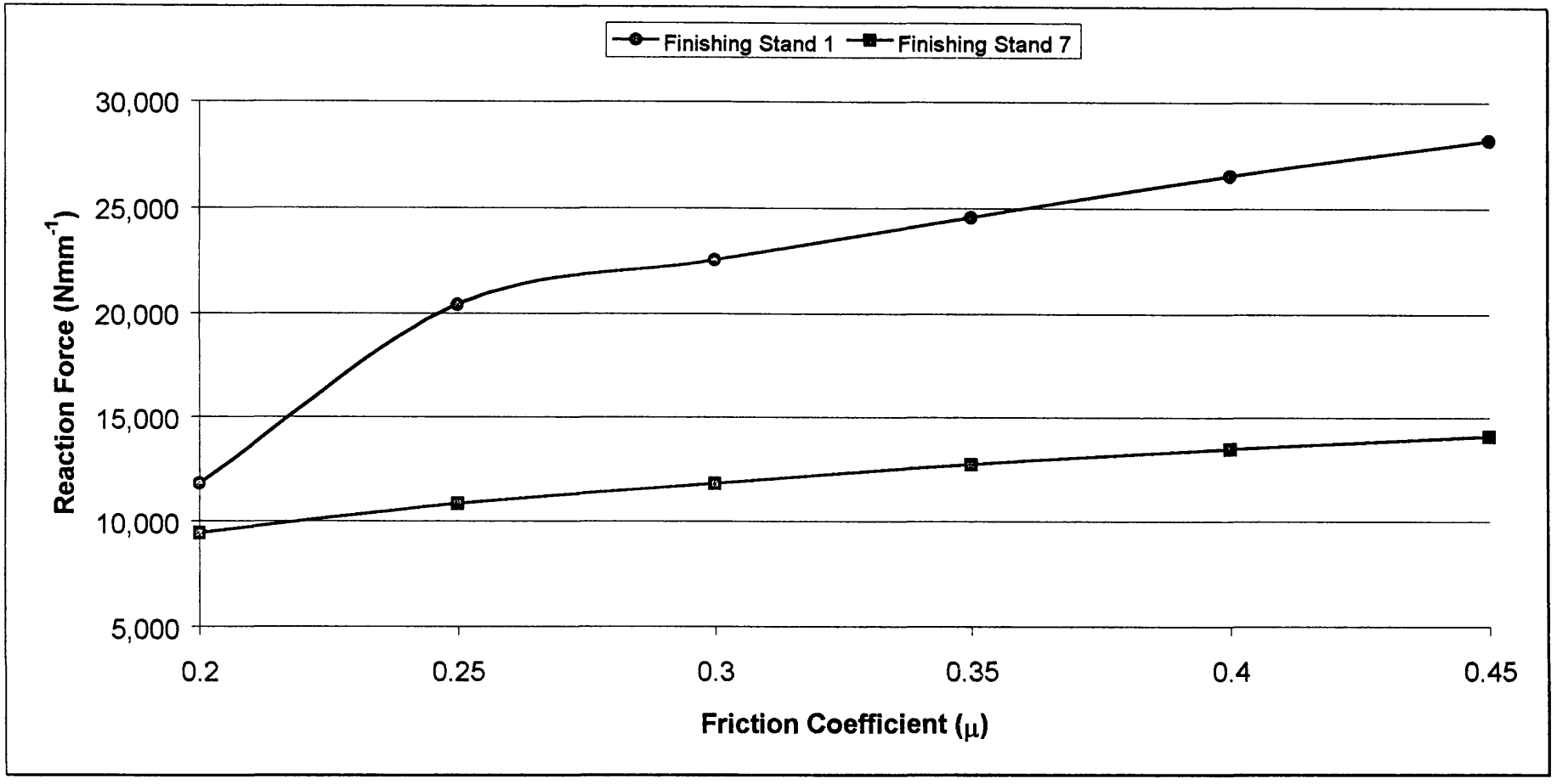

Figure 8.49 Rolling Loads for Stands 1 and 7 with Varying Coefficient of Friction

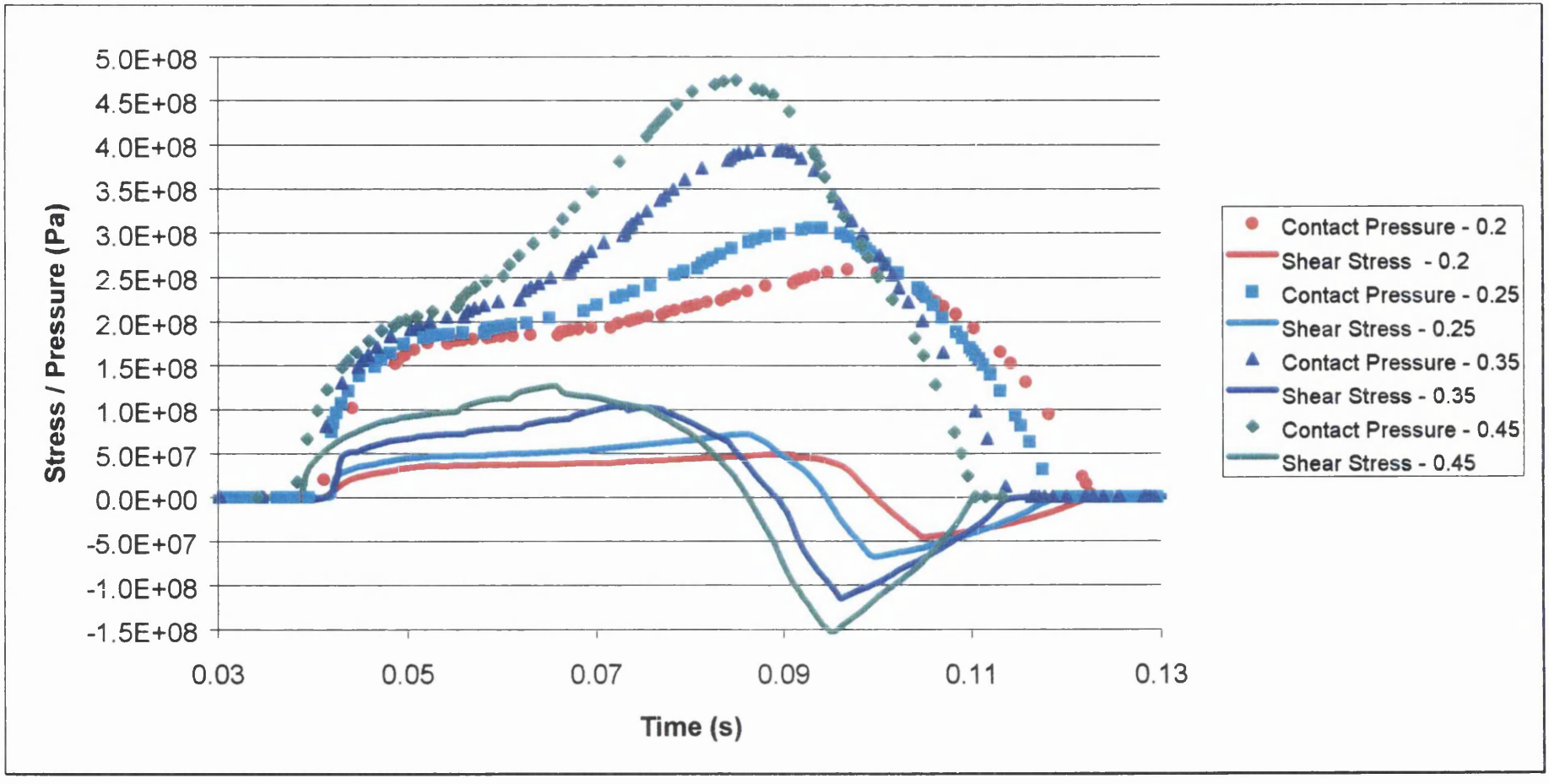

Figure 8.50 Contact Pressures and Shear Stresses for Stand 1 with Varying Friction Coefficients

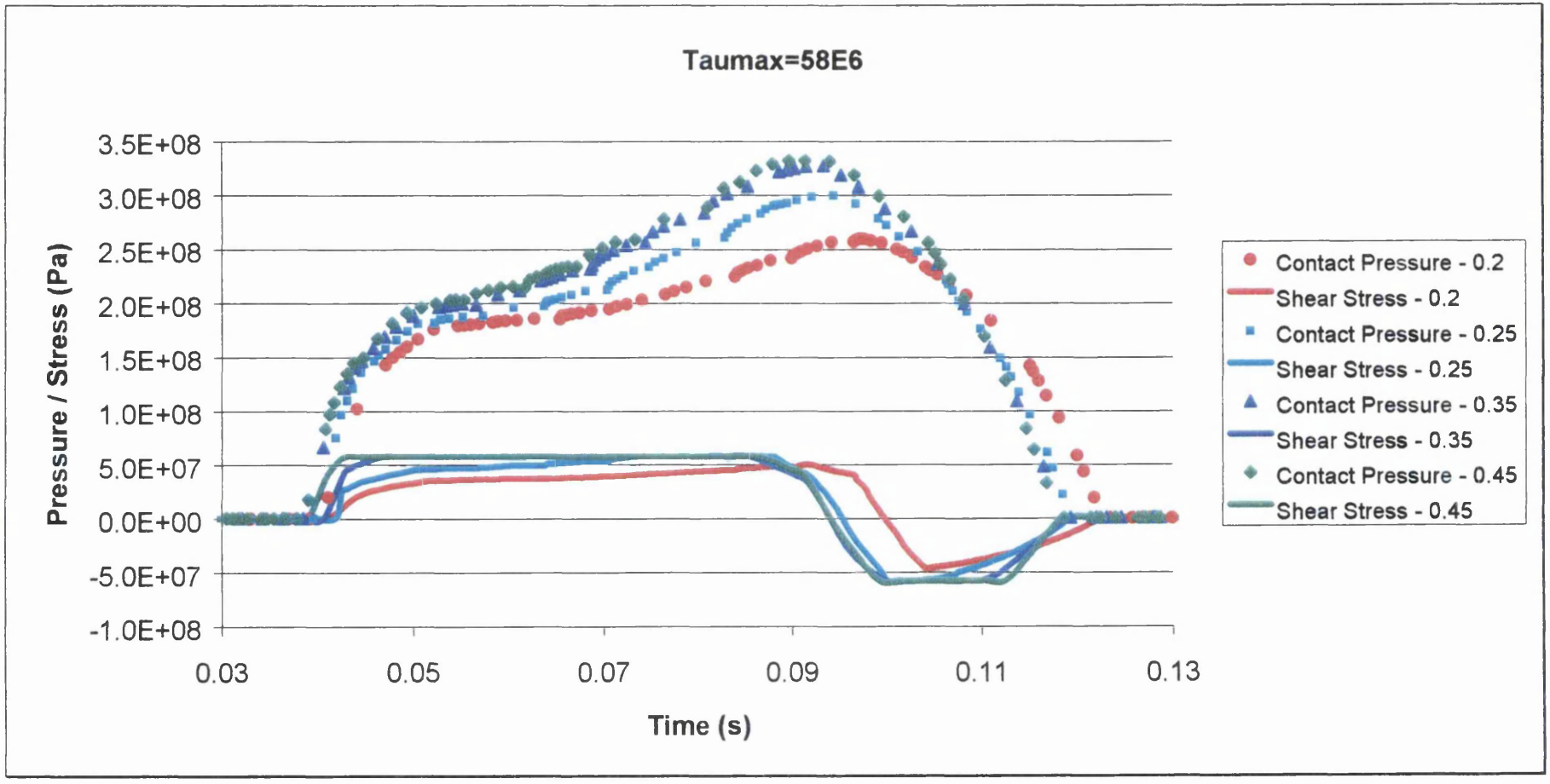

Figure 8.51 Contact Pressures and Shear Stresses for Stand 1 with a Constant Shear Stress Law

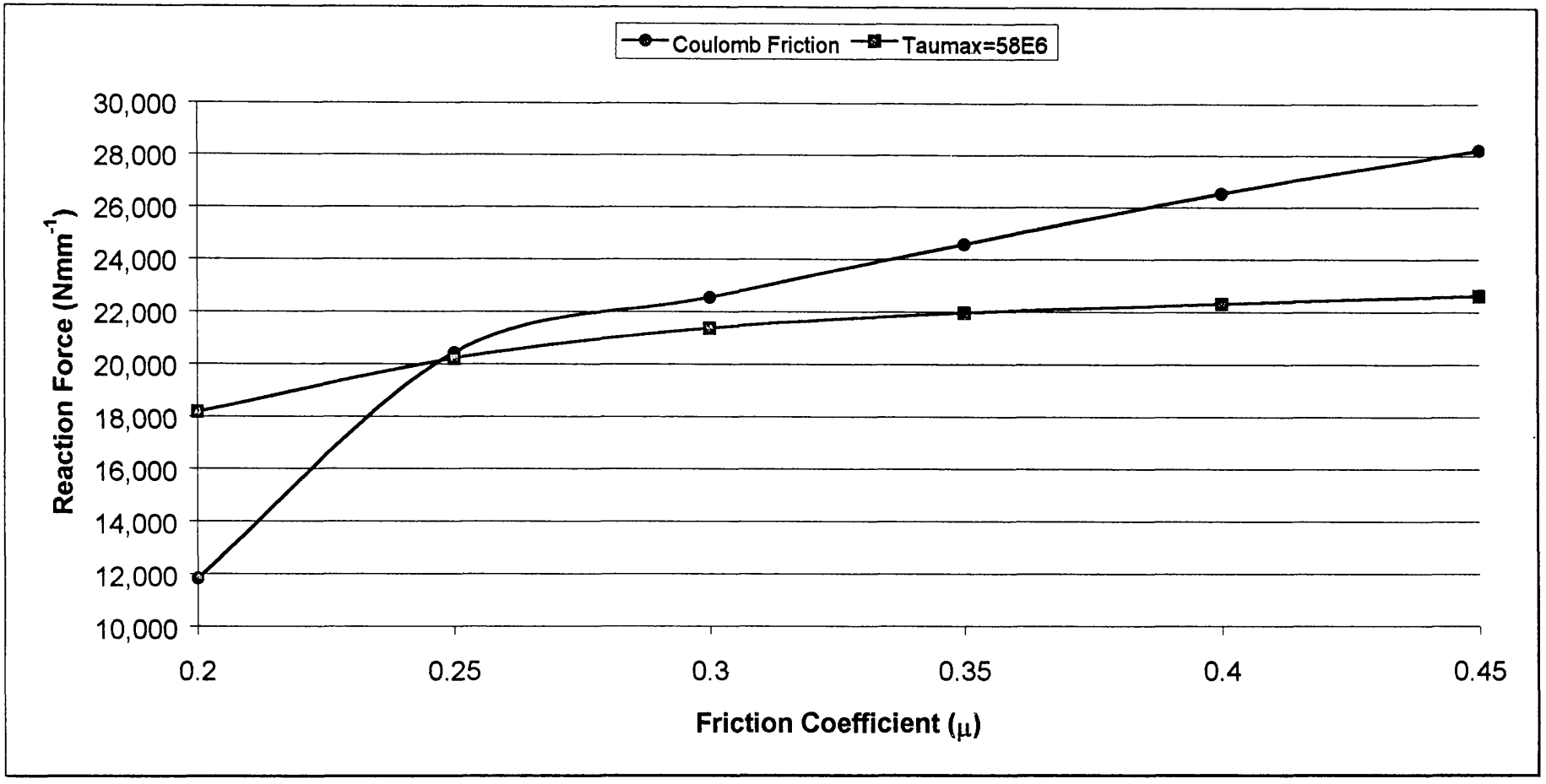

Figure 8.52 Rolling Loads for Stand 1 with Coulomb and Maximum Shear Stress Laws

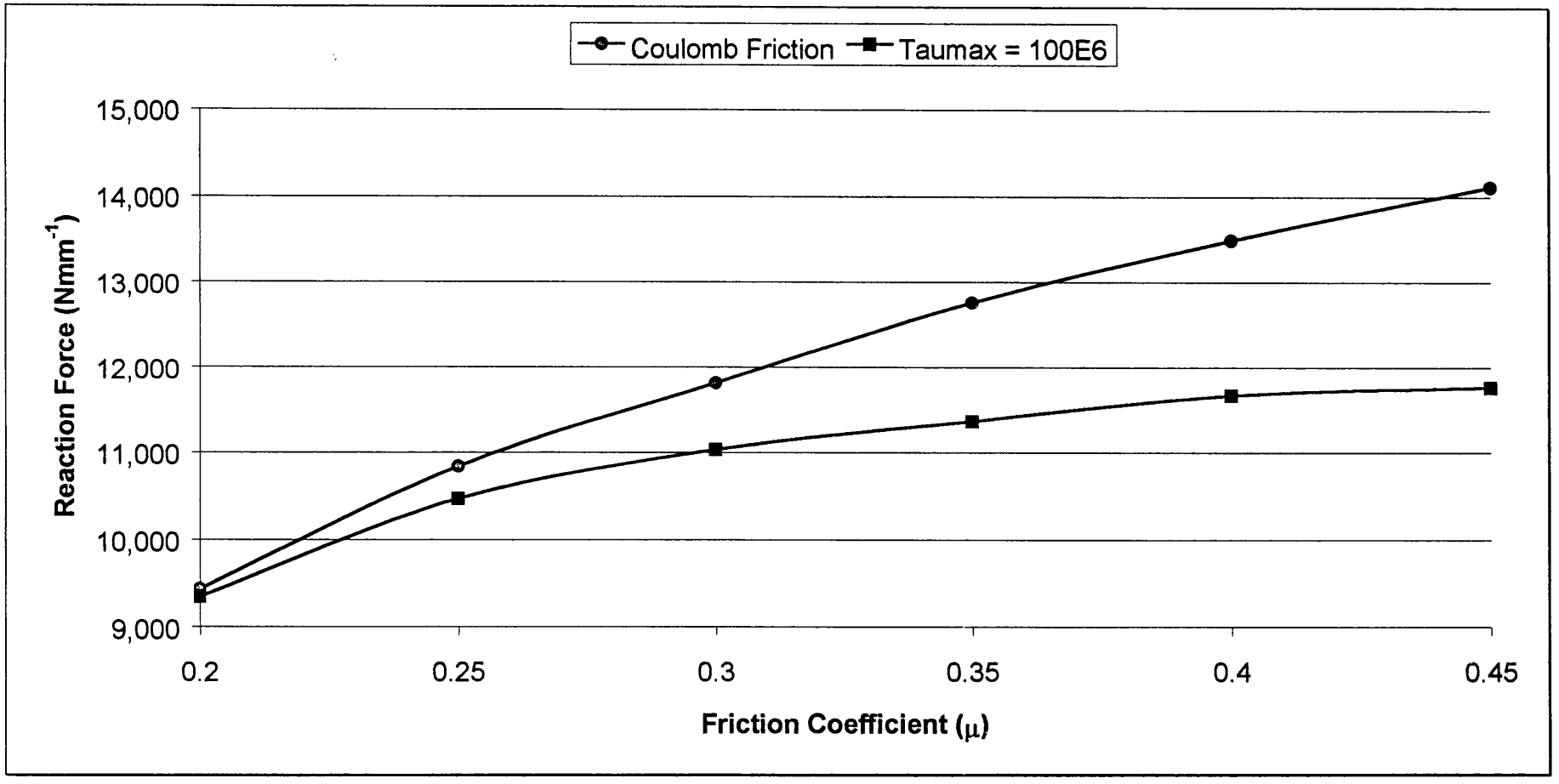

Figure 8.53 Rolling Loads for Stand 7 with Coulomb and Maximum Shear Stress Friction Laws

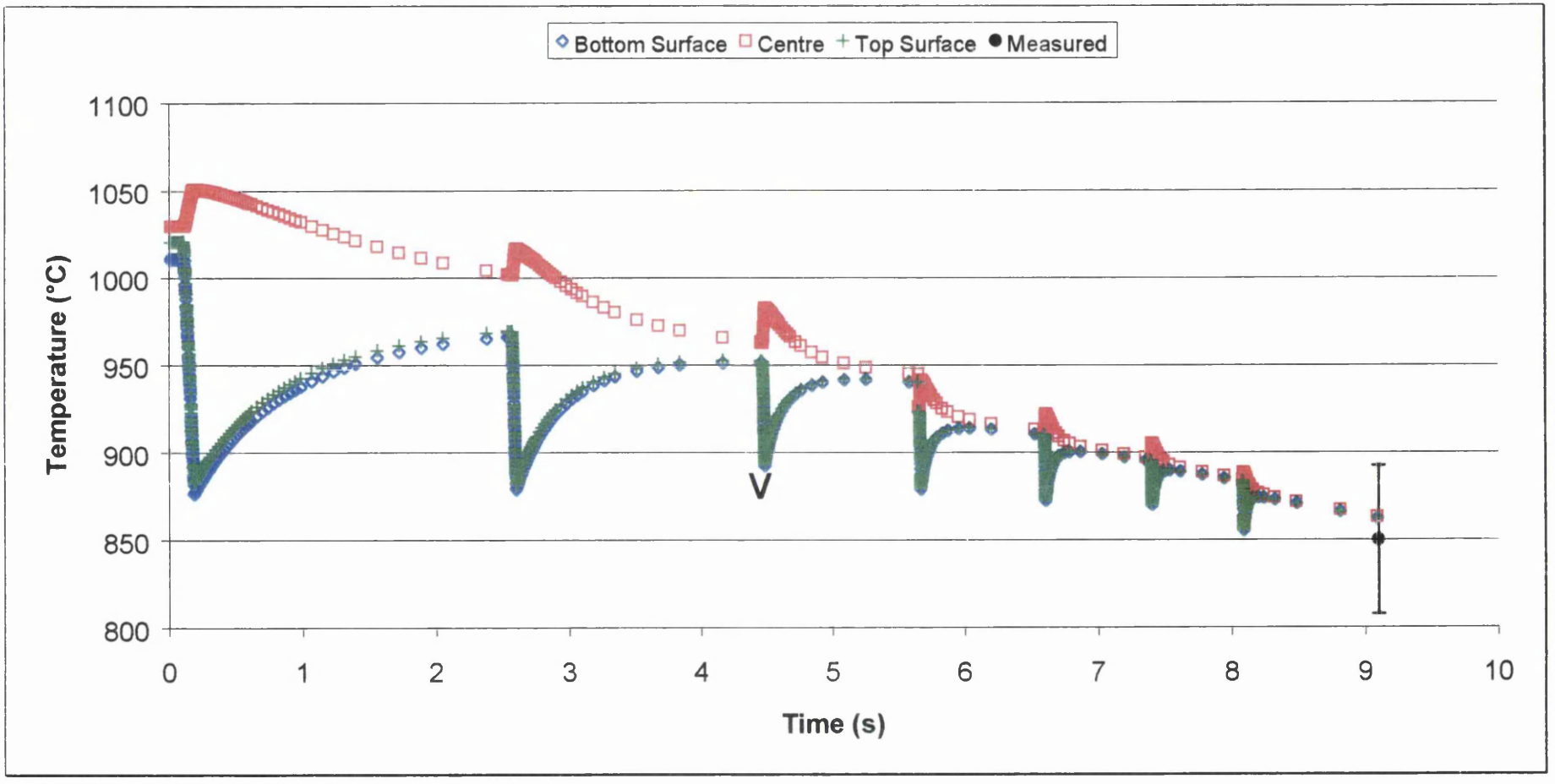

Figure 8.54 Thermal Evolution of High Carbon Steel within the Finishing Mill.

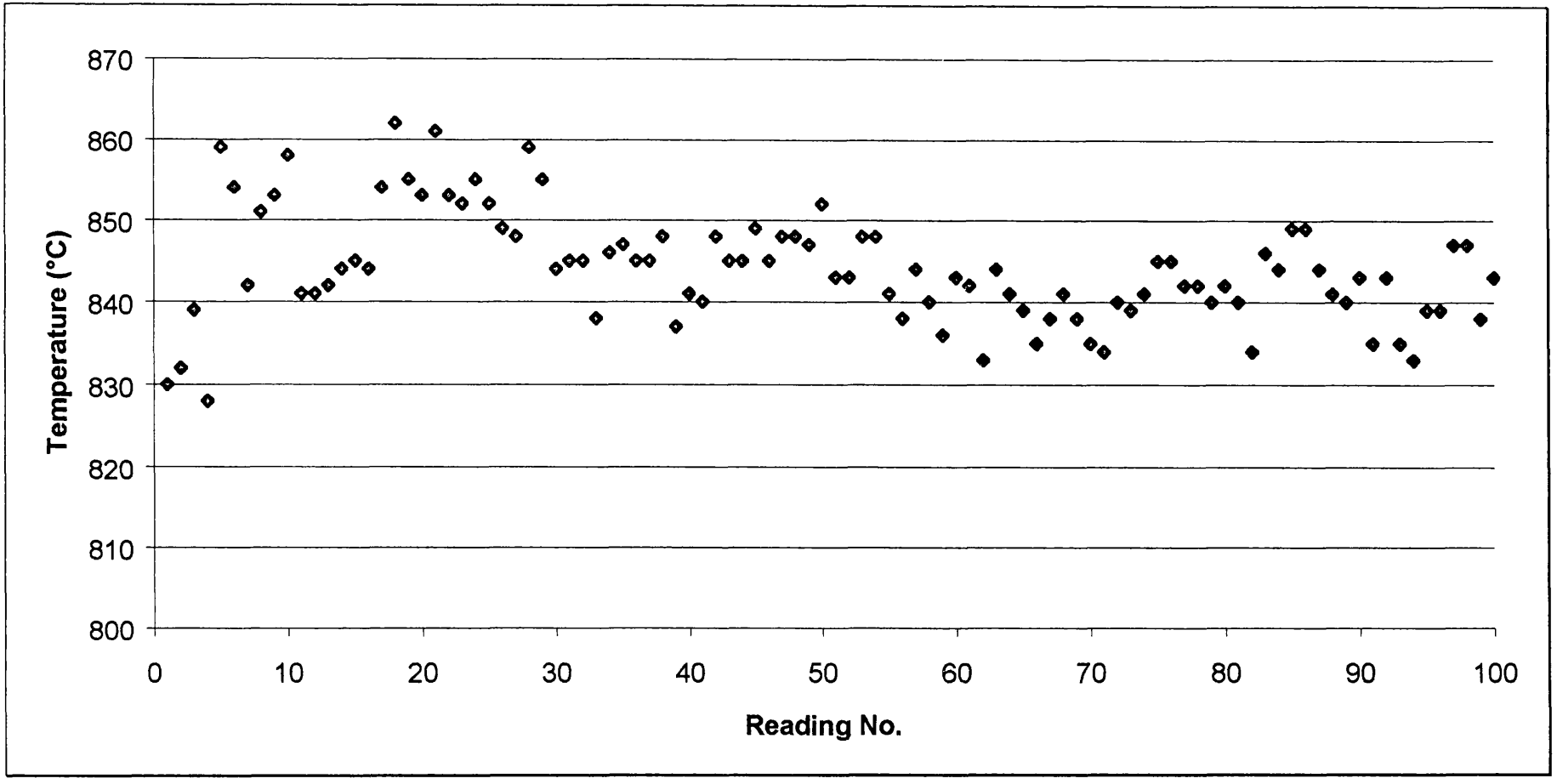

Figure 8.55 Measured Finishing Mill Exit Temperatures fro the High Carbon Steel. Coil No. 8334801

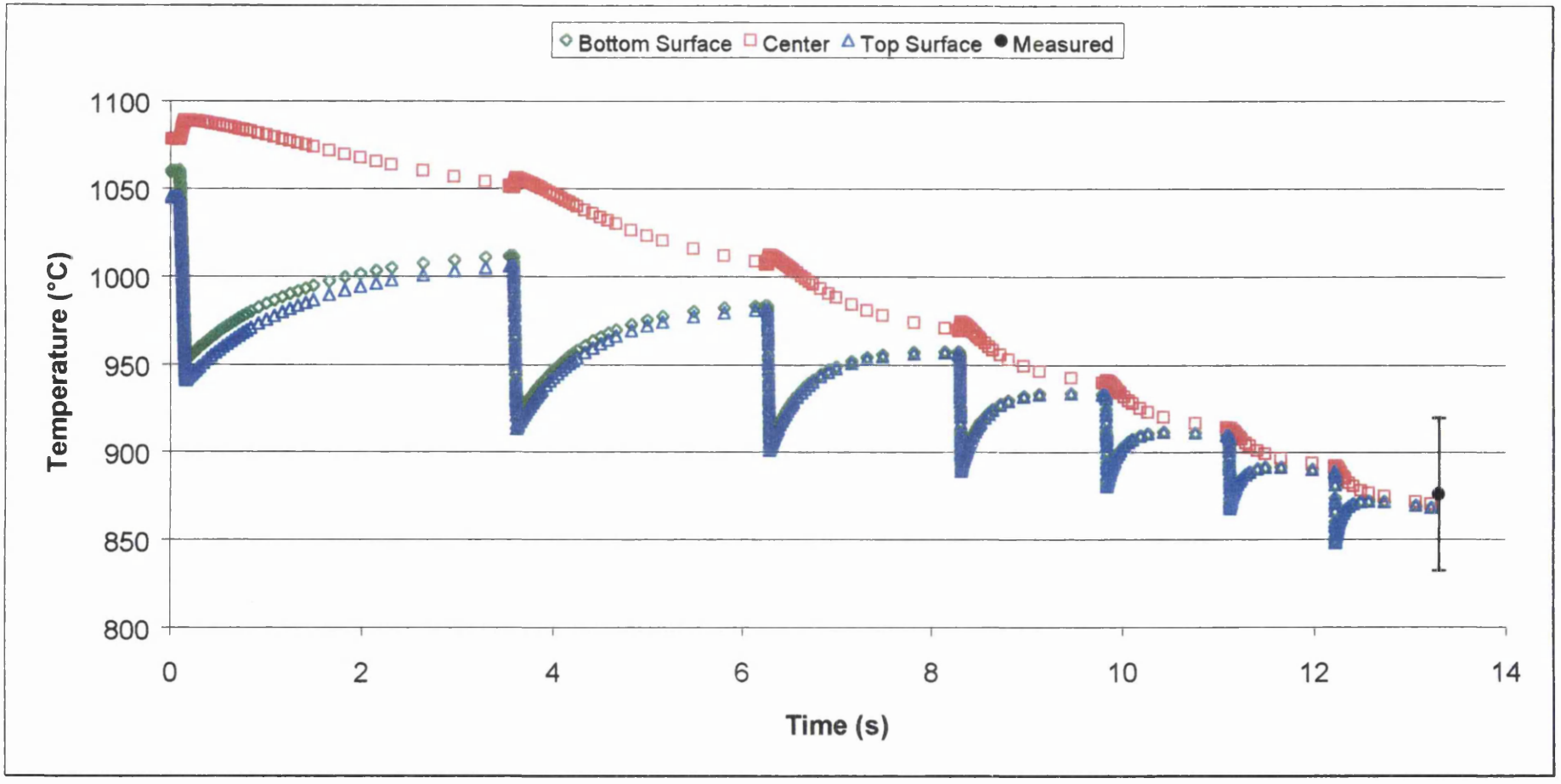

Figure 8.56 Thermal Evolution of the Carbon Manganese Steel within the Finishing Mill

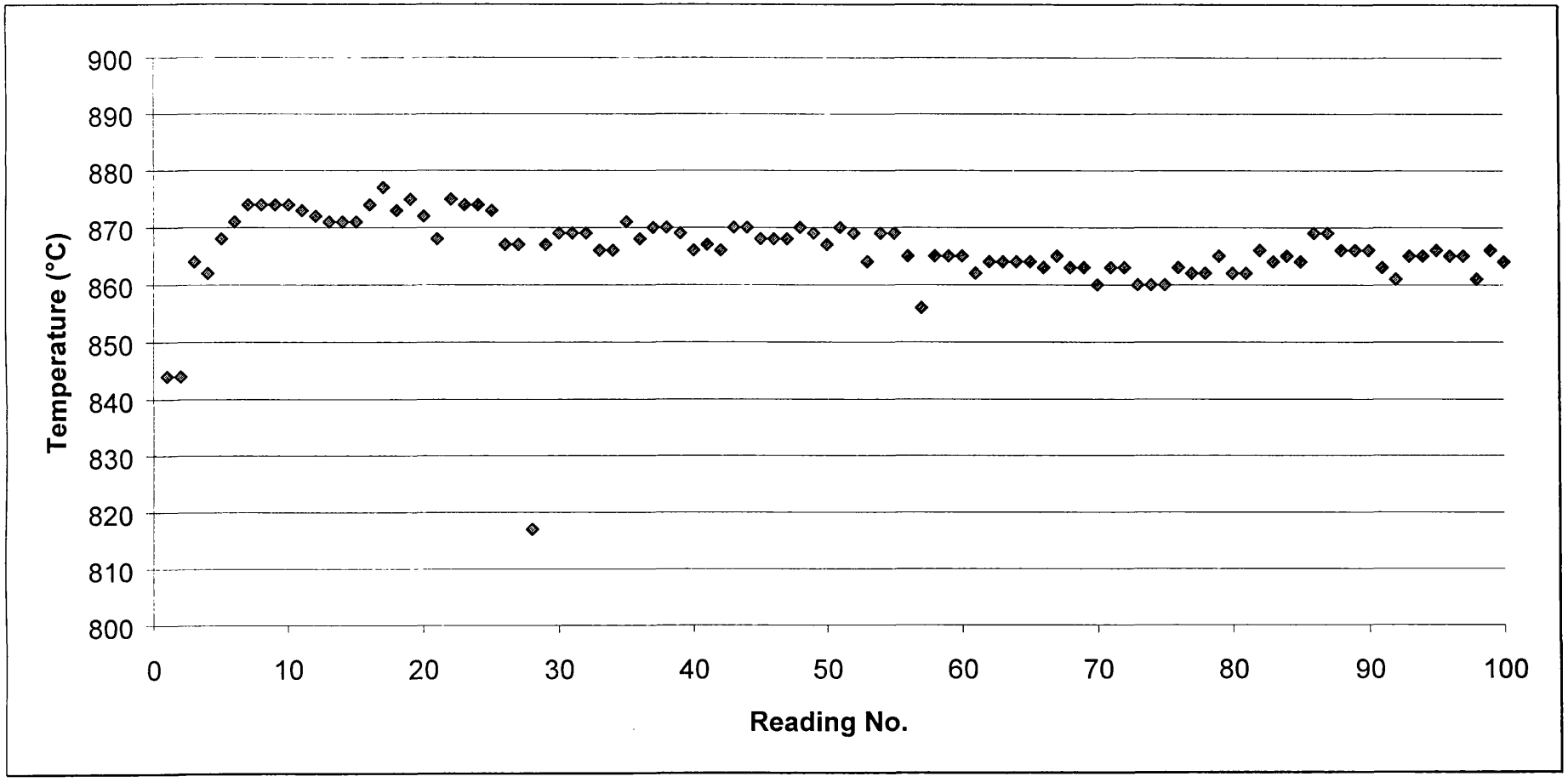

Figure 8.57 Measured Finishing Mill Exit Temperatures for the Carbon Manganese Steel. Coil No. 6314003

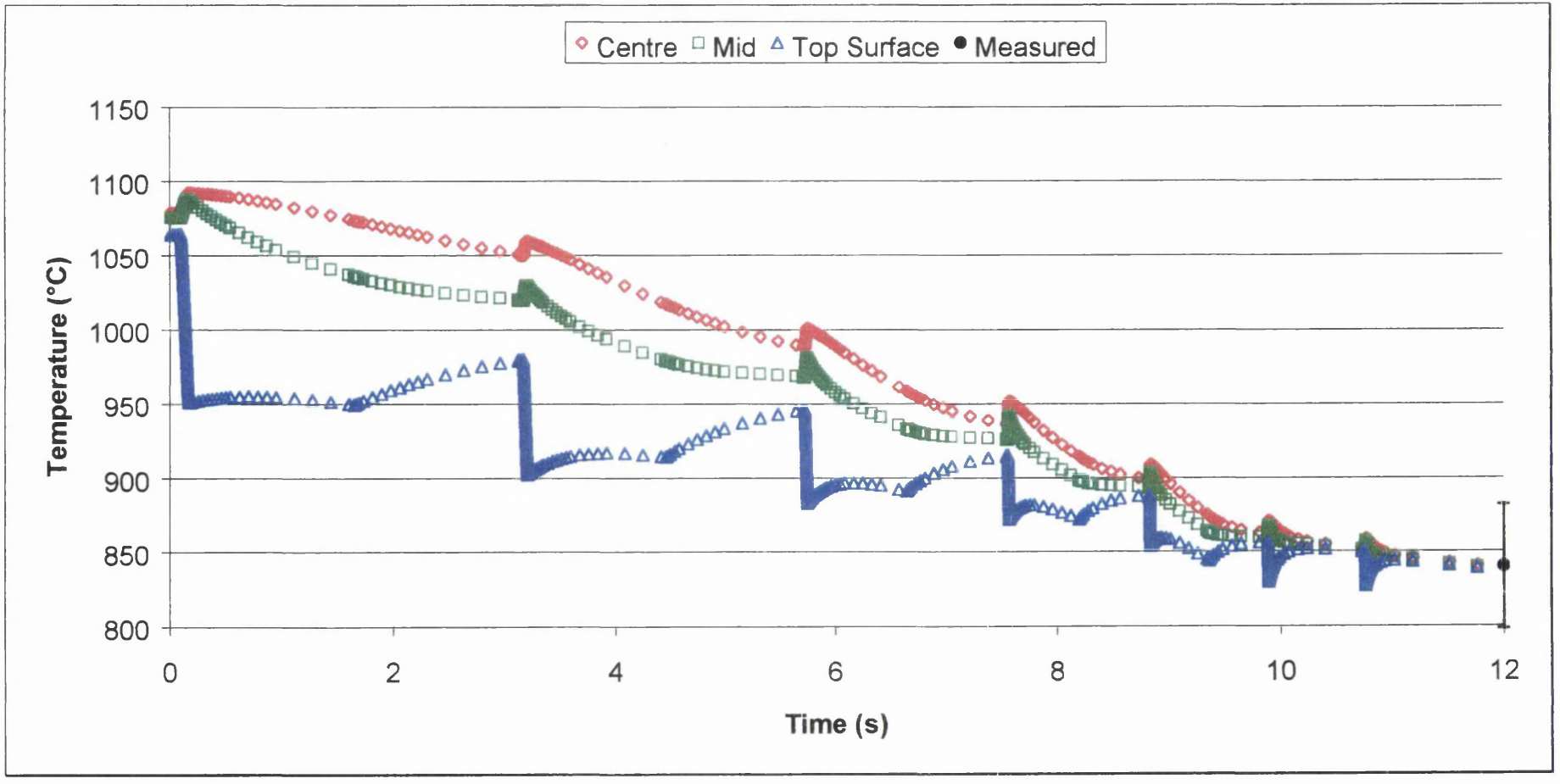

Figure 8.58 Thermal Evolution of the Low Carbon Steel within the Finishing Mill

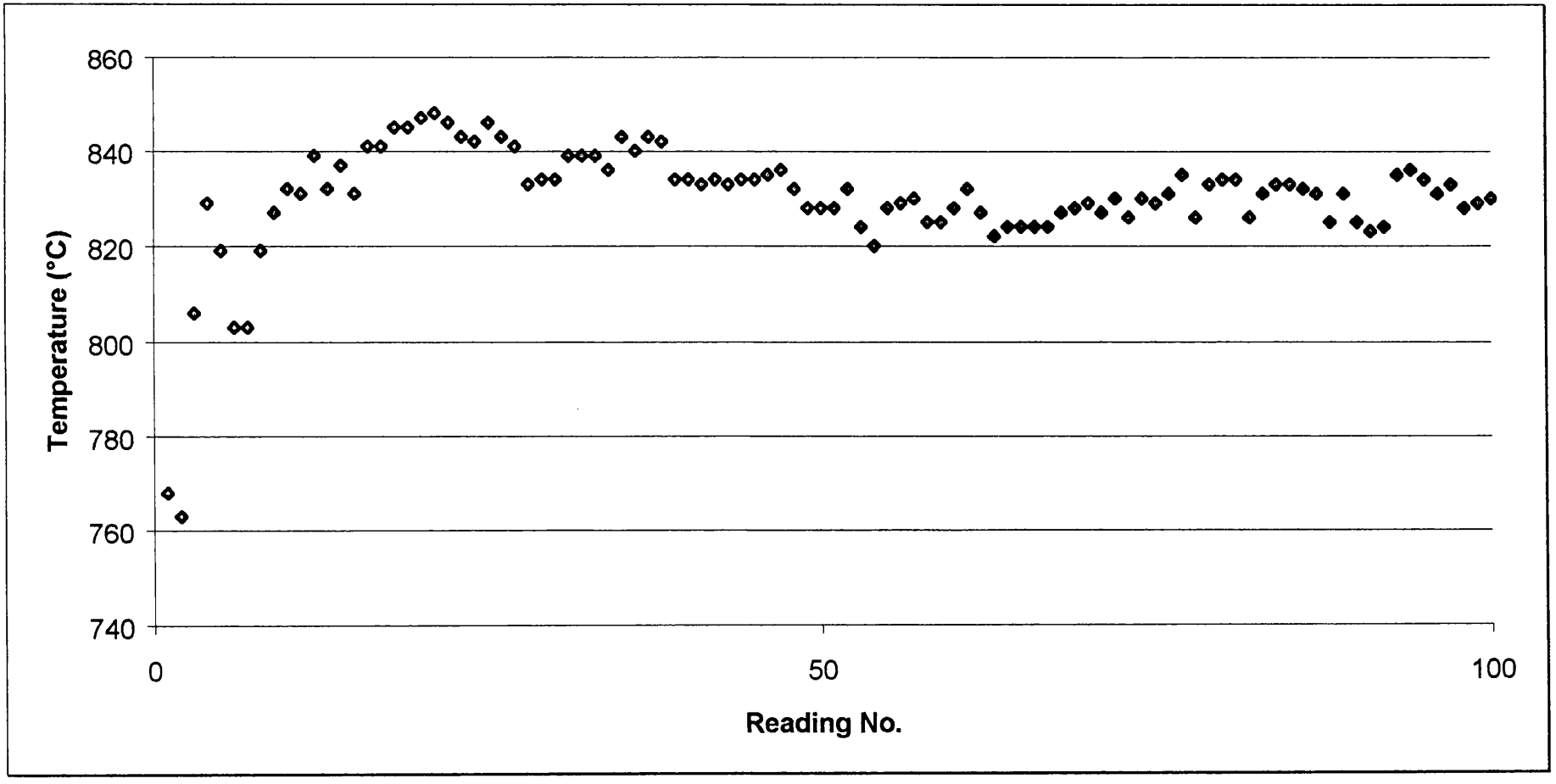

Figure 8.59 Measured Finishing Mill Exit Temperature for the Low Carbon Steel. Coil No. 3681301

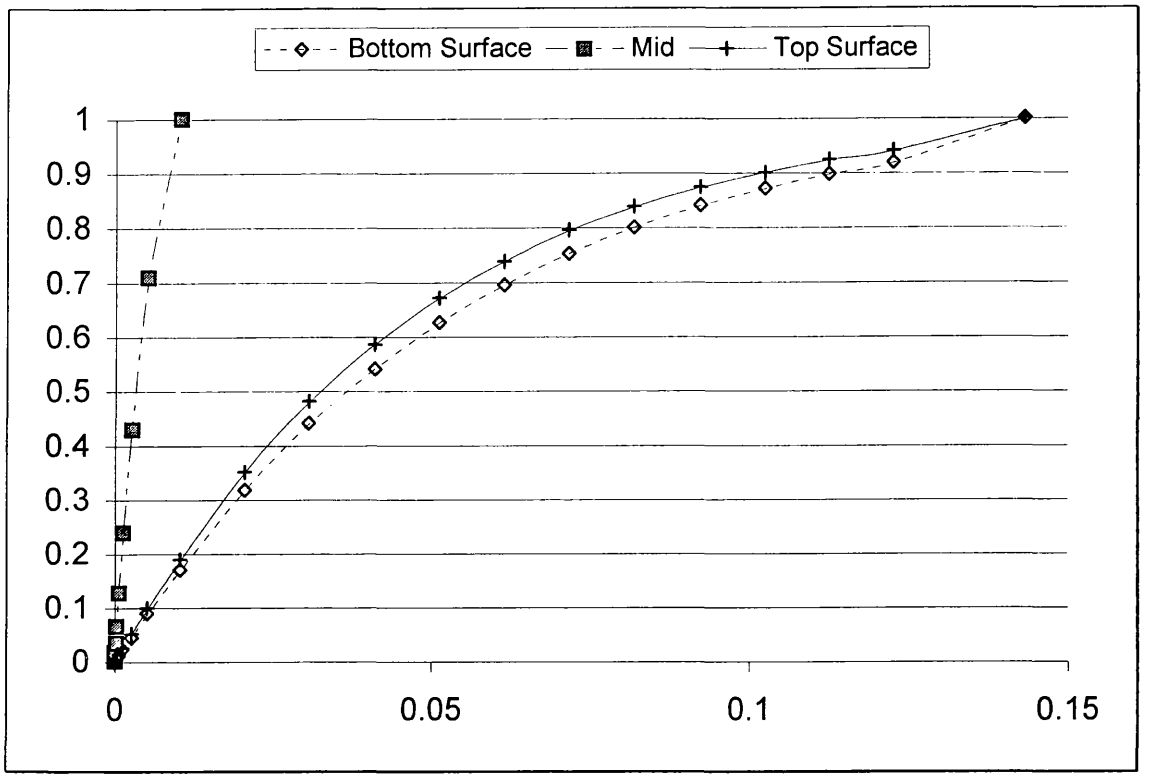

Figure 8.60 Fractional Softening for High Carbon Steel-Interstand 1

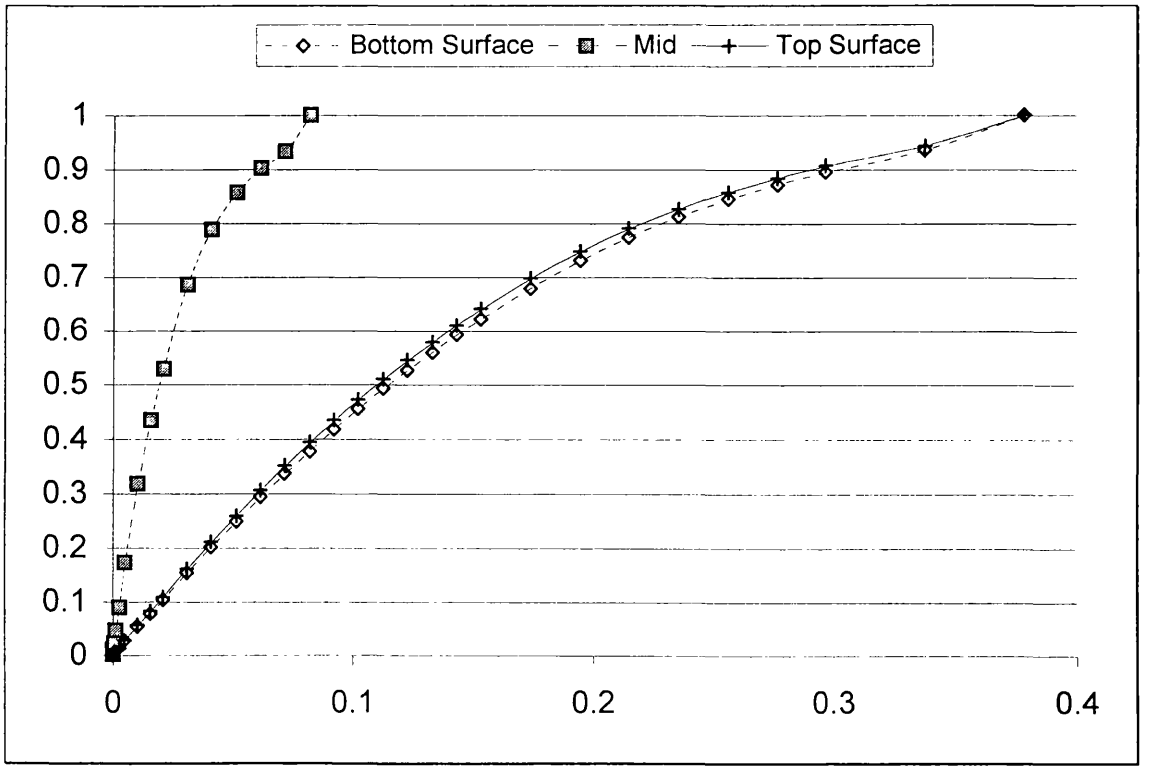

Figure 8.61 Fractional Softening for High Carbon Steel-Interstand 2

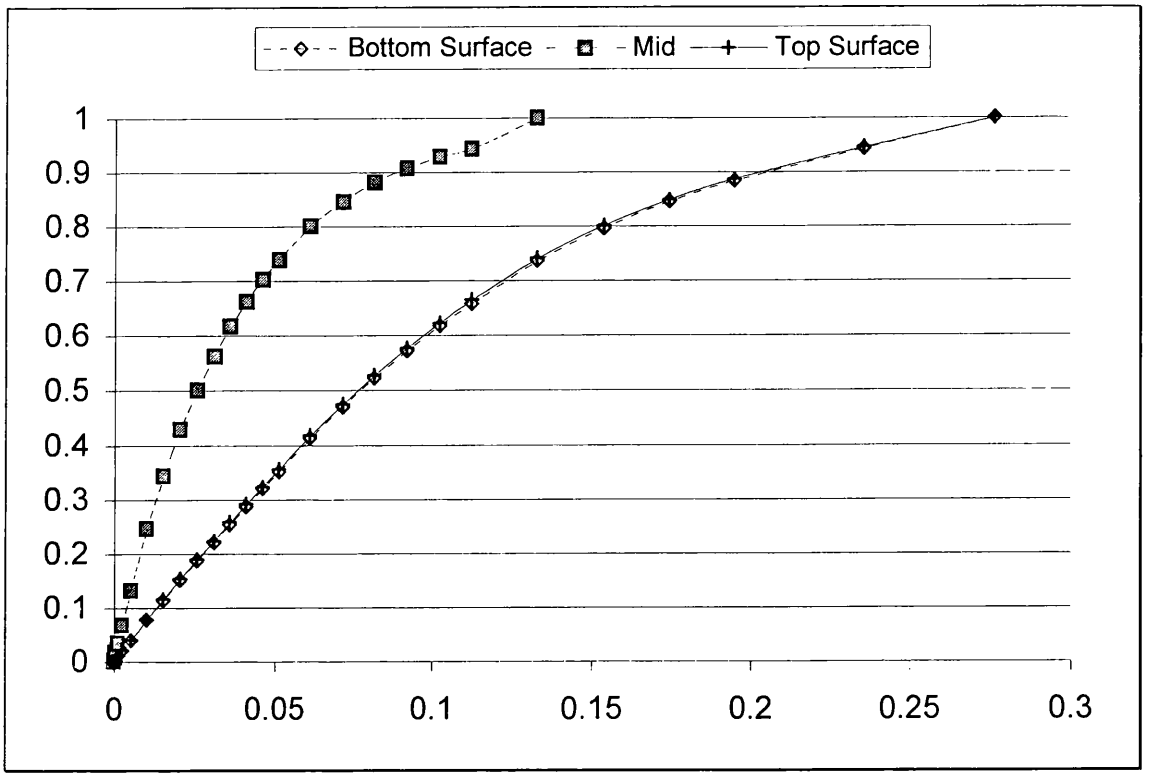

Figure 8.62 Fractional Softening for High Carbon Steel-Interstand 3

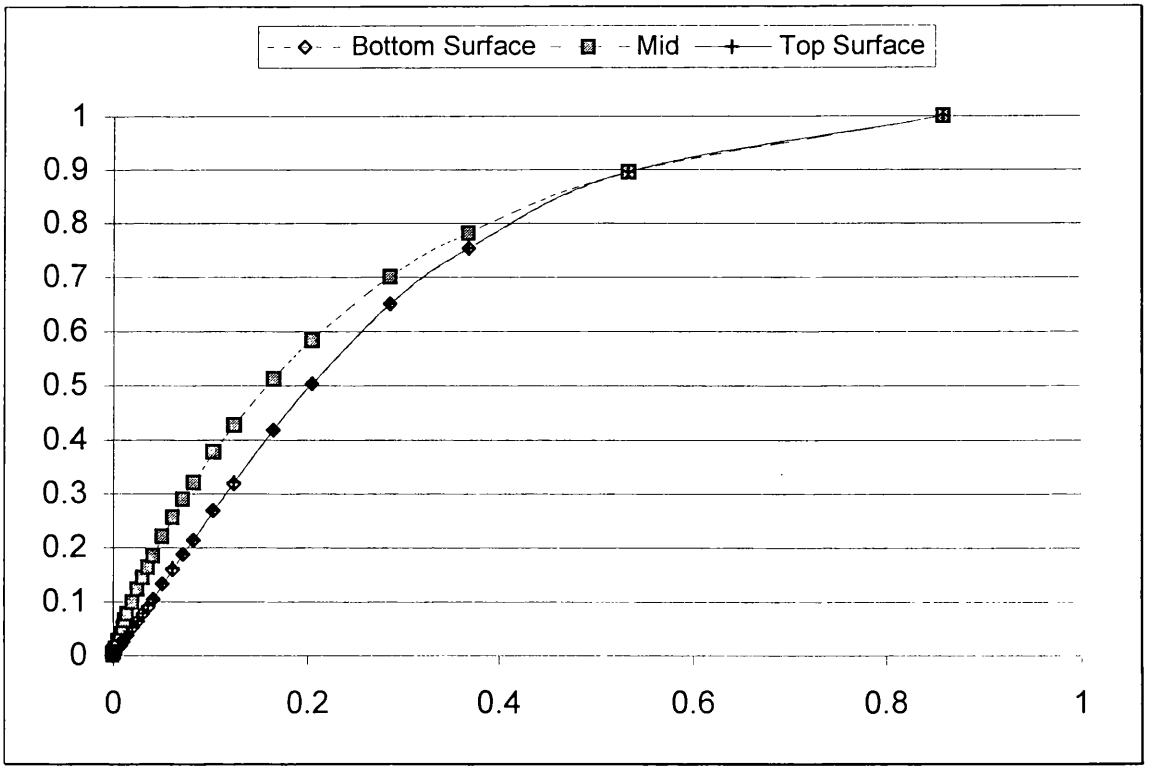

Figure 8.63 Fractional Softening for High Carbon Steel-Interstand 4

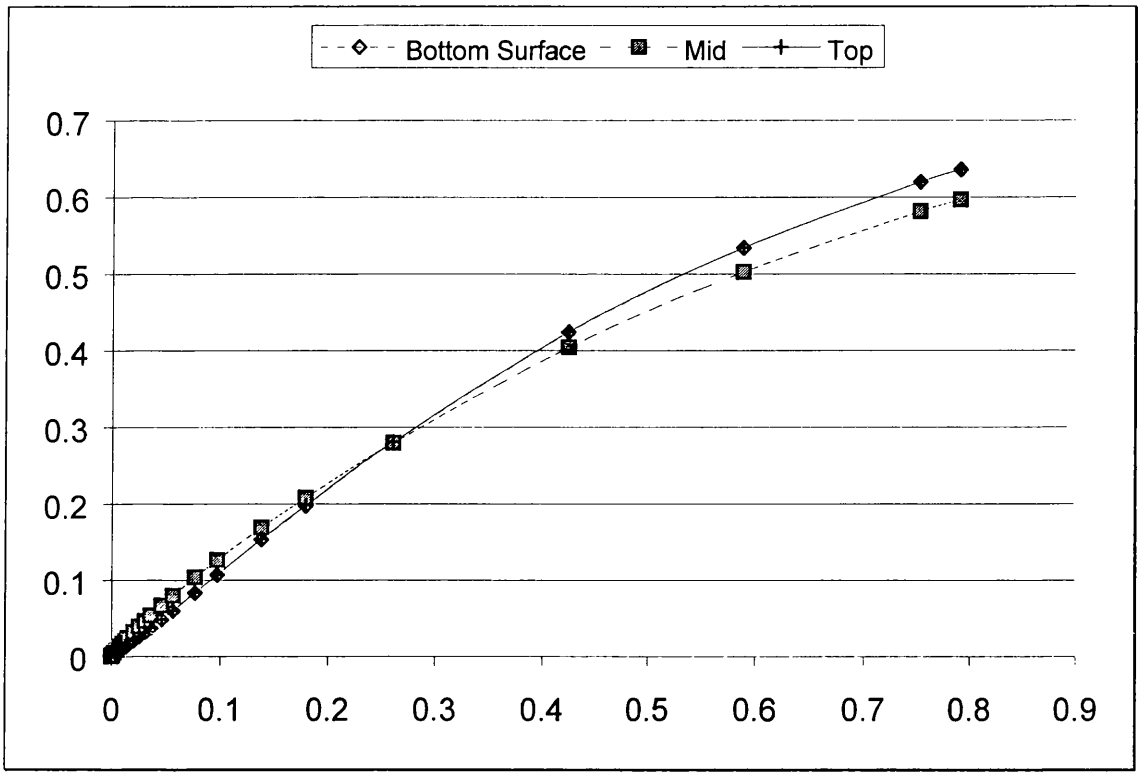

Figure 8.64 Fractional Softening for High Carbon Steel-Interstand 5

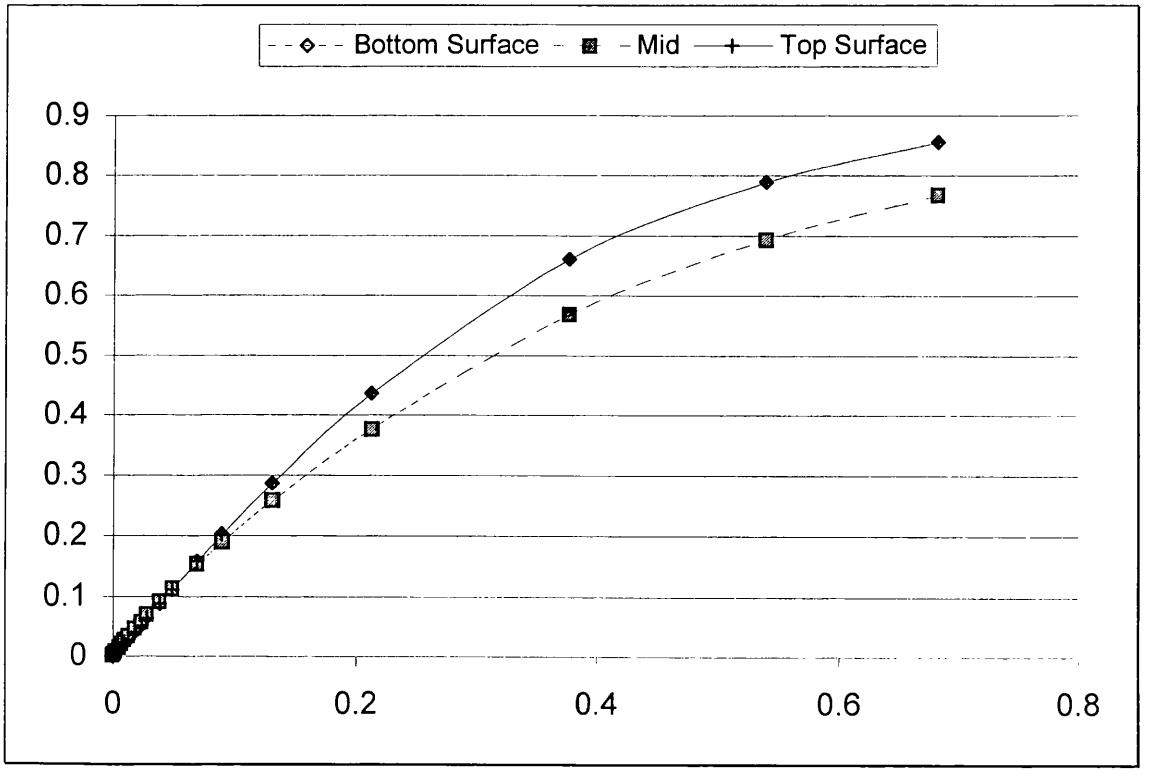

Figure 8.65 Fractional Softening for High Carbon Steel-Interstand 6

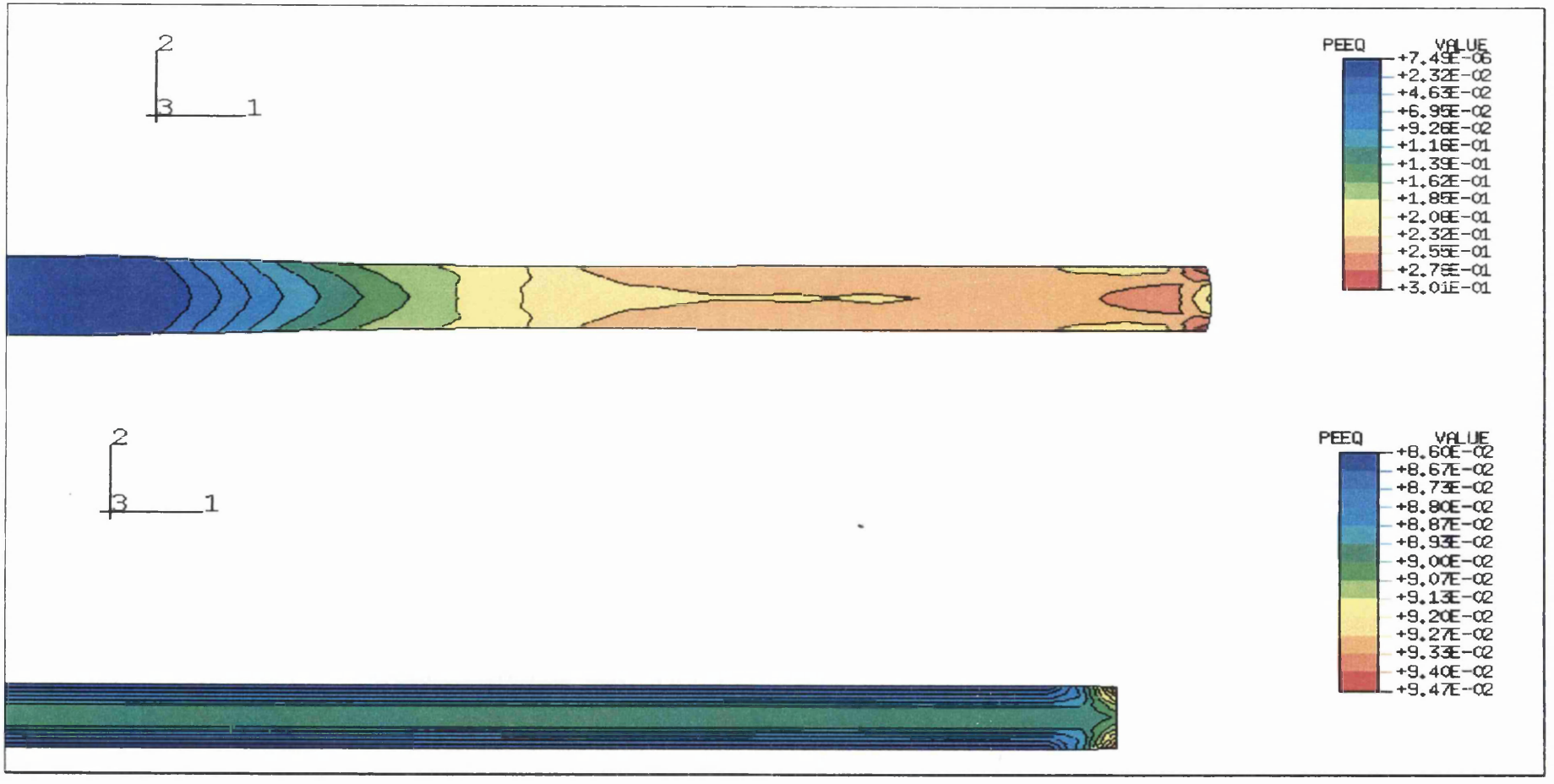

Figure 8.66 Equivalent Plastic Strain and Initial Plastic Strain For Stands 5 and 6 respectively for the High Carbon Steel.

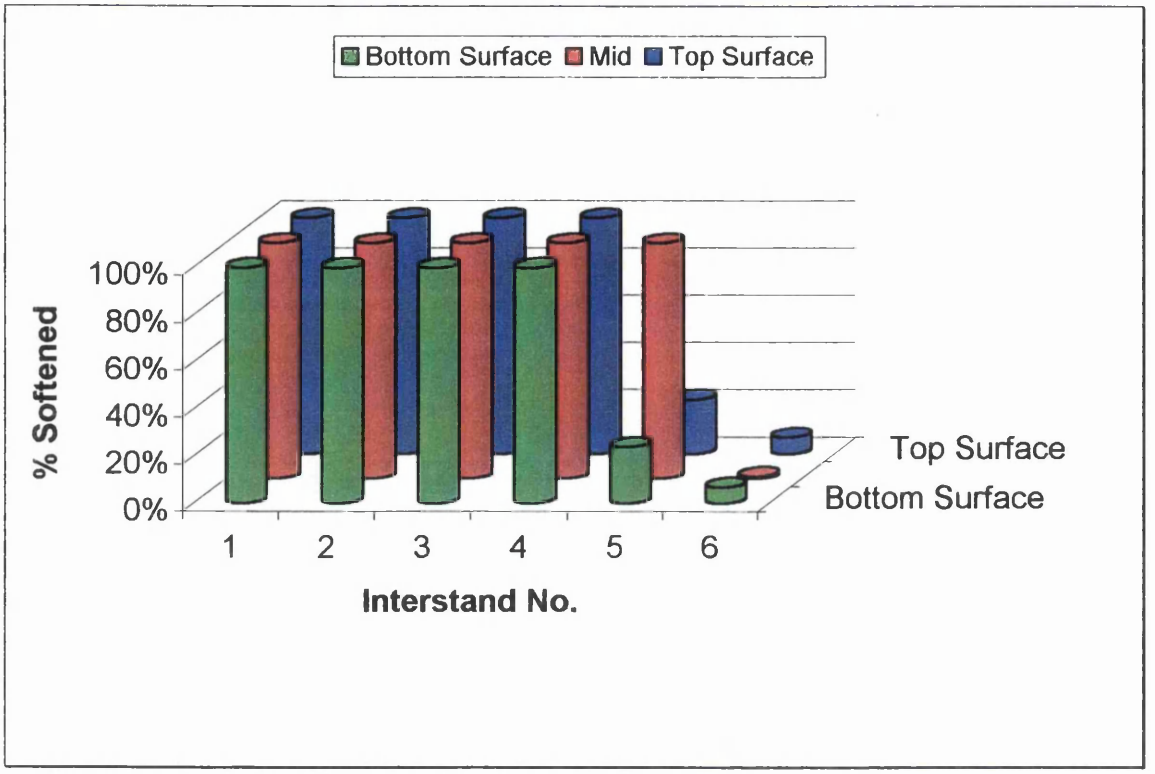

Figure 8.67 Fraction Softened for the Carbon Manganese Steel

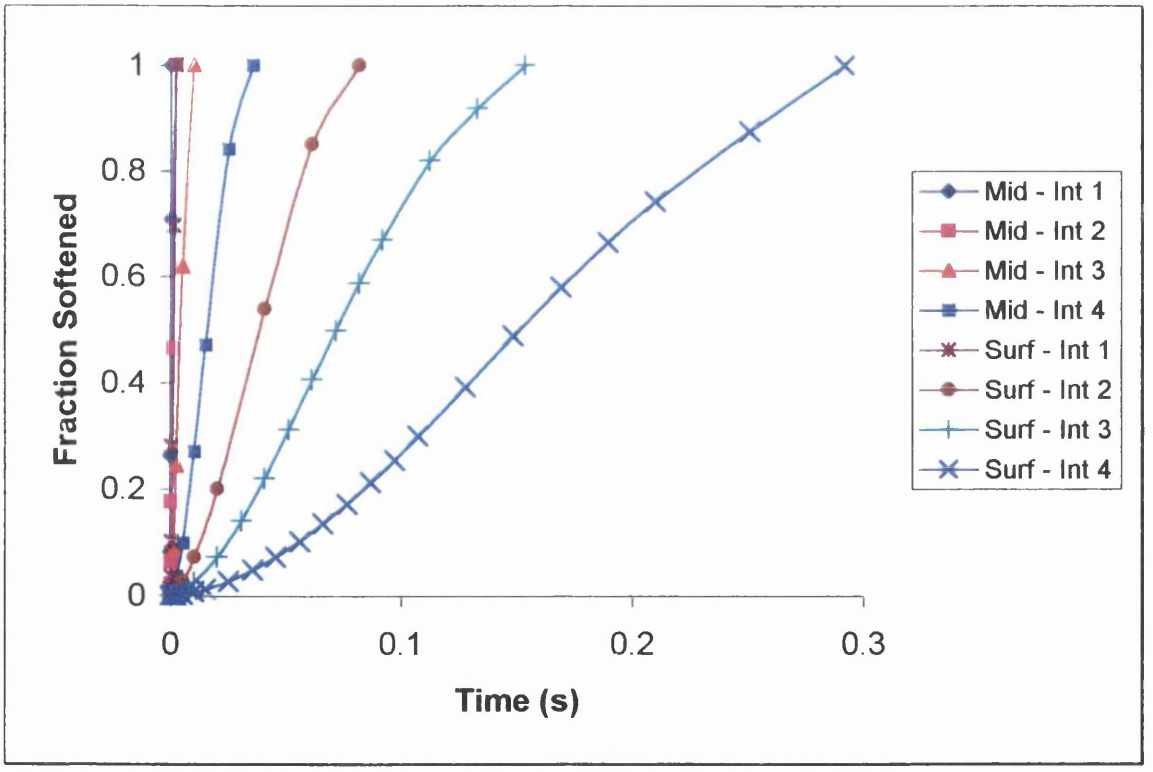

Figure 8.68 Fraction Softened for the Carbon Manganese Steel. Interstands 1-4

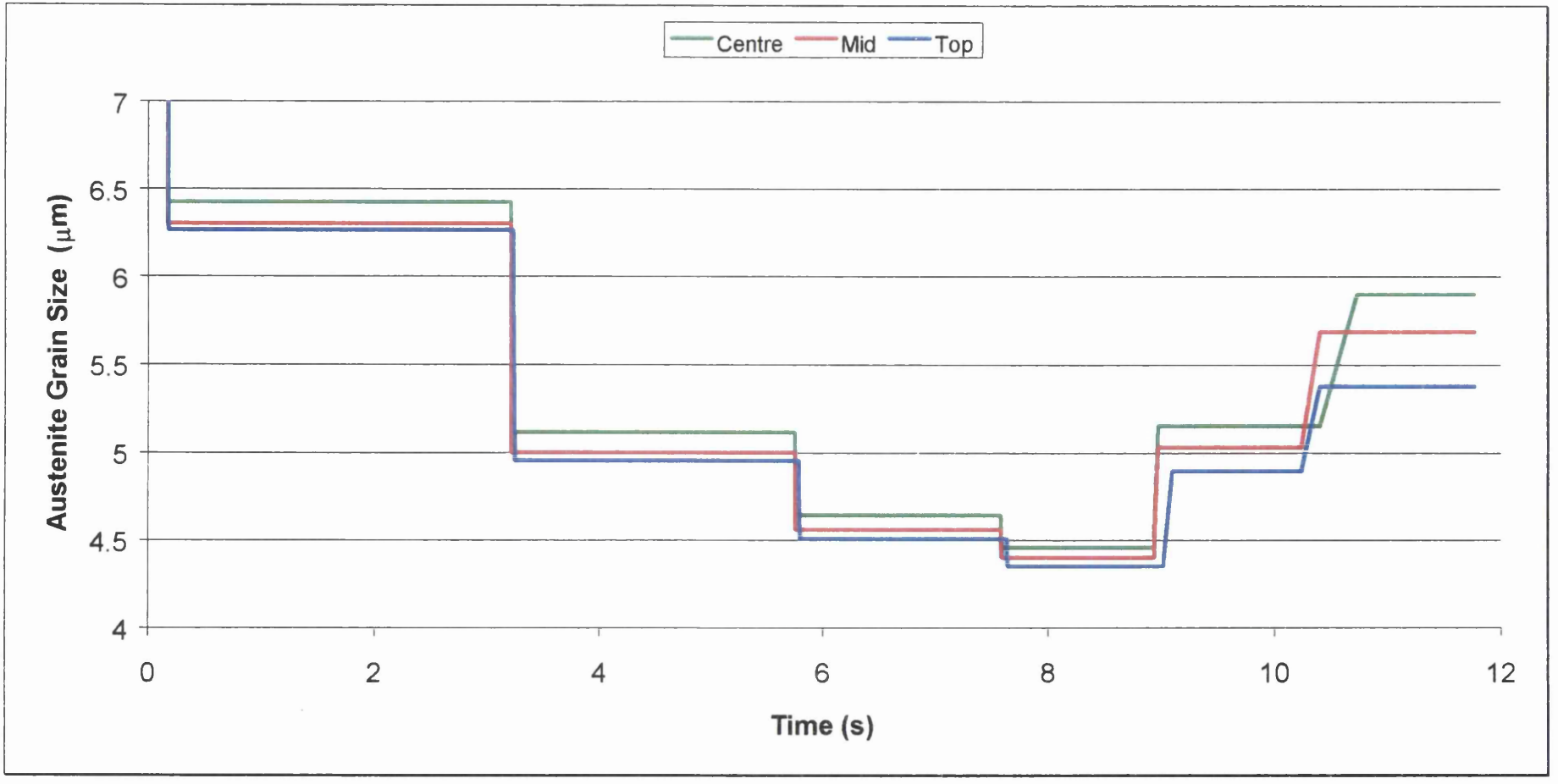

Figure 8.69 Recrystallised Austenite Grain Size for the Low Carbon Steel [100]

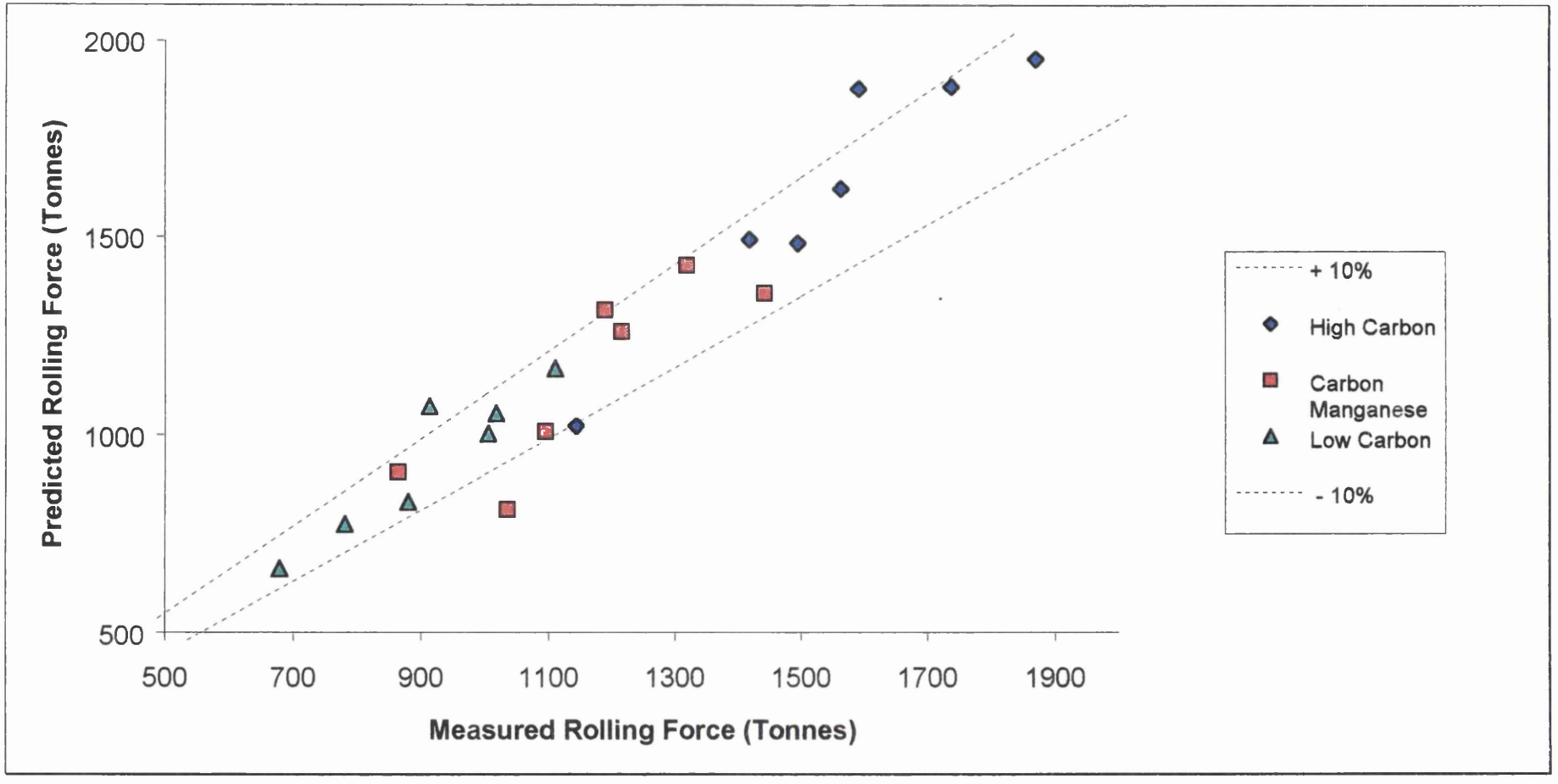

Figure 8.70 Predicted Vs. Measured Rolling Forces for the Finishing Mill Simulations

9 Conclusions and Future Work

9.1 Conclusions

1. A combined thermal-mechanical and microstructural Finite-Element model of the finishing mill has been successfully developed to investigate the effects of process variables such as temperature distribution, microstructural evolution and their consequential effects on the mechanical behaviour of the strip during rolling.

2. The finishing mill was effectively modelled as two distinct physical problems. The roll-gap was considered as a two-dimensional plane strain problem with an elasto-thermoviscoplastic material model. The interpass periods were modelled as a 2-dimensional heat transfer problem with microstructural algorithms to calculate the fractional softening parameters between deformations.

3. The combined thermal-mechanical and microstructural model provided rolling load sensitivities to temperature and friction that are useful during the development and validation of on-line control systems.

4. The University of Wales-Swansea provided all the facilities necessary for the examination and analysis of the hot deformation characteristics of the High Carbon Steel. The equipment was capable of temperatures up to 1373K and strain rates of $40s^{-1}$. The experimental matrix controlled the deformation parameters that enabled all the laboratory results to be extrapolated to those conditions encountered within a commercial finishing mill.

5. Testing carried out at Temperatures between 1123 and 1373K and strain rates from 0.0001 to $40s^{-1}$ revealed the High Carbon material exhibited increasing flow

stress with increasing strain rate or decreasing temperature in agreement with current understanding of the deformation of austenite.

6. The High Carbon steel examined demonstrated deformation behaviour associated with dynamic recovery. Any decrease in flow stress after the maximum stress, as seen during the experiments at the higher strain rates, was associated with adiabatic heating of the specimen during deformation.

7. The hyperbolic sine law was utilised to define three critical flow stresses of yield, maximum and stress at large strain on the true stress/stain curves. Regression analysis was used to discover the best-fit constants for the calculation of σ_y, σ_p and σ_L. The methods applicability was demonstrated by providing a comparable measure of the deformation activation energy, **Q,** to materials of similar composition.

8. The strain at peak stress, ε_p, was simply defined as a function of temperature and strain rate. The strain at which the maximum stress was observed increased with increasing flow stress due to either a lower deformation temperature or increasing strain rate or any combination of the two.

9. The complete flow stress curve at constant strain rate and temperature was defined with elastic and plastic components. The recoverable elastic behaviour was assumed linear and temperature dependant. Evolution of stress between yield and maximum stress was accurately defined with a binomial relationship between true stress and true strain. The linear interpolation between the maximum stress and the stress at large strain accounted for any softening due to adiabatic heating.

10. During the interrupted compression testing both equipment and software proved sensitive to the softening kinetics of the high Carbon steel. Increasing temperature and strain rate resulted in an increase in the softening kinetics of the material tested. Results from the double deformation testing revealed a sigmoidal relationship between fractional softening and interrupt time.

11. Fractional softening was calculated from a combination of Avrami type equations and calculation of the time to 50% softened. All exponents were maintained constant and regression analysis provided the best fit to the experimental data. The Avrami equation was differentiated with respect to time to permit incremental calculation of fraction softened during interstand periods

12. Fortran 90 subroutines linked the roll-gap models to subsequent interstand analyses. The interstand models effectively calculated the thermal evolution during the interpass periods using two-dimensional Finite-Element heat transfer techniques. Temperature dependent material properties were incorporated within the interstand model with radiation and convection boundary conditions applied to the upper and lower surfaces of the strip.

13. Recrystallisation routines calculated the fraction softened and recrystallised grain size, for the Low Carbon steel, as a combination of the strain rate and strain from the previous roll-gap analysis and the thermal evolution during the interstand period.

14. Total strain varies with position through the gauge. This strain is a complex function of the geometry of the roll-gap and material characteristics. Results of the simulations of commercial finishing rolling at Port Talbot and Llanwern show the majority of deformation to be taking place just beneath the surface of the strip with the minimum strain occurring along the centre line of the rolled material.

15. The interstand model calculated the fraction restored from an average effective strain rate for the roll-gap analysis. Results showed the surface to have a greater average strain rate due to the heterogeneous deformation taking place near the roll/strip interface. This strain rate was particularly sensitive to the friction factor prescribed to simulate the mechanical interactions at the interface.

16. Temperature was the most dominant parameter when modelling the softening kinetics within a finishing mill. Due to the rapid surface chilling from conduction to the work rolls and heating along the centre line due to the plastic dissipation during the deformation a considerable temperature gradient was shown to exist through the gauge of the strip at exit of the roll-gap.

17. During the interstand periods further cooling takes place at the surfaces due to radiation and convection to the surroundings. However, these cooling effects cannot maintain a uniform thermal profile and the surface temperature rebounded to a near constant value slightly less than that prior to rolling. The centre of the strip cools steadily during the interstand period due to the thermal flux created by the low surface temperatures. Validation of interstand temperatures were impossible within current Corus hot strip finishing mills but investigation should be made into future opportunities to install and measure surface temperatures between the finishing stands.

18. The calculation of the rate of softening was a complex function of the mechanical deformation history and current thermal effects. Softening at the surface is a balance between the low surface temperatures and the high equivalent strains and strain rates. Conversely, softening towards the centreline of the material was a function of the higher bulk temperatures and relatively moderate equivalent strains and strain rates.

19. The work has shown that Finite-Element roll-gap models can work extremely well, but perhaps more importantly, lend themselves well to being coupled with metallurgical algorithms to complete a thermo-mechanical and microstructural simulation of commercial hot strip finishing mills.

9.2 Future work

1. A contact pressure dependent heat transfer coefficient was specified at the roll/strip interface to accurately describe the surface chilling due to conduction to the work rolls. Although the conduction coefficients used within this research adequately described these thermal losses, further investigations should be made into quantitatively characterising this phenomenon as functions of commercial finishing rolling parameters.

2. No flow stress predictions were carried out below Ar_3 as the material analysis was only carried out within the austenite temperature range. If further developments into ferritic hot rolling take place investigations into the hot deformation characteristics below the Ar_3 temperature may have to be investigated.

3. No optical investigation into the microstructural phenomena was completed during this research due to the difficulties encountered when attempting to reveal the prior austenite grain boundaries. If recrystallised grain sizes are required optical investigation would be required.

4. Future models of the roll-gap should include both strip and work-roll temperature models to account for thermal crowns within the rolls and their effects upon the shape of the strip.

5. Due to developments in strip cooling practices it may be necessary, in the future, to describe these cooling boundary conditions as functions of the processing parameters such as coolant flow or pressure.

6. Friction should be further investigated to derive scale and flow stress dependencies for a range of materials and temperatures. Within the roll-gap Finite-Element program friction subroutines should be added to take account of these new parameters to further understanding of this phenomenon.

10 References

[1] FORD H., "Researches into the deformation of Metals by Cold Rolling", *Proc. Instn, Mech. Engrs.*, 1948, **159**, pp. 115-143.

[2] KARMAN V. T., "On the Theory of Rolling", *Zeit. Fur angew. Math. u Mech.*, **5**, p. 139.

[3] OROWAN, E., "The Calculation of Roll Pressure in Hot and Cold Flat Rolling", *Proc. Inst. Mech. Engrs.*, (1943), pp. 150-152.

[4] SIMS, R. B., "Calculation of Roll Force and Torque in Hot Rolling Mills", *Proc. Inst. Mech. Engrs.*, (1954), pp. 191-219.

[5] SIMS, R.B., "Calculation of Roll Force and Torque in Cold Rolling by Graphical and Experimental Methods", *Journ. of Iron and Steel Inst.*, (1954), pp. 137-152.

[6] LARKE, E. C., "The Rolling of Strip, Sheet and Plate", *Science Paperbacks, Ltd.*, London (1957), pp. 304-306.

[7] COOK, P. M. and McCRUM, A. W., "The Calculation of Load and Torque in Hot Flat Rolling", B.I.S.R.A., London, March (1958), PP. 7-9.

[8] JOHNSTON, W., SOWERBY, R. and VENTER, R. D., "Plane Strain Slip-line Fields for Metal Deformation Processes". A source book and bibliography. Pergammon Press, England, (1982), pp. 128-131.

[9] ALEXANDER J. M., "A Slip Line Field for the Hot Rolling Process", *Proc. Inst. Mech. Engrs.* 169 (1955) **109**, pp. 1021-1030.

[10] FORD H. and ALEXANDER J. M., "Simplified Hot Rolling Calculations", *Journ. Inst. Metals* **92**, (1963-64), pp.397-403.

[11] CRANE F. A. A. and ALEXANDER J. M., "Slip-Line Fields and Deformation in Hot Rolling of Strip", *Journ. Inst. Metals*. **96** (1968), pp.289-300.

[12] DENTON, K. and CRANE, F. A. A., "Roll Load and Torque in the Hot Rolling of Steel Strip". *Journ. of Iron and Steel Inst.*, (1972), pp. 606-617.

[13] GUPTA, S. and FORD, H. "Calculation Method for Hot Rolling of Steel Sheet and Strip", *Journ. of Iron and Steel Inst.*, (1967), pp. 186-190.

[14] ARGYRIS J. H., "Energy Theorems and Structural Analysis", *Aircraft Engineering* **26** (1954), pp. 383-394.

[15] ARGYRIS J. H., "Energy Theorems and Structural Analysis", *Aircraft Engineering* **27** (1955), pp. 44-58

[16] CLOUGH R.W., "The Finite-Element Method in Plane Stress Analysis", *Proc. American Soc. Civil Engineers, 2nd Conf. Electronic Computation,* **23** (1960), pp. 345-378.

[17] PILLINGER I., "The Elastic-Plastic Finite-Element Method" Numerical Modelling of Material Deformation Processes, (Eds P Hartley, I Pillinger and C Sturgess), Spinger-Verlag, London, (1992), pp. 225.

[18] FREDRICKSON A. G., "Principles and Applications of Rheology", (Eds. Neal R. Amundson), Prentice Hall Inc Englewood Cliffs N. J. (1964), p. 1.

[19] CHEN C.C. and KOBAYASHI S., "Rigid Plastic Finite Element Analysis of Ring Compression". *Applications of Numerical Methods to Forming Processes. ASME Applied Mechanics Division*, Vol. **28**, (1978), pp. 163-174.

[20] SHIMA S., "Rigid-Plastic Finite Element Analysis of Strip Rolling", *Proc. 4th Int. Conf. on Prod. Eng.*, (1980), p. 82-84.

[21] LI G. J. and KOBAYASHI S., "Spread Analysis in Rolling by the Rigid-Plastic, Finite Element Method", Numerical Methods in Industrial Forming Processes, (Eds. J. F. T. Pittman, R. D. Wood, J. M. Alexander and O. C. Zienkiewiewicz), (1982). Pineridge Press Swansea, pp. 777-786.

[22] LI G. J. and KOBAYASHI S., "Analysis of Spread in Rolling by the Rigid-Plastic, Finite Element Method", Numerical Analysis of Forming Processes, (Eds. J. F. T. Pittman, O. C. Zienkiewiewicz, R. D. Wood and J. M. Alexander), (1984). Wiley and Sons, Swansea, pp. 71-88.

[23] MORI K. and OSAKADA K., "Simulation of Three-Dimensional Rolling by the Rigid-Plastic Finite Element Method", Numerical Methods in Industrial Forming Processes, (Eds. J. F. T. Pittman, R. D. Wood, J. M. Alexander and O. C. Zienkiewiewicz), Pineridge Press Swansea, (1982), pp. 747-756.

[24] MORI K. and OSAKADA K., "Finite Element Simulation of Three-Dimensional Deformation in Shape Rolling". Numerical Methods in Industrial Forming Processes (Eds. E. G. Thompson, R.D. Wood & O. C. Zienkiewicz and A. Samuelsson), Pineridge Press Swansea, (1989), pp. 337-342.

[25] YAMADA K., OGAWA S. and ATAKA M., "Three-Dimensional Analysis of Flat Rolling using Rigid-Plastic Finite Element Method Coupled with Roll Deformation analysis". Numerical Methods in Industrial Forming Processes (Eds. J.-L. Chenot, R. D. Wood and O. C. Zienkiweicz), Pineridge Press Swansea, (1992), pp. 755-761.

[26] YANAGIMOTO J. and KIUCHI M., "Three-Dimensional Simulation System for Coupled Elastic/rigid-plastic Deformations of Rolls and Workpieces in Strip Rolling Processes". Numerical Methods in Industrial Forming Processes (Eds. J.-L. Chenot, R. D. Wood and O. C. Zienkiwicz), Pineridge Press Swansea, (1992), pp. 763-768.

[27] CORNFIELD C. and JOHNSON R. H., "Theoretical Predictions of Plastic Flow in Hot Rolling Including the effect of various Temperature Distributions", *Journ. Iron and Steel Inst.* **211** (1973), pp. 567-573.

[28] LEE C. H. and KOBAYASHI S., "New Solutions to Rigid Plastic Deformation Problems Using a Matrix Method", *Journ. Engng. Ind. Trans. ASME* **95** (1973), pp. 865-873.

[29] ZIENKIEWICZ O. C. and GODPOLE P.N. "Flow of Plastic and Viscoplastic Solids with Special Reference to Extrusion and Forging Problems", *Int. Journ. Num. Meth. Engng.* **8** (1974), pp. 3-16.

[30] KUMAR A., SAMARASEKERA I. V. and HAWBOLT E. B., "Roll-Bite Deformation During the Hot Rolling of Steel Strip", *Journ. Materials. Processing Technology*, **30** (1992), pp. 91-114.

[31] JIN, D., STACHOWIAK, R. G., SAMARASEKERA, I.V. and BRIMACOMBE, J. K., "Mathematical Modelling of Deformation during Hot Rolling", *36th MWSP Conf., Proc.*, ISS-AIME, Vol. **32**, (1995), pp. 401-407.

[32] MARCAL P. V. and KING I. P, "Elastic Plastic Analysis of Two Dimensional Stress Systems by the Finite Element Method", *Int. Journ. Mech. Sci.*, **9** (1967), pp. 143-155.

[33] YAMADA Y., YOSHURA N. and SAKURAI T, "Plastic Stress-Strain Matrix and its Application for the Solution of Elastic-Plastic Problems by the Finite Element Method", *Int. Journ. Mech. Sci.*, **10** (1968), pp. 343-354.

[34] ZIENKIEWICZ O. C., VALLIAPPAN S, and KING I. P., "Elasto-Plastic Solutions of Engineering Problems 'initial Stress' Finite Element Approach", *Int. J. Num. Meth. Engng.* **1** (1969), pp. 75-100.

[35] HARTLEY P., PILLINGER I., STURGESS C., "Numerical modelling of Material Defprmation Processes", Springer-Verlag, London, (1992), pp. 252-354.

[36] OWEN D. R. J. and HINTON E., "Finite Elements in Plasticity: Theory and Practice", Swansea. Pineridge Press, (1980).

[37] BRIDGMAN, P. W., "Studies in Large Plastic Flow and Fracture", McGraw Hill, New York (1952).

[38] AMICI E., DEMOFONTI G., LUBRANO M. and PIETROSANTI C., "Application of the Finite Element Method to the Simulation of Rolling Process of Flat and Long Products", Numerical Methods in industrial Forming Processes. Numiform (Eds. E. G. Thompson, R. D. Wood & O. C. Zienkiewicz and A. Samuelsson), (1989), pp. 293-301.

[39] LINDGREN L. E. and EDBERG J., "Contact Forces and Deformations in Plate Rolling", Numerical Methods in industrial Forming Processes. Numiform (Eds. E. G. Thompson, R. D. Wood & O. C. Zienkiewicz and A. Samuelsson), (1989), pp.331-336.

[40] FUKUMURA, M., FUJIKAKE, M. and FUJITA, F., "Elasto-Plastic Finite Element Simulation of the Flat Rolling Process by Dynamic Explicit Method", *2nd Int. Conf. on Modelling of Metal Rolling Processes*, (Eds. J.H. Beynon, P. Ingham, H. Teichert and K. Waterson), December 9 – 11 (1996), London, pp. 264 – 274.

[41] BOËR C. R., GUDMUNSON P. and REBELO N., "Comparison of Elasto-Plastic FEM, Rigid-Plastic FEM and Experiments for Cylinder Upsetting", (Eds. J. F. T. Pittman, O. C. Zienkiewiewicz, R. D. Wood and J. M. Alexander), Wiley and Sons, Swansea, (1984), pp. 217-226.

[42] THOMPSON E. G. and BERMAN H. M., "Steady State Analysis of Elasto-Viscoplastic Flow During Rolling", (Eds. J. F. T. Pittman, O. C. Zienkiewiewicz, R. D. Wood and J. M. Alexander), Wiley and Sons, Swansea, (1984), pp. 71-88.

[43] KOBAYASHI S., "Thermoviscoplastic Analysis of Metal Forming Problems by the Finite Element Method", (Eds. J. F. T. Pittman, O. C. Zienkiewiewicz, R. D. Wood and J. M. Alexander), Pinewood Press, Swansea, (1984), pp. 17-69.

[44] HOLLANDER F., "A Model to Calculate the Complete Temperature Distribution in Steel During Hot Rolling", *Proc. Conf. Mathematical Models in Metallurgical Process Development organised by the Iron and Steel Inst.*, London 1969, Published in the Journ. Iron and Steel Inst., ISI **123** (1970), pp. 46-78.

[45] SEREDYNSKI, F., "Prediction of Plate Cooling during Rolling-Mill Operation," *Journ. of Iron and Steel Inst,.* (1973), pp. 197-203.

[46] YANAGI K. I., "Prediction of Strip Temperatures for Hot Strip Mills". Originally published in Mitsubishi Juko Giho **11** (1974), No., 53 in Japanese. Eng. version received August 19, (1974).

[47] TSENG AMPERE A., "A Finite-Difference Thermal Model of Flat Rolling", Numerical Methods in Industrial Forming Processes, (Eds. J. F. T. Pittman, R. D. Wood, J. M. Alexander and O. C. Zienkiewiewicz), (1982). Pinewood Press, Swansea, pp. 767-776.

[48] DEVADAS, C. and SAMARASEKERA, I.V., "Heat Transfer during Hot Rolling of Steel Strip", *Ironmaking and Steelmaking* Vol. **13**, (1986), No. 6, pp. 311 – 321.

[49] COLÁS, R. and SELLARS, C.M., "Computed Temperature Profiles of Hot Rolled Plate and Strip during Accelerated Cooling", *Proc. of the Int. Symp. on Accelerated Cooling of Rolled Steel*, (Eds. G.E. Ruddle and A.F. Crawley), Winnipeg, Canada, August 24 – 25 (1987), pp. 121-130.

[50] PIETRZYK M. and LENARD J.G., "A Study of Heat Transfer During Hot Rolling", *Numiform 89* (Ed. Thompson) (1989), pp. 343-348.

[51] JOHNSON W. and KUDO H., "The Use of the Upper-Bound Solutions for the Determination of Temperature Distributions in Fast Hot Rolling and Axisymmetric Extrusion Processes", *Int. Journ. Mech. Sci.*, Vol. **1**, (1960), p. 175

[52] TAY A. O., STEVENSON M. G. and DAVIS G. V., "Using the Finite-Element Method to Determine Temperature Distributions in Orthogonal Machining", *Proc. Inst. Mech. Engr.* Vol. **188**, (1974), p. 236

[53] ALTAN T. and KOBAYASHI S., "A Numerical Method for Estimating the Temperature Distributions in Extrusion Through Conical Dies", *Trans ASME, J. Engr. Ind*, Vol. **90** (1968), p. 107

[54] BISHOP J. F. W., "An Approximate Method for Determining the Temperature Reached in Steady Stat Motion Problems of Plane Plastic Strain", *Q. J. Mech. App. Math.*, Vol **9**, (1956), p. 236

[55] LAHOTI G. and ALTAN T., "Prediction of Temperature Distribution in Axisymmetric Compression and Torsion", *Trans. ASME, J. Engr. Materials Technology,* Vol. **97** (1975), p. 113.

[56] MAGPAL V., LAHOTI G. D. and ALTAN T., "A Numerical Method for Simultaneaous Prediction of Metal Flow and Temperatures in Upset Forging of Rings", *Trans. ASME, J Engr. Ind.* Vol. **109** (1978), p. 413

[57] CULLING D. L., "Computer Simulation of the Mechanical and Thermal Aspects in the Finishing Section for the Hot Rolling of Strip Steel", EngD. Thesis University of Wales-Swansea .(1996)

[58] ODEN J. T., BHANDARI D. R., YAGWA G. and CHUNG T.J., "A New Approach to the Finite Element Formulation and Solution of a Class of Problems in Coupled

Thermoelastoviscoplasticity of Crystalline Solids", *Nuclear Engineering and Design* **24**: (1973), pp. 420-430.

[59] HSU C., T., "Computer Simulations of Hot Rolling of Steel", PhD Thesis University of Wales-Swansea. (1985)

[60] LENARD J. G. and PIETRZYK M., "Thermal-Mechanical Modelling of a Hot Strip Mill", *Advanced Technology of Plasticity* , **2**, (1990), pp. 601-605.

[61] CHEN, W.C., SAMARASEKERA, I.V., KUMAR, A. and HAWBOLT, E.B., "Mathematical Modelling of Heat Flow and Deformation during Rough Rolling", *Ironmaking and Steelmaking*, Vol. **20**, (1993), No. 2, pp. 113-125.

[62] BERTRAND C. C., MONITMITONNET P and CHENOT J. L., "A Three-Diemsional Analysis of Hot Rolling with a Steady State Thermomechanical Approach", Numerical Methods in Industrial Forming Proceses. *Numiform* (Eds. E. G. Thompson, R. D. Wood & O. C. Zienkiewicz and A. Samuelsson), (1989), pp. 303-308.

[63] TOO J. J. M. and BARNES K. R., "Application of Numerical Method for the Simulation of Hot Rolling of Metals", Numerical Methods in Industrial Forming Proceses. *Numiform* (Eds. E. G. Thompson, R. D. Wood & O. C. Zienkiewicz and A. Samuelsson), (1989), pp. 367-374.

[64] TSENG. A., GUNDERIA A. S. and SUN P. F., "Heat Transfer of Roll and Strip Cooling in Steel Rolling", *Proc. Int. Symp. Mathematical Modelling of Hot Rolling Steel,* (Ed. S. Yue), (1990), pp. 177-189.

[65] SAMARASEKERA I. V., "The Importance of Characterising Heat Transfer in ot Rolling of Steel Strip", *Proc. Int. Symp. Mathematical Modelling of Hot Rolling Steel,* (Ed. S. Yue), (1990), pp. 148-167.

[66] FLETCHER, J. D. and BEYNON. J.H., "Heat Transfer Conditions in Roll Gap in Hot Strip Rolling", *Ironmaking and Steelmaking*, Vol. **23**, (1996), No. 1, pp. 52-57.

[67] MURATA, K., MORISE, H., MITSUTSUKA, M., NAITO, H., KIMATSU, T. and SHIDA, S., "Heat Transfer between Metals in Contact and its Application to Protection of Rolls", *Transactions ISIJ*, Vol. **24**, (1984).

[68] YUEN, W.Y.D., "On the Heat Transfer of a Moving Composite Strip Compressed by Two Rotating Cylinders", *Journ. of Heat Transfer*, August Vol. **107,** (1985), pp. 541-548.

[69] SELLARS C. M., "Computer Modelling of Hot-Working Processes", *Materials Science and Technology*, **1** (1985), pp. 325-331.

[70] PIETRZYK, M. and LENARD, J.G., "Experimental Substantiation of Modelling Heat Transfer in Hot Flat Rolling", *ASME Proc. of National Heat Transfer Conf.*, Houston, (1988), pp. 47-53.

[71] BURTE, P.R., IM Yong-Taek, ALTAN, T., SEMIATAN, S.L., "Measurement and Analysis of Heat Transfer and Friction during Hot Forging", *Trans, of the ASME Journ. Eng. Ind.*, November Vol. **112**, (1990), pp. 332-339.

[72] DEVADAS, C., SAMARASEKERA, I.V. and INROPERA, F.P., "The Thermal and Metallurgical State of Steel Strip during Hot Rolling: Part 1. Characterisation of Heat Transfer", *Metallurgical Transactions A*, Vol. **22**, (1991), pp. 307-319.

[73] CHEN, W.C., SAMARASEKERA, I.V., KUMAR, A. and HAWBOLT, E.B., "Fundamental Phenomena Governing Heat Transfer during Rolling", *Metallurgical Transactions A*. June Vol. **24**, (1993), pp. 1307-1320.

[74] HLADY, C.O., BRIMACOMBE, J.K., SAMARASEKERA, I.V. and HAWBOLT, E.B., "Heat Transfer in the Hot Rolling of Metals", Metallurgical and Material Transactions B, October Vol. **26**, (1995), pp. 1019-1027.

[75] LI, Y.H. and SELLARS, C.M., "Evaluation of Interfacial Heat Transfer and its Effects on Hot Forming Processes", *Modelling of Metal Rolling Processes Symp.* 7: *Cooling in Rolling Mills*, London, June **7** (1995).

[76] LI y. H. and SELLARS C. M., "Evaluation of Interfacial Heat Transfer and its Effects on Hot Forming Processes", *Ironmaking and Steelmaking*, **23** (1996), pp. 58-61.

[77] LI Y. H. and SELLARS C. M., "Modelling Deformation behaviour of Oxide Scales and their Effects on Interfacial Heat Transfer and Friction During Hot Steel Roling", 2nd Int. Conf. On Modelling of Metal Rolling Processes (Eds. J. H. Beynon, P Ingham, H Teichert and K Waterson), Dec 9-11 (1996), pp.192-201.

[78] LI Y. H. and SELLARS C. M., " Effects of Scale Deformation Patterns and Contact Heat Transfer on Secondary Oxide Growth", *2nd Int. Conf. On Hydraulic Descaling in Rolling Mills*, Oct (1997).

[79] FLECHER J.D. and BEYNON J. H., "Heat Transfer Conditions in roll gap in Hot Strip Rolling", *Ironmaking and Steelmaking,* **23**, (1996), pp.52-57.

[80] TSENG A. A., ASHUTOSH S., GUNDERIA S. and SUN, P. F., "Cooling of Roll and Strip in Steel Rolling", *Steel Research,* **5** (1991), pp. 207-214.

[81] CHEN Shih-Jiun and KOTHARI, J., "Temperature Distribution and Heat Transfer of a Moving Metal Strip Cooled by a Water Jet", *ASME Winter Annual Meeting*, November 27 – December 2, Chicago, (1988).

[82] ZUMBRUNNEN, D.A., VISKANTA, R., INCROPERA, F.P., "The Effect of Surface Motion on Forced Convection Film Boiling Heat Transfer", *Journ. of Heat Transfer*, Vol. **3**, (1986), pp. 760 –766.

[83] PACKO M, KUSUAK H and PIETRZYK M., "Modelling Water Cooling of Steel Strip During Hot Rolling", *Steel Research,* **64** (1993), pp. 128-131.

[84] HORSKY J., RAUDENSKY M and KOTRBACEK P., "Experimental Study of Long Product Cooling in Hot Rolling", *Journ. Mat. Process Technology,* **80-81** (1998), pp. 337-340.

[85] SCHEY J. A., "Metal Deformation Processes / Friction and Lubrication", Marcel Dekker Inc, New York, (1970).

[86] PETTY D. M., "Friction Models for Finite Element Modelling", *Journ of Mater. Process. Technology,* **45**, (1994), pp. 7-12.

[87] BAY N., "Friction and Adhesion in Metal Forming and Cold Welding" *Technical University of Denmark,* Extracts from DSc thesis, 1985.

[88] COULOMB C. A., "Theories des Machines Simple", *Memoires de Mathematique et de Physique de l'academie Royal.*, (1785), pp. 161-342.

[89] BAY N. and WANHEIM T., "Real Area of Contact and Friction Stress at High Pressure Sliding Contact", *Wear*, **38**, (1976), pp. 201-209.

[90] RUDKINS N. T., "A Study of Surface Friction to Improve the Finite Element Simulation of Hot Rolling". PhD Thesis University of Birmingham (1997).

[91] MUNTHER P. A. and LENARD J. G., "A Study of Friction During Hot Rolling of Steels", *Scandinavian Journ. of Metallurgy,* **26**, (1997), pp. 231-240.

[92] EKELUND S., "Analysis of Factors Influencing Rolling Pressure and Power Consumption in the Hot Rolling of Steel", *Steel*, **93**, (1993), pp. 38-42.

[93] RUDKINS N. T., HARTLEY P., PILLINGER I. and PETTY D., "Friction Modelling and Experimentation Observations in Hot Ring Compression Tests", *Journ of Materials Process Technology,* **60**, (1996), pp. 349-353.

[94] LI Y. H., BEYNON J.H. and SELLARS C. M., "Determination of Friction in Hot Rolling by Forward/Backward Slip Measurements", *6th Int. Conf. On Technology of Plasticity*, (1999), pp. 19-24

[95] CHUN-HUI L., "Modelling the Frictional Boundary Conditions in a Rolling Process", *Journ. of Mater. Process Technology,* **59**, (1995), pp. 373-380

[96] BAY N. and WANHEIM T., "Real Area of Contact and Friction Stress at High Pressure Sliding Contact", *Wear*, **38**, (1976), pp. 201-209.

[97] SAMARASEKERA, I. V., WELLS M. A., JIN D., HLADY C. O. BRIMACOMBE J. K. and HAWBOLT E. B., "Application of Microstructural Engineering to the Processing of Lightweight Materials", *Materials Characterisation,* **35**, (1995), pp. 69-79.

[98] SELLARS C. M. and TEGART W. J. McG., "Hot Workability", *Int. Metallurgical Reviews*, Vol **17**, (1972), pp. 1-24.

[99] KOSTER, W. "Die Temperaturabhangigkeit des Elastizitatsmoduls Reiner Metalle", *Zeitschrift Für Metallkunde*, Vol **89**, (1948), pp.1-9.

[100] BEYNON J. H. and SELLARS C. M., "Modelling Microstructure and its Effects During Multipass Hot Rolling", *ISIJ Int.* Vol. **32**, 3 (1992), pp. 359-367.

[101] DOHERTY R. D., HIGHES D. A., HUMPHREYS F. J., JONAS J. J., JENSEN D. J., KASSNER M. E., KING W. E., McNELLEY T. R., McQUEEN H. J. and ROLLETT

A. D., "Current Issues in Recrystallisation-A Review", *Materials Science and Engineering* A, (1997), pp. 219-247.

[102] TEGART W. J. McG. and GITTINS A., "The Hot Deformation of Austenite", (Ed. J. B. Balance) The Hot Deformation of Austenite, AIME, New York, (1997), pp. 1-46.

[103] FAREGUE P., "Prediction of High Temperature Flow Stresses through a Dynamic Recrystallisation Model", *Proc. int. conf. Advancement in Hot Deformation Textures and Microstructures*, (Eds. J. J. Jonas, T. R. Bielerand and K. J. Bonman). The Mierals, Metals and Materials Society, (1994), pp. 75-94.

[104] LAASRAOUI A., JONAS, J. J., and BARAGER D., "Mathematical Modelling of the Hot Rolling of Steel", *Proc., Int. Symp. CIM,* (1990), p. 86.

[105] ANDERSON J. G., and EVANS R. W., "Modelling Flow Stress Evolution During Elevated Temperature Deformation of Two Low Carbon Steels", *Ironmaking and Steelmaking* Vol. **23**, No 2, (1996), pp. 130-135.

[106] ANDERSON J. G., "Microstructural Algorithms for the Computer Simulations of the Hot Strip Rolling of Steel", Eng D thesis University of Wales Swansea (1996).

[107] SELLARS C. M. and WHITEMAN J. A., "Recrystallisation and Grain Growth in Hot Rolling", *Metal Science* (1979), pp. 187-194.

[108] DJAIC R. A. P. and JONAS J. J., "Static Recrystallisation of Austenite Between Intervals of Hot Working", *Journ. of Iron and Steel Inst.* (1972), pp. 256-261.

[109] SUN W.P. and HAWBOLT E. B., "Prediction of the Onset of Static Recrystallisation After Hot Deformation", *ISIJ Int.*, Vol **35** (1995), No 7, pp. 908-913.

[110] MILITZER M., GIUMELLI A., HAWBOLT, E. B.and MEADOWCROFT T. R., "Austenite and Ferrite Grain Size Evolution in Plain Carbon Steel", *36th MWSP Conf. Proc*, ISS-AIME, Vol **32**, (1995), pp. 375-384.

[111] SUN W. P., MILITZER M., HAWBOLT, E. B. and MEADOWCROFT T. R., "Analysis and Modelling of Austenite Grain Refinement and Growth During Hot Rolling", *Iron and Steelmaking* (1998) pp. 85-94

[112] MEDINA S. F., "Microstructural Modelling for Low Alloy and Microalloyed Steels", *2nd Int Conf. Modelling of Metal Rolling Process*ses (Eds. J. H. Beynon, P. Ingahm, H Teichert and K. Waterson, (1996), pp.501-510.

[113] COLAS R., ELIZONDO L., and LEDUC L. A., "Mathematical Modelling of a Continuous Thin Strip Mill", *2nd Int Conf. Modelling of Metal Rolling Processes* (Eds. J. H. Beynon, P. Ingahm, H Teichert and K. Waterson, (1996), pp. 12-22.

[114] BIANCHI J. H. and PETRONE1 E., "Modelling of Multipass Rolling of Steel Plates", *Numerical Methods in Industrial Forming Processes* (Eds. J. –L. Chenot, R. D. Wood and O. C. Zienkiewicz), (1992), pp. 701-706.

[115] ZHANG X., HODGSON P.D. and THOMPSON P. F., "The Effects of Through-Thickness Strain Distribution on the Static Recrystallisation of Hot Rolled Austenitic Stainless Steel Strip", *Journ Materials processing Technology*, **60**, (1996), pp. 615-619.

[116] PIETRZYK M. and KEDZIERSKI Z. and LENARD J. G., "Finite Element Simulation of Mechanical, Thermal and Structural Phenomena in the Hot Rolling Process", *Numerical Methods in Industrial Forming Processes* (Eds. J. –L. Chenot, R. D. Wood and O. C. Zienkiewicz), (1992), pp.749-754.

[117] DUNSTAN G. R., "A Laboratory Simulation of Commercial Hot Rolling", PhD Thesis, University of Wales-Swansea (1969).

[118] EVANS R. W., "The Plane Strain Compression Test for the Determination of Hot Working Properties", (Eds. J. F. T. Pittman, R. D. Wood, J. M. Alexander and O. C. Zienkiewiewicz), (1982). Pineridge Press, Swansea, pp. 481-490.

[119] Getting Started With ABAQUS 1-1.

[120] ABAQUS Theory manual. Ver 5.8.

[121] LEE P. J., "Control of Shape and Profile in Hot Rolled Steel Strip", EngDoc Thesis, University of Wales, Swansea (1997).

[122] HODGSON P. D., BROWNE K. M., GIBBSR. K., PHAM T. T. and COLLINSON D. C., "The Mathematical Modelling of Temperature and Microstructure During Spray Cooling", *Proc. 1st Intern. Conf. On Quenching and Control of Distortion*, Chicago, (1992) pp. 41-49.

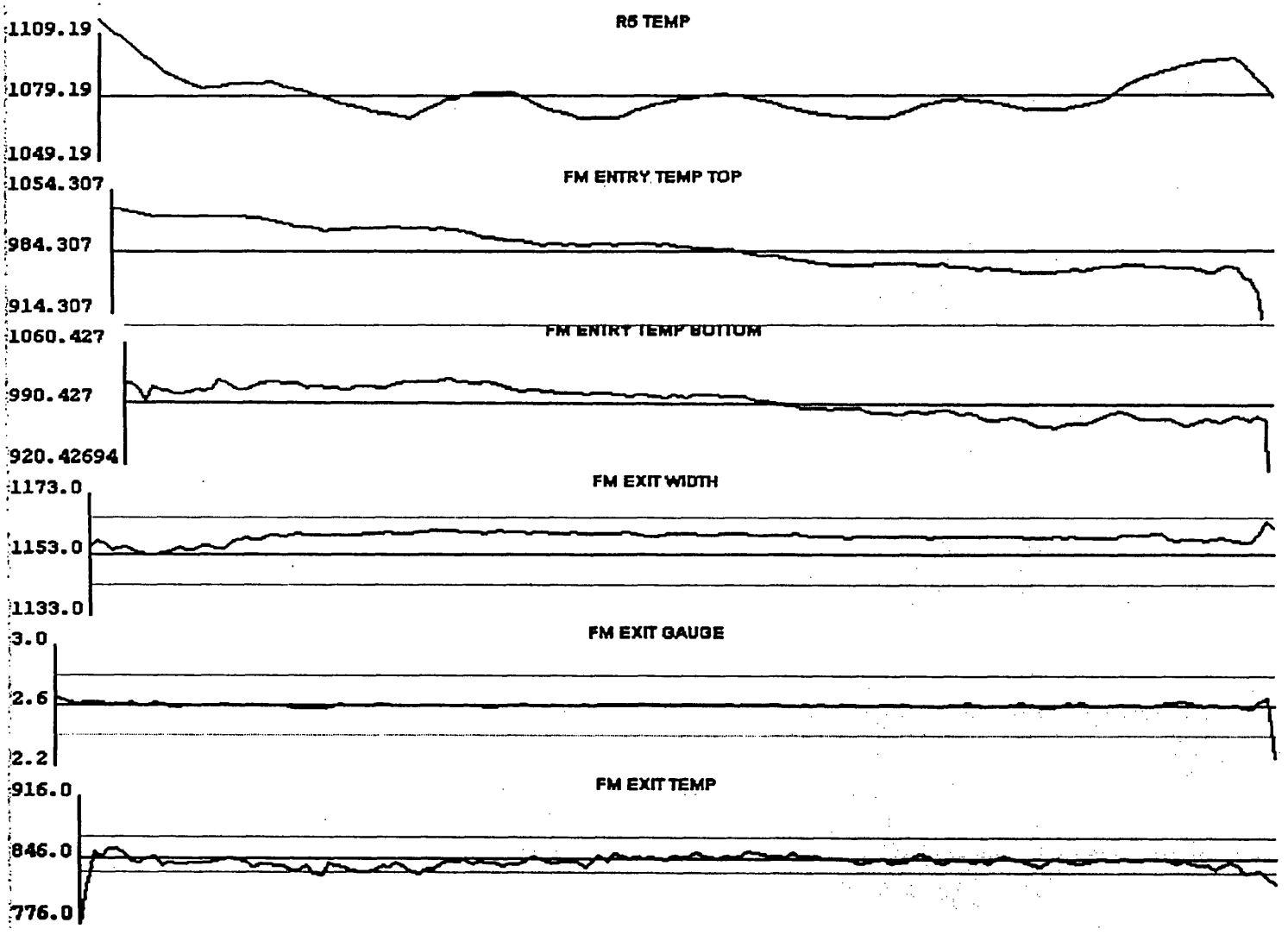

Finishing Mill Data For High Carbon. Coil No. 8334801

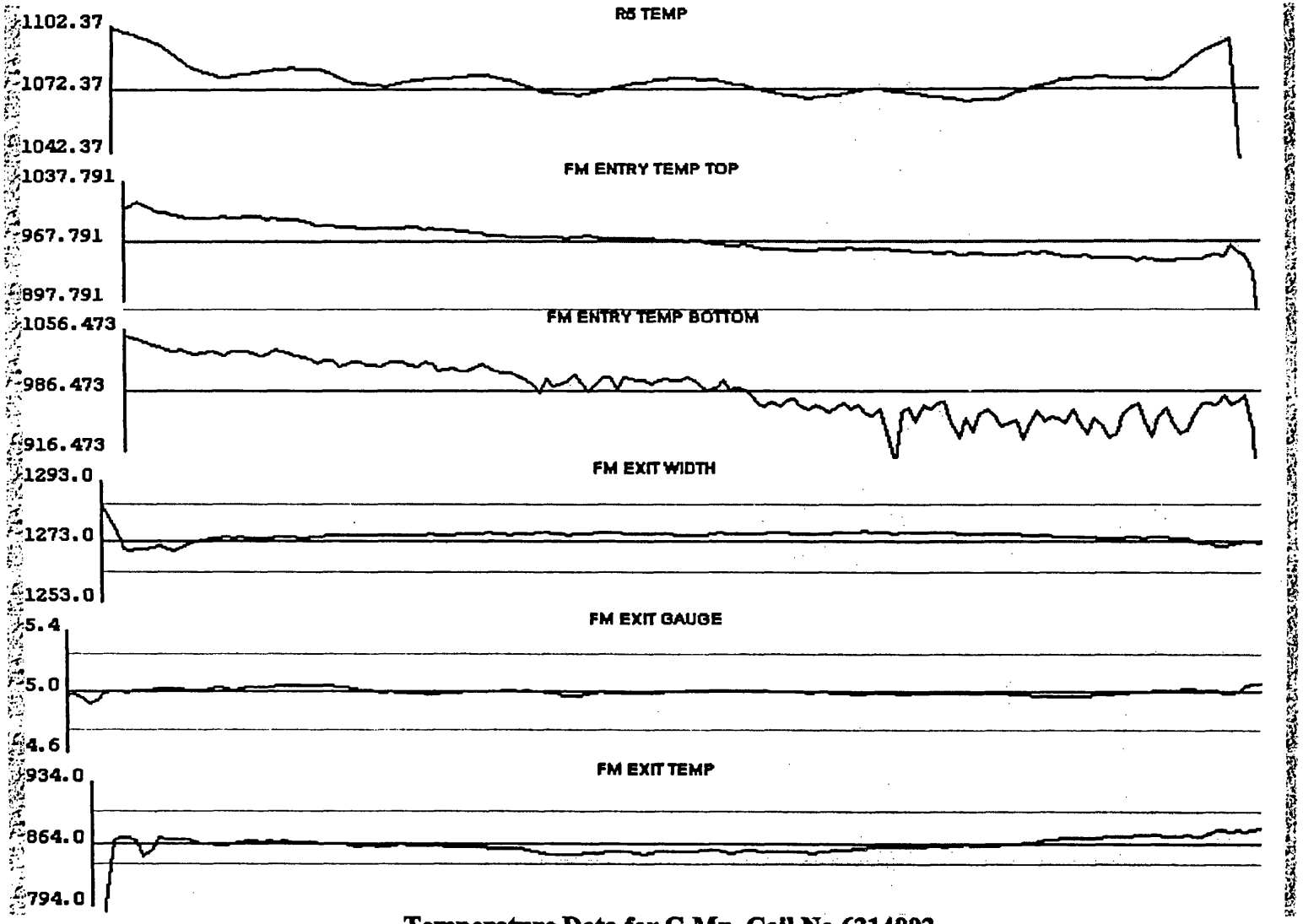

Temperature Data for C-Mn. Coil No.6314003

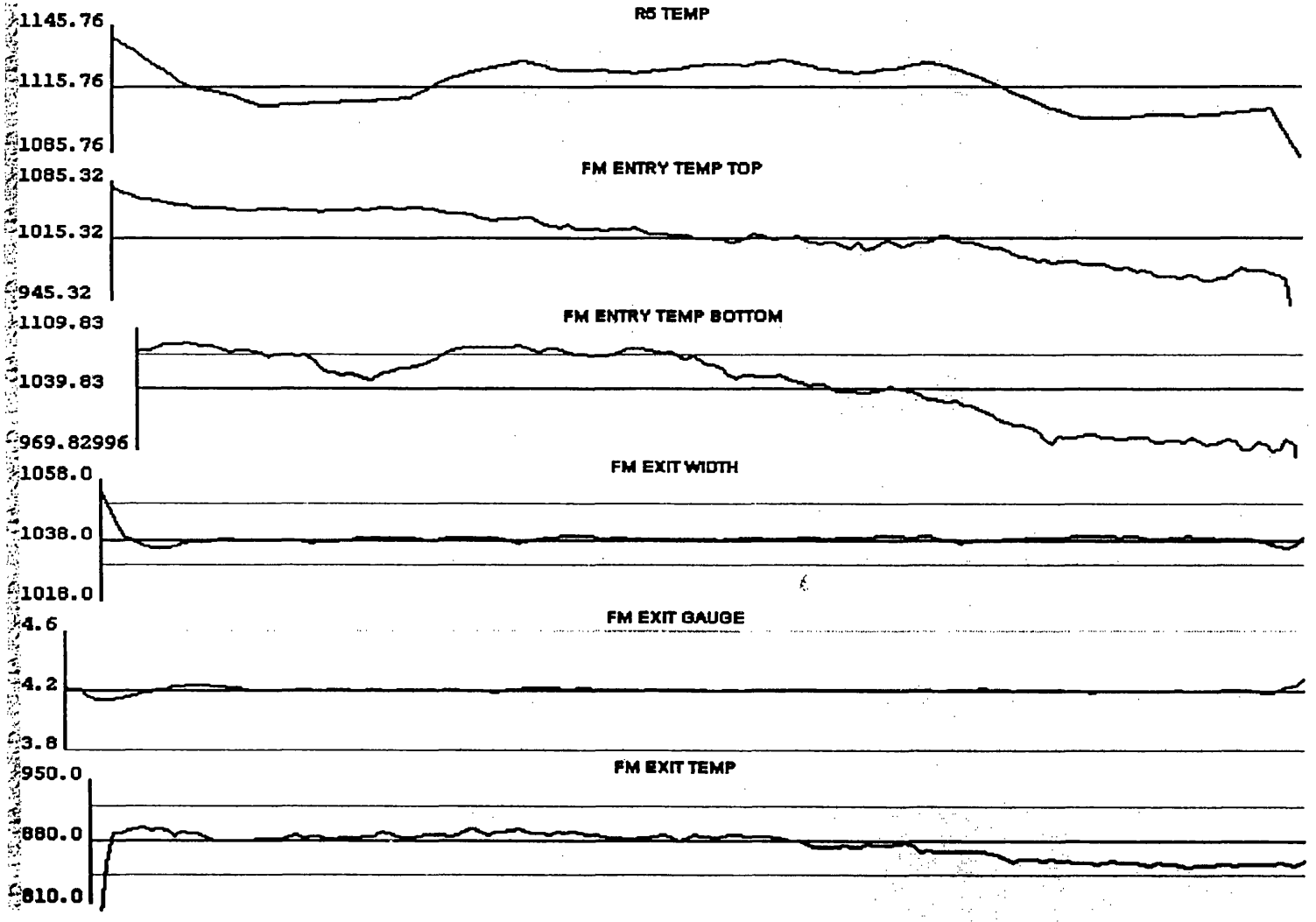

Finishing Mill Data For Low Carbon. Coil No. 3681301

ENOG-A LIVE FILE 17:35:21 29/11/00

Analysis Specification For Grade 2946 Account Code : 1

Desc. : HIGH CARBON PPC Classification : 678

	C	Si	Mn	P	S	Cr	Mo	Ni	S.Al
Aim									
Min	0.7500	0.1500	0.6500			0.1500			0.0200
Max	0.8000	0.3000	0.8500	0.0200	0.0080	0.2300	0.0500	0.2000	0.0500
REF/LIMIT									

	T.Al	As	B	Cu	N	Nb	Sn	Ti	V
Aim									
Min									
Max			0.0005	0.1500	0.0090	0.0100	0.0300	0.0100	
REF/LIMIT									

Comment about Grade Priority: HIGH CARBON GRADE

Ratios From To

Al/N

Ti/C

Mn/S

Cev

Bucket No. : 7946

Grade Priority : 99

User ref : 4225

Schedulable : Y

Orderable : Y

GE Code : 67

Suitability for { Slab Dunking : N

{ Coil Quenching : N

OPTION ( )

HARD COPIES OF THIS SCREEN FOR INFORMATION ONLY - NOT SUBJECT TO AMENDMENT

LLANWERN HOT STRIP MILL : ROLLING PRACTICE

VERSION 1.4 15/4/98

PRODUCT: >0.5% CARBON	GRADES: 5945 5935 2945 2935
ISSUE	PRACTICE REQUIREMENT
SCHEDULING:	
REHEATING:	-
DROP OUT TEMPERATURE	1250°C-1280°C
FURNACE PRACTICE	120 SEC GAP TIMEON ENTRY TO HEATING ZONES <=2.5MM PRODUCTS: SLABS TO BE HOT CHARGED
ROUGHING:	-
ROUGHER DESCALING	**reduce to hsb,r5,r3&r1 descaling on <=3mm products if required to aid rolling in fin mill**
DELAY TABLE:	-
TRANSFER BAR THICKNESS	35MM
ENCO PANEL REQUIREMENTS	DOWN
CROP SHEAR	**DOUBLE CROP HE of 5945 grade <=3mm gauge**
FSB	
FINISHING MILL	IF CONDITIONS ARE NOT FAVOURABLE THEN INITIALLY ROLL 2.0MM GAUGE TO 2.5MM TO STABILISE FIN. MILL THEN ROLL AT 2.0mm
FINISHING TEMP:	LIMIT MILL ACCELERATION TO MAINTAIN FT AT TARGET
ROLL COOLING	4 PUMPS ON ROLL COOLING
THREAD SPEED	FOR GAUGES =<3MM LIMIT THREAD SPEED TO 670/680 M/MIN
SCALE SUPPRESSION	OFF
F1 BOT ENTRY SPRAY	OFF
F2 ENTRY SPRAYS	ALL OFF
INTERSTAND REQUIREMENT	
ROT COOLING	-
COOLING STATEGY	COOLING STRATEGY 22
SPECIAL INSTRUCTIONS	Coiling Temp: 625°C FOR C>0.68% & GAUGES =<2.5MM COILING TEMP 650°C

COILING	**For gauges >= 4.5mm dry coiling practice** **mandrel cooling water off** **pinch roll cooling water off** **Elkuch sprays off** **use coil car to ensure tight oputer laps achieved off** **coiler mandrel**
INSPECTION REQUIREMENTS UNILUX COIL PIT OTHER	
OTHER REQUIREMENTS	<2.5MM PRODUCT:COOL BORE VERTICAL
WIDTH&GAUGE VARIATIONS:	

LLANWERN HOT STRIP MILL : ROLLING PRACTICE

PRODUCT: C-Mn 350/NP242	GRADES:5724
ISSUE	PRACTICE REQUIREMENT
SCHEDULING:	
REHEATING: DROP OUT TEMPERATURE	1250°C - 1280°C
ROUGHING: ROUGHER DESCALING	
DELAY TABLE: ENCO PANEL REQUIREMENTS	>=3MM MIMIMAL CRAWL SPEED <3MM 70M/MIN, 70M/MIN &150M/MIN >=3MM PANELS UP <3MM PANELS DOWN
FSB	FULL ON
FINISHING MILL FINISHING TEMP: ENTRY TEMP REQUIREMENTS SCALE SUPPRESSION F1 BOT ENTRY SPRAY F2 ENTRY SPRAYS INTERSTAND REQUIREMENT	>=3MM : 820°C-840°C HOLD FM SPEED IF REQUIRED <3MM : 820°C-860°C HOLD FM SPEED IF REQUIRED >=4MM AIM ENTRY TEMP 980°C 3MM-4MM AIM ENTRY TEMP: 1000°C <3MM MIN ENTRY TEMP 1000°C -ELSE ROLL TO 5MM ALT GAUGE >=3MM ALL ON <3MM NO INTERSTAND WATER ON HE, APPLY F1 INTERSTAND AFTER HE HAS THREADED THROUGH F2
ROT COOLING COOLING STATEGY SPECIAL INSTRUCTIONS	INTERRUPT COOLING >=4MM : 650-700°C GAP TEMP 400-450°C C TEMP 3-4MM : 630-670°C GAP TEMP 425-475°C C TEMP <3MM : 630-670°C GAP TEMP 450-500°C C TEMP MODIFY GAP&CTEMPS AT TIME OF ROLLING ENSURE ALL ROT CAPABILITY CHECKS ARE CARRIED OUT PRIOR TO ROLLING
COILING	

INSPECTION REQUIREMENTS
UNILUX
COIL PIT
OTHER